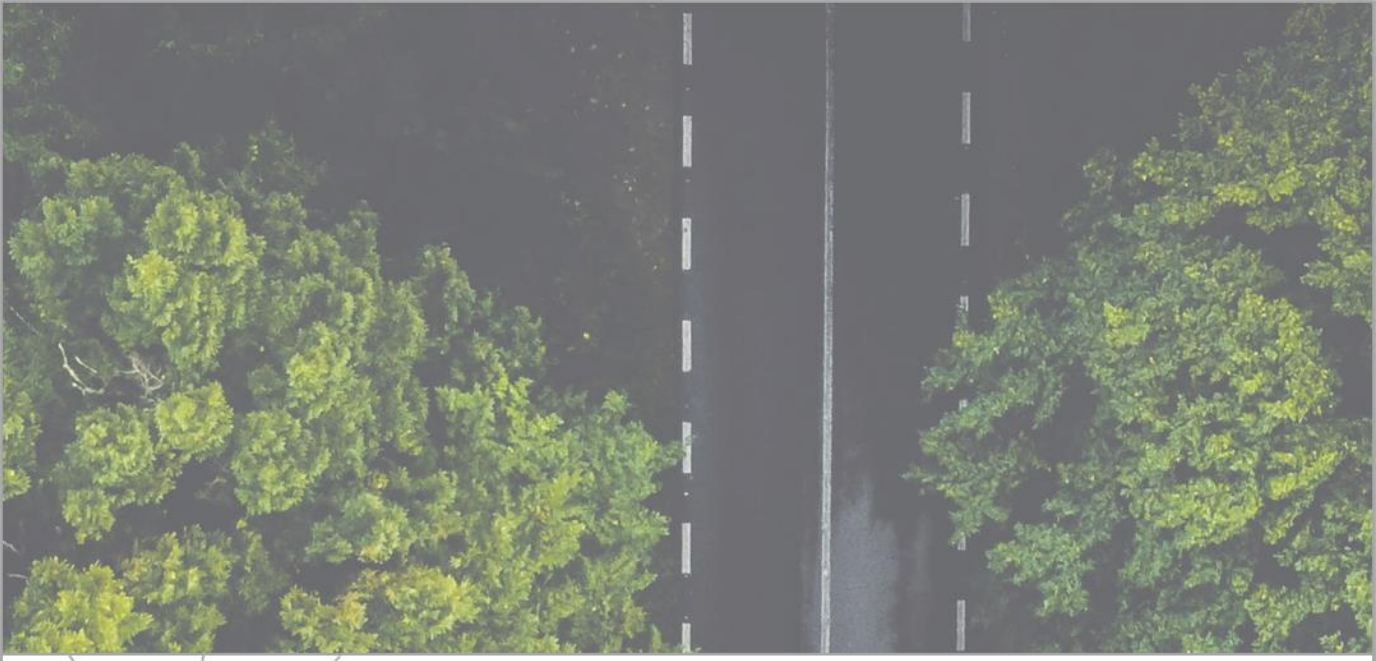

eman ta zabal zazu
Universidad del País Vasco
Euskal Herriko Unibertsitatea

Nuevas formulaciones de PUR más sostenibles para componentes estructurales

Novel sustainable PUR formulations for structural components

2022

Oihane Echeverria Altuna

Oihane Echeverria Altuna
Escuela de Ingeniería de Gipuzkoa
Donostia - San Sebastián, 2022

(cc) 2022 Oihane Echeverria Altuna, (cc by 4.0)

Tesis Doctoral

NUEVAS FORMULACIONES DE PUR MÁS SOSTENIBLES PARA COMPONENTES ESTRUCTURALES

NOVEL SUSTAINABLE PUR FORMULATIONS FOR STRUCTURAL COMPONENTS

Presentada por:

Oihane Echeverria Altuna

Supervisado por:

Arantxa Eceiza Mendiguren

Isabel Harismendy Ramirez de Arellano

en el

Departamento de Ingeniería Química y del Medio Ambiente

perteneciente a la

Universidad del País Vasco

Donostia - San Sebastián, 2022

Agradecimientos

Jada urte batzuk joan dira proiektu honetan sartu nintzenetik, edota hobeto esanda sartu ginenetik. Izan ere, lan hau soilik nire egitea egiari traizio egitea litzateke. Horregatik, ezer baino lehen nire bizitzako etapa honen parte izan zareten eta laguntza eskaini didazuen guztioi eskertu nahiko nizueke.

En primer lugar, quiero agradecer la orientación y el respaldo de mis dos directoras ha sido la clave para conseguir acabar este proyecto. Gracias a las dos por creer en mí, en mi trabajo y apoyarme cada día. Gracias a Isabel, por darme la oportunidad de equivocarme y ayudarme a mejorar. Arantxari eskertu nahi nioke laguntzeko beti duen prestutasuna eta aurrera ateratzeko trasminitzen duen indar hori. Plazer bat izan da zuekin lau urte hauetan lan egitea.

Del mismo modo quiero agradecer a los compañeros de Tecnalia que han hecho posible este trabajo. Aunque no pueda mencionar a todas las personas que me han ayudado, me gustaría agradecer a los compañeros del grupo de composites y al de los polímeros sostenibles. Una mención especial a Olatz y Amaia por las horas que han pasado en planta intentando sacar las piezas de composite, animándome cuando las cosas no salían y alegrándose tanto como yo cuando salían. Agradecer a los compañeros de ensayos mecánicos, en especial a Jorge por correr en el último momento y acabar con los ensayos de nuestros poliuretanos.

Me gustaría resaltar también la ayuda de los compañeros del grupo GMT de la EHU/UPV. No solía bajar todos los días, pero llegar al

laboratorio de la facultad siempre ha sido tranquilizador, siempre me sentía arropada de compañeros dispuestos a enseñarme. En especial Tamara e Izaskun que me han ayudado con los ensayos de caracterización y también Eider y Ana que me han proporcionado componentes necesarios para las formulaciones desarrolladas en la tesis. También, me gustaría mencionar a los compañeros de SGIker, Loli por la ayuda con algunos de los ensayos de caracterización, y a JI por el apoyo técnico brindado para la interpretación de los NMR.

Me gustaría destacar el trabajo de Gorka (EHU/UPV) a la hora de formular los móldelos DDDAS y la ayuda de Pablo en toda la parte de las tecnologías RTM 4.0.

También me gustaría agradecer a Tecnalia, en especial a Cristina y Patxi, la oportunidad brindada gracias a la cual he continuado formándome en el ámbito de los polímeros y materiales. Por otro lado, me gustaría agradecer a la EHU/UPV la oportunidad que me ha dado de presentar mi trabajo bajo su respaldo en el Departamento de Ingeniería Química y del Medio Ambiente.

Agradecer al Gobierno Vasco la financiación a través de los ELKARTEK AVANSITE KK-2020/00019 para el desarrollo de las formulaciones de BIO-PUR para componentes estructurales de automoción y NEOMAT KK-2021/00059 en la línea de desarrollo de resinas de BIO-PUR para palas y otros componentes para energía offshore. Del mismo modo agradecer la financiación de la EHU/UPV Grupo de Investigación (GIU18/216) y del Gobierno Vasco Grupo de Investigación Consolidado del Sistema Universitario Vasco (IT1333-19 y IT1690-22).

Eta ezin ahaztu nire sare ikustezina, hor ez dagoela dirudien arren badagoena. Ostiraleroko ohituraz iluntze aldera atera eta une goxo eta dibertigarriez blaitzen eta berpizten nauena. Ez da hain erraza salto egitea sarerik ez dagoenean. Eskerrik asko sarea osatzen duzuen lagunei.

Azkenik, etxekoei. Egunerokotasunean, eta batez ere, azken hilabete hauetan urperatzen ninduen berunaren kontra, gorantz tira egiten zuen aingura hegoduna izategatik.

Resumen gráfico

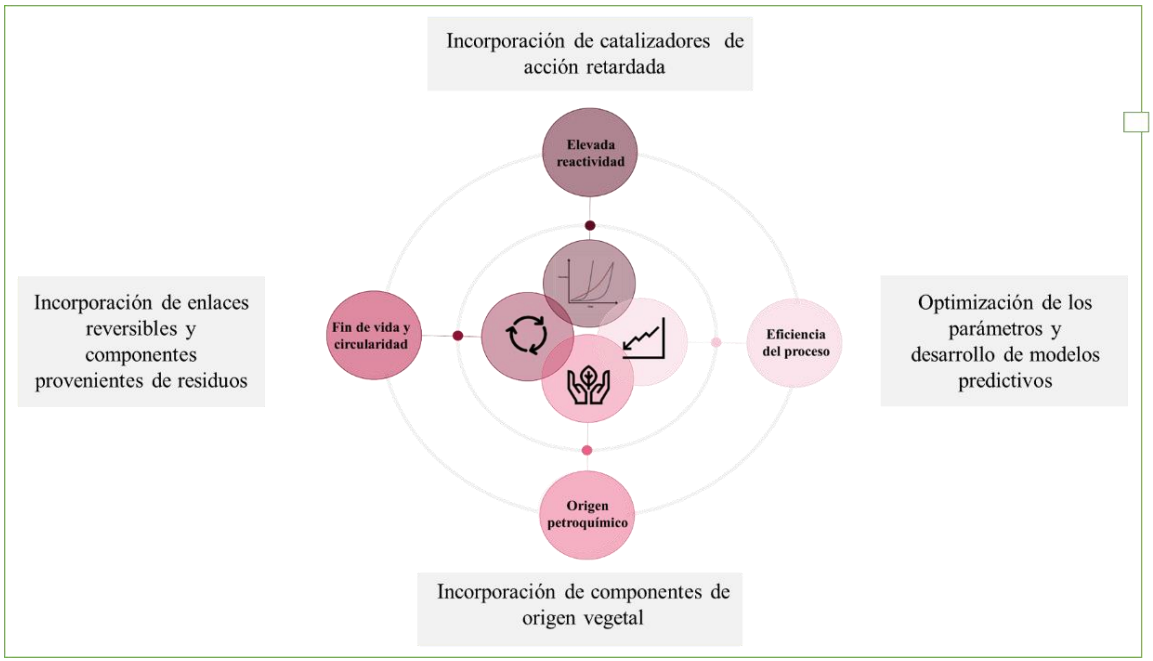

Resumen

Aportar soluciones hacia la descarbonización de la industria de la automoción se ha convertido en uno de los principales retos para el sector. En este contexto, uno de los grandes desafíos es el aligeramiento de los componentes estructurales y los composites se presentan como una de las soluciones más competitivas.

Dentro de las diferentes alternativas de fabricación de piezas estructurales de composite, se encuentra el moldeo por transferencia de resina (RTM) que ofrece la ventaja de ser más eficiente tanto en costes y tiempos como en consumo energético. Por ello, actualmente las resinas de curado rápido y altas prestaciones, específicas para el RTM están suscitando gran interés. Entre las resinas de curado rápido se encuentran los poliuretanos termoestables (PUR).

Las ventajas que ofrece la tecnología basada en PUR frente a otras alternativas son su tenacidad y resistencia a fatiga, que las hace especialmente atractivas para componentes sometidos a cargas cíclicas, así como su baja viscosidad y ciclos de curado rápidos. Sin embargo, actualmente no son alternativas del todo sostenibles, debido al origen petroquímico de sus componentes y su baja reciclabilidad.

En este trabajo se ha desarrollado una investigación en la línea de nuevas formulaciones de base poliuretano más sostenibles, siendo el reto principal el que fueran válidas para aplicaciones estructurales y además viables para el proceso de RTM. Más concretamente, se ha optimizado

la formulación para la fabricación de una ballesta de suspensión para el sector automoción.

En cuanto a la procesabilidad, los PUR en general poseen bajas viscosidades, pero su elevada reactividad provoca un aumento de viscosidad prematuro imposibilitando la adecuada impregnación de las fibras en el proceso de RTM. Por ello, en la primera parte de este trabajo, se han desarrollado catalizadores específicos de acción retardada para controlar y adecuar su reactividad a los requisitos del proceso.

Por otra parte, se ha trabajado en la mejora del impacto medioambiental de las resinas formuladas. Con este objetivo, se han incorporado en la formulación de los PUR componentes de origen vegetal (BIO-PUR), en concreto polioles derivados de aceites vegetales. Se ha estudiado el efecto de las características de los polioles biobasados en la reactividad, viscosidad y propiedades finales de los BIO-PURs. Basándose en este estudio se ha podido formular un BIO-PUR con un contenido de componentes biobasados de hasta 29%, que tras su optimización mediante la incorporación de agentes de entrecruzamiento y catalizadores, resulta adecuado para la fabricación de componentes estructurales por RTM.

La formulación desarrollada se ha validado mediante la fabricación por RTM y ensayo de composites reforzados con fibra de vidrio, seleccionándose los parámetros de fabricación tras un estudio preliminar de su efecto en la calidad. Por otra parte, se ha desarrollado un modelo basado en la metodología de sistemas de aplicación basados en datos dinámicos (DDDAS) de cara a mejorar la robustez del proceso.

Asimismo, debido a la gran demanda en general de soluciones de composites estructurales más sostenibles, se ha estudiado la viabilidad de los BIO-PUR’s para otros sectores como el de la energía en aplicaciones como la eólica, en este caso mediante el proceso de infusión.

Por último, se han estudiado nuevas líneas de investigación hacía la mejora de la circularidad y fin de vida de los BIO-PURs. La reciclabilidad se ha abordado a nivel exploratorio con un estudio de viabilidad preliminar incorporando enlaces dinámicos de tipo Diels-Alder. Por otra parte, se ha abordado el tema de la revalorización de residuos, estudiando la incorporación en las formulaciones del monómero BHET obtenido del reciclado químico de botellas de PET recogidas del mar.

Abstract

The achievement of novel solutions towards the decarbonization of the automotive industry has become one of the major challenges for the sector. One of the main issues is the lightening of structural components, and to this end, composites are one of the most competitive solutions.

Among the different alternatives for manufacturing structural composite parts, resin transfer molding (RTM) offers the advantage of being more efficient in terms of costs, time, and energy consumption. This is reason why high-performance, fast-curing resins specific for RTM are gaining increasing interest. Thermosetting polyurethanes (PUR) are among the most promising the fast-curing resins.

The advantages offered by PUR-based technology are its toughness and resistance to fatigue, which makes it especially attractive for components subjected to cyclic loading, as well as its low viscosity and fast curing cycles. However, they are currently not fully sustainable alternatives, due to the petrochemical origin of their components and their low recyclability.

In this work research in the field of more sustainable polyurethanes resins has been carried out facing the challenge of developing formulations for structural composite applications and also suitable for the RTM process. More specifically, the formulation has been optimized for a leaf spring for the automotive sector.

In terms of processability, PUR presents low viscosities, but their high reactivity causes a premature increase of viscosity, limiting the impregnation of fibres in the RTM process. For this reason, in the first part of this work, specific delayed-action catalysts have been developed to control and adapt their reactivity to the process requirements.

On the other hand, in order to improve the resins sustainability, components with renewable origin have been incorporated in the formulation, concretely polyols derived from vegetable oils. For this purpose, the effect of the characteristics of biobased polyols on the reactivity, viscosity and final properties of BIO-PURs has been studied. Based on this study, a novel BIO-PUR with a content of biobased components of up to 29% has been selected. After it's optimization, incorporating cross-linking agents and catalysts, a formulation suitable for manufacturing of structural components by RTM has been developed.

The developed formulation has been validated by manufacturing by RTM and testing glass fibre reinforced composites. The election of the process parameters has been performed after a preliminary study of their effect on quality. On the other hand, a model based on the DDDAS methodology has been developed to improve the robustness of the process.

Likewise, due to the great demand in general for more sustainable structural composite solutions, the BIO-PUR has been validated for other sectors such as wind energy. In this case, the process studied was infusion.

Finally, new research lines have been studied to improve the BIO-PURs circularity and their end of life. Recyclability has been addressed at an exploratory level with a preliminary feasibility study incorporating dynamic Diels-Alder type bonds. On the other hand, the issue of waste recovery has been addressed, studying the BHET, a monomer obtained from the chemical recycling of PET bottles collected from the sea, incorporation in the formulation.

Laburpena

Autogintza industriaren deskarbonizazioa sektorearen lehentasun nagusien artean kokatzen da. Honetarako, erronka azpimarragarrienetarikoa egiturazko osagaien arintzea da, konpositeak alternatiba lehiakorrenen artean aurkitzen direlarik.

Egiturako konpositeen fabrikazio prozesu mota ezberdinen artean transferentzia bidezko moldekatzea (RTM) topatzen da. Bera izanik, prozesuaren kostua, denbora eta kontsumo energetikoa kontuan hartuz gero alternatiba eraginkorrenetakoa. Hau dela eta, RTM prozesuetarako diseinatutako ontze erreakzio azkarrak eta propietate altuak eskaintzen dituzten erretxinek sektorearen arreta piztu dute. Ontze erreakzio azkarreko erretxinen artean poliuretano termoegonkorrak (PUR) aurkitzen dira.

PURetan oinarritutako teknologiak hainbat abantaila eskaintzen ditu; hala nola, biskositate baxuak, ontze erreakzio azkarrak, eta nabarmengarrienak, zailtasun handia eta nekearekiko erresistentzia bikaina. Horrela ba, PURak bereziki interesgarriak dira karga ziklikoak jasan behar dituzten aplikazioetarako. Alabaina, egun ez dira material erabat jasangarriak, euren jatorri ez-berriztagarria eta birziklagarritasun maila baxua dela eta.

Lan honen ardatza PUR jasangarrien garapena izan da, jorratu den ikerketa lerroa, RTMrako egokiak diren eta egiturazko aplikazioetarako beharrezko eskakizunak betetzen dituzten PURen

diseinua izanik. Gainera, formulazio berria autogintza sektorerako interesa duen konpositezko baleztetarako egokitu da.

Prozesagarritasunari dagokionez, nahiz eta PURek biskositate baxuak eskaini, duten erreaktibotasun altua dela eta, biskositatea garaizegi hasten da handitzen, RTM prozesuetan nahitaezko den zuntzen blaitze egokia galaraziz. Ondorioz, ikerkuntza lan honen lehen zatian PUREn erreaktibotasuna kontrolatze eta egokitze aldera, erreakzioa atzeratzeko gaitasuna duten katalizatzaile espezifikoak garatu dira.

Bestalde, PUREn ingurumen-inpaktua murrizteko helburuz, formulazioetan jatorri berriztagarrietatik eratorritako konposatuak gehitu dira, zehazki erabili diren osagaiak landare olioetatik eratorritako poliolak izan dira. Ezaugarri ezberdinetako poliolak erabiliz BIO-PURak garatu dira, honi esker poliolen ezaugarriek formulazio berrien erreaktibotasunetan, biskositateetan eta amaierako propietateetan duten eragina aztertu da. Ikerketa honetan oinarrituz, gurutzaketa areagotzeko ahalmena duten osagaiak eta katalizatzaileak gehituz BIO-PURak optimizatu dira. Horrela,% 29ko jatorri berriztagarria duen BIO-PUR berria garatu da, zein RTM bidez fabrikatutako konposite egituraletarako egokia den.

Erretxina berriaren egokitasuna frogatze aldera, konposite plaka bat fabrikatu da RTM bidez, zeini amaierako kalitatea aztertu zaion eta mekanikoki karakterizatu den. Bestalde, DDDAS metodologian oinarrituriko modelo bat garatu da fabrikazio prozesuaren irmotasuna hobetzeko helburuz.

Halaber, egun material jasangarrietan beste sektore batzuk duten interesa ikusita, garatutako BIO-PURaren egokitasuna aztertu da beste

industria eta prozesu batzuetarako; hala nola, industria eoliko eta fotoboltaikorako infusio bidez egindako konpositeetarako.

Azkenik, BIO-PURen zirkularitatea eta bizi amaiera hobetze aldera bi estrategia ezberdin aztertu dira. Lehenari dagokionez, BIO-PURaren birziklagarritasunaren hobetze aldera egitura kimikoan Diels-Alder motako lotura dinamikoak gehitzeak duen eragina aztertu da. Bigarren estrategiari dagokionez, hondakinen balioa handitzeko eta materialen zirkularitatea hobetzeko asmoz, formulazio berrietan itsasotik bildutako PET botilen birziklapen kimikotik eratorritako BHET monomeroa formulazioetan gehitu da.

Índice

1. MOTIVACIÓN Y ORGANIZACIÓN DE LA TESIS 1

1.1. MOTIVACIÓN 2

1.2. ORGANIZACIÓN DE LA TESIS 5

2. INTRODUCCIÓN Y OBJETIVOS 9

2.1. INTRODUCCIÓN 10

2.1.1. Composites 10

2.1.2. Aplicación (Ballesta) 14

2.1.3. RTM 17

2.1.4. Poliuretanos 19

2.1.5. Propiedades de los PUR 29

2.2. ASPECTOS A MEJORAR RESPECTO AL ESTADO DEL ARTE 31

2.2.1. Reactividad 32

2.2.2. Sostenibilidad 33

2.3. OBJETIVOS 36

2.4. REFERENCIAS 38

3. REACTIVITY CONTROL 55

3.1. GRAPHICAL ABASTRACT 56

3.2. ABSTRACT 57

3.3. INTRODUCTION....57
3.4. EXPERIMENTAL....57
3.4.1. Materials....60
3.4.2. Synthesis....61
3.5. CHARACTERISATION....65
3.5.1. Rheological characterisation....65
3.5.2. Differential scanning calorimetry (DSC)....65
3.6. RESULTS AND DISCUSSION....66
3.6.1. Rheological characterization....66
3.6.2. Differential scanning calorimetry (DSC)....73
3.6.3. Modelling and process simulation....78
3.7. CONCLUSIONS....89
3.8. REFERENCES....90
4. BIOBASED POLYOLS....95
4.1. GRAPHICAL ABSTRACT....96
4.2. ABSTRACT....97
4.3. INTRODUCTION....97
4.4. EXPERIMENTAL....99
4.4.1. Materials....99
4.4.2. Synthesis....101
4.5. CHARACTERIZATION....103
4.5.1. Rheological characterization....103

4.5.2. Differential scanning calorimetry (DSC) 103
4.5.3. Dynamic mechanical analysis (DMA) 103
4.5.4. Thermal stability (TGA) 104
4.5.5. Mechanical properties 104
4.6. RESULTS AND DISCUSSION 104
4.6.1. Rheology 104
4.6.2. Differential scanning calorimetry (DSC) 107
4.6.3. Dynamical mechanical analysis (DMA) 109
4.6.4. Thermal stability (TGA) 113
4.6.5. Mechanical properties 116
4.7. CONCLUSIONS 117
4.8. REFERENCES 119
5. BIO-PUR SYSTEM OPTIMIZATION 125
5.1. GRAPHICAL ABSTRACT 126
5.2. ABSTRACT 127
5.3. INTRODUCTION 128
5.4. EXPERIMENTAL 129
5.4.1. Materials 129
5.4.2. Samples preparation 132
5.5. CHARACTERIZATION 132
5.5.1. Rheological characterization 132
5.5.2. Differential scanning calorimetry (DSC) 133

5.5.3. Dynamic mechanical analysis (DMA) 134
5.5.4. Mechanical properties 134
5.6. RESULTS AND DISCUSSION 134
5.6.1. Rheological characterization 134
5.6.2. Differential scanning calorimetry (DSC) 136
5.6.3. Dynamical mechanical analysis (DMA) 138
5.6.4. Mechanical properties 140
5.6.5. Modelling and process simulation 141
5.7. CONCLUSIONS 148
5.8. REFERENCES 149
6. BIO-PUR SYSTEM OPTIMIZATION 151
6.1. GRAPHICAL ABSTRACT 152
6.2. ABSTRACT 153
6.3. INTRODUCTION 154
6.4. EXPERIMENTAL 160
6.4.1. Materials 160
6.5. CHARACTERIZATION 161
6.5.1. Permeability test 161
6.5.2. Void content 163
6.5.3. Dynamic mechanical analysis (DMA) 163
6.5.4. Mechanical properties 163
6.5.5. Density 164

6.5.6. Fibre and void Volume Fraction 164

6.6. RESULTS AND DISCUSSION 164

6.6.1. Permeability 164

6.6.2. Void content 167

6.6.3. Composite manufacturing and testing 173

6.6.4. Devopment of the DDDAS process control system 177

6.7. CONCLUSIONS 192

6.8. REFERENCES 194

7. OTHER APPLICATIONS: WIND ENERGY 201

7.1. GRAPHICAL ABSTRACT 202

7.2. ABSTRACT 203

7.3. INTRODUCTION 203

7.4. EXPERIMENTAL 205

7.4.1. Materials 205

7.5. CHARACTERIZATION 206

7.5.1. Mechanical properties 206

7.5.2. Density 207

7.5.3. Fibre and void volume fraction 207

7.6. RESULTS 207

7.6.1. Infusion process development 207

7.6.3. Composite manufacturing and testing 219

7.7. CONCLUSIONS 220

7.8. REFERENCES 222

8. END OF LIFE / RECYCLABILITY 225

8.1. GRAPHICAL ABSTRACT 226

8.2. ABSTRACT 227

8.3. INTRODUCTION 227

8.4. EXPERIMENTAL 234

8.4.1. Materials 234

8.4.2. Synthesis 235

8.5. CHARACTERIZATION 237

8.5.1. Characterization of Triol-DA and BHET 237

8.5.2. Characterization of BIO-PUR-DA and BIO-PUR-R systems 238

8.6. RESULTS 240

8.6.1. Synthesis of BIO-PUR containing dynamic covalent bonds (BIO-PUR-DA) 240

8.6.2. Synthesis of BIO-PUR with recycled components 252

8.7. CONCLUSIONS 260

8.8. REFERENCES 262

9. CONCLUSIONES FINALES Y SUGERENCIAS PARA FUTUROS TRABAJOS 267

9.1. CONCLUSIONES GENERALES 268

9.2. TRABAJOS FUTUROS 272

9.3. PUBLICACIONES Y CONTRIBUCIONES A CONGRESOS 281

9.4. REFERENCIAS 285

ANEXO I: Figuras y tablas 287

ANEXO II: Abreviaturas y símbolos..... 299

ANEXO III: Materiales 303

1

MOTIVACIÓN Y ORGANIZACIÓN DE LA TESIS

1. MOTIVACIÓN Y ORGANIZACIÓN DE LA TESIS

1.1. MOTIVACIÓN 2

1.2. ORGANIZACIÓN DE LA TESIS 5

En este primer capítulo se describe la motivación para empezar con esta tesis y también se presenta la organización del trabajo.

1.1. MOTIVACIÓN

La creciente preocupación por el medioambiente está impulsando el desarrollo de medios de trasporte más sostenibles. En este contexto, uno de los desafíos para abordar la reducción del impacto medioambiental de los vehículos está asociado a la cantidad de CO_2 que emiten. Por ello, es imprescindible minimizar el consumo de energía y/o combustible necesario en su vida útil y una de las soluciones es el aligeramiento de su estructura. Una disminución de peso del 10% en un vehículo de tamaño medio puede reducir sus emisiones de CO_2 en un 5.6%.

En esta carrera emprendida hacia el aligeramiento, los materiales juegan un papel relevante en los vehículos sostenibles del futuro, y los composites de matriz polimérica se presentan como uno de los candidatos más sólidos. Este interés se debe en gran medida a la buena combinación de propiedades mecánicas y ligereza, pero además facilitan la libertad de diseño, posibilitan la integración de funciones, la reducción de componentes y presentan alta resistencia a la corrosión.

Sin embargo, la utilización de estos materiales para soluciones ligeras en el mercado de la automoción es todavía incipiente debido al coste de producción de estos componentes y la limitada capacidad

productiva, teniendo en cuenta los elevados tiempos de proceso de las tecnologías de fabricación actuales.

Por ello, los fabricantes de automoción, junto con los fabricantes de resinas, están trabajando en el desarrollo de materiales más reactivos y procesos que permitan aumentar las cadencias de producción y reducir los tiempos de proceso a pocos minutos, como por ejemplo el HP-RTM (Moldeo por Transferencia de Resina, RTM, de alta presión) y el C-RTM (compresión RTM de alta presión). Concretamente, en el caso de las resinas para RTM, se buscan formulaciones de curado ultra-rápido (procesos de 2-5 min) y bajas viscosidades para optimizar al máximo los ciclos de curado e inyección. En esta carrera, las resinas epoxi actualmente utilizadas compiten con algunos termoplásticos, como la poliamida y con las resinas acrílicas y poliuretanos.

La tecnología basada en resinas de poliuretano (PUR), ofrece frente a otras alternativas, la ventaja de poseer gran tenacidad y resistencia a la fatiga, lo cual las hace especialmente atractivas para elementos sujetos a impactos o a cargas cíclicas como los elementos de suspensión. Sin embargo, el desarrollo principal de los PUR se ha centrado tradicionalmente en aplicaciones de bajas prestaciones y procesos como proyección, moldeo por inyección de resina reforzada (R-RIM), moldeo por inyección de resina estructural (S-RIM) o casting lo que hace que su aplicación en componentes estructurales no sea inmediata. Ejemplo de ello es, que en la actualidad existen formulaciones comerciales de PUR para RTM, pero debido a sus altas reactividades y elevada exotermia no se han implantado en la mayoría de las cadenas de producción industrial.

Además, los PUR actualmente utilizados presentan algunos inconvenientes desde el punto de vista de la sostenibilidad como el origen petroquímico de sus componentes y su baja reciclabilidad. Este problema es de gran relevancia y ha suscitado un gran interés en los últimos años debido a la demanda tanto a nivel legislativo, como de la sociedad de productos más ecológicos.

Esto hace que cada vez se esté trabajando más en buscar soluciones que permitan la síntesis de poliuretanos más sostenibles, como aquellos que incorporan elevados contenidos de carbono renovable o biobasados, BIO-PUR. Actualmente, el desarrollo de nuevos BIO-PUR está en auge, pero la mayoría de estos desarrollos están dirigidos a otro tipo de aplicaciones de menor requisito estructural como biomédicas, aislamiento, recubrimientos y adhesivos.

Por último, uno de los mayores retos de los PUR, como resinas termoestables, es su fin de vida. Los PUR están formados por una red tridimensional constituida por enlaces covalentes, por lo que estos materiales son infusibles e insolubles, de manera que no se pueden ni reprocesar ni reciclar. El desarrollo de resinas termoestables de tipo PUR que en determinadas condiciones se comporten como materiales termoplásticos es otro ámbito que también despierta gran interés.

En este contexto, el objetivo principal de esta tesis ha sido el desarrollo de formulaciones de base poliuretano más sostenibles, siendo el reto principal el que fueran válidas para aplicaciones estructurales y además viables para el proceso de RTM.

Para ello, se ha trabajado en aportar soluciones en estas tres direcciones; control de la reactividad, origen renovable y fin de vida más sostenible.

1.2. ORGANIZACIÓN DE LA TESIS

Esta tesis está estructurada en nueve capítulos incluido este primero (**capítulo 1**) donde se describe la motivación por la que se empezó con este trabajo de investigación y la descripción de las diferentes secciones que lo forman.

En el **capítulo 2** se ha realizado la revisión del estado del arte de los composites estructurales para automoción. El objetivo principal de este capítulo es introducir los poliuretanos termoestables y exponer las ventajas que presentan estos materiales para su aplicación en composites estructurales. Además, se han identificado los aspectos a mejorar para su implementación en la industria y gracias a ello se han establecido los objetivos de la tesis que se describen en este mismo capítulo.

Los dos grandes retos que presentan los poliuretanos termoestables son la procesabilidad y la sostenibilidad. Estas líneas se han desarrollado en las siguientes secciones experimentales donde se ha escogido el formato e idioma (inglés) comúnmente utilizado para la redacción de artículos científicos. Por esta razón, se solicita la indulgencia del lector por las repeticiones inherentes a esta forma de redacción.

El **capítulo 3** se enfoca al desarrollo de catalizadores de acción retardada para controlar y adecuar la reactividad de los PUR a los requisitos del proceso de RTM.

En el **capítulo 4** se sintetizan diferentes BIO-PURs a partir de diferentes polioles derivados de aceites vegetales de diferentes características y se estudia el efecto de dichas características en las propiedades de los BIO-PURs con el objetivo de establecer los requisitos para la aplicación.

La formulación más prometedora se optimiza en el **capítulo 5**, donde se mejoran las propiedades finales (térmicas y mecánicas) mediante la adición de agentes de entrecruzamiento biobasados para cumplir con los requisitos de las piezas estructurales de automoción.

La nueva resina optimizada se valida en el **capítulo 6** con la fabricación por RTM y ensayo de composites reforzados con fibra de vidrio. En este capítulo se estudia el efecto de los parámetros del proceso en la calidad del composite de cara a su optimización y se desarrolla un modelo DDDAS para mejorar su robustez.

Tras validar el BIO-PUR desarrollado para aplicaciones estructurales de automoción, en el **capítulo 7** se estudia su viabilidad para otro tipo de aplicaciones como la eólica, utilizándose en este caso para la fabricación el proceso de infusión.

Por último, en el **capítulo 8** se exploran nuevas líneas de investigación para la mejora de fin de vida y circularidad. Para ello, se estudia la viabilidad de incorporar enlaces dinámicos de tipo Diels-Alder en la formulación de cara a mejorar la reciclabilidad de los materiales

desarrollados y por otra parte se aborda el tema de la revalorización de residuos mediante la incorporación de tereftalato de bis (2-hidroxietilo), BHET, reciclado de politereftarato de etileno, PET, altamente degradado en la formulación.

Finalmente, en el **capítulo 9**, se resumen las conclusiones generales de todo el trabajo realizado en esta tesis, así como las futuras líneas de investigación.

2

INTRODUCCIÓN Y OBJETIVOS

2. INTRODUCCIÓN Y OBJETIVOS

2.1. INTRODUCCIÓN 10
2.1.1. Composites 10
2.1.2. Aplicación (Ballesta) 12
2.1.3. RTM 17
2.1.4. Poliuretanos 19
2.1.5. Propiedades de los PUR 28
2.2. ASPECTOS A MEJORAR RESPECTO AL ESTADO DEL ARTE 31
2.2.1. Reactividad 32
2.2.2. Sostenibilidad 33
2.3. OBJETIVOS 36
2.4. REFERENCIAS 38

2.1. INTRODUCCIÓN

En este capítulo se pone en contexto y se presentan los objetivos de la tesis. Se realiza una revisión bibliográfica y el estudio del arte de los composites para componentes estructurales de automoción. Además de ello, se introduce la química de los poliuretanos y las ventajas que pueden presentar frente a otras alternativas utilizadas actualmente en este tipo de aplicaciones. Por otra parte, las resinas basadas en la tecnología de poliuretano también presentan algunos retos y desventajas que también se exponen en este capítulo.

El objetivo fundamental de este capítulo es introducir de manera general estas resinas. Por esta razón, y tratando de evitar repeticiones, no se presentará una revisión bibliográfica global ya que en los capítulos siguientes se recoge el estado del arte específico de cada temática.

2.1.1.Composites

La creciente preocupación por el medio ambiente ha impulsado a la industria de la automoción a invertir en desarrollos sostenibles. Ejemplo de ello es la fuerte apuesta del sector por la electrificación de los vehículos. Otro de los grandes desafíos del sector es el aligeramiento de los vehículos, ya que la reducción de peso está directamente ligada a la cantidad de energía y/o combustible necesario en su vida útil [1]. Los objetivos en cuestión de emisiones de CO_2 fijados para Europa en 2020 son de 95 g CO_2 km^{-1}, lo cual requiere una reducción del peso del

vehículo de 200-300 kg [2,3]. En este contexto, los composites de matriz polimérica se postulan como uno de los candidatos más interesantes.

Los composites son materiales heterogéneos constituidos por más de dos fases inmiscibles de diferente naturaleza y estructuras que combinados presentan propiedades mejoradas. Hay diferentes tipos de composites, pero los que presentan la mejor combinación resistencia/peso son los composites de matriz polimérica reforzados con fibras continuas. Debido a sus superiores propiedades mecánicas en combinación con su ligereza, estos composites son una alternativa que suscita gran interés. En el camino hacia un transporte cada vez más sostenible, donde se requieren vehículos con diseños más aerodinámicos y menos pesados, el potencial de los composites reside en que se pueden fabricar piezas con geometrías complejas y con mejor relación resistencia/peso *Figura 2.1*.

Sin embargo, la utilización de estos materiales para soluciones ligeras en el mercado de la automoción es todavía incipiente debido al coste de las materias primas y la limitada capacidad productiva de las tecnologías de fabricación actuales. Ejemplo de ello, que podamos ver algunos modelos exclusivos de grandes marcas o los coches de carreras fabricados con composite, pero que los veamos de manera limitada en la carretera en nuestro día a día.

En la *Figura 2.2* se presentan las piezas estructurales que en la actualidad se están fabricando y/o sería viable fabricar en composi

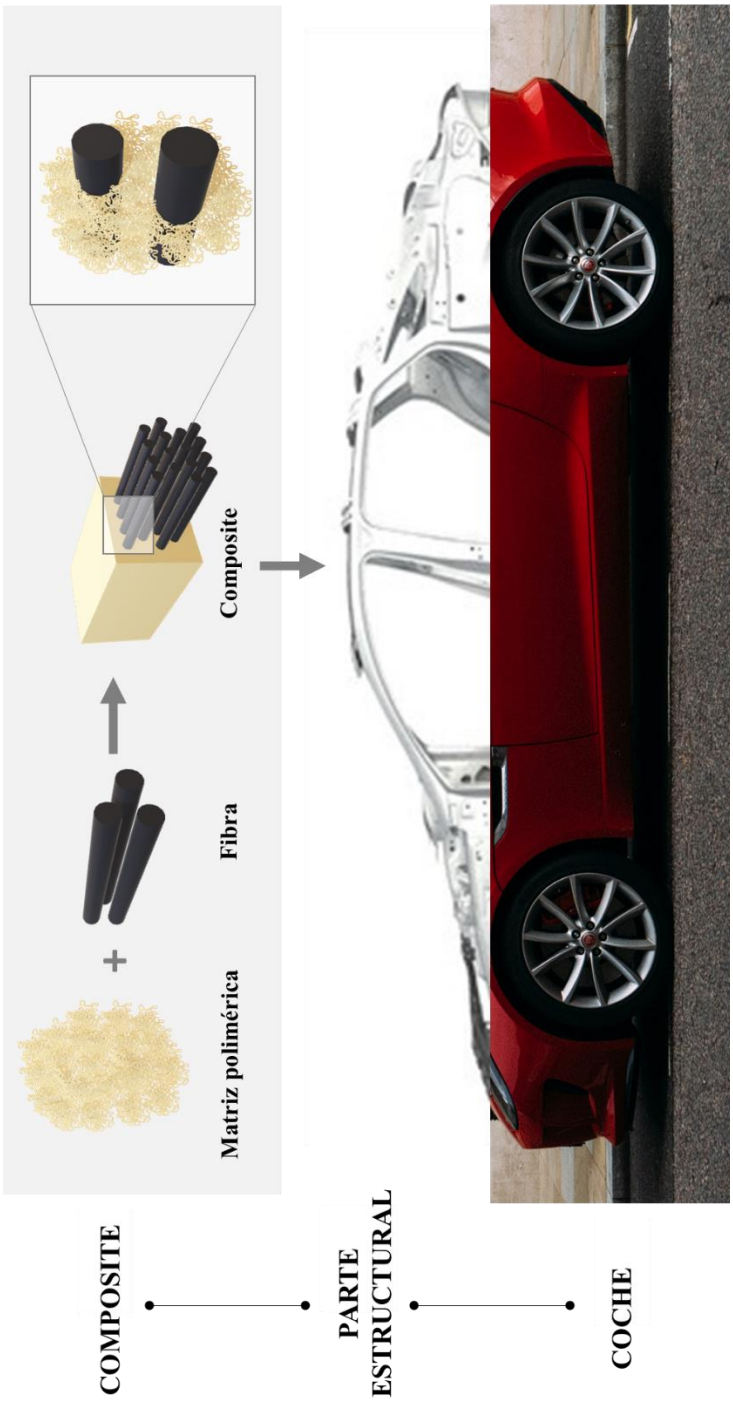

Figura 2.1. Composite para soluciones estructurales ligeras en automoción.

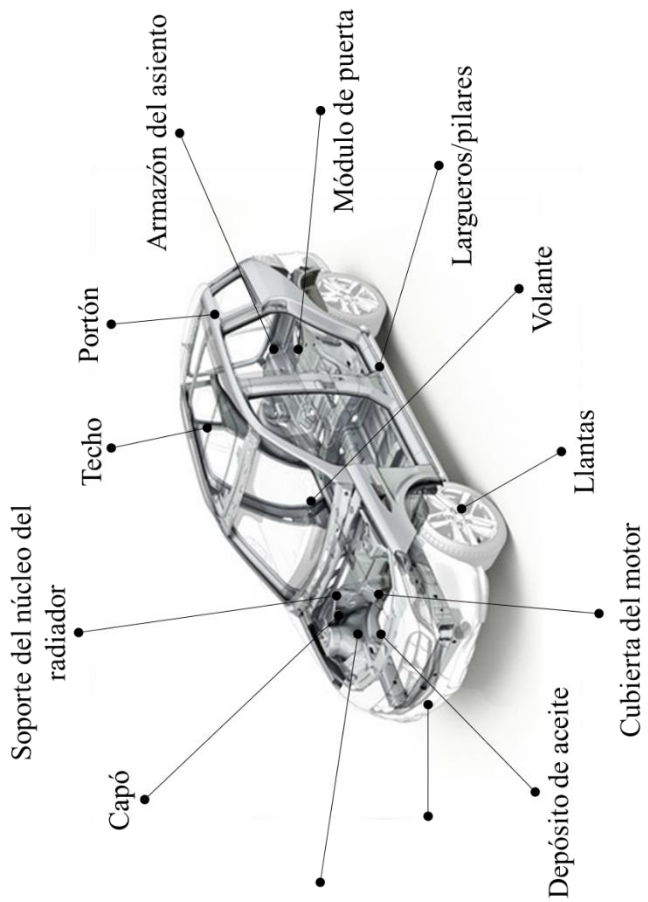

Figura 2.2.Piezas estructurales en composite

2.1.2.Aplicación (Ballesta)

Entre las aplicaciones que se mencionan en la sección anterior se encuentran las ballestas fabricadas en composite. Actualmente, existen varios fabricantes que además de las tradicionales ballestas metálicas, están fabricando ballestas en composite (*Tabla 2.1)*. Tal y como se ha comentado, la reducción de peso está directamente ligada a las emisiones de CO_2, y en el caso de las ballestas, se ha conseguido una reducción de peso entre el 50 - 80%. Además, las ballestas de composite pueden presentar ventajas frente a las metálicas, como mejora en propiedades de amortiguación, excelente resistencia a la fatiga y disminución en términos de vibración/ruido [4].

Las ballestas de composite actuales son principalmente de resina epoxi y fibra de vidrio (*Tabla 2.2)* [5-15]. Las fibras de vidrio son utilizadas para diferentes aplicaciones debido en gran parte a su bajo coste y la elevada resistencia a fatiga, siendo la mejor alternativa para las piezas estructurales que van a tener que soportar el pandeo en su vida útil, como las ballestas. En cuanto a la resina (*Tabla 2.2*), es indudable que, en la actualidad, debido a sus elevadas prestaciones, la mayoría de las piezas de composite en el mercado son de base epoxi [16-20]. Sin embargo, existen desarrollos donde se están explorando otras alternativas como los poliuretanos [21,22] y los polímeros termoplásticos, como la poliamida y resinas acrílicas [23,24].

Tabla 2.1.Fabricantes de ballestas de composite.

Fabricante	
Benteler-SGL [5,6]	
IFC Composite [7]	
Rassini [8]	
Ziur composites [9]	
Hyperco [10]	
Owen springs [11,12]	
Mubea [13]	
Hendrickson [14]	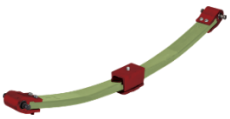
ARC Industries [15]	

Tabla 2.2. Tecnologías y materiales empleados en la fabricación de ballestas de composite.

Propietario	Tecnología	Materiales
SGL carbon [16,17]	Preimpregnado	Epoxi + fibra de vidrio
Hexcel [18]	Preimpregnado	Epoxi + fibra de vidrio
Mubea [13]	Preimpregnado	Epoxi + fibra de vidrio
Chomarat Group + Huntsman + KraussMaffei [19]	HP-RTM	Epoxi + fibra de vidrio
Henkel + Benteler [20]	HP-RTM	Poliuretano + fibra de vidrio
MBHA + Huntsman [21]	HP-RTM	Poliuretano + fibra de vidrio
Fraunhofer ICT [22]	RTM	ε-Caprolactama (termoplástico) + fibra de vidrio
Fraunhofer IMWS + IFC Composite [23]	Cintas Unidireccionales	Fibra de vidrio + polímero termoplástico

Estas ballestas se fabrican utilizando diferentes tipos de procesos. Uno de los grandes retos de los composites es el elevado coste de producción. Necesitan ser adaptados a la producción en masa, reduciendo tiempos de proceso y disminuyendo los costes. Tradicionalmente, la industria del composite ha estado basada en un alto componente manual, por lo que se precisa avanzar en su automatización para aumentar la eficiencia, algo que se puede conseguir a través de procesos como el conformado, HP-RTM y C-RTM [25].

Para el caso particular de las ballestas, el RTM resulta una solución competitiva, ya que se pueden conseguir composites con altas prestaciones con un proceso altamente automatizado y se evita trabajar con materiales preimpregnados que presentan desventajas desde el punto de vista de la vida útil y del coste inicial del material.

2.1.3.RTM

Tal y como se ha comentado en el apartado anterior, el RTM está entre los procesos que permiten la reducción de los tiempos de proceso a pocos minutos y aumentar las cadencias de producción.

Básicamente, el proceso de RTM consiste en la inyección de una resina en un molde cerrado en el cual se han colocado previamente refuerzos de fibra que suelen estar previamente preformados. Una vez colocado el refuerzo en la cavidad del molde, la resina se inyecta mediante presión y/o vacío e impregna el refuerzo y finalmente se solidifica y alcanza las propiedades finales en el proceso de curado (*Figura 2.3*). Las ventajas que presenta el RTM frente a otros procesos son los buenos acabados de las piezas y la capacidad de fabricar piezas de geometrías complejas y altamente integradas en un solo paso.

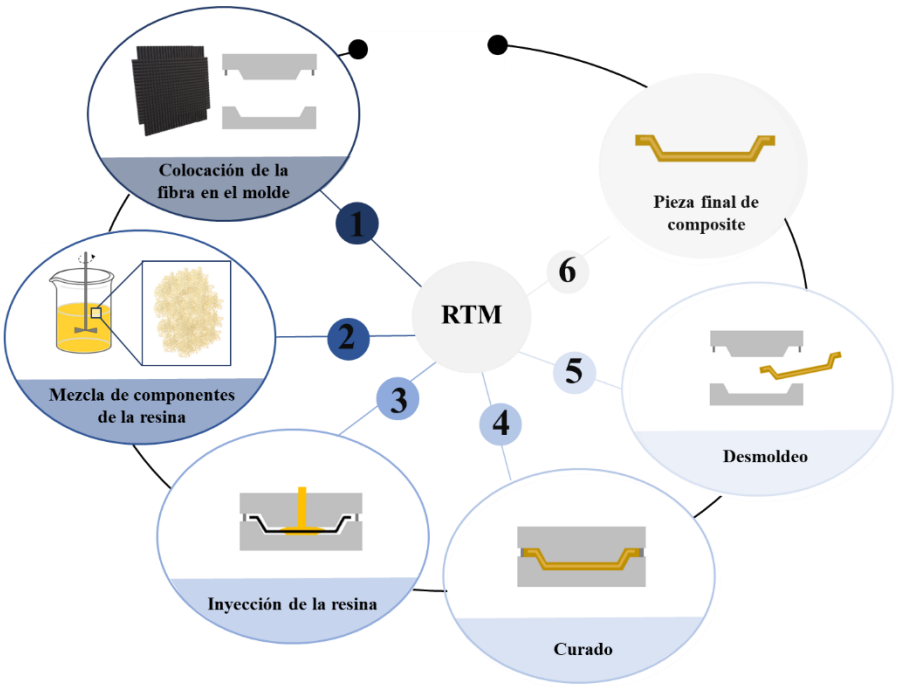

Figura 2.3. Etapas principales del proceso RTM.

El gran inconveniente actual del RTM es la dificultad para trabajar en serie en tiempos cortos. Para aumentar las cadencias de producción y reducir los tiempos de proceso, se puede trabajar a alta presión de inyección en el RTM de alta presión (HP-RTM) o también en el RTM con compresión (C-RTM). Pero, para ello es imprescindible el desarrollo de nuevas resinas específicas para este tipo de procesos. Formulaciones con curado ultra-rápido (procesos de 2-5 min) y bajas viscosidades para optimizar al máximo los ciclos de inyección y curado [24]. Las resinas epoxi son las más utilizadas actualmente en composites estructurales, pero en la actualidad se están desarrollando nuevas alternativas termoplásticas, como la poliamida y resinas acrílicas, y poliuretanos [25–29].

2.1.4.Poliuretanos

En cuanto a la historia de esta familia de polímeros, el primer trabajo se atribuye a Wurtz, A. en 1848 con su estudio sobre los isocianatos [30]. En los siguientes años se estudió la química de los isocianatos y se sintetizaron gran variedad de ellos [31,32], pero el desarrollo industrial de los poliuretanos no comenzó hasta el año 1937 en Alemania, con la primera patente sobre poliuretanos de Bayer y sus colaboradores [33,34]. Hoy en día los poliuretanos, tanto en su versión termoplástica como termoestable, constituyen una de las familias de polímeros más importantes y con mayor crecimiento del mercado, siendo la quinta que más se produce en Europa y la séptima a nivel mundial [35].

Cabe destacar que los poliuretanos se caracterizan por su gran versatilidad, debido a la amplia gama de reactivos disponibles para la síntesis, incluso de origen renovable. Esto hace que los poliuretanos puedan ser sintetizados con diferentes estructuras químicas y por lo tanto con propiedades muy diferentes, abarcando desde materiales flexibles a materiales de alta rigidez, tanto en forma de materiales compactos como de espumas. En sus diferentes formas (elastómeros, adhesivos, recubrimientos, espumas flexibles y rígidas) son un componente clave de la industria del plástico, ocupando un lugar destacado en la producción de polímeros en Europa, y a nivel mundial. Los poliuretanos cubren una amplia gama de aplicaciones en diferentes sectores tales como la construcción, textiles, aislamiento térmico y acústico, deportes, automoción o biomedicina [36].

Química de los poliuretanos

Los poliuretanos se caractrizan por los grupos uretano de sus cadenas. Este grupo funcional se genera mediante la reacción de poliadición entre el grupo funcional hidroxilo y el isocianato, como se puede observar en la *Figura 2.4*.

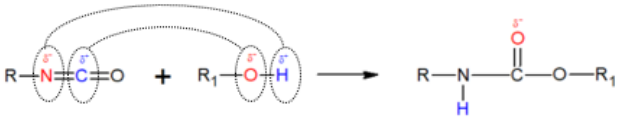

Figura 2.4. Formación del grupo uretano.

Reactivos

En la síntesis de los poliuretanos tanto termoplásticos como termoestables se utilizan dos componentes base, el poliol y el isocianato. La elección de estos componentes es fundamental, ya que la procesabilidad y las propiedades finales estarán directamente relacionados con la naturaleza de estos dos reactivos [37].

Isocianato

Los isocianatos se forman mediante la fosgenación de las aminas. En la *Figura 2.5* se muestra el grupo funcional y sus estructuras de resonancia. Los más utilizados en el mercado para la síntesis de los poliuretanos se recogen en la *Tabla 2.3*.

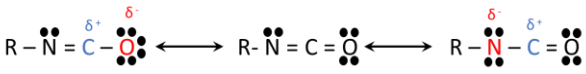

Figura 2.5. El grupo isocianato y sus estructuras de resonancia.

Cabe destacar que los isocianatos aromáticos MDI, pMDI y TDI son los más utilizados en la industria, tanto en la síntesis de poliuretanos termoplásticos, poliuretanos termoestables de alto entrecruzamiento y elastómeros, como de espumas flexibles y rígidas [38,39]. En general el MDI se utiliza en la síntesis de poliuretanos termoplásticos, el TDI en la síntesis de espumas flexibles y el pMDI para sintetizar poliuretanos con mayor entrecruzamiento como las espumas rígidas o los termoestables compactos. Los isocianatos aromáticos presentan la característica de que son más reactivos que los alifáticos, y por lo tanto más adecuados en aplicaciones industriales de alta producción. Presentan el inconveniente de que desarrollan coloración por absorción de radiación ultravioleta, aspecto no deseable en ciertas aplicaciones. Otro inconveniente es que entre los productos de degradación producen aminas aromáticas más tóxicas que las alifáticas. Los isocianatos alifáticos, aunque más caros y menos reactivos, se emplean en aplicaciones en los que la estabilidad a la luz es crítica como en algunos recubrimientos o piezas estéticas [40–43].

En los últimos años, las políticas medioambientales han impulsado el interés por los isocianatos de origen renovable (*Table 4.2*). Entre los comerciales destacan el diisocianato de dimerilo (DDI) [44–46], diisocianato de etil éster L-lisina (L-LDI) y triisocianato de etil éster L-lisina (LLTI) [44,46,47], alofanato en base a diisocianato de hexametileno y aceite de palma (TolonateTM X Flo 100, Vencorex) [48–51] y trímero de isocianurato de pentametilendiisocianto (Desmodur® eco N 7300, Covestro) [28,52,53], pero este tipo te diisocianatos presentan algunas desventajas como baja reactividad y las propiedades mecánicas de los poliuretanos no llegan a ser la de lo poliuretanos sintetizados con disocianatos aromáticos.

Tabla 2.3. Isocianatos más utilizados en la síntesis de los poliuretanos.

Diisocianato	Estructura química
2,4- o 2,6-Tolueno diisocianato **(TDI)**	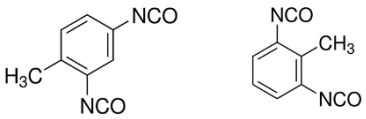
4,4'-Difenil metano diisocianato **(MDI)**	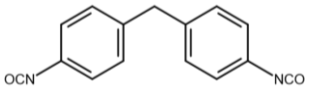
4,4'-Difenil metano diisocianato polimérico **(pMDI)**	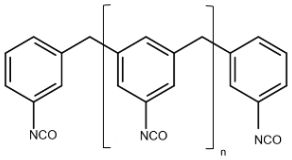
1,6- Hexametilen diisocianato **(HDI)**	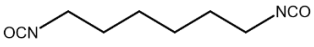
Isoforone diisocianato **(IPDI)**	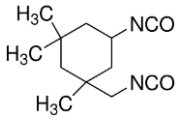
Diciclohexilmetano-4,4'-diisocianato metileno-bis-(4-isocianatociclohexano) **(H_{12}MDI)**	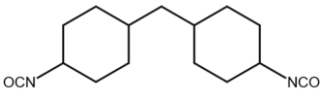

Tabla 2.4. Isocianatos biobasados comerciales.

Diisocianato	Estructura química
Diisocianato de dimerilo **(DDI)**	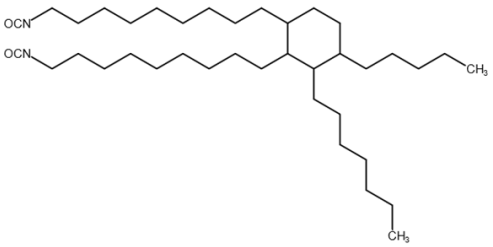
Diisocianato de etil ester L-lisina **(L-LDI)**	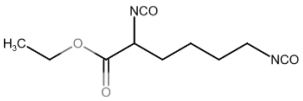
Alofanato en base a diisocianato de hexametileno y aceite de palma **(TolonateTM X Flo 100)**	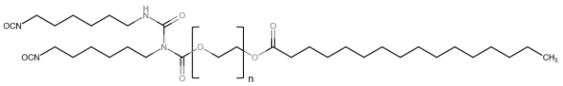
Trímero de isocianurato de pentametilendiisocianto (**Desmodur® eco N 7300**)	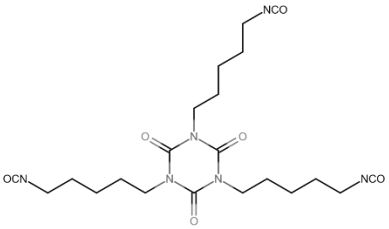

Polioles

Los polioles son macromoléculas con grupos hidroxilo con masas moleculares entre 250-10000 g mol^{-1}[54,55]. Los polioles más utilizados en la síntesis de los poliuretanos se pueden clasificar en dos grandes grupos, poliéster y poliéter y presentan funcionalidades entre 2-

8, permitiendo la síntesis de una gran variedad de poliuretanos. Los polioles con funcionalidades bajas (2-3) se utilizan para sintetizar poliuretanos flexibles y los de funcionalidades altas (3-8) se utilizan en la síntesis de poliuretanos con mayor entrecruzamiento, poliuretanos rígidos.

Los polioles suelen tener una temperatura de transición vítrea (T_g) muy baja, por ello a temperatura ambiente las cadenas del poliol suelen tener movilidad y aportan flexibilidad al poliuretano. En cuanto a la microestructura pueden ser amorfos o semicristalinos, presentando además una temperatura de fusión (T_m) en torno a la temperatura ambiente.

La mayoría de los polioles comerciales que se utilizan actualmente son de origen petroquímico. Sin embargo, los de origen renovable, más atractivos desde el punto de vista de la sostenibilidad, están suscitando cada vez más interés, en concreto los polioles derivados de aceites vegetales. Los aceites vegetales son trigliceroles, conocidos como triglicéridos, formados por la esterificación de tres ácidos grasos y una molécula de glicerina. Son muchos los polioles renovables utilizados en la síntesis de poliuretanos con propiedades comparables a las de los sintetizados con polioles de origen petroquímico, tales como derivados de aceite de palma [56–58], canola [59–61], ricino [62–66], soja [67–70], girasol [71–73] y linaza [74,75].

Como ya se ha mencionado dependiendo de la funcionalidad de los constituyentes, se pueden sintetizar poliuretanos termoplásticos y poliuretanos termoestables con diferentes propiedades y para diferentes aplicaciones.

Poliuretanos termoplásticos (TPU)

Los poliuretanos termoplásticos se forman mediante la reacción de adición entre los isocianatos de un diisocianato y los grupos hidroxilo de un macrodiol o de un diol de baja masa molecular, denominado extendedor de cadena, formando en la mayoría de los casos una estructura amorfa o semicristalina. Las cadenas poliméricas, que contienen el grupo uretano, además de los enlaces covalentes de la propia cadena, forman otros enlaces secundarios entre diferentes cadenas, como se muestra en la *Figura 2.6*. Los poliuretanos termoplásticos están constituidos por segmentos termodinámicamente incompatibles [76,77], el rígido y el flexible. El diisocianato y el extendedor de cadena constituyen el segmento rígido y el macrodiol el segmento flexible. Estos segmentos, forman (micro)dominios o (micro)fases separadas que resultan en la estructura que se muestra en la *Figura 2.6* [54]. En cuanto a las propiedades, el segmento flexible controla las propiedades del material a bajas temperaturas, aportando flexibilidad, ductilidad y capacidad de recuperación. El segmento rígido controla las propiedades del poliuretano a temperaturas elevadas. Este segmento y los dominios que forma, actúan como refuerzo de elevado módulo elástico. En general los TPU no presentan transiciones vítreas superiores a 120 ºC y tampoco las propiedades mecánicas son lo suficientemente altas para su aplicación en componentes estructurales de automoción [36,78–81].

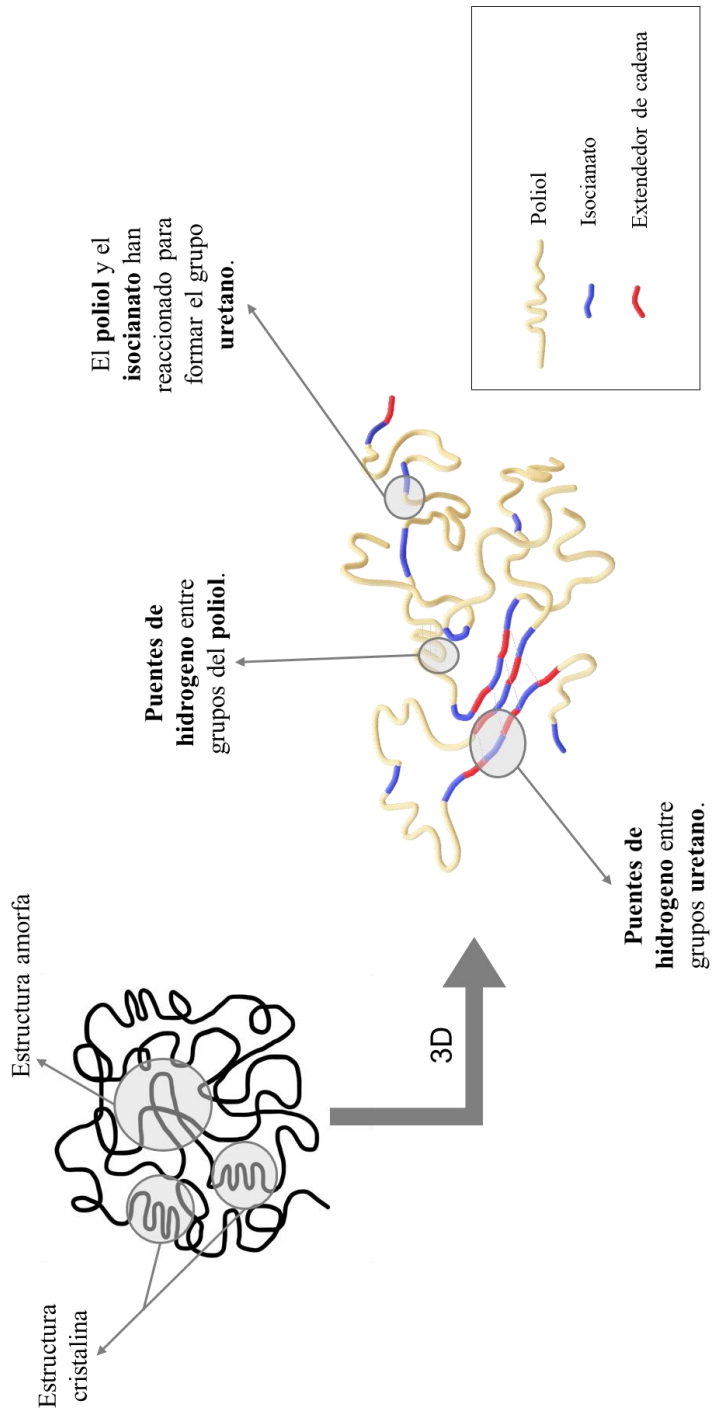

Figura 2.6. Estructura de los poliuretanos termoplásticos.

Poliuretanos termoestables (PUR)

Los poliuretanos termoestables pasan de estado líquido a solido mediante el proceso de curado en el que el isocianato de un diisocianato o isocianato con funcionalidad mayor reacciona con el grupo hidroxilo de un poliol creando una red tridimensional como se muestra en la *Figura 2.7* [82]. Los constituyentes se unen mediante enlaces covalentes en una reacción irreversible donde se obtiene un material insoluble e infusible. La estructura del poliuretano es totalmente amorfa y los entrecruzamientos aportan rigidez al material. Esto hace que sean los elegidos para aquellas aplicaciones donde se requieran altas propiedades mecánicas como es el caso de la aplicación objetivo.

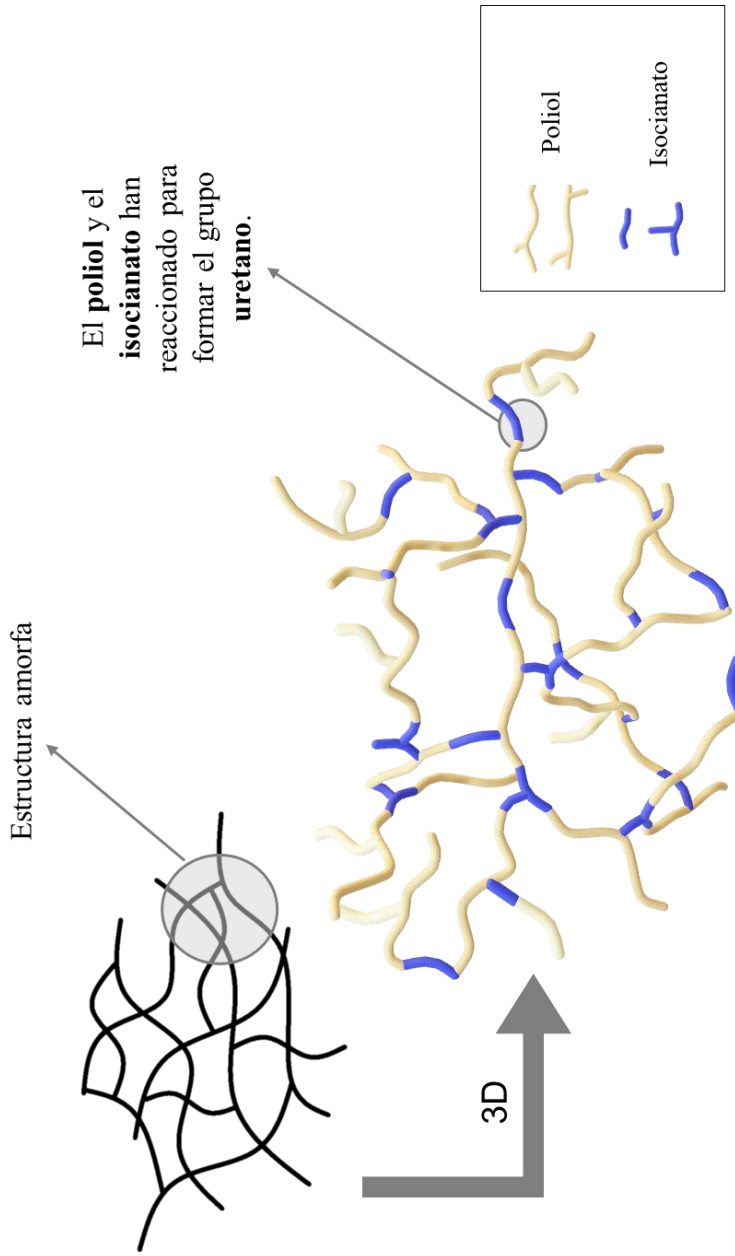

Figura 2.7. Estructura de los poliuretanos termoestables (red tridimensional).

2.1.5.Propiedades de los PUR

En los últimos años los PURs han suscitado interés como matriz de composite ya que presentan algunas ventajas frente a las alternativas convencionales (*Figura 2.8*) como buena adhesión con las fibras (carbono, vidrio, aramida y de origen vegetal), elevadas propiedades térmicas, curados ultra-rápidos, bajas viscosidades y altas propiedades mecánicas [36].

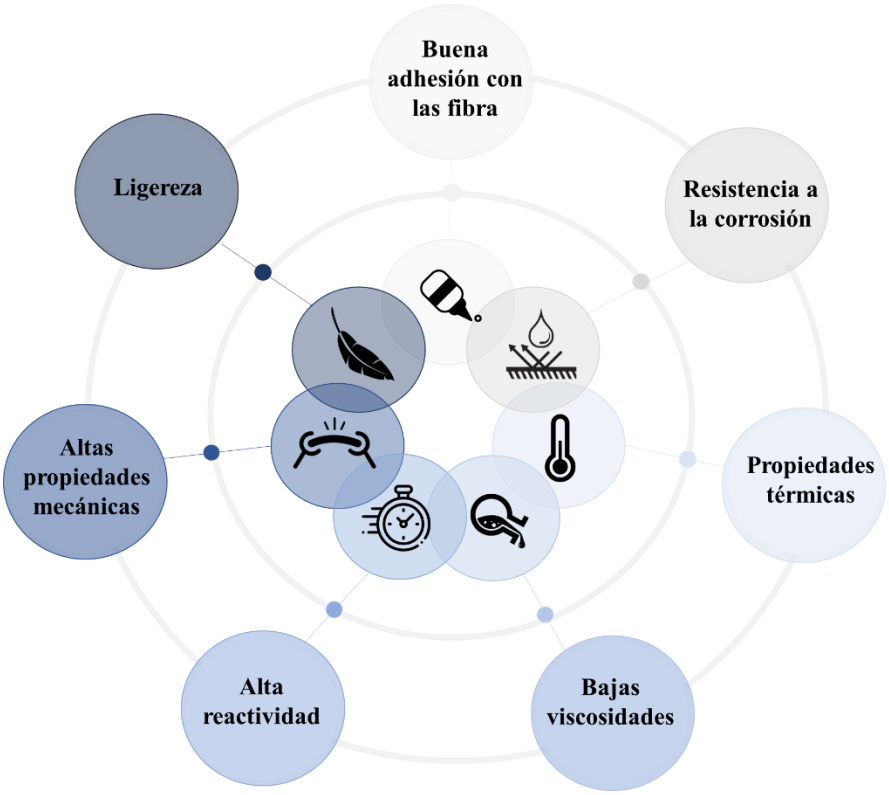

Figura 2.8.Propiedades de los PUR.

En la búsqueda de soluciones para RTM, las bajas viscosidades iniciales y las altas reactividades convierten a los poliuretanos en una alternativa a tener en cuenta. De ahí que, en la actualidad, en el mercado

existan varias alternativas de PUR de altas prestaciones para RTM, como se muestran en la *Tabla 2.5*.

Tabla 2.5. Resinas poliuretano termoestables comerciales.

Suministrador	Sistema de PUR	Aplicación
Henkel [85]	Max	Sistema de suspensión - ballesta Parte de la consola central Módulo del asiento Techo del vehículo
Dow [86]	Voraforce	Piezas interiores estéticas Parachoques Guardabarros
Huntsman [87]	Vitrox	Sistema de suspensión - ballesta Piezas interiores del vehículo Módulo del asiento Cajas de batería EV
Covestro [88–90]	Baydur	Componentes de carbono para vehículos. Tanques de presión Palas para turbinas eólicas
Basf [91]	Elastolit	Componentes estructurales Paneles de la carrocería

Entre estas propiedades, cabe destacar la resistencia a fatiga de estos materiales. Esto los hace especialmente interesantes en el caso de piezas estructurales de automoción que estén sujetas a impactos y/o a cargas cíclicas, como las ballestas. Un ejemplo de ello es que en la actualidad, una de las casas más reconocidas, Volvo, está empezando a fabricar ballestas de base poliuretano para algunas de las líneas más exclusivas XC90, sedán de lujo S90 y modelos de camioneta V90 [5,6]. Otro de los sectores es la energía eólica donde se ha empezado a explorar la fabricación de palas de PUR [83,84].

2.2. ASPECTOS A MEJORAR RESPECTO AL ESTADO DEL ARTE

A pesar de las ventajas que presentan los PUR, su uso principal se ha centrado tradicionalmente en aplicaciones de bajas prestaciones y procesos de proyección, R-RIM, S-RIM o casting lo que hace que su aplicación en componentes estructurales no sea inmediata. Además, actualmente las formulaciones de poliuretano presentan algunas dificultades de procesabilidad para su integración en procesos RTM. Por otra parte, también presentan desafíos desde el punto de vista de la sostenibilidad (*Figura 2.9*).

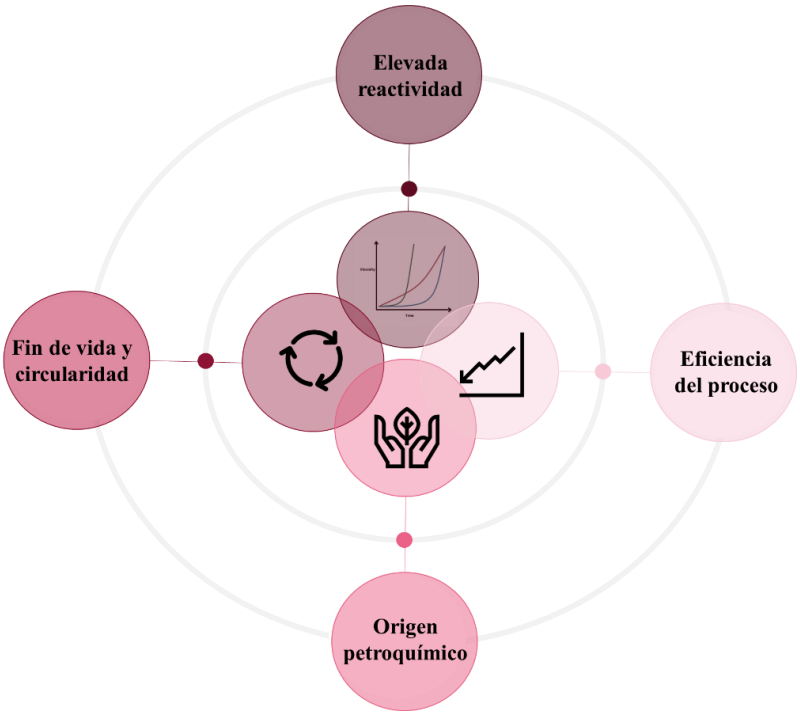

Figura 2.9. Retos que presentan los poliuretanos.

2.2.1.Reactividad

En cuanto a la procesabilidad para RTM, los PUR en general poseen bajas viscosidades, pero su elevada reactividad provoca un aumento de viscosidad prematuro imposibilitando la correcta impregnación de las fibras. Para que las resinas sean adecuadas para RTM es necesaria una cierta latencia en la primera parte del proceso, manteniendo una viscosidad baja durante el llenado seguida de un curado posterior rápido [27,92–94]. Esta evolución de la viscosidad se podría ajustar utilizando catalizadores específicos de acción retardada.

En el caso de los catalizadores para PUR, los más utilizados por la industria se centran en acelerar la reacción de curado, como las aminas terciarias [95,96] o los catalizadores organometálicos [97–99]. Este tipo

de catalizadores son muy eficientes y conocidos, pero no son adecuados ya que las resinas resultan demasiado reactivas para el proceso de RTM. Otra de las soluciones utilizadas son los catalizadores de acción retardada. Este tipo de catalizadores, también basados en aminas terciarias y catalizadores organometálicos suelen activarse con la temperatura o retrasan la reacción desde el primer momento [100]. En ambos casos, no se consigue la combinación latencia / curado rápido requerida para las formulaciones para RTM. De ahí surge la necesidad de desarrollar catalizadores específicos para el caso particular de los PUR para RTM.

2.2.2.Sostenibilidad

Uno de los aspectos más críticos de los nuevos desarrollos de materiales es su sostenibilidad. La sostenibilidad se puede definir y cuantificar de diferentes maneras, pero para poder tener una idea más realista, es recomendable tener en cuenta todo el ciclo de vida del material desde la extracción u origen de los materiales, pasando por procesos de producción, hasta su fin de vida [101,102].

Figura 2.10. Ciclo de vida de materiales.

En este sentido, los poliuretanos presentan diferentes desafíos:

Origen

Actualmente, las formulaciones de PUR para componentes estructurales están basadas en componentes de origen petroquímico. Sin embargo, en los últimos años se ha sintetizado una gran variedad de polioles derivados de aceites vegetales, aceites como el de palma [56–58], canola [59–61], ricino [62–66], soja [67–70], girasol [71–73] y linaza [74,75]. Debido a la gran variedad de polioles disponibles, el desarrollo de nuevos BIO-PUR está en auge, pero están dirigidos a otro tipo de aplicaciones como biomédicas [103], aislamiento [104–106], recubrimientos [107–109] y adhesivos[110,111] y no existen desarrollos para matrices de altas prestaciones.

Eficiencia del proceso

Otro de los retos que plantea la sostenibilidad, es que los procesos de producción también tienen que ser eficientes, tanto desde el punto de vista de consumo energético, como de la tasa de piezas defectuosas.

El proceso de RTM es un proceso en el que el aseguramiento de la calidad sigue siendo un reto debido al gran número de variables involucradas. Por ejemplo, las incertidumbres del material afectan negativamente en la impregnación produciendo defectos de porosidad y áreas secas que llevan a la generación de deshechos con el consiguiente coste económico y medioambiental [112].

A pesar de que ya se han realizado algunos avances de cara a poder predecir en tiempo real la calidad del proceso queda todavía

mucho camino por recorrer en este sentido, sobre todo en cuanto a su implementación [113,114].

Fin de vida y circularidad

En líneas generales, los materiales para que sean totalmente sostenibles deben poseer las "tres R" de la economía circular: reutilizable, reciclable, recuperable. En este sentido, los BIO-PUR, como resinas termoestables presentan grandes retos.

En cuanto al fin de vida, los PUR están formados por una red tridimensional constituida por enlaces covalentes, por lo que estos materiales son infusibles e insolubles, de manera que no se pueden ni reprocesar ni reciclar [115].

Se está investigando en aportar nuevas soluciones para aportar reciclabilidad a los PUR, como incorporar enlaces dinámicos de tipo disulfuros [116] o de tipo Diels Alder [117,118] pero al igual que ocurría con los biopoliuretanos, no existen desarrollos para el caso matrices de altas prestaciones

Por otro lado, la síntesis de BIO-PUR a partir de monómeros reciclados podría ser una alternativa interesante de cara a mejorar su circularidad. Por ejemplo, se ha visto que mediante el proceso de reciclado químico del politereftalato de etileno (PET) proveniente de envases plásticos altamente degradados en ambiente marino se puede producir un poliol, el Bis(2-Hidroxyethil) tereftalato BHET [119,120] válido para la síntesis de los BIO-PUR, ya que posee grupos hidroxilo capaces de reaccionar con el isocianato. Sin embargo, todavía no se ha

estudiado su viabilidad para la síntesis de resinas para moldeo por vía líquida (RTM o infusión).

2.3. OBJETIVOS

El objetivo principal de esta tesis es el desarrollo de formulaciones de base poliuretano más sostenibles, siendo el reto principal el que sean válidas para aplicaciones estructurales y además viables para el proceso de RTM.

En base a este objetivo principal, se han definido los siguientes objetivos técnicos de cara a poder aportar soluciones en cuanto al control de la reactividad, origen de las materias primas, eficiencia del proceso y fin de vida:

- **Objetivo I:** Control de la **reactividad** mediante el desarrollo de sistemas catalíticos específicos de doble efecto para optimizar la evolución de la viscosidad de los PUR. En estos procesos es necesaria una baja viscosidad para reducir los tiempos de llenado e impregnar adecuadamente el refuerzo y tras ello las resinas para RTM deben presentar curados rápidos.

- **Objetivo II:** Incorporación de componentes de **origen** vegetal en la formulación, en concreto polioles derivados de aceites vegetales. Para ello es necesario el estudio del efecto de las características de los bio-polioles y otros componentes como los agentes de entrecruzamiento en la viscosidad, reactividad y propiedades finales

de los BIO-PUR de cara a identificar las características más adecuadas para la aplicación objetivo.

- **Objetivo III:** Mejora de la **eficiencia del proceso.** Esto implica el estudio del efecto de las condiciones de proceso en la calidad final de las piezas y el control de las mismas mediante el modelo basado en la metodología DDDAS.

- **Objetivo IV: Demostrar la viabilidad del sistema** desarrollado para aplicaciones estructurales tanto para aplicaciones de automoción como de otro tipo de sectores donde podrían ser de interés.

- **Objetivo V:** Explorar nuevas líneas de investigación para la **mejora de fin de vida y circularidad** con la incorporación en la formulación de monómeros obtenidos a partir del reciclado químico de Politereftalato de etileno (PET) altamente degradado en ambiente marino, y de enlaces dinámicos con el fin de aumentar la reprocesabilidad y reciclabilidad del composite final.

2.4. REFERENCIAS

[1] Cheah, L. W.; Heywood, J. B.: Cars on a Diet : The Material and Energy Impacts of Passenger Vehicle Weight Reduction in the U . S . Engineering, (2010).

[2] Kawajiri, K.; Kobayashi, M.; Sakamoto, K.: Lightweight materials equal lightweight greenhouse gas emissions?: A historical analysis of greenhouse gases of vehicle material substitution. J. Clean. Prod. (2020), 253.

[3] European Environment Agency: Average CO2 emissions from newly registered motor vehicles — European Environment Agency. 2019, (2019).

[4] Automotive Composite Leaf Springs Market Size, Share, Trend, Forecast, & Competitive Analysis: 2018-2023;

[5] Ernst-Siebert, R.; Grasser, S.: Mass production of composite leaf springs. Lightweight Design worldwide, 11 (2018). http://doi:10.1007/s41777-018-0013-0.

[6] Benteler SGL to supply composite leaf springs for new Volvo XC90 Available online: https://www.compositesworld.com/news/benteler-sgl-to-supply-composite-leaf-springs-for-new-volvo-xc90 (accessed on Aug 1, 2022).

[7] World's first glass fiber leaf spring for 40-ton trucks Available online: https://www.compositesworld.com/news/worlds-first-glass-fiber-leaf-spring-for-40-ton-trucks (accessed on Aug 1, 2022).

[8] Grace Nehls: Hexion partners with Rassini for composite leaf spring application in new Ford F-150 model Available online: https://www.compositesworld.com/news/hexion-partners-with-

rassini-for-composite-leaf-spring-application-in-new-ford-f-150-model (accessed on Aug 1, 2022).

[9] Ziur Composites Products Available online: https://ziurcomposites.com/en/products/ (accessed on Aug 1, 2022).

[10] Hypercoils Composite leaf springs Available online: https://www.hypercoils.com/composite-leaf-springs (accessed on Aug 1, 2022).

[11] Carbon fibre leaf spring Available online: http://www.owensprings.co.uk/category/product-news/page/2/ (accessed on Aug 1, 2022).

[12] Owensprings carbon fibre composite leaf springs Available online: http://www.owensprings.co.uk/carbon-fibre-leaf-springs-composite-leaf-springs/ (accessed on Aug 1, 2022).

[13] Mubea composite components. Available online: https://www.mubea.com/en/composite-components (accessed on Aug 1, 2022)

[14] Hendrickson composite spring liteflex heavy duty Available online: https://www.hendrickson-intl.com/products/liteflex/liteflex-heavy-duty (accessed on Aug 1, 2022).

[15] Why ARC Composite Leaf Spring Suspensions are Better? Available online: https://www.arcsuspension.in/blog/arc-suspension/why-arc-composite-leaf-spring-suspensions-are-better-an-nv-dyanics-case-study-on-ford-endeavour (accessed on Aug 1, 2022).

[16] SGL Carbon produces composite leaf springs for Ford Transit Available online: https://www.sglcarbon.com/en/newsroom/news/press-report/sgl-carbon-produces-composite-leaf-springs-for-ford-transit/ (accessed on Aug 3, 2022).

[17] Hannah Mason: SGL Carbon produces composite leaf springs for Ford Transit Available online: https://www.compositesworld.com/news/sgl-carbon-produces-composite-leaf-springs-for-ford-transit (accessed on Aug 3, 2022).

[18] Hexcel Suspension parts Available online: https://www.hexcel.com/Markets/Industrial/automotivesuspensionparts (accessed on Aug 3, 2022).

[19] Hannah Mason: Chomarat glass fiber reinforcement lightens mass-produced auto parts Available online: https://www.compositesworld.com/news/chomarat-glass-fiber-reinforcement-lightens-mass-produced-auto-parts (accessed on Aug 3, 2022).

[20] Ginger Gardiner: 500,000 parts per year? No problem! Available online: https://www.compositesworld.com/articles/500000-parts-per-year-no-problem- (accessed on Feb 2, 2022).

[21] Ginger Gardiner: CAMX 2018: Second look, more new developments Available online: https://www.compositesworld.com/articles/camx-2018-second-look-more-new-developments (accessed on Aug 3, 2022).

[22] Thomas Siebel: Thermoplastic Composite Leaf Spring is Ready for Series. Springer Professional, (2020).

[23] Lightweight concepts for leaf springs Available online: https://www.imws.fraunhofer.de/en/kompetenzfelder/kunststoffe/highlights/leichtbau-konzepte-fuer-blattfedern.html (accessed on Aug 3, 2022).

[24] Malnati, P.; Sloan, J.: Fast and faster: Rapid-cure resins drive down cycle times. CompositesWorld, (2019).

[25] Imre, B.; Pukánszky, B.: Recent advances in bio-based polymers and composites: Preface to the BiPoCo 2012 Special Section. In European Polymer Journal; (2013); Vol. 49.

[26] Grace Nehls: DNV lowers the partial reduction factor γm1 of wind turbine blades using aging-resistant PU Available online: https://www.compositesworld.com/news/dnv-lowers-the-partial-reduction-factor-m1-of-wind-turbine-blades-using-aging-resistant-pu (accessed on Feb 2, 2022).

[27] Kreiling, S.; Fetscher, F.: Progress with polyurethane matrix resin technology: high-speed resin transfer molding processes and application examples. In SPE ACCE; Novi (Detroit), (2013).

[28] Kurańska, M.; Cabulis, U.; Auguścik, M.; Prociak, A.; Ryszkowska, J.; Kirpluks, M.: Bio-based polyurethane-polyisocyanurate composites with an intumescent flame retardant. Polymer Degradation and Stability, 127 (2016). http://doi:10.1016/j.polymdegradstab.2016.02.005.

[29] de Sousa, R. R.; Miranda, E. A.; Batalha, G. F.; dos Santos, D. J.: Bio-based polyurethane applied as matrix of fiberglass reinforced composite. Journal of Achievements in Materials and Manufacturing Engineering, 81 (2017). http://doi:10.5604/01.3001.0010.2031.

[30] WURTZ, A.: recherches sur les éthers cyaniques et leurs dérivés. Comptes rendus hebdomadaires des séances de l'Académie des sciences, 27, 241 (1848).

[31] Petrović, Z. S.; Ferguson, J.: Polyurethane elastomers; Vol. 16;.

[32] Hofmann, A. W.: Ueber die Einwirkung des Broms in alkalischer Lösung auf Amide. Berichte der deutschen chemischen Gesellschaft, 14 (1881). http://doi:10.1002/cber.188101402242.

[33] Bayer, O.: Das Di-Isocyanat-Polyadditionsverfahren (Polyurethane). Angewandte Chemie, 59, 257–272 (1947). http://doi:10.1002/ange.19470590901.

[34] Otto Bayer; Werner Siefken; Heinrich Rinke; L. Orthner; H. Schild: A process for the production of polyurethanes and polyureas (1937).

[35] Global Polyurethane Market Research Report 2018. ;

[36] Atiqah, A.; Mastura, M.; Ali, B.; Jawaid, M.; Sapuan, S.: A Review on Polyurethane and its Polymer Composites. Current Organic Synthesis, 14 (2016). http://doi:10.2174/1570179413666160831124749.

[37] Janik, H.; Sienkiewicz, M.; Kucinska-Lipka: Polyurethanes, Handbook of thermoset plastics;

[38] Guo, Q.: Thermosets: Structure, properties, and applications: Second edition;

[39] Thomson, T.: Polyurethanes as specialty chemicals: Principles and applications;

[40] Golling, F. E.; Pires, R.; Hecking, A.; Weikard, J.; Richter, F.; Danielmeier, K.; Dijkstra, D.: Polyurethanes for coatings and adhesives – chemistry and applications. Polym. Int. (2019), 68.

[41] Gürses, C.; Karaaslan-Tunç, M. G.; Keleştemur, Ü.; Balcıoğlu, S.; Gülgen, S.; Köytepe, S.; Ateş, B.: Aliphatic Polyurethane Films Based on Hexamethylene Diisocyanate and Saccharides for Biocompatible Transparent Coating on Optic Medical Devices. Starch/Staerke, 74 (2022). http://doi:10.1002/star.202100214.

[42] Fernández-D'Arlas, B.; Alonso-Varona, A.; Palomares, T.; Corcuera, M. A.; Eceiza, A.: Studies on the morphology, properties and biocompatibility of aliphatic diisocyanate-polycarbonate polyurethanes. Polymer Degradation and Stability, 122 (2015). http://doi:10.1016/j.polymdegradstab.2015.10.023.

[43] Gómez-Fernández, S.; Ugarte, L.; Calvo-Correas, T.; Peña-Rodríguez, C.; Corcuera, M. A.; Eceiza, A.: Properties of flexible polyurethane foams containing isocyanate functionalized kraft lignin. Industrial Crops and Products, 100 (2017). http://doi:10.1016/j.indcrop.2017.02.005.

[44] Zheng, B. H.; Guan, L. F.; Li, Y. Bin; Luo, G.; Liu, X. W.: Mechanical properties of polyurethane cured by DDI/IPDI and its application in PBX. Hanneng Cailiao/Chinese Journal of Energetic Materials, 24 (2016). http://doi:10.11943/j.issn.1006-9941.2016.03.002.

[45] Li, Y.; Noordover, B. A. J.; Van Benthem, R. A. T. M.; Koning, C. E.: Chain extension of dimer fatty acid- and sugar-based polyurethanes in aqueous dispersions. European Polymer Journal, 52 (2014). http://doi:10.1016/j.eurpolymj.2013.12.007.

[46] Li, Y.; Noordover, B. A. J.; Van Benthem, R. A. T. M.; Koning, C. E.: Property profile of poly(urethane urea) dispersions containing dimer fatty acid-, sugar- and amino acid-based building blocks. European Polymer Journal, 59 (2014). http://doi:10.1016/j.eurpolymj.2014.06.016.

[47] Wang, Z.; Yu, L.; Ding, M.; Tan, H.; Li, J.; Fu, Q.: Preparation and rapid degradation of nontoxic biodegradable polyurethanes based on poly(lactic acid)-poly(ethylene glycol)-poly(lactic acid) and l-lysine diisocyanate. Polymer Chemistry, 2 (2011). http://doi:10.1039/c0py00235f.

[48] Gurunathan, T.; Chung, J. S.: Physicochemical properties of amino-silane-terminated vegetable oil-based waterborne polyurethane nanocomposites. ACS Sustainable Chemistry and Engineering, 4 (2016). http://doi:10.1021/acssuschemeng.6b00768.

[49] Sahoo, S.; Kalita, H.; Mohanty, S.; Nayak, S. K.: Meticulous study on curing kinetics of green polyurethane-clay

nanocomposite adhesive derived from plant oil: Evaluation of decomposition activation energy using TGA analysis. Journal of Macromolecular Science, Part A: Pure and Applied Chemistry, 54 (2017). http://doi:10.1080/10601325.2017.1336727.

[50] Cifarelli, A.; Boggioni, L.; Vignali, A.; Tritto, I.; Bertini, F.; Losio, S.: Flexible polyurethane foams from epoxidized vegetable oils and a bio-based diisocyanate. Polymers, 13 (2021). http://doi:10.3390/polym13040612.

[51] Morales-Cerrada, R.; Tavernier, R.; Caillol, S.: Fully Bio-Based Thermosetting Polyurethanes from Bio-Based Polyols and Isocyanates. Polymers, 13, 1255 (2021). http://doi:10.3390/polym13081255.

[52] Sasaki, N.; Yokoyama, T.; Tanaka, T.: PROPERTIES OF ISOCYANURATE-TYPE CROSSLINKED POLYURETHANES. J Polym Sci Part A-1 Polym Chem, 11 (1973). http://doi:10.1002/pol.1973.170110801.

[53] Morales-Cerrada, R.; Tavernier, R.; Caillol, S.: Fully bio-based thermosetting polyurethanes from bio-based polyols and isocyanates. Polymers, 13 (2021). http://doi:10.3390/polym13081255.

[54] Szycher, M.: Szycher's handbook of polyurethanes: Second edition;

[55] Ionescu, M.: Chemistry and technology of polyols for polyurethanes. .; Vol. 56;.

[56] Tanaka, R.; Hirose, S.; Hatakeyama, H.: Preparation and characterization of polyurethane foams using a palm oil-based polyol. Bioresource Technology, 99 (2008). http://doi:10.1016/j.biortech.2007.07.007.

[57] Yeoh, F. H.; Lee, C. S.; Kang, Y. B.; Wong, S. F.; Cheng, S. F.; Ng, W. S.: Production of biodegradable palm oil-based polyurethane as potential biomaterial for biomedical

applications. Polymers, 12 (2020). http://doi:10.3390/POLYM12081842.

[58] Vural Kök, B.; Aydoğmuş, E.; Yilmaz, M.; Akpolat, M.: Investigation on the properties of new palm-oil-based polyurethane modified bitumen. Construction and Building Materials, 289 (2021). http://doi:10.1016/j.conbuildmat.2021.123152.

[59] Kong, X.; Liu, G.; Curtis, J. M.: Novel polyurethane produced from canola oil based poly(ether ester) polyols: Synthesis, characterization and properties. European Polymer Journal, 48 (2012). http://doi:10.1016/j.eurpolymj.2012.08.012.

[60] Aydoğmuş, E.; Kamişli, F.: New commercial polyurethane synthesized with biopolyol obtained from canola oil: Optimization, characterization, and thermophysical properties. Journal of Molecular Structure, 1256 (2022). http://doi:10.1016/j.molstruc.2022.132495.

[61] Kong, X.; Yue, J.; Narine, S. S.: Physical properties of canola oil based polyurethane networks. Biomacromolecules, 8 (2007). http://doi:10.1021/bm0704018.

[62] Ristić, I. S.; Bjelović, Z. D.; Holló, B.; Mészáros Szécsényi, K.; Budinski-Simendić, J.; Lazić, N.; Kićanović, M.: Thermal stability of polyurethane materials based on castor oil as polyol component. Journal of Thermal Analysis and Calorimetry, 111, 1083–1091 (2013). http://doi:10.1007/s10973-012-2497-x.

[63] Corcuera, M. A.; Saralegi, A.; Fernandez-d'Arlas, B.; Mondragon, I.; Eceiza, A.: Shape memory polyurethanes based on polyols derived from renewable resources. In Macromolecular Symposia; (2012); Vol. 321–322.

[64] Corcuera, M. A.; Rueda, L.; Fernandez D'Arlas, B.; Arbelaiz, A.; Marieta, C.; Mondragon, I.; Eceiza, A.: Microstructure and

properties of polyurethanes derived from castor oil. In Polymer Degradation and Stability; (2010); Vol. 95.

[65] Alaa, M. A.; Yusoh, K.; Hasany, S. F.: Pure polyurethane and castor oil based polyurethane: Synthesis and characterization. Journal of Mechanical Engineering and Sciences, 8 (2015). http://doi:10.15282/jmes.8.2015.25.0147.

[66] Chen, Y. C.; Tai, W.: Castor oil-based polyurethane resin for low-density composites with bamboo charcoal. Polymers, 10 (2018). http://doi:10.3390/polym10101100.

[67] Acik, G.; Kamaci, M.; Altinkok, C.; Karabulut, H. R. F.; Tasdelen, M. A.: Synthesis and properties of soybean oil-based biodegradable polyurethane films. Progress in Organic Coatings, 123 (2018). http://doi:10.1016/j.porgcoat.2018.07.020.

[68] Fang, Z.; Qiu, C.; Ji, D.; Yang, Z.; Zhu, N.; Meng, J.; Hu, X.; Guo, K.: Development of High-Performance Biodegradable Rigid Polyurethane Foams Using Full Modified Soy-Based Polyols. Journal of Agricultural and Food Chemistry, 67 (2019). http://doi:10.1021/acs.jafc.8b05342.

[69] Tan, S.; Abraham, T.; Ference, D.; MacOsko, C. W.: Rigid polyurethane foams from a soybean oil-based Polyol. Polymer, 52 (2011). http://doi:10.1016/j.polymer.2011.04.040.

[70] Miao, S.; Sun, L.; Wang, P.; Liu, R.; Su, Z.; Zhang, S.: Soybean oil-based polyurethane networks as candidate biomaterials: Synthesis and biocompatibility. European Journal of Lipid Science and Technology, 114 (2012). http://doi:10.1002/ejlt.201200050.

[71] Das, B.; Konwar, U.; Mandal, M.; Karak, N.: Sunflower oil based biodegradable hyperbranched polyurethane as a thin film material. Industrial Crops and Products, 44 (2013). http://doi:10.1016/j.indcrop.2012.11.028.

[72] Omrani, I.; Babanejad, N.; Shendi, H. K.; Nabid, M. R.: Preparation and evaluation of a novel sunflower oil-based waterborne polyurethane nanoparticles for sustained delivery of hydrophobic drug. European Journal of Lipid Science and Technology, 119 (2017). http://doi:10.1002/ejlt.201600283.

[73] Doley, S.; Dolui, S. K.: Solvent and catalyst-free synthesis of sunflower oil based polyurethane through non-isocyanate route and its coatings properties. European Polymer Journal, 102 (2018). http://doi:10.1016/j.eurpolymj.2018.03.030.

[74] Lee, J. H.; Kim, S. H.; Oh, K. W.: Bio-based polyurethane foams with castor oil based multifunctional polyols for improved compressive properties. Polymers, 13 (2021). http://doi:10.3390/polym13040576.

[75] Bähr, M.; Mülhaupt, R.: Linseed and soybean oil-based polyurethanes prepared via the non-isocyanate route and catalytic carbon dioxide conversion. Green Chemistry, 14 (2012). http://doi:10.1039/c2gc16230j.

[76] Gardiner, G.: The rise of HP-RTM Available online: https://www.compositesworld.com/articles/hp-rtm-on-the-rise (accessed on Oct 4, 2021).

[77] Hentschel, T.; Münstedl, H.: Thermoplastic polyurethane - The material used for the Erlanger silver catheter. Infection, 27 (1999). http://doi:10.1007/BF02561617.

[78] Khalifa, M.; Anandhan, S.; Wuzella, G.; Lammer, H.; Mahendran, A. R.: Thermoplastic polyurethane composites reinforced with renewable and sustainable fillers–a review. Polym. Technol. Mater. (2020), 59.

[79] Nguyen Dang, L.; Le Hoang, S.; Malin, M.; Weisser, J.; Walter, T.; Schnabelrauch, M.; Seppälä, J.: Synthesis and characterization of castor oil-segmented thermoplastic polyurethane with controlled mechanical properties. European

Polymer Journal, 81 (2016). http://doi:10.1016/j.eurpolymj.2016.05.024.

[80] Hu, S.; Shou, T.; Fu, G.; Zhao, X.; Wang, Z.; Zhang, L.: New Stratagem for Designing High-Performance Thermoplastic Polyurethane by Using a New Chain Extender. Macromolecular Chemistry and Physics, 222 (2021). http://doi:10.1002/macp.202000439.

[81] Hablot, E.; Zheng, D.; Bouquey, M.; Avérous, L.: Polyurethanes based on castor oil: Kinetics, chemical, mechanical and thermal properties. Macromolecular Materials and Engineering, 293 (2008). http://doi:10.1002/mame.200800185.

[82] F Zafar; E Sharmin: Polyurethane; Zafar, F., Ed.; InTech; ISBN 978-953-51-0726-2.

[83] Covestro: Covestro polyurethane resin composites: an easy choice for wind turbine blades Available online: https://solutions.covestro.com/en/highlights/articles/stories/2020/covestro-polyurethane-solutions-easy-choice-wind-turbine-rotor-blades (accessed on Aug 15, 2022).

[84] Grace Nehls: DNV lowers the partial reduction factor γm1 of wind turbine blades using aging-resistant PU Available online: https://www.compositesworld.com/news/dnv-lowers-the-partial-reduction-factor-m1-of-wind-turbine-blades-using-aging-resistant-pu (accessed on Aug 15, 2022).

[85] Henkel: Composite Solutions for theAutomotive Industry Available online: https://www.google.com/url?sa=t&rct=j&q=&esrc=s&source=web&cd=&ved=2ahUKEwi3gZ7d6Nf5AhUByRoKHfsjAr8QFnoECAcQAQ&url=https%3A%2F%2Fdm.henkel-dam.com%2Fis%2Fcontent%2Fhenkel%2Fbrochure-composite-solutions-automotive-industry&usg=AOvVaw34HQFBMZ7H0Fz6Q97E3gkt (accessed on Aug 21, 2022).

[86] Dow: Light, Strong, Durable – Solutions for Efficient Composites Fabrication Dow VORAFORCETM Composite Systems Available online: https://www.google.com/url?sa=t&rct=j&q=&esrc=s&source=web&cd=&ved=2ahUKEwinv9r859f5AhXQw4UKHbRhCMIQFnoECAYQAQ&url=https%3A%2F%2Fwww.dow.com%2Fcontent%2Fdam%2Fdcc%2Fdocuments%2Fen-us%2Fcatalog-selguide%2F880%2F880-07301-01-dow-voraforce-composite-systems-selection-guide.pdf&usg=AOvVaw2mw6Drr4J_GPOmMHT2xtW8 (accessed on Aug 21, 2022).

[87] Huntsman: Polyurethanes VITROX® and RIMLINE® composite solutions Lightweight design with innovative chemistry Available online: https://www.google.com/url?sa=t&rct=j&q=&esrc=s&source=web&cd=&cad=rja&uact=8&ved=2ahUKEwjTg_iR6Nf5AhVY_IUKHQuhBr4QFnoECAIQAQ&url=https%3A%2F%2Fhuntsman-pimcore.equisolve-dev.com%2FDocuments%2FAutomotive%2520Composites%2520Portfolio.pdf&usg=AOvVaw1esakagMG69RLlAl3QAZxy (accessed on Aug 21, 2022).

[88] Covestro: Polyurethane made for carbon in cars Available online: https://solutions.covestro.com/en/highlights/articles/stories/composites-thermoset/baydur--automotive (accessed on Aug 21, 2022).

[89] CompositesWorld: Composites 2010 Product Showcase Available online: https://www.compositesworld.com/articles/composites-2010-product-showcase (accessed on Aug 21, 2022).

[90] Manson H.: Covestro delivers first order of polyurethane resin for wind blades.

[91] Basf: BECAUSE PASSION FOR CARS RUNS THROUGH OUR VEINS BASF polyurethanes for automotive enthusiasts

Available online: https://www.google.com/url?sa=t&rct=j&q=&esrc=s&source=web&cd=&cad=rja&uact=8&ved=2ahUKEwig-M-G7Nf5AhVWwIUKHXGhCcEQFnoECCwQAQ&url=https%3A%2F%2Fdownload.basf.com%2Fp1%2F8a8082587fd4b608017ff4e4f2b30092%2Fen%2FBASF_Polyurethanes_for_Automotive_Enthusiasts_Brochure_English.pdf%3Fview&usg=AOvVaw0gbUh2l1H16yq7DynpLYdx (accessed on Aug 21, 2022).

[92] Wood, K.: Composite leaf springs: Saving weight in production (2014).

[93] Bareis, D.; Heberer, D.; Connolly, M.: Advances in Urethane Composites: Resins With Tunable Reaction Times. In COMPOSITES 2011; (2011).

[94] Angst, P.; Emig, J.; Albrecht, P.: Sandwich opens huge potential for lightweight engineering. Jec Composites Magazine, , 21–24 (2019).

[95] Li, R.; Liu, L.; Liu, Y.; Wang, B.; Yang, J. J.; Zhang, J.: Research progress of amine catalyst for polyurethane
. New Materials and Intelligent Manufacturing (NMIM), 1, 54–57 (2018).

[96] Jürgen, R.; Holger, C.; Cor, W.: New Catalysts for Low VOC in Flexible Slabstock Foam. Journal of Cellular Plastics, 37, 207–220 (2001).

[97] Silva, A. L.; Bordado, J. C.: Recent Developments in Polyurethane Catalysis: Catalytic Mechanisms Review. Catalysis Reviews, 46, 31–51 (2004).

[98] Schellekens, Y.; Trimpont, B. Van; Goelen, P. J.; Binnemans, K.; Smet, M.; Persoons, M. A.; Vos, D. De: Tin-free catalysts for the production of aliphatic thermoplastic polyurethanes. Green chemistry, 16, 441–447 (2014). http://doi:10.1039/c4gc00873a.

[99] Akindoyo, J. O.; Beg, M. D. H.; Ghazali, S.; Islam, M. R.; Jeyaratnam, N.; Yuvaraj, A. R.: Polyurethane types, synthesis

and applications - a review. RSC advances, 6, 114453–114482 (2016). http://doi:10.1039/c6ra14525f.

[100] Jones, F. N.; Nichols, M. E.; Pappas, S. P.; Webster, D. C.: Organic Coatings; 4th ed.; John Wiley & Sons, Incorporated: Newark; ISBN 111902689X.

[101] Steinmann, Z. J. N.; Huijbregts, M. A. J.; Reijnders, L.: How to define the quality of materials in a circular economy? Resour. Conserv. Recycl. (2019), 141.

[102] Wulf, C.; Werker, J.; Ball, C.; Zapp, P.; Kuckshinrichs, W.: Review of sustainability assessment approaches based on life cycles. Sustain. (2019), 11.

[103] Wendels, S.; Avérous, L.: Biobased polyurethanes for biomedical applications. Bioact. Mater. (2021), 6.

[104] Peyrton, J.; Avérous, L.: Structure-properties relationships of cellular materials from biobased polyurethane foams. Mater. Sci. Eng. R Reports (2021), 145.

[105] Gama, N. V.; Soares, B.; Freire, C. S. R.; Silva, R.; Neto, C. P.; Barros-Timmons, A.; Ferreira, A.: Bio-based polyurethane foams toward applications beyond thermal insulation. Materials and Design, 76 (2015). http://doi:10.1016/j.matdes.2015.03.032.

[106] Mort, R.; Vorst, K.; Curtzwiler, G.; Jiang, S.: Biobased foams for thermal insulation: Material selection, processing, modelling, and performance. RSC Adv. (2021), 11.

[107] Patil, C. K.; Rajput, S. D.; Marathe, R. J.; Kulkarni, R. D.; Phadnis, H.; Sohn, D.; Mahulikar, P. P.; Gite, V. V.: Synthesis of bio-based polyurethane coatings from vegetable oil and dicarboxylic acids. Progress in Organic Coatings, 106 (2017). http://doi:10.1016/j.porgcoat.2016.11.024.

[108] Paraskar, P. M.; Prabhudesai, M. S.; Hatkar, V. M.; Kulkarni, R. D.: Vegetable oil based polyurethane coatings – A sustainable approach: A review. Prog. Org. Coatings (2021), 156.

[109] Noreen, A.; Zia, K. M.; Zuber, M.; Tabasum, S.; Zahoor, A. F.: Bio-based polyurethane: An efficient and environment friendly coating systems: A review. Prog. Org. Coatings (2016), 91.

[110] Tenorio-Alfonso, A.; Sánchez, M. C.; Franco, J. M.: Preparation, characterization and mechanical properties of bio-based polyurethane adhesives from isocyanate-functionalized cellulose acetate and castor oil for bonding wood. Polymers, 9 (2017). http://doi:10.3390/polym9040132.

[111] Zain, N. M.; Roslin, E. N.; Ahmad, S.: Preliminary study on bio-based polyurethane adhesive/aluminum laminated composites for automotive applications. International Journal of Adhesion and Adhesives, 71 (2016). http://doi:10.1016/j.ijadhadh.2016.08.001.

[112] Mesogitis, T. S.; Skordos, A. A.; Long, A. C.: Uncertainty in the manufacturing of fibrous thermosetting composites: A review. Composites Part A: Applied Science and Manufacturing, 57, 67–75 (2014). http://doi:10.1016/j.compositesa.2013.11.004.

[113] Mendikute, J.; Plazaola, J.; Baskaran, M.; Zugasti, E.; Aretxabaleta, L.; Aurrekoetxea, J.: Impregnation quality diagnosis in Resin Transfer Moulding by machine learning. Composites Part B: Engineering, 221 (2021). http://doi:10.1016/j.compositesb.2021.108973.

[114] Chinesta, F.; Cueto, E.; Abisset-Chavanne, E.; Duval, J. L.; Khaldi, F. El: Virtual, Digital and Hybrid Twins: A New Paradigm in Data-Based Engineering and Engineered Data. Archives of Computational Methods in Engineering, 27 (2020). http://doi:10.1007/s11831-018-9301-4.

[115] Jin, Y.; Lei, Z.; Taynton, P.; Huang, S.; Zhang, W.: Malleable and Recyclable Thermosets: The Next Generation of Plastics. Matter, 1, 1456–1493 (2019). http://doi:10.1016/j.matt.2019.09.004.

[116] Erice, A.; Azcune, I.; Ruiz De Luzuriaga, A.; Ruipérez, F.; Irigoyen, M.; Matxain, J. M.; Asua, J. M.; Grande, H. J.; Rekondo, A.: Effect of Regioisomerism on Processability and Mechanical Properties of Amine/Urea Exchange Based Poly(urea-urethane) Vitrimers. ACS Applied Polymer Materials, 1 (2019). http://doi:10.1021/acsapm.9b00589.

[117] Turkenburg, D. H.; van Bracht, H.; Funke, B.; Schmider, M.; Janke, D.; Fischer, H. R.: Polyurethane adhesives containing Diels–Alder-based thermoreversible bonds. Journal of Applied Polymer Science, 134 (2017). http://doi:10.1002/app.44972.

[118] Du, P.; Liu, X.; Zheng, Z.; Wang, X.; Joncheray, T.; Zhang, Y.: Synthesis and characterization of linear self-healing polyurethane based on thermally reversible Diels-Alder reaction. RSC Advances, 3 (2013). http://doi:10.1039/c3ra42278j.

[119] Mendiburu-Valor, E.; Mondragon, G.; González, N.; Kortaberria, G.; Eceiza, A.; Peña-Rodriguez, C.: Improving the Efficiency for the Production of Bis-(2-Hydroxyethyl) Terephtalate (BHET) from the Glycolysis Reaction of Poly(Ethylene Terephtalate) (PET) in a Pressure Reactor. Polymers, 13, 1461 (2021). http://doi:10.3390/polym13091461.

[120] Mendiburu-Valor, E.; Mondragon, G.; González, N.; Kortaberria, G.; Martin, L.; Eceiza, A.; Peña-Rodriguez, C.: Valorization of urban and marine PET waste by optimized chemical recycling. Resources, Conservation and Recycling, 184, 106413 (2022). http://doi:10.1016/j.resconrec.2022.106413.

3

REACTIVITY CONTROL

3. REACTIVITY CONTROL

3.1. GRAPHICAL ABASTRACT 56
3.2. ABSTRACT 57
3.3. INTRODUCTION 57
3.4. EXPERIMENTAL 57
3.4.1. Materials 60
3.4.2. Synthesis 61
3.5. CHARACTERISATION 65
3.5.1. Rheological characterisation 65
3.5.2. Differential scanning calorimetry (DSC) 65
3.6. RESULTS AND DISCUSSION 66
3.6.1. Rheological characterization 66
3.6.2. Differential scanning calorimetry (DSC) 73
3.6.3. Modelling and process simulation 78
3.7. CONCLUSIONS 89
3.8. REFERENCES 90

3.1. GRAPHICAL ABASTRACT

PUR for successful RTM process

Low viscosity

to achieve a good wetting

+

Fast cure

to reduce process times

Controllable reaction

catalyst

- A two-component catalyst system has been developed
- The catalyst is generated *in situ*
- It provides latency first and fast curing later
- A structural part was simulated demonstrating the suitability of the formulation

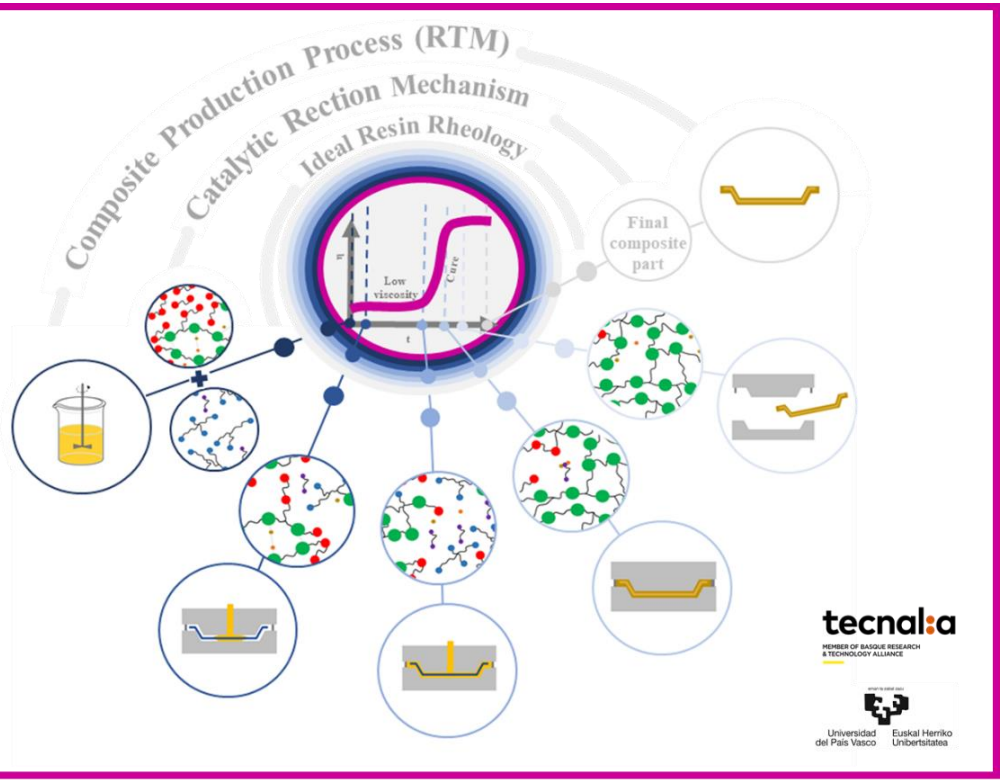

3.2. ABSTRACT

The high reactivity of PUR's hinders some manufacturing processes like Resin Transfer Moulding (RTM). The work presented in this chapter aimed to achieve a PU resin (PUR) formulation with the required latency and reactivity for the RTM. For this purpose, different catalytic systems based on an epoxide and LiCl were investigated. The reactivity of the systems was evaluated through Differential Scanning Calorimetry (DSC) and rheology tests, and the curing reaction and viscosity were modelled. Furthermore, the RTM process of a representative composite part was simulated. Results demonstrated the processability improvements when the LiCl was incorporated into the isocyanate component of the formulation combined with a monool or a diol. It was observed that these combinations contribute to the encapsulation of the LiCl between the as formed urethane groups by hydrogen bonding, providing the desired latency and acting as a delayed action catalyst. Once the reaction started and the encapsulation was deactivated, an alkoxide was formed to act as a catalyst. Encapsulation was more effective with the diol, providing a higher latency.

3.3. INTRODUCTION

In the mass-production of automobiles, speed is paramount, and the newly developed materials should allow high production rates. This is why some developments in the field of PU's for composites are

targeting the RTM process [1,2], which allows the application of short cycle times in the production of structural composites components. For a successful RTM process, the novel PU thermoset resins (PUR) should have initially low viscosity to achieve a good wetting and fast and controllable reaction to allow fast curing. The high reactivity and short cure times of PURs [2–5] result in an abrupt and premature increase in viscosity that makes them not suitable for RTM. Therefore, it is necessary to develop new catalyst formulations to achieve a certain latency to maintain a low viscosity in the wetting step.

Different types of catalysts are used for PUR, the most common being the low molecular weight tertiary amines, such as 1,4-diazabicyclo[2.2.2]octane (DABCO) and 2-[2-(dimethylamino)ethoxy]-N,N-dimethylethanamine (BDMAEE), widely used in rigid and elastic foams [6,7]. However, due to their low molecular weight, they have the tendency to release volatile organic compounds (VOC). Reactive amine catalysts functionalised with isocyanate reactive groups (urea, amino or hydroxyl) can bond to the polymer and reduce VOC release [7–9]. In any case, tertiary amines, reactive or not, accelerate the reaction from the beginning, the curing is very fast, and they do not provide the necessary latency to the PUR for RTM.

Organometallic catalysts have also been extensively used in polyurethane reactions [9–11], being inorganic and organic tin compounds, and more specifically tin alkoxides, the most common [12,13]. Despite their efficiency, they are susceptible to moisture, reducing their catalytic activity [9]. Another disadvantage is their toxicity due to the residues formed [14].

Delayed action catalysts formed by tertiary amines blocked with organic acids, which can be thermally activated, have been investigated [15]. However, organic carboxylates have a strong corrosive action, causing a faster deterioration of the machine and storage containers due to the release of carboxylic acid [9]. Therefore, they are not a feasible alternative for the RTM process. In addition to the tertiary amines with delayed action catalyst, there are organometallic compounds with delayed action, but in most cases, they are formed by mercury and heavy metals [16]. Another solution of delayed action catalysts consists of using polymers capable of containing or bonding the catalyst in order to encapsulate or link the catalyst to the polymer [9,17,18]. In this context, some authors propose to encapsulate one component of the catalyst system within the reaction components through electrostatic interactions [19,20]. After the component release, the catalyst is formed in situ, and it acts to accelerate the reaction. Pelzer et al. [21] studied the effect of different halides in the catalytic coupling with an epoxide in the presence of different ratios of 4,4'-diphenylmethane diisocyanate (MDI). They observed that at high MDI contents, the intermediate alkoxide formed by the coupling between epoxide and ammonium halide catalyses the formation of isocyanurate. It was shown that when the halide was chloride, the catalysed reaction that leads to the formation of isocyanurate prevails over other paths. Moreover, the ability of LiCl was reported to coordinate with urethane groups forming a stable complex via electrostatic interactions [22,23], as well as to form stable intermolecular hydrogen bonding interactions with hydroxyl groups [24]. In this context, adding a stabilised halide salt within a hydroxyl group containing molecule to the isocyanate component to form an urethane prepolymer can be envisaged as an effective strategy for

encapsulating the halide salt of the catalyst system within one of the reaction components.

The aim of this chapter was to achieve a PUR formulation with the required latency and reactivity for the RTM manufacturing of structural PUR based composites. More specifically, the target application was an automotive component subjected to cycling loadings, such as leaf springs. For this purpose, different catalytic systems based on an epoxide and LiCl, separately incorporated within the reaction components, were investigated. The reactivity of the PUR systems was evaluated through differential scanning calorimetry, and rheology tests and the curing reaction and viscosity were modelled. The chemo-rheological resin models considering the viscosity dependence on temperature and curing degree were employed to effectively predict the resin systems-viscosity evolution with time. Finally, in order to evaluate the different alternatives and find the best process parameters of the injection and curing stages of the RTM process, a representative composite part has been simulated with ESI's PAM-RTM software.

3.4. EXPERIMENTAL

3.4.1.Materials

In this chapter a high reactivity and low viscosity two-component commercial thermoset polyurethane resin, supplied by Dow Chemical (Milano, Italia) was employed. The first PUR component was constituted by a polyether-polyol (Voraforce TR 1551-Polyol, OH-number = 527

mg KOH g^{-1} and viscosity = 750 mPa s). Hydroxyl number of Voraforce 1551 was determined according to ASTM D 4274-88. The second component was an isocyanate (Voraforce TR 1500-Isocyanate, NCO equivalent weight = 136 g eq^{-1} and viscosity = 130 mPa s). NCO equivalent weight was determined according to the ASTM D2572-97. Three different catalyst systems were evaluated. CAT1 is a two-component system formed by an epoxide (1,4-butanediol diglycidyl ether, BDDE) and a halide salt (LiCl). CAT2 is formed by BDDE and LiCl dissolved in a low molecular mass biobased cyclic diol (1,4:3,6-dianhydro-D-glucitol or D-isosorbide, DAS). CAT3 is formed by BDDE and LiCl dissolved in a low molecular mass aliphatic monool (diethylene glycol butyl ether, BDG). All the catalysts components were supplied by Sigma Aldrich (St. Louis, USA), and used as received.

3.4.2.Synthesis

Four PUR systems were synthesised, three catalysed and one without additional catalyst as reference. The isocyanate index was maintained constant (equal to 1.2) for all the PUR systems studied. Designation and composition of the PUR systems are summarised in the *Table 3.1*. All formulations are based on 150 parts by weight of isocyanate (pbw).

Before the polyurethane synthesis reaction, both polyol and isocyanate were degassed separately under vacuum at 1000 mbar and 1000 rpm for 30 min. The non-catalysed system (PUR-REF) consists of the reaction of previously degassed polyol and isocyanate components. The reaction components were prepared as shown in *Figure 3.1a*.

Table 3.1. Designation and composition of synthesised thermoset polyurethanes.

System	Components ratio (pbw)					
	Polyol	*Isocyanate*	*LiCl*	*BDDE*	*DAS*	*BDG*
PUR-REF	100	150	-	-	-	-
PUR-CAT1	99.92	150	2.31	5.56	-	-
PUR-CAT2	83	150	2.31	5.56	10.19	-
PUR-CAT3	92.6	150	2.31	5.56	-	10.19

The catalysed PUR systems (PU-CAT1, PU-CAT2 and PU-CAT3) consist of the reaction of a polyol and epoxide based mixture (Part A) and an isocyanate based prepolymer (Part B) formed just before the mixing of both components *(Figure 3.1b).* For part A preparation the polyol and epoxide were mixed at room temperature (RT) and under nitrogen at 1000 rpm for 15 min, obtaining the Part A mixture. For part B, the LiCl is used alone (CAT1) or dissolved in DAS (CAT2) or in BDG (CAT3) after mixing for 30min at 1000 rpm and 80 ºC under nitrogen. After that it was mixed with isocyanate at 1000 rpm and 50 ºC for 4 h under nitrogen to obtain the isocyanate prepolymer. Finally, Part A mixture and isocyanate prepolymer were mixed with the same procedure as for the uncatalysed system (*Figure 3.1a*).

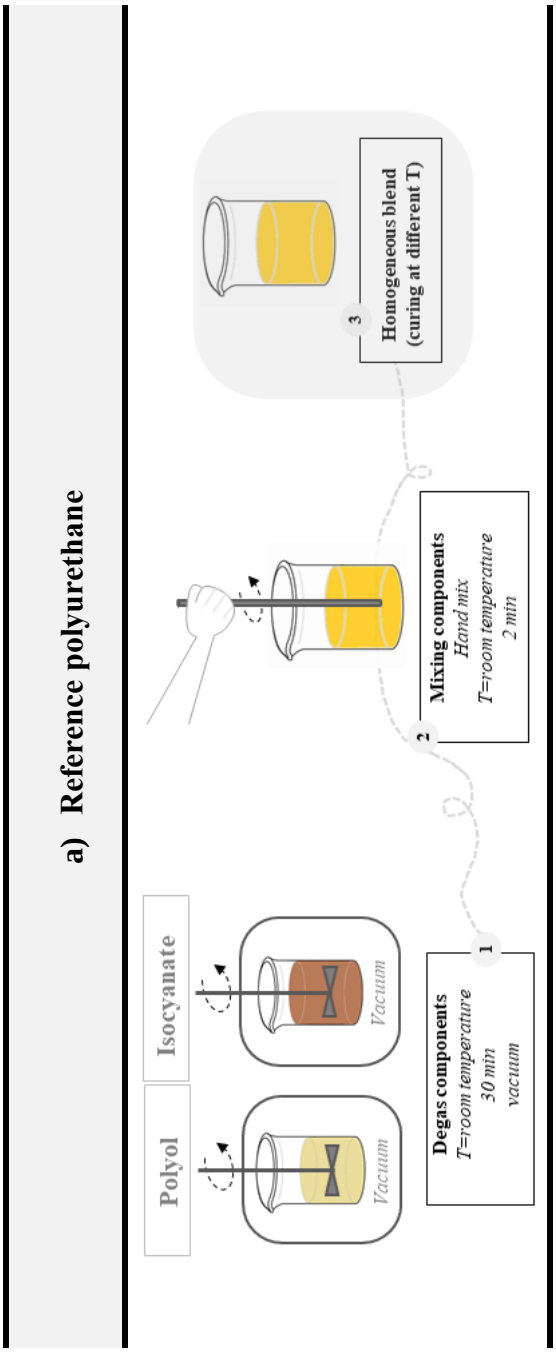

Figure 3.1. a) Reference polyurethane sample preparation.

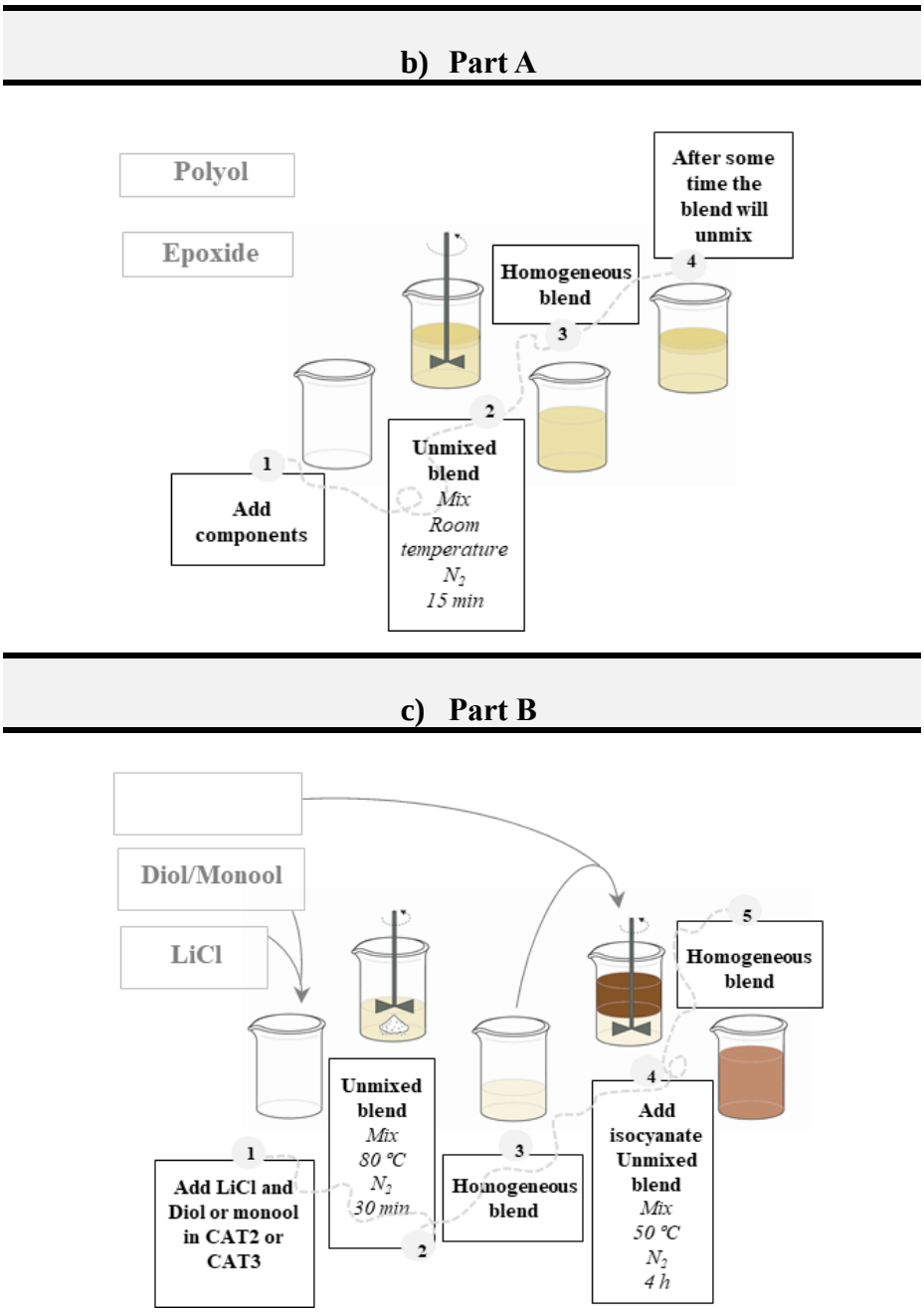

Figure 3.1. b) Part A preparation of the catalysed systems and c) Part B preparation of the catalysed systems.

3.5. CHARACTERIZATION

3.5.1.Rheological characterization

Rheological tests were carried out on a HAAKE RheoStress 6000 Rheometer (Thermo Fisher Scientific, Massachusetts, USA), running in an oscillating stress mode at a frequency of 1 Hz. Amplitude was held constant in the Linear Viscoelastic Range (LVR) throughout the test. A gap separation of 1 mm and disposable parallel plates of 60 mm diameter were used. Experiments were performed at both isothermal or time sweep test, and dynamic or temperature sweep test conditions. Time sweep tests were carried out at different temperatures ranging from 50 to 90 ºC whereas temperature sweep tests were performed from 25 to 200 ºC at a constant heating rate of 5 ºC min^{-1}. Storage and loss moduli, G' and G" respectively, and complex viscosity, η*, were measured over time or temperature in isothermal or dynamic conditions. The gelation time, t_{gel}, was taken as G' and G" crossover (G' = G").

3.5.2.Differential scanning calorimetry (DSC)

Differential scanning calorimetry (DSC) tests were carried out on a TA Instruments DSC Q100 (TA Instruments, New Castle, USA) calorimeter in both dynamic and isothermal conditions. The dynamic experiments were performed from 20 to 200 ºC at three heating rates 5, 10 and 20 ºC min^{-1}. Isothermal experiments were performed at temperatures ranging from 50 to 120 ºC. All samples were subjected to a subsequent dynamic scan from 20 to 200 ºC at 10 ºC min^{-1} to determine

the residual heat of reaction and the glass transition temperature, T_g, of the cured material. The T_g was taken as the midpoint of the heat capacity change and the total heat of reaction (H_T) was calculated from the integration of the area of the exothermic peaks.

The curing rates ($d\alpha/dt$) from the heat flow curves obtained in the dynamic and isothermal DSC tests equation (3.1) were integrated to calculate the degree of cure (α) profiles equation (3.2).

$$H = \frac{dH}{dt} = \frac{d\alpha}{dt} H_T \qquad (3.1)$$

$$\alpha = \int_0^t \frac{d\alpha}{dt} dt \qquad (3.2)$$

where *H* is the instantaneous heat evolved during the polymerisation reaction of the resin, and H_T is the total heat after the curing process.

3.6. RESULTS AND DISCUSSION

3.6.1.Rheological characterization

Viscosity during the resin curing evolves with time and depends on degree of cure and temperature. In the case of a resin system suitable for high production rate RTM, a combination of low reactivity in the first part of the process and high reactivity in the following steps is necessary. *Figure 3.2a* shows schematically the desired viscosity evolution curve for the suitable RTM resin system. Some latency is needed in the first

part of the process (resin injection) to maintain a low viscosity value and to facilitate the fibre impregnation. Then, a high reactivity is desired to reduce curing times and allow fast production cycles.

Viscosity results from oscillatory temperature sweep tests of the four PUR systems are shown in *Figure 3.2b*. As has already been mentioned, the latency in the first part of the curing reaction is necessary to guarantee low viscosity values and obtain an adequate mould filling. Normally, for RTM resin systems, process temperatures are in the range of 90-120 ºC to reach the final target properties in process times ranging from 3 to 10 minutes. Therefore, results showed that the PUR-REF system would not be suitable. The viscosity starts increasing at temperatures lower than 70 ºC, which means that this system will start to react in a few seconds at the target temperatures and will not have the necessary latency. In the case of the PUR-CAT1 the results have been unsatisfactory since the curing is accelerated, and the viscosity increase starts earlier, and it is faster than the reference system. Moreover, this system shows higher viscosity values from the beginning. For the PUR-CAT2 system, the viscosity increase starts at a higher temperature showing that the catalyst system provides latency. Furthermore, the shape of the curve at the viscosity increase is similar to the observed for the reference one, which means the cure is fast. PUR-CAT3 system does not show any appreciable improvement compared to the reference systems at this temperature range.

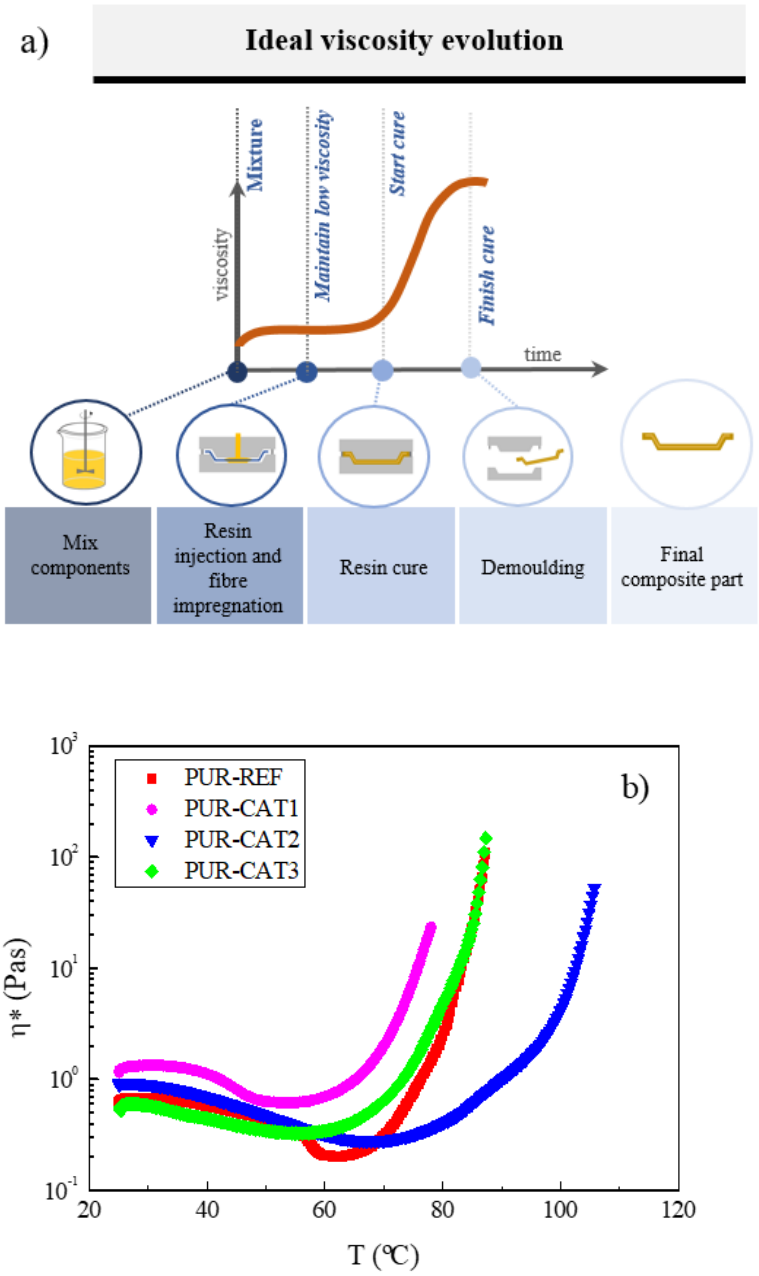

Figure 3.2. a) Ideal viscosity evolution for the PUR RTM resin systems and b) complex viscosity evolution with temperature for the different PUR.

Oscillatory time sweep tests were performed at temperatures between 50 and 90 ºC *(Figure 3.3)*.

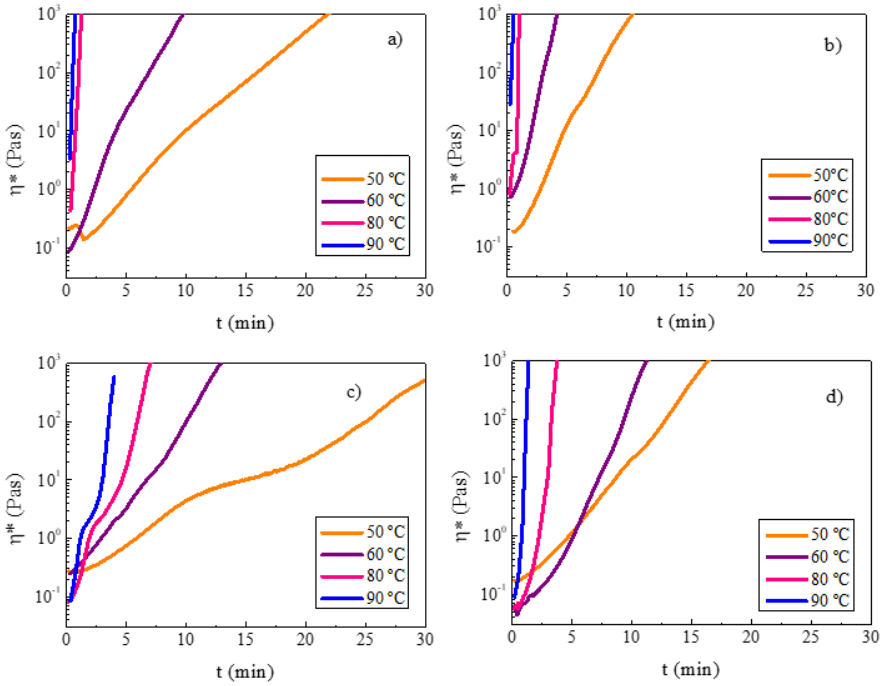

Figure 3.3. Complex viscosity evolution with time at different temperatures, a) PUR-REF, b) PUR-CAT1, c) PUR-CAT2 and d) PUR-CAT3.

Results are in accordance with previous temperature sweep tests. The PUR-REF cure is ultra-fast at temperatures higher than 60 ºC and not suitable for RTM. For PUR-CAT1, the cure reaction is accelerated at high temperatures worsening the material processability for RTM. PUR-CAT3 only provided a slight improvement compared to the reference. For PUR-CAT2, however, it can be observed that the desired latency is obtained in the first part of the reaction. This delayed action catalytic system seems to be suitable for RTM processing and fulfils the

function to provide both latency at the beginning and fast curing at the end of the reaction to the polyurethane resin.

Gel times, t_{gel}, were determined as the G' and G" moduli crossover in the time sweep tests. The obtained t_{gel} values for each PUR system at the studied temperatures are represented in *Figure 3.4*.

Results show that PUR-CAT2 provides latency to polyurethane system, increasing the gel times for all the temperatures studied. In this case, although the best results are obtained for PUR-CAT-2, the improvement of latency is also appreciated for PUR-CAT-3.

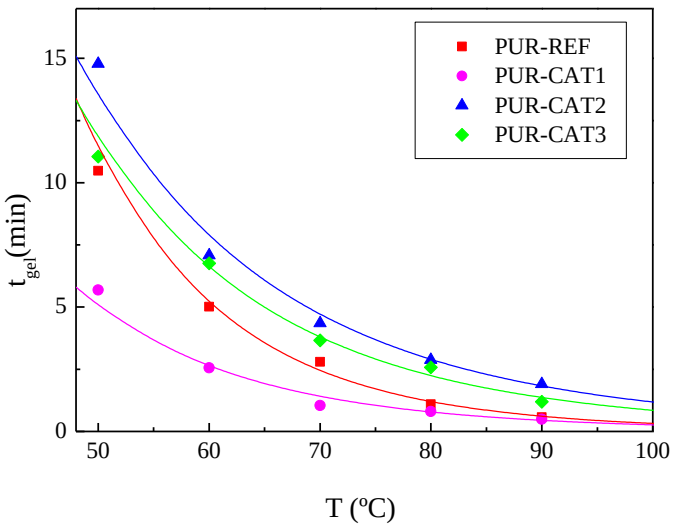

Figure 3.4. Gel time vs temperature for the studied PUR systems.

Again, the lower gel times or the higher reactivities are obtained for PUR-CAT1, showing that this catalyst system is capable of accelerating the reaction, but it cannot provide latency. In PUR-CAT1 the dissociated lithium and chloride encounters the epoxide unimpeded,

and they can create an alkoxide, which acts accelerating the reaction of polyurethane [21,25].

The behaviour observed in PUR-CAT-2 and PUR-CAT-3 can be attributed to the developed catalytic system, which is based on the generation of the catalyst *in situ*, once the reaction between part A and part B is initiated. The urethane groups formed once the monool or diol and the isocyanate are mixed to prepare the part B are able to encapsulate the lithium salt through the formation of a polydentate complex with the salt [22,24]. The encapsulation process involves several steps. In the first step of the part B preparation, the lithium salt is dissociated in the diol or monool due to the electrostatic interactions (*Figure 3.5a)*.

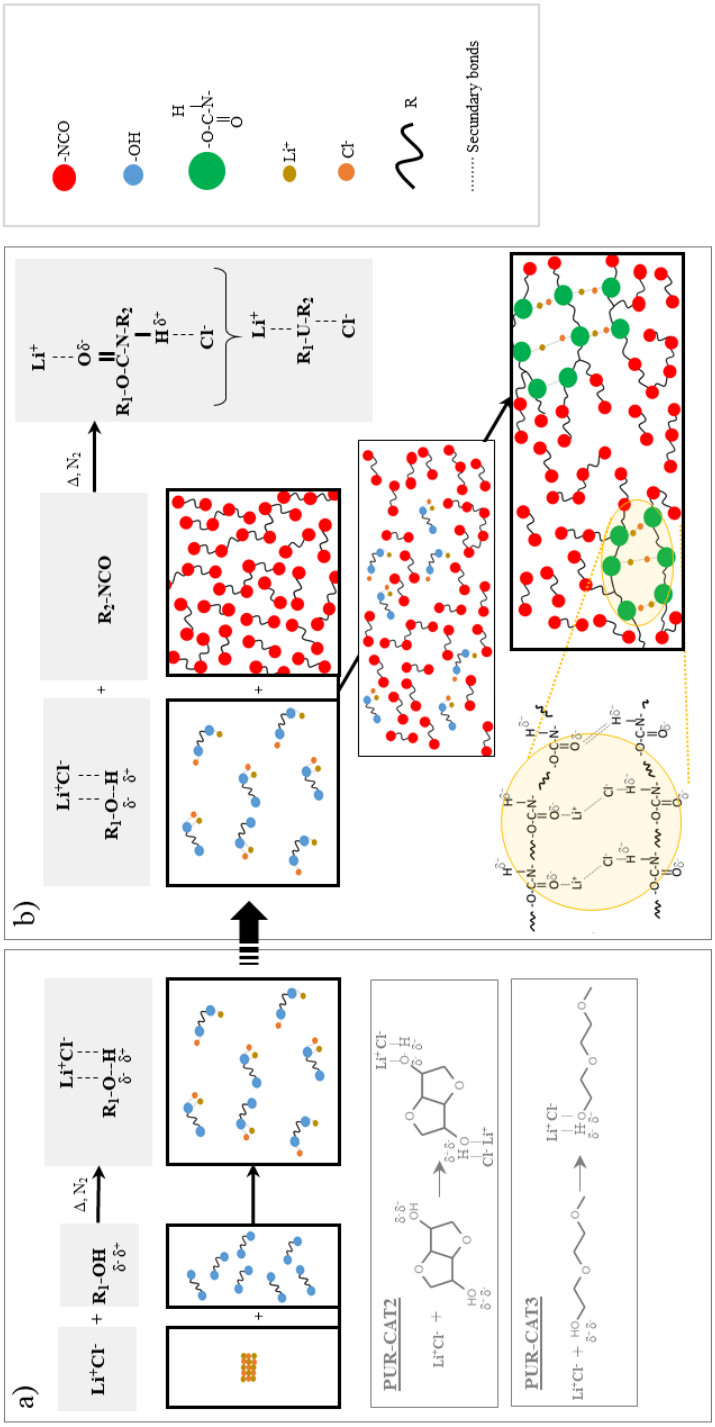

Figure 3.5. Scheme of the salt encapsulation. a) Salt dissociation in DAS and BDG and b) urethane formation with DAS or BDG and salt encapsulation.

In the second step of the part B preparation, the isocyanate reacts with the hydroxyl groups of the diol or monool, creating urethane groups. Thanks to the electrostatic interaction, the lithium cation and chloride anion can be associated with the urethane groups [22,23] and create a monodentate or bidentate complex. *Figure 3.5b* shows the chemical structure evolution in this second step. The salt is caught between the urethane groups encapsulating via electrostatic interactions. In addition, the urethane groups are capable of creating hydrogen bonds among them increasing the encapsulation effectiveness, being stringer in the case of diol. Due to the lack of urethane groups in the PUR-CAT1 Part B, the encapsulation of the LiCl is not possible. For this reason, the CAT1 accelerates the reaction from the beginning and does not provide any latency. Therefore, this system has been discarded as a suitable alternative for the RTM process.

3.6.2.Differential scanning calorimetry (DSC)

The curing reaction of PUR-REF, PUR-CAT2 and PUR-CAT3 was also characterised by both dynamical and isothermal DSC tests. *Figure 3.6a-c* shows the thermograms obtained in dynamic conditions for the different systems at 5, 10 and 20 ºC min^{-1}. The total heat of reaction, taken as the value obtained at 10 ºC min^{-1} was 311 J g^{-1} for the PUR-REF system whereas for the catalysed systems PUR-CAT2 and PUR-CAT3 were 282 J g^{-1} and 301 J g^{-1} respectively. The enthalpy difference could be due to the fact that in catalysed systems, the diol and monool were mixed with the isocyanate to form an urethane prepolymer during the Part B preparation. In this step, some isocyanate groups react with hydroxyl groups of the monool or diol in order to produce urethane

groups as shown in the *Figure 3.5b*. The heat released in this step was not measured in the later DSC cure.

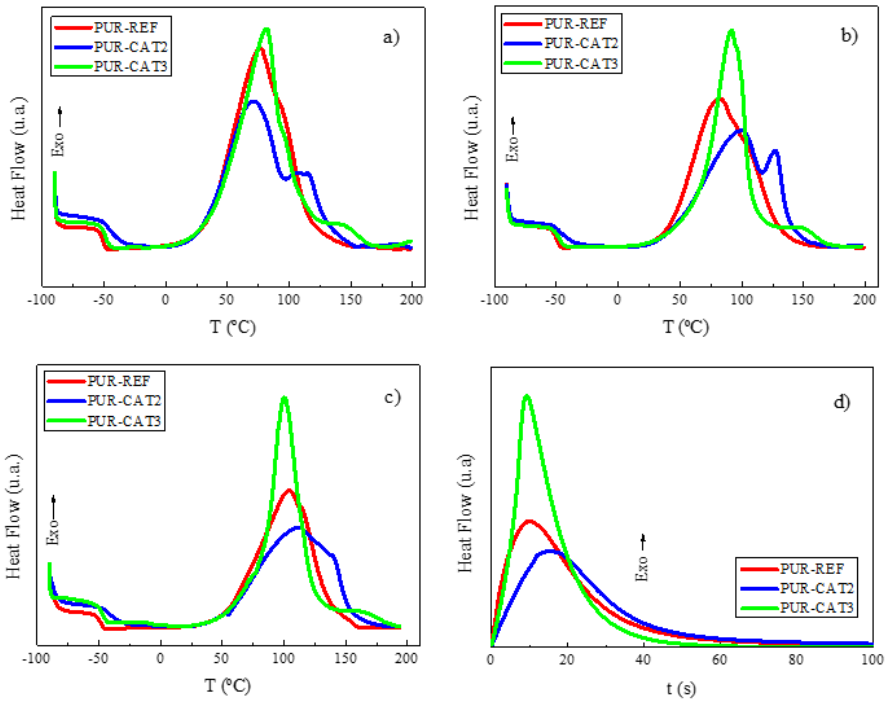

Figure 3.6. Dynamic DSC thermograms for the different PUR systems at a) 5 ºC min^{-1}, b) 10 ºC min^{-1} and c) 20 ºC min^{-1}, and d) isothermal DSC thermograms for the different PUR systems at 120 ºC.

As can be seen in the figures, the reaction is delayed for the catalysed systems. For instance, at 10 ºC min^{-1} PUR-REF system peak has a maximum at 80 ºC, whereas it appears at 97 and 93 ºC for PUR-CAT2 and PUR-CAT3, respectively. However, it is not evident for the PUR-CAT3 system presented in *Figure 3.6*c-d at high reaction rates (20 ºC min $^{-1}$ and isothermal at 120 ºC). Furthermore, the shape of the heat flow curve changes and a second peak or an overlapped peak can be appreciated at a higher temperature. This could be attributed to a two-

step catalytic mechanism. The first peak in the PUR-CAT2 and in the PUR-CAT3 is associated with polyurethane reaction. At the beginning of the reaction, when the two parts of the system (Part A and Part B) are mixed, due to LiCl is encapsulated, a delay in the reaction is observed, providing the necessary latency (*Figure 3.7, First step).*

Once the reaction progresses, the heat released is able to break down hydrogen bonds between urethane groups, the encapsulation is destabilised, and the LiCl encounters the epoxide. LiCl activates the ring opening of the epoxy group, forming an alkoxide, which acts as a catalyst accelerating the reaction of the polyurethane system, as well as reacting with isocyanate group in excess forming isocyanurate [21,24]. The second peak in PUR-CAT2 and PUR-CAT3 could be associated with the isocyanurate and additional network formation [26] (*Figure 3.7, Second step*). This second peak appears at 127 ºC in the case of PUR-CAT2 dynamic test at 10 ºC min^{-1}, whereas for PUR-CAT3 the maximum appears at higher temperatures 150 ºC. In the case of PUR-REF systems, although the second peak was overlapped with the main reaction peak, a shoulder was also appreciated. This can involve the achievement of a lower maximum degree of cure at the process temperatures. This effect is also appreciated at the other heating rates studied *(Figure 3.6).*

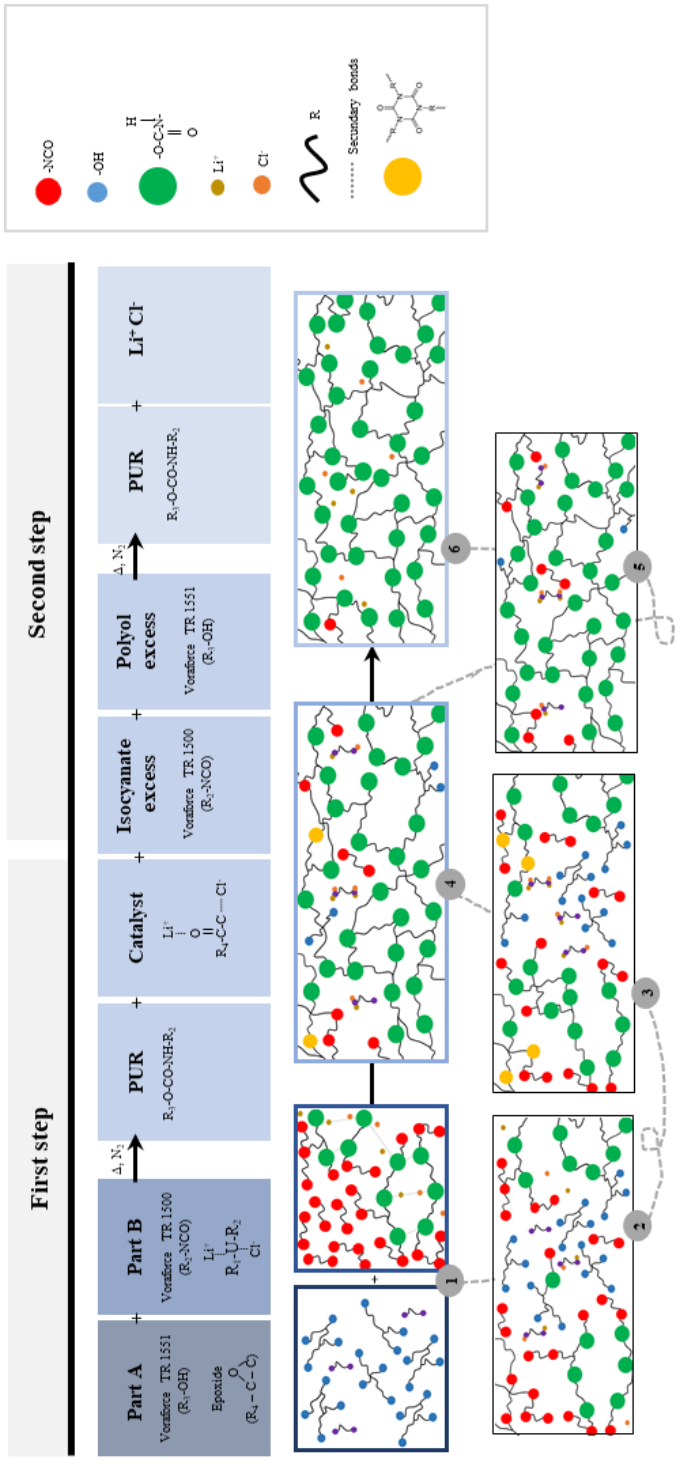

Figure 3.7. a) Scheme of the catalyst mechanism, catalyst production in situ and polyurethane curing.

The T_g calculated from the second DSC scan at 10 ºC min^{-1} gives values of 130 ºC for PUR-REF, 133 ºC for PUR-CAT2 and 93 ºC for PUR-CAT3. The changes in T_g are attributed to the effect of the diol and monool on the crosslinking density of the polyurethane. It was expected that crosslinking density decreased with the addition of the diol and monool in the formulation, since both have lower functionality than the Voraforce TR 1551 Polyol (*Figure 3.8*).

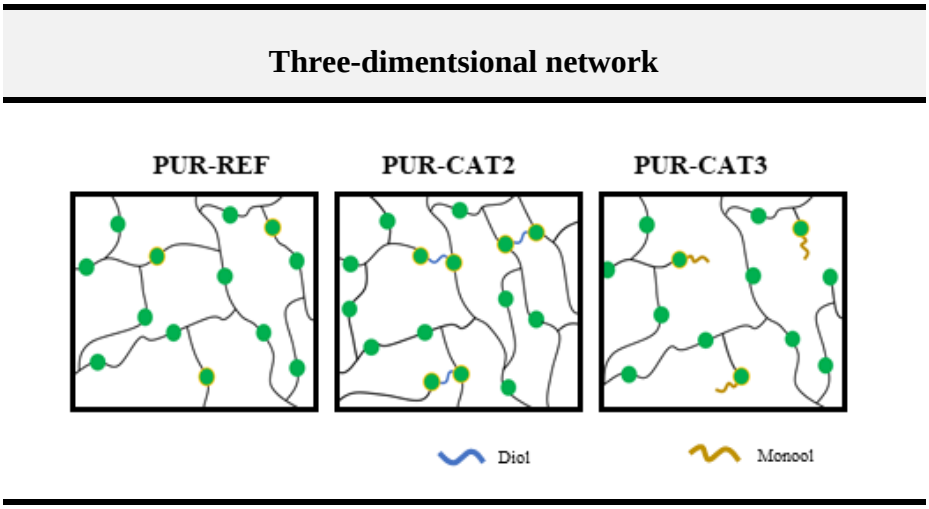

Figure 3.8. Polyurethane three-dimensional network for PUR-REF, PUR-CAT2 and PUR-CAT3 systems.

Nevertheless, in the case of the diol, which has been integrated into PUR-CAT2 system, the T_g value is maintained. This can be attributed to the cycloaliphatic diol structure, which also provides steric hindrance that affects polymer mobility. On the other hand, the monool of PUR-CAT3 is aliphatic and monofunctional and reduces the crosslinking density as shown in *Figure 3.8,* where a schematic representation of the three-dimensional network of the polyurethane systems PUR-REF, PUR-CAT2 and PUR-CAT3 is depicted.

Isothermal experiments were carried out at temperatures ranging between 50 and 120 ºC. *Figure 3.6d* shows as an example the results obtained at 120 ºC (target process temperature). As for the dynamic tests, a shift of the maximum of the heat flow is observed with the addition of the catalyst, suggesting an increase in the latency of the system, being more remarkable for PUR-CAT2 system.

3.6.3.Modelling and process simulation

Once the reactivity of the PUR systems was evaluated, the curing reaction and viscosity were modelled. For the cure kinetic modelling, the degree of cure curves obtained from the dynamic and isothermal DSC tests were fitted to the Kamal-Sourour equation *(3.3)* [27]. In order to consider the diffusion effect and have a good fitting in all the degree of cure ranges, we completed the model with a diffusion factor F(α) *(3.3)* [28].

$$\frac{d\alpha}{dt} = \left(k_1 e^{-\frac{E1}{T}} + k_2 e^{-\frac{E2}{T}} \alpha^m\right)(1-\alpha)^n F(\alpha) \qquad (3.3)$$

$$F(\alpha) = \frac{1}{1 + e^{(Ed(\alpha - \alpha_c))}} \qquad (3.4)$$

where

$$E_d = E_{d1} + E_{d2}\, T \qquad (3.5)$$

and

$$\alpha_c = \alpha_{c1} + \alpha_{c2}\, T \qquad (3.6)$$

are temperature dependent adjustable parameters.

In this equation α is the degree of cure, dα/dt is the reaction rate, n and m the reaction orders and T the temperature. The variables k_1, E_1 and k_2, E_2 are the preexponential factors and activation energies of the n^{th} and m^{th} order reactions, respectively and F(α) corresponds to the diffusion factor. The kinetic model parameters for each of the PUR systems are summarised in *Table* 3.2.

Table 3.2. Kinetic model parameters for the different PUR resin systems.

		PUR-REF	**PUR-CAT2**	**PUR-CAT3**
K_1	s^{-1}	4.45E+08	1.38E+08	2.49E+11
E_1	ºK	8.80E+03	1.53E+04	1.10E+04
K_2	s^{-1}	2.05E+06	1.79E+06	2.05E+06
E_2	ºK	9.10E+03	6.79E+03	1.26E+04
m		3.00E-01	2.50E-01	2.40E-01
n		1.80E+00	2.30E+00	3.14E+00
α_{c1}		6.10E-01	1.54E-01	-3.29E-01
α_{c2}		1.00E-03	2.00E-03	3.00E-03
E_{d1}		-1.76E+06	-1.34E+03	-6.15E+02
E_{d2}		7.67E+03	6.90E+00	3.65E+00

The activation energies for the first part of the reaction, E_1, are higher for the catalysed than for the reference systems (1.53E+04, 1.10E+04 and 8.80E+03 ºK for PUR-CAT2, PUR-CAT3 and PUR-REF, respectively), confirming their higher latency. The activation energy for the second part, E_2, is clearly higher for PUR-CAT3 (1.26E+04, 9.10E+03 and 6.79E+03 ºK for PUR-CAT3, PUR-REF and PUR-CAT2, respectively) showing a delay of the final part of the cure. For PUR-CAT2 however, the activation energy remains low. As it can be seen in *Figure 3.9* there is a good correlation between the experimental results and the proposed models for all the systems studied.

Figure 3.9d compares the maximum degrees of cure obtained at each temperature for the different resin systems. As it can be seen, at the temperature range studied, the maximum degree of cure for the catalysed systems is lower than for the uncatalysed system. In the case of PUR-REF maximum degrees of cure from 0.93 to 1 (full cure, at 120 ºC) are obtained and for PUR-CAT2 and PUR-CAT3 the maximum at 120 ºC are 0.94 and 0.85, respectively. For PUR-CAT2 the maximum degree of cure of 0.94 is good enough to avoid postcuring whereas for PUR-CAT3 system would require a postcure at higher temperatures. This is in agreement with the results from the dynamic DSC scans (*Figure 3.6a-c)*, where a peak appears at temperatures above 120 ºC for PUR-CAT3. Due to the requirement of postcure process, which is an important disadvantage, the PUR-CAT3 systems were discarded as a real alternative for RTM resin.

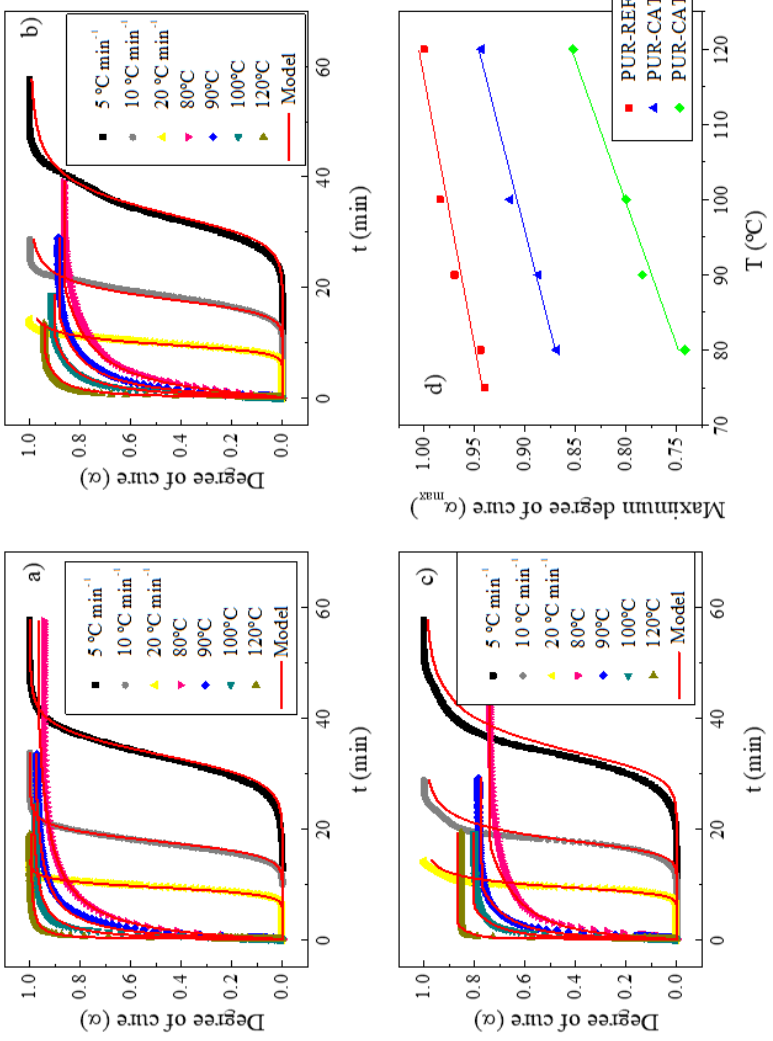

Figure 3.9. Degree of cure curves from DSC isothermal and dynamic tests (symbols) and models fitting (lines), a) PUR-REF, b) PUR-CAT2 and c) PUR-CAT3, and d) maximum degree of cure at different temperatures.

For the viscosity modelling, the results from the time and temperature sweeps tests for PUR-REF and PUR-CAT2 were fitted to the following equation based on Castro-Macosko model *(3.7)* [29]:

$$\eta^* = \eta_0 e^{\frac{E}{T}} \frac{1}{(1-\alpha)}^{p1+p2\alpha} \quad (3.7)$$

where η* is the resin viscosity at a given degree of cure (α), temperature (T) and activation energy (E), and η_0, p1 and p2 are adjustable parameters, which are shown in *Table 3.3*.

As it can be seen in *Figure 3.10*, there is a good fitting for both systems in the pregel stage. Also, again it is demonstrated that the catalytic system is capable of delaying the reaction. The PUR-REF system reaches a viscosity of 1000 Pa.s at 80 ºC in one minute, whereas the viscosity of the PUR-CAT2 at this time is lower than 1 Pa.s. At 90 ºC, this difference is more significant, where the PUR-REF reaches a viscosity of 1000 Pa.s in half a minute, whereas for PUR-CAT2 the viscosity is 0.12 Pa.s. The difference in the reactivity is also reflected in the model's parameters shown in *Table 3.3*.

Table 3.3. Viscosity model parameters.

		PUR-REF	**PUR-CAT2**
η_0	Pa s	1.22E-04	1.50E-03
E	ºK	2383	3979
p1		1.93	9.82
p2		52.42	-10.4

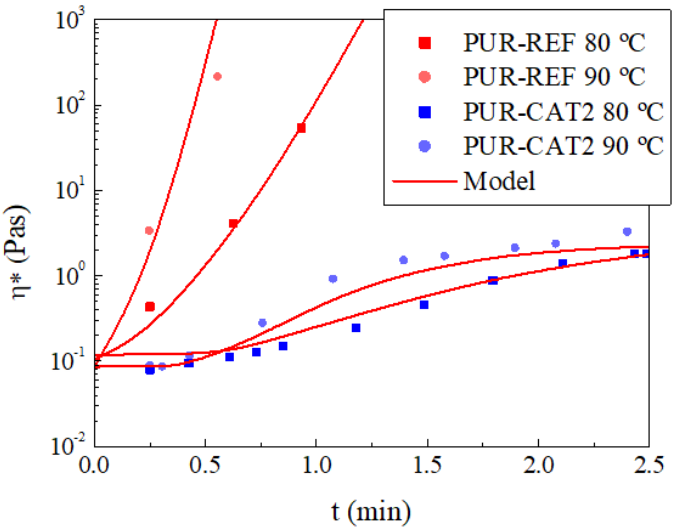

Figure 3.10. Viscosity evolution with time at 80 and 90 ºC for PUR-REF and PUR-CAT2 systems. Experimental results (symbols) and the rheological model (red lines).

Finally, in order to evaluate the PUR systems suitability for manufacturing structural parts by RTM, a representative composite part has been simulated with ESI's PAM-RTM software. The composite part simulated was a leaf spring reinforced with 47% fibre volume content of high fatigue resistance (ultra-fatigue) unidirectional glass fibre (Ultra Fatigue UD, U-V-E-PB-1176g/m²-1200mm, Saertex, Saerbeck, Germany). These parts are normally produced with a linear, lateral injection strategy with the resin inlet at the middle point of the part and the outlets at the ends *(Figure 3.11a)* so for the evaluations, only half length of the real part was considered. The mesh dimensions used in the simulations are shown in *Figure 3.11*b.

a)

b)

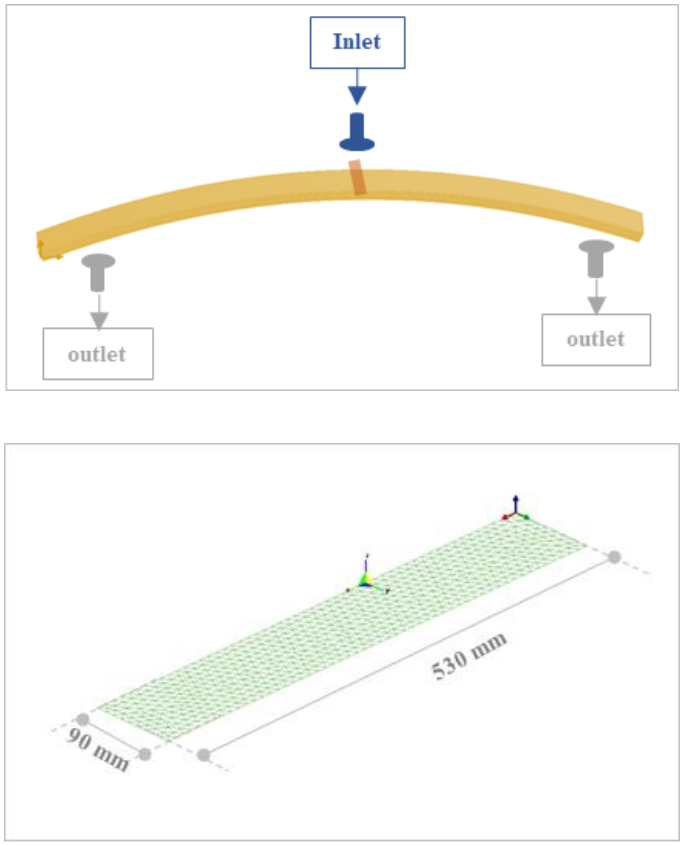

Figure 3.11. a) Injection strategy and b) mesh used in the simulation of a reinforced leaf spring.

The flow of the polyurethane resin through the glass fibre fabric can be described by Darcy's law *(3.8)*.

$$Q = -\frac{S\,K}{\phi\,\eta}\nabla P \qquad (3.8)$$

where Q denotes the resin flow rate, K is the preform permeability, S is the cross-sectional area, ϕ is the porosity, η is the resin viscosity, and P represents the pressure. On the other hand, as mentioned previously,

resin viscosity depends on resin temperature and time (degree of cure) as described in equation *(3.7)*.

The temperature used for the simulations was 120 ºC in all the cases, which is a standard temperature for the production of composite automotive parts. Also, two different injection strategies were considered, at constant pressure and a constant flow. In the case of constant pressure injections, the simulations have been carried out at different pressures ranging from 70 to 100 bar. PUR-REF is not able to fill the mould in any case, as shown in *(Figure 3.12)*. This happens because the viscosity starts to increase in a few seconds, and the resin gels, making it impossible to continue mould filling. PUR-REF lack of latency makes this resin system not suitable for the manufacture of leaf springs by RTM. However, PUR-CAT2 system simulations results are satisfactory (*Figure 3.13*). Simulations show the processability of PUR-CAT2 at moderate pressures. At pressures higher than 70 bar, this system can fill the mould in a few seconds. After the mould filling the curing is fast, and in four minutes, the curing is completed without post-curing processes. The PUR-CAT2 provides enough latency to be suitable for RTM.

The simulations at a constant flow rate of 1 Kg min^{-1} and 100 bar maximum pressure strengthen the previous results *(Figure 3.14)*. The PUR-REF is not capable of filling the mould, and it reaches the maximum pressure and gels before in a few seconds. In the simulation with PUR-CAT2 system, the maximum pressure is reached in 5 seconds, and there is a decrease in filling rate, but the mould is fully filled in only 14 seconds.

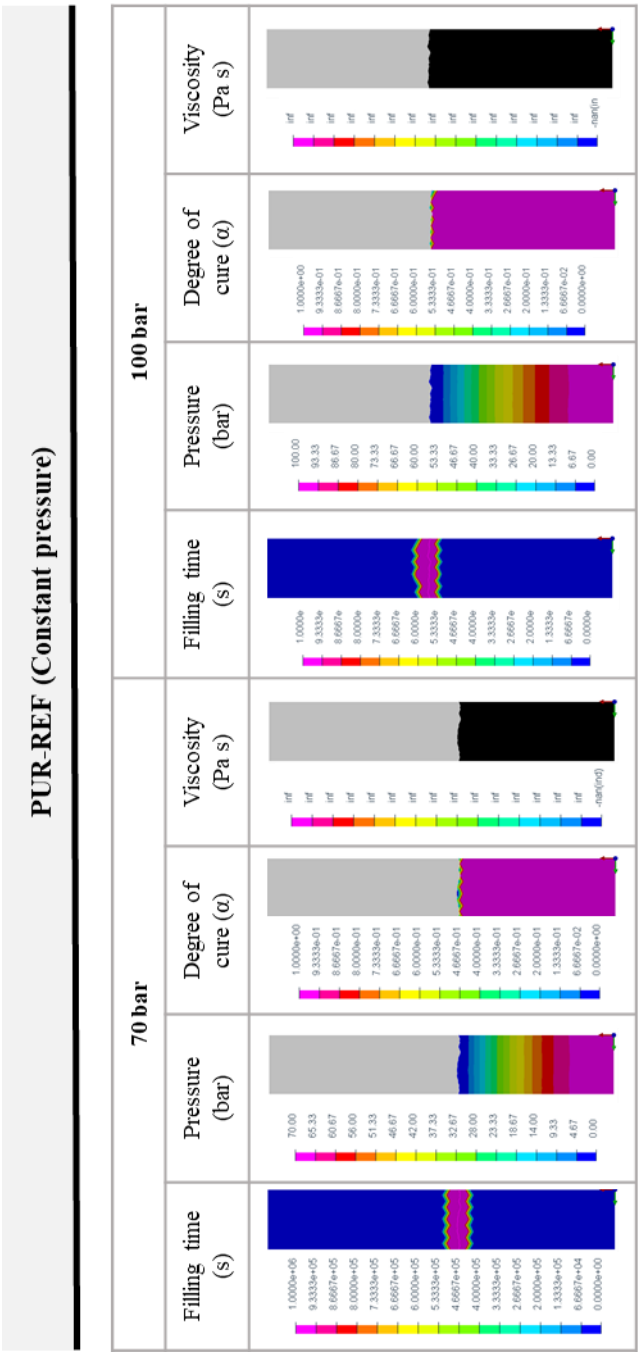

Figure 3.12. Leaf spring simulation at 120ºC with constant pressure for PUR-REF.

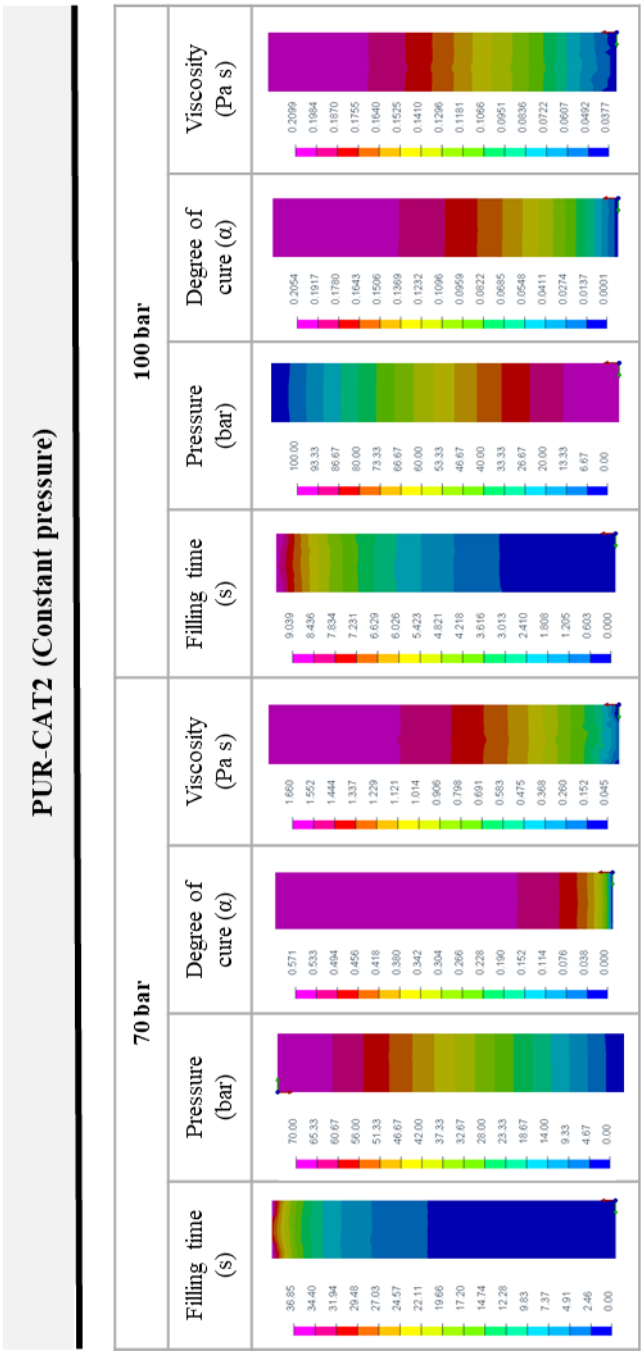

Figure 3.13. Leaf spring simulation at 120ºC with constant pressure for PUR-CAT2.

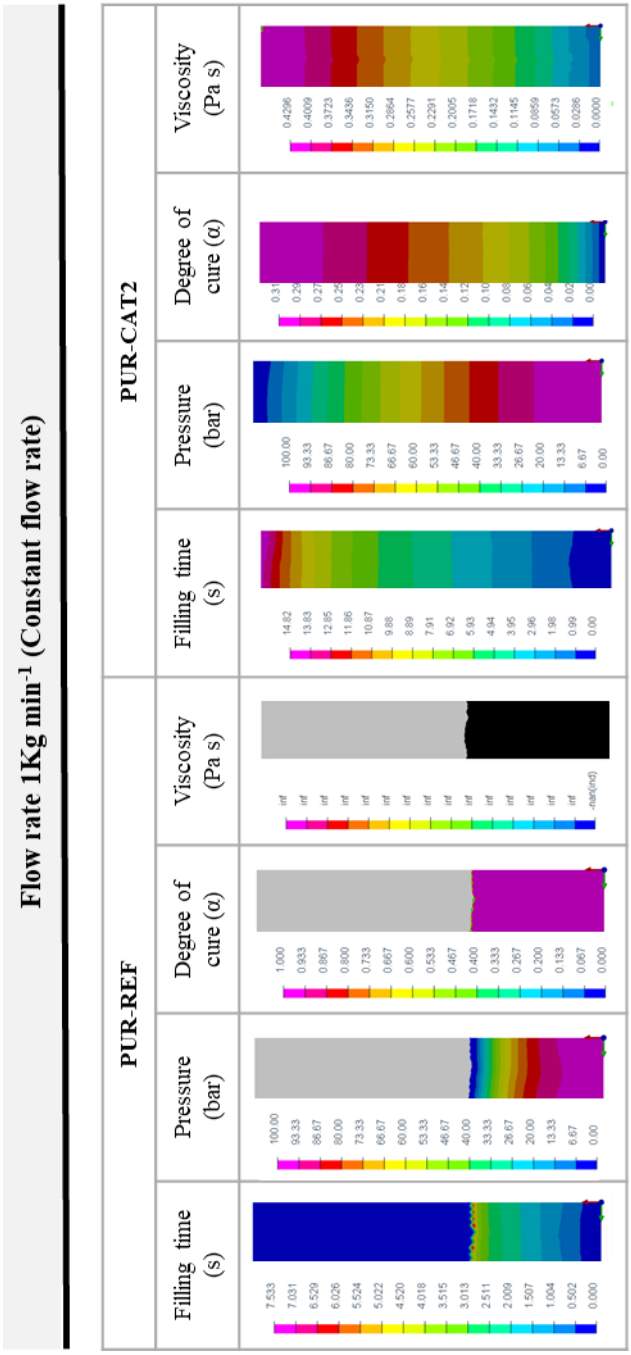

Figure 3.14. Leaf spring simulation at 120ºC with constant flow rate for PUR-REF and PUR-CAT2.

3.7. CONCLUSIONS

In this work, different catalytic systems based on an epoxide and LiCl were investigated to achieve the required reactivity for the RTM manufacturing. DSC, rheology and RTM simulation results showed that the PUR-REF commercial system is not suitable for the target application due to the abrupt increase of viscosity during the mould filling step. It is necessary to provide latency to the resin system. When the LiCl was used alone, as in PUR-CAT1, the salt and the epoxide could form an alkoxide, which acted as a catalyst accelerating the reaction, but the curing rate was increased from the beginning of the reaction, worsening the PUR processability. Adding the diol or monool in the isocyanate component of the formulations, as for PUR-CAT2 (DAS diol) and PUR-CAT3 (BDG monool), delayed the curing in the first part of the reaction and provided latency in both systems. This is a result of the capability of urethane groups, formed by isocyanate component and diol or triol, to encapsulate the lithium halide via electrostatic interactions. When the reaction progressed, the heat released could break down hydrogen bonds, and the encapsulation was destabilised. After that, the LiCl encountered the epoxide to form alkoxide, and it acted as a catalyst. The delayed action catalyst with DAS (PUR-CAT2) showed more effective encapsulation. Moreover, for PUR-CAT2 the maximum curing degree obtained was good enough to avoid postcuring, with a T_g of 133 ºC, whereas the PUR-CAT3 system would require a postcure at a higher temperature to achieve the required properties. The RTM simulations demonstrated the PUR-CAT2 processability improvements and the capability to manufacture real structural parts.

3.8. REFERENCES

[1] Mason, H.: SGL Carbon produces composite leaf springs for Ford Transit (2019).

[2] Wood, K.: Composite leaf springs: Saving weight in production (2014).

[3] Kreiling, S.; Fetscher, F.: Progress with polyurethane matrix resin technology: high-speed resin transfer molding processes and application examples. In SPE ACCE; Novi (Detroit), (2013).

[4] Bareis, D.; Heberer, D.; Connolly, M.: Advances in Urethane Composites: Resins With Tunable Reaction Times. In COMPOSITES 2011; (2011).

[5] Angst, P.; Emig, J.; Albrecht, P.: Sandwich opens huge potential for lightweight engineering. Jec Composites Magazine, 21–24 (2019).

[6] Li, R.; Liu, L.; Liu, Y.; Wang, B.; Yang, J. J.; Zhang, J.: Research progress of amine catalyst for polyurethane
. New Materials and Intelligent Manufacturing (NMIM), 1, 54–57 (2018).

[7] Jürgen, R.; Holger, C.; Cor, W.: New Catalysts for Low VOC in Flexible Slabstock Foam. Journal of Cellular Plastics, 37, 207–220 (2001).

[8] Huhtasaari, M. S.; Plaumann, R.; Grimminger, J.; Kniss, J. G.; Womack, F. D.: Catalysts and Silicone Surfactants for Reduced VOC Emissions of Polyester Slabstock Foam; 1st ed.; CRC Press: Columbus, Ohio;

[9] Silva, A. L.; Bordado, J. C.: Recent Developments in Polyurethane Catalysis: Catalytic Mechanisms Review. Catalysis Reviews, 46, 31–51 (2004).

[10] Schellekens, Y.; Trimpont, B. Van; Goelen, P. J.; Binnemans, K.; Smet, M.; Persoons, M. A.; Vos, D. De: Tin-free catalysts for the

production of aliphatic thermoplastic polyurethanes. Green chemistry, 16, 441–447 (2014). http://doi:10.1039/c4gc00873a.

[11] Akindoyo, J. O.; Beg, M. D. H.; Ghazali, S.; Islam, M. R.; Jeyaratnam, N.; Yuvaraj, A. R.: Polyurethane types, synthesis and applications - a review. RSC advances, 6, 114453–114482 (2016). http://doi:10.1039/c6ra14525f.

[12] Devendra, R.; Edmonds, N. R.; Söhnel, T.: Computational and experimental investigations of the urethane formation mechanism in the presence of organotin(IV) carboxylate catalysts. Journal of molecular catalysis A: Chemical, 366, 126–139 (2013). http://doi:10.1016/j.molcata.2012.09.015.

[13] Devendra, R.; N.R.Edmonds; Söhnel, T.: Organotin carboxylate catalyst in urethane formation in a polar solvent: an experimental and computational study. RSC advances, 5, 48935–48945 (2015). http://doi:10.1039/C5RA03367E.

[14] Fent, K.: Organotin compounds in municipal wastewater and sewage sludge: contamination, fate in treatment process and ecotoxicological consequences. Science of the total environment, 185, 151–160 (1996). http://doi:https://doi.org/10.1016/0048-9697(95)05048-5.

[15] Jones, F. N.; Nichols, M. E.; Pappas, S. P.; Webster, D. C.: Organic Coatings; 4th ed.; John Wiley & Sons, Incorporated: Newark; ISBN 111902689X.

[16] Christman, D. L.; le, G.; Merkl, B. A.: Trimerization catalysts and organo-mercury compounds as Co-catalysts for the preparation of noncellular polyurethane elastomers (1984).

[17] Gao, Y.; Dong, H.; Liu, L.; Yu, Y.; Tang, Z.; Bai, C.; Schmidt, T.; Feng, Y.; Chen, H.: Tin-Containing Crystalline Copolymers as Latent Catalysts for Polyurethanes. ACS applied polymer materials, 2, 4531–4540 (2020). http://doi:10.1021/acsapm.0c00627.

[18] Bitler, S. P.; Kamp, D. A.; Wanthal, M. A.; Sendijarevic, A.; Altarribasanpons, M.; Wang, J.; Frish, K. C.: Novel delayed

action catalysts for polyurethane applications. . In In Polyurethane World Congress; CRC Press: The Netherlands, (1997); pp. 338–345.

[19] Verbeke, H.; Verbeke, H. G. G.; Giannini, G.; Esbelin, C.: In-situ formation of polyurethane catalyst (2016).

[20] Liese, J.; Schütte, M.; Eling, B.: Polyurethane system with long pot life and rapid hardening (2015).

[21] Pelzer, T.; Eling, B.; Thomas, H.-J.; Luinstra, G. A.: Toward polymers with oxazolidin-2-one building blocks through tetra-n-butyl-ammonium halides (Cl, Br, I) catalyzed coupling of epoxides with isocyanates. European polymer journal, 107, 1–8 (2018). http://doi:10.1016/j.eurpolymj.2018.07.039.

[22] Yalcinkaya, F.; Yalcinkaya, B.; Jirsak, O.: Influence of Salts on Electrospinning of Aqueous and Nonaqueous Polymer Solutions. Journal of Nanomaterials, 2015, 1–12 (2015). http://doi:10.1155/2015/134251.

[23] Verdolotti, L.; Colini, S.; Porta, G.; Iannace, S.: Effects of the addition of LiCl, LiClO4, and LiCF3SO3 salts on the chemical structure, density, electrical, and mechanical properties of rigid polyurethane foam composite. Polymer engineering and science, 51, 1137–1144 (2011). http://doi:10.1002/pen.21846.

[24] Zhang, M.; Lai, W.; Su, L.; Lin, Y.; Wu, G.: A synthetic strategy toward isosorbide polycarbonate with a high molecular weight: the effect of intermolecular hydrogen bonding between isosorbide and metal chlorides. Polymer chemistry, 10, 3380–3389 (2019). http://doi:10.1039/C9PY00331B.

[25] Pankratoc, V. A.; Frenkel, T. M.; Fainleib, A. M.: 2-Oxazolidinones. Russian Chemical Reviews, 52, 1018–1052 (1983).

[26] Li, J.; Jiang, S.; Ding, L.; Wang, L.: Reaction kinetics and properties of MDI base poly (urethane-isocyanurate) network polymers. Designed Monomers and Polymers, 24 (2021). http://doi:10.1080/15685551.2021.1971858.

[27] Kamal, M. R.; Sourour, S.: Kinetics and thermal characterization of thermoset cure. Polymer engineering and science, 13, 59–64 (1973). http://doi:10.1002/pen.760130110.

[28] Chern, C. S.; Poehlein, G. W.: A kinetic model for curing reactions of epoxides with amines. Polymer engineering and science, 27, 788–795 (1987). http://doi:10.1002/pen.760271104.

[29] Castro, J. M.; Macosko, C. W.; Perry, S. J.: Viscosity changes during urethane polymerization with phase separation. Polymer communications, 25, 82–87 (1984).

4

BIOBASED POLYOLS

4. BIOBASED POLYOLS

4.1. GRAPHICAL ABSTRACT 96
4.2. ABSTRACT 97
4.3. INTRODUCTION 97
4.4. EXPERIMENTAL 99
4.4.1. Materials 99
4.4.2. Synthesis 101
4.5. CHARACTERIZATION 103
4.5.1. Rheological characterization 103
4.5.2. Differential scanning calorimetry (DSC) 103
4.5.3. Dynamic mechanical analysis (DMA) 103
4.5.4. Thermal stability (TGA) 104
4.5.5. Mechanical properties 104
4.6. RESULTS AND DISCUSSION 104
4.6.1. Rheology 104
4.6.2. Differential scanning calorimetry (DSC) 107
4.6.3. Dynamical mechanical analysis (DMA) 109
4.6.4. Thermal stability (TGA) 113
4.6.5. Mechanical properties 116
4.7. CONCLUSIONS 117
4.8. REFERENCES 119

4.1. GRAPHICAL ABSTRACT

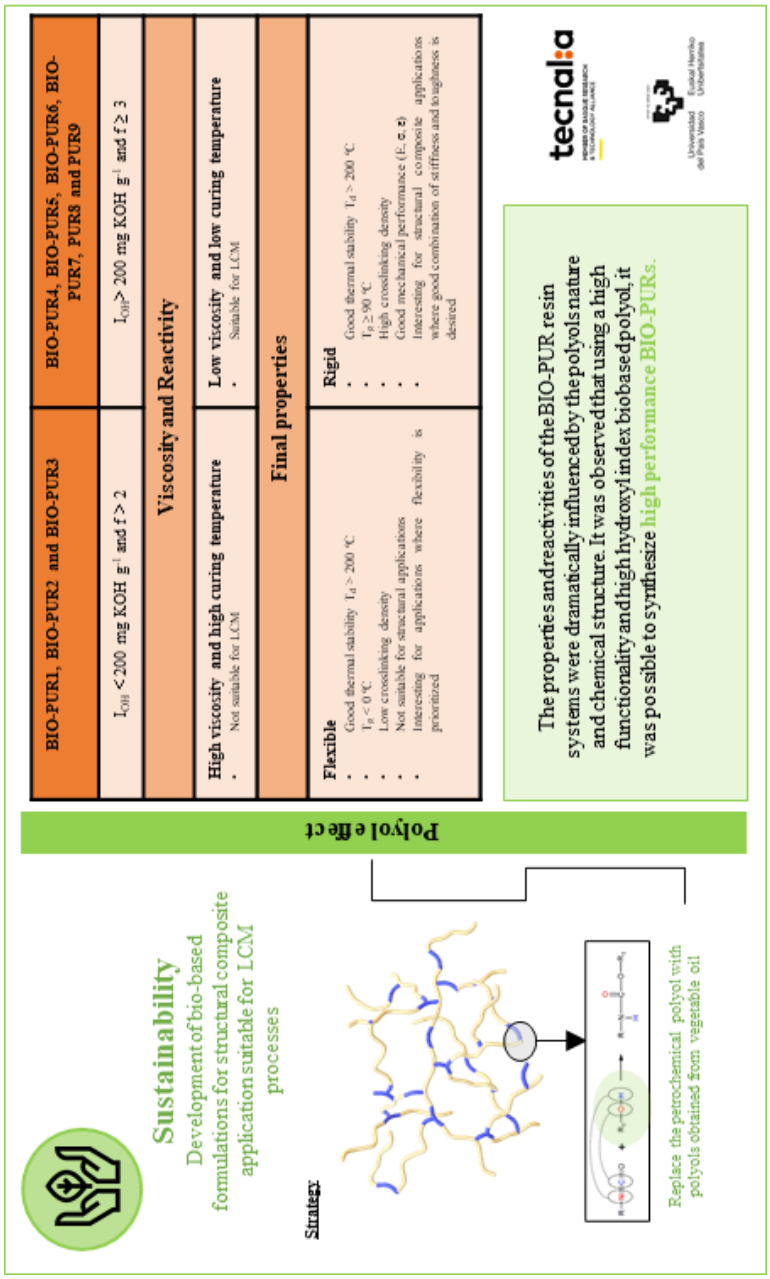

4.2. ABSTRACT

Actually, a broad range of biobased polyols are available in the market, but there is not a specific formulation for high-performance PURs composites. The aim of this chapter was to study the effect of biobased polyol chemical structure in the PUR characteristics (reactivity, viscosity and final properties). In addition, biobased polyol features to synthesize BIO-PURs suitable for structural applications were stablished. The viscosity and reactivity were studied by means of rheology and differential scanning calorimetry (DSC). Thermal and mechanical properties were studied through thermogravimetric analysis (TGA), dynamic mechanical analysis (DMA) and flexural tests. The results obtained demonstrated the dramatical influence of polyols nature on BIO-PUR/PUR properties and their effect on the crosslink density. It was observed that using a high functionality and high hydroxyl index biobased polyol, it was possible to synthesize high-performance BIO-PUR suitable for structural composites.

4.3. INTRODUCTION

In general, the interest on developing PUR formulations based on renewable resources is significantly increasing due to environmental, geopolitical and economical concerns derived from the commonly used fossil-based starting materials [1,2]. Actually, many biobased polyols,

mainly derived from vegetable oils, are available in the market to synthesize biobased PURs (BIO-PUR).

Vegetable oils are one of the cheapest and most abundant sustainable sources available in the world [3,4]. The use of biological sources as platform chemicals for polyol synthesis has numerous advantages, including inherent biodegradability and limited toxicity [5]. The most used oils are castor, soybean, sunflower, palm, canola and eucalyptus. Nowadays, there are different routes for the synthesis of polyols from these oils, which provide the possibility to produce a wide variety of biobased polyols [6,7].

BIO-PUR based on polyols derived from vegetable oils are being developed for a huge variety of applications. For instance, PU's are gaining increasing interest for biomedical applications due to their tuneable properties and the possibility of obtaining shape memory materials [8–10]. In this context, BIO-PU's have shown great biocompatibility and degradation properties compared to petrochemical based ones [11,12]. Also, BIO-PU's have shown their suitability for coatings [13–15], adhesives [16–18] or foams [19–21].

However, despite the intensive investigation on BIO-PURs, there is not a high-performance formulation suitable for structural applications. A biobased alternative suitable for structural composites should have low initial viscosity, latency and fast cure to allow fast and low-cost manufacturing processes together with high mechanical properties [22]. These characteristics are directly correlated to components nature, so a good selection of the biobased polyol is critical.

The aim of this work was to study the effect of the biobased polyols structure on the reactivity, viscosity and final properties of the BIO-PUR resin systems in order to find the keys to formulate biobased systems suitable for high-performance composites. For this purpose, several BIO-PUR based on biobased polyols with different characteristics, such as functionality and OH index, were formulated, and compared to PURs based on petrochemical polyols. The viscosity and reactivity of the different BIO-PUR/PUR resin systems were studied by means of rheology and differential scanning calorimetry (DSC). Thermal and mechanical properties were evaluated by thermogravimetric analysis (TGA), dynamic mechanical analysis (DMA) and flexural tests.

4.4. EXPERIMENTAL

4.4.1.Materials

Different renewably sourced commercial polyols were employed in the synthesis of BIO-PURs. Their renewable content, hydroxyl index (I_{OH}), functionality (f), equivalent weight and viscosity values, provided by the supplier or determined in their absence, are summarized in Table 1. Moreover, two petrochemical origin polyols were also used for comparative purposes (***¡Error! No se encuentra el origen de la referencia.***). The second component was an isocyanate (Voraforce TR1500-Isocyanate from Dow Chemical, NCO equivalent weight = 136 $g \cdot eq^{-1}$ and viscosity = 130 mPa·s). NCO equivalent weight was determined according to the ASTM D2572-97

Table 4.1. Propesties of polyols.

	I_{OH}	f	Viscosity at 25 ºC	Renewable content	Equivalent weight
	mg KOH g^{-}		*mPas*	*%*	*g OH eq^{-1}*
Polyol-1	60	3.1	24600	73	935
Polyol-2	86	2.5	5000	80	652
Polyol-3	71	>2	11000	56	790
Polyol-4	203	4	27050	60	276
Polyol-5	400	3	1500	80	141
Polyol-6*	330	4	3000	80	170
Polyol-7	280	4	1385	80	200
Polyol-8**	400	3	373	0	140
Polyol-9**	490	5	22750	0	114

* 25% of secondary OH groups according to data sheet
** 100% of secondary OH groups according to data sheet

4.4.2. Synthesis

Nine BIO-PUR/PUR systems were synthesised, seven with a biobased polyol, BIO-PUR1 to BIO-PUR7, and two with a petroleum derived polyol, PUR8 and PUR9, as references. The isocyanate index was maintained constant (equal to 1.2) for all the PUR/BIO-PUR systems studied. The designation, composition and renewable content of the BIO-PUR/ PUR systems are summarized in *Table 4.2.* All formulations are based on 100 parts by weight of polyol (pbw).

Table 4.2. Summary of synthesized BIO-PUR/PUR systems.

System	Polyol (pbw)	Isocyanate (pbw)	Renewable content %
BIO-PUR1	100 (Polyol-1)	17.5	63.1
BIO-PUR2	100 (Polyol-2)	25.1	63.9
BIO-PUR3	100 (Polyol-3)	20.7	71.3
BIO-PUR4	100 (Polyol-4)	80.6	33.2
BIO-PUR5	100 (Polyol-5)	116.7	36.9
BIO-PUR6	100 (Polyol-6)	96.3	40.8
BIO-PUR7	100 (Polyol-7)	81.7	44.0
PUR8	100 (Polyol-8)	116.7	0
PUR9	100 (Polyol-9)	143.0	0

The renewable content of BIO-PURs was determined according to the weight percentage and renewable content of the biobased components. All BIO-PURs have a renewable content higher than 33%.

BIO-PUR/PURs were synthesised using one-step bulk polymerization process, according to the reactant's ratios shown in Table 2. Before the BIO-PUR/ PUR synthesis reaction, all components, polyols and isocyanate, were degassed under vacuum to remove any trace of moisture. The reaction components were prepared as shown in *Figure 4.1a*. The BIO-PUR/PUR plates were manufactured by casting the resin into a mould and curing it in an oven at 120 ºC for 1 hour (*Figure 4.1b*).

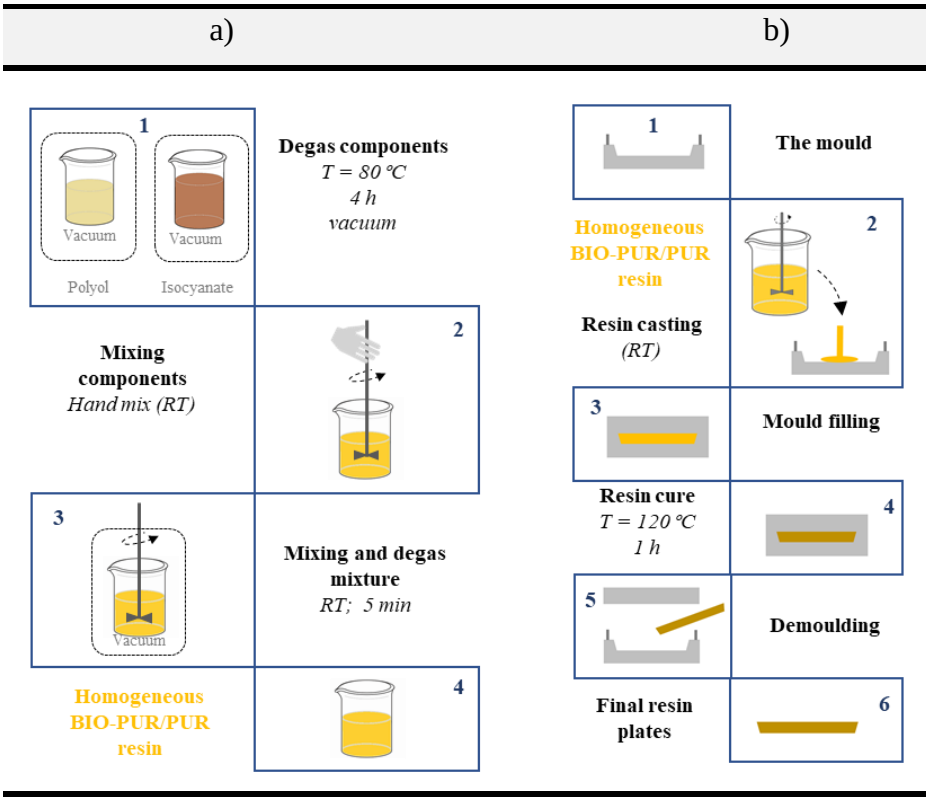

Figure 4.1. a) BIO-PUR/ PUR sample preparation and b) resin plates casting process.

4.5. CHARACTERIZATION

4.5.1.Rheological characterization

Rheological tests were carried out on a HAAKE RheoStress 6000 Rheometer (Thermo Fisher Scientific, Massachusetts, USA), running in an oscillating stress mode at a frequency of 1 Hz. Amplitude was held constant in the Linear Viscoelastic Range (LVR) throughout the test. A gap separation of 1 mm and disposable parallel plates of 60 mm diameter were used. Experiments were performed at dynamic or temperature sweep test conditions. Temperature sweep tests were performed from 25 to 200 ºC at a constant heating rate of 5 ºC min^{-1}. Storage and loss moduli, G' and G'' respectively, and complex viscosity, η*, were measured over temperature.

4.5.2.Differential scanning calorimetry (DSC)

Differential scanning calorimetry (DSC) tests were carried out on a TA Instruments DSC Q100 (TA Instruments, New Castle, USA) calorimeter in dynamic conditions. The experiments were performed from -90 to 200 ºC at 10 ºC min^{-1} heating rate. All samples were subjected to a subsequent dynamic scan from -90 to 200 ºC at 10 ºC min^{-1} to evaluate the presence of residual curing.

4.5.3.Dynamic mechanical analysis (DMA)

Dynamic mechanical analysis (DMA) tests were carried out using the Gabo Eplexor100N (Netzch, Selb, Germany) dynamic

mechanical analyser. Temperature scans were performed from -40 to 200 ºC at 2 ºC min^{-1} heating rate and at a frequency of 1 Hz. The sample dimensions were 2.2 x 5 x 50 mm^3. The T_g of the PUR resin systems was taken at the temperature value of the maximum of tan δ, [23,24].

4.5.4.Thermal stability (TGA)

The thermal stability of the cured PURs was analysed by thermogravimetric analysis (TGA) using a Mettler Toledo TGA/SDTA851 (Mettler Toledo, Columbus, USA) equipment. Temperature scans were performed from RT to 600 ºC at a heating rate of 10 ºC min^{-1}, under nitrogen atmosphere.

4.5.5.Mechanical properties

The flexural tests were carried out at RT using a Instron 5967 (Instron, Norwood, USA) equipment, with a 3-point bending device, according to ISO 178 standard.

4.6. RESULTS AND DISCUSSION

4.6.1.Rheology

Liquid composite moulding process (LCM) in its different versions such RTM, H-RTM, C-RTM or infusion is used more and more to produce structural composites because of its numerous advantages.

In these processes the viscosity is a critical factor. Some latency is needed in the first part of the process to maintain a low viscosity value

and to facilitate the fibre impregnation. Then, a high reactivity is desired to reduce curing times and allow fast production cycles.

Before curing, the BIO-PUR systems showed in general higher viscosity values than the two petroleum derived references PURs (*Figure 4.2*). This can be related to i) the lowest content of low viscosity isocyanate and ii) the different polyol nature.

Among the different BIO-PURs, BIO-PUR1 showed the highest initial viscosity value and BIO-PUR5 showed the lowest one due to their lowest and highest isocyanate content, respectively. On the other hand, the polyols properties such as, functionality, hydroxy number and molecular weight also affected directly on the component's viscosity. The viscosity of the polyols depends on the functionality or hydroxyl number due to the quantity of hydroxyl groups capable of forming hydrogen bonds [25]. This is the reason why Polyol-4 and Polyol-9 showed very high viscosity values (22750 and 27050 mPas, respectively). However, after mixing them with isocyanate, the hydrogen bonds concentration decreased and viscosity value decreases down to 3990 and 1140 mPas respectively. The effect of the molecular wight could be observed on BIO-PUR1, this systems present the highest viscosity value because of the effect of the Polyol-1 high molecular weight [26,17].

Figure 4.2 shows results of the complex viscosity evolution for the different BIO-PUR/PURs resins. At low temperatures viscosity decreased with temperature until the curing started accompanied by an abrupt increase of viscosity. Regarding the effect of hydroxyl index value and polyol functionality in the reactivity, it can be observed that in the case of biobased polyols with the lowest hydroxyl index value (I_{OH} <

100 *mg KOH* g^{-1}), BIO-PUR1, BIO-PUR2 and BIO-PUR3, the curing started at higher temperatures, showing a higher latency. At these hydroxyl indexes, the increase of the functionality results in an increase of the reactivity of the system showing lower curing starting temperature as in the BIO-PUR1. For higher hydroxyl index value (I_{OH} > 200 *mg KOH* g^{-1}), there was a decrease of reaction starting temperature as for BIO-PUR4 with functionality 4. This effect was observed even for the lowest functionality system such BIO-PUR5 were its lower functionality (f=3) was compensated by its higher hydroxyl value (I_{OH} = 400 *mg KOH* g^{-1}).

However, these were not the only factors affecting the resins viscosity evolution. In addition to I_{OH} and functionality, the type of hydroxyl group, primary or secondary, has to be considered. In this way, if we compare BIO-PUR6 and BIO-PUR7, both with the same functionality, it can be observed that although BIO-PUR6 has a higher hydroxyl index, the curing started at higher temperature. This can be attributed to the fact that the polyol employed in BIO-PUR6 has a secondary hydroxyl group that is less reactive than primary hydroxyl group [28-30]. The same effect can be seen in the reference PUR8 and PUR9 systems, which contain only secondary hydroxyl groups. Regarding PUR9, it can be also observed that an increase of I_{OH} and functionality results in a faster curing.

Comparing the different options, it can be seen that BIO-PURs based on polyols with high functionality (f = 4) and high OH index (200 mg KOH g^{-1} < I_{OH} < 330 mg KOH g^{-1}) like BIO-PUR4, BIO-PUR6 and BIO-PUR7, or polyols with f = 3 and I_{OH} = 400 mg KOH g^{-1} like BIO-

PUR5, could provide promising viscosity and reactivity to formulate systems for LCM processes.

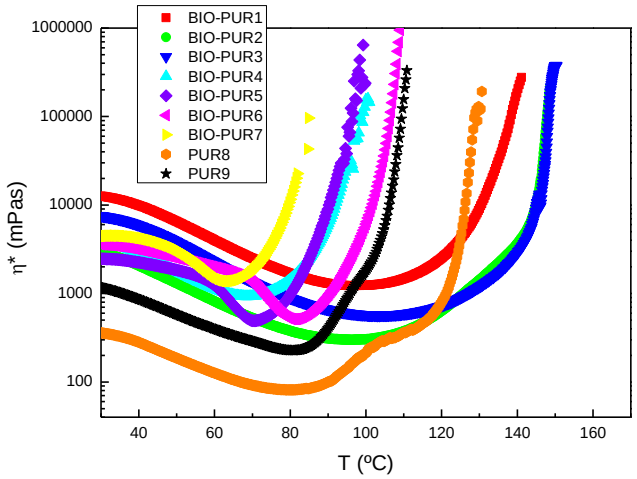

Figure 4.2. Complex viscosity evolution with temperature of the different BIO-PUR and PUR.

4.6.2.Differential scanning calorimetry (DSC)

The curing reaction of BIO-PURs was also characterised by dynamical DSC tests (*Figure 4.3*). The obtained thermograms were in accordance with rheological tests results. The resin systems formulated with polyols with high functionality and OH index higher than 200 mg KOH g^{-1} presented the fastest cures. BIO-PURs based on polyols with OH index lower than 100 mg KOH g^{-1} exhibited significantly slower curing reactions. As can be seen in *Figure 4.3*, the exothermic peaks corresponding to the curing of BIO-PUR1, BIO-PUR2 and BIO-PUR3 started and finished at higher temperatures. Also, BIO-PUR6 and PUR8 and PUR9 presented slower cures than their counterparts with similar functionality and OH index, due to the different hydroxyl group type. These results demonstrate that BIO-PUR/PURs reactivity directly

correlated with the polyol OH index, functionality and secondary hydroxyl group content.

The total heat of reaction is summarized in the *Table 4.3*. For the different BIO-PUR/PUR systems, the total heat of reaction increased with the increase of I_{OH}, which is mainly related with the total hydroxyl or isocyanate groups content, thus the formed urethane groups density. However, other factors should be also considered such as the functionality and hydroxyl group type. BIO-PURs showed in general lower total heat release than PURs, which is of interest for structural composite manufacturing processes to avoid overheating due to exotherm, especially in the case of thick laminates.

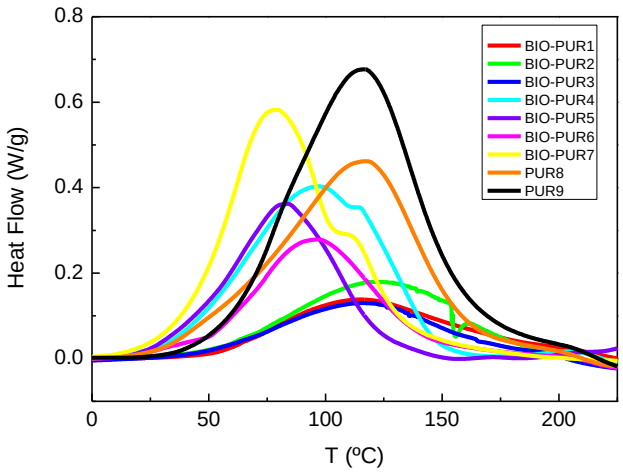

Figure 4.3. Dynamic DSC thermograms.

Table 4.3. Total heat of cure reaction of different BIO-PUR/PUR's systems.

System	Total heat of reaction ($J\ g^{-1}$)
BIO-PUR-1	72
BIO-PUR2	99
BIO-PUR-3	73
BIO-PUR-4	164
BIO-PUR-5	121
BIO-PUR-6	109
BIO-PUR-7	211
PUR-8	207
PUR9	278

4.6.3.Dynamical mechanical analysis (DMA)

BIO-PUR/PURs plates for DMA were prepared by casting and curing 1 h at 120 ºC. BIO-PUR1, BIO-PUR2 and BIO-PUR3 presented high flexibility, while the other systems were stiffer at RT (*Figure 4.4*).

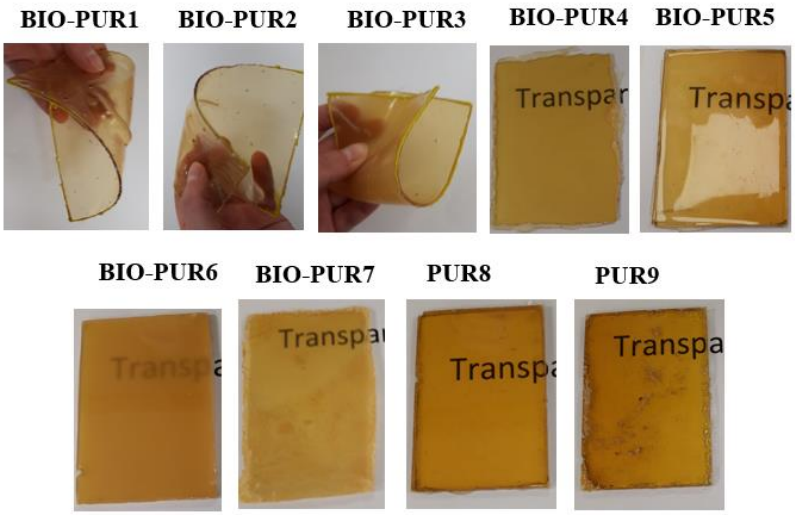

Figure 4.4. BIO-PURs and PURs plates.

Figure 4.5 shows tan δ and storage modulus, E', as a function of temperature for the synthesized BIO-PUR's and PUR's systems. Flexible BIO-PURs with low OH index (I_{OH} <100 mg KOH g^{-1}), showed T_g values below RT (*Figure 4.5a*), while BIO-PURs with I_{OH} > 200 mg KOH g^{-1} showed T_g values above RT (*Figure 4.5a*).

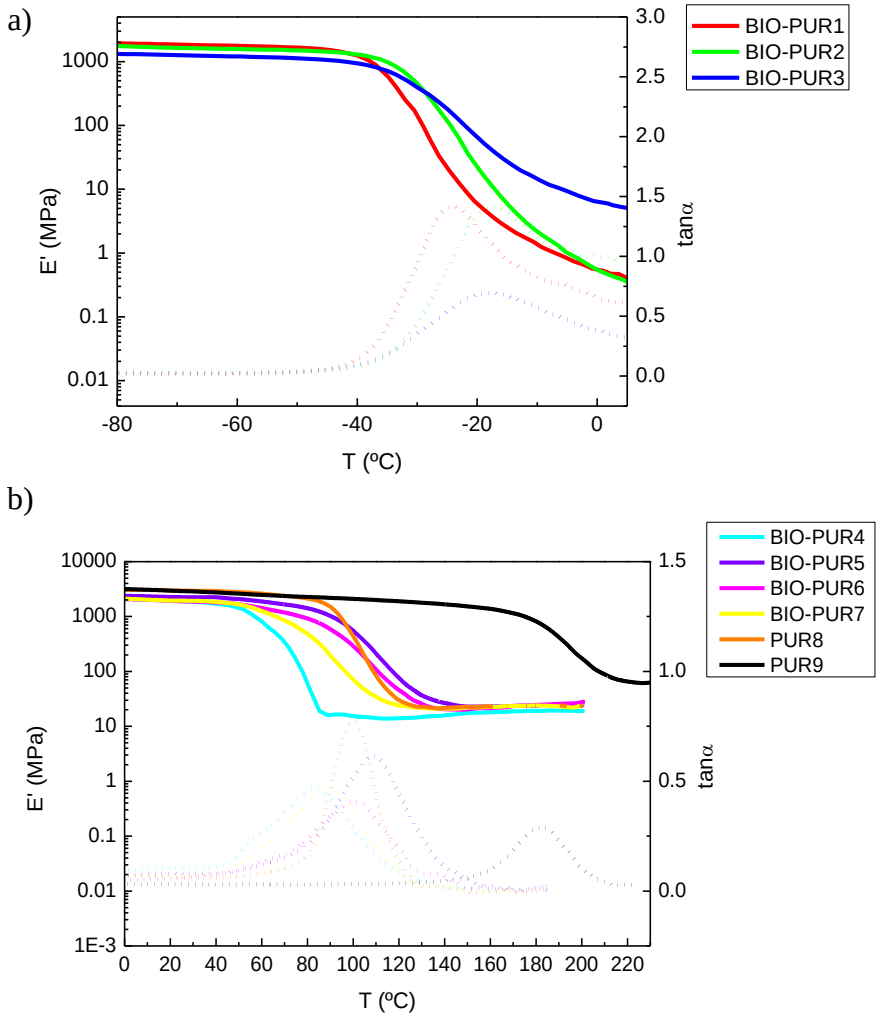

Figure 4.5. Curves of loss factor (tan δ, dashed line) and storage modulus (E', continuous line) vs temperature. a) Flexible BIO-PUR systems flexural geometry and b) Rigid BIO-PUR and PUR systems.

The cross-linking density was calculated from the storage modulus in the rubbery interval according to equation (4.1) [23,24].

$$v(mol\ m^{-3}) = \frac{E'_{T_g+50}}{3\ R\ (T_g + 50)} \qquad (4.1)$$

where E'_{Tg+50} is the storage modulus in the rubbery region (at T_g + 50 ºC), R is the universal gas constant (8.314 J mol^{-1} K^{-1}) and Tα is the glass transition temperature in Kelvin. Results are shown in *Table 4.4.*

Table 4.4. Crosslinking density and T_g values of different BIO-PUR/PUR systems.

System	v (mol m^{-3})	E' (T_g+50) (MPa)	T_g (ºC)	E' (25 ºC) (GPa)
BIO-PUR-1	---	---	-17	---
BIO-PUR2	---	---	-17	---
BIO-PUR-3	---	---	-25	---
BIO-PUR-4	1516	15.6	90	1.8
BIO-PUR-5	2145	23.7	119	2.3
BIO-PUR-6	1938	20.5	101	2.1
BIO-PUR-7	1992	20.9	97	2.0
PUR-8	1830	23.3	108	2.9
PUR9	8020	106.3	187	3.0

As it can be observed in *Figure* 4.6, where the structure of the synthesised BIO-PUR7PURs is schematically represented, BIO-PUR1-3 systems presented a low crosslinking density network that resulted in T_g values below RT. In addition, above T_g temperature these formulations showed very high flexibility, the polymer chains presented high mobility, so that caused very high elongation and low resistance during the DMA tests (*Figure 5a*). Despite not shown here, the same results were obtained in tensile geometry. Consequently, the test did not provide accurate results above 0 ºC and the crosslinking density

determination was not possible for these systems. BIO-PUR1-3 systems could be interesting for flexible components but there are not suitable for the target structural composite applications.

In contrast, BIO-PUR4-7, PUR8 and PUR9 presented higher T_g values, due to the higher crosslinking density network and the lower chain mobility (*Figure 4.5b* and *Figure 4.6)*. If we compare BIO-PUR 4-7, BIO-PUR5 showed the highest T_g value and storage modulus (E'). This is due to its higher urethane density, which is comparable to the PUR8 reference system with a slightly lower T_g and crosslink density. PUR9 ref system showed the higher T_g and storage modulus values according to higher crosslinking density.

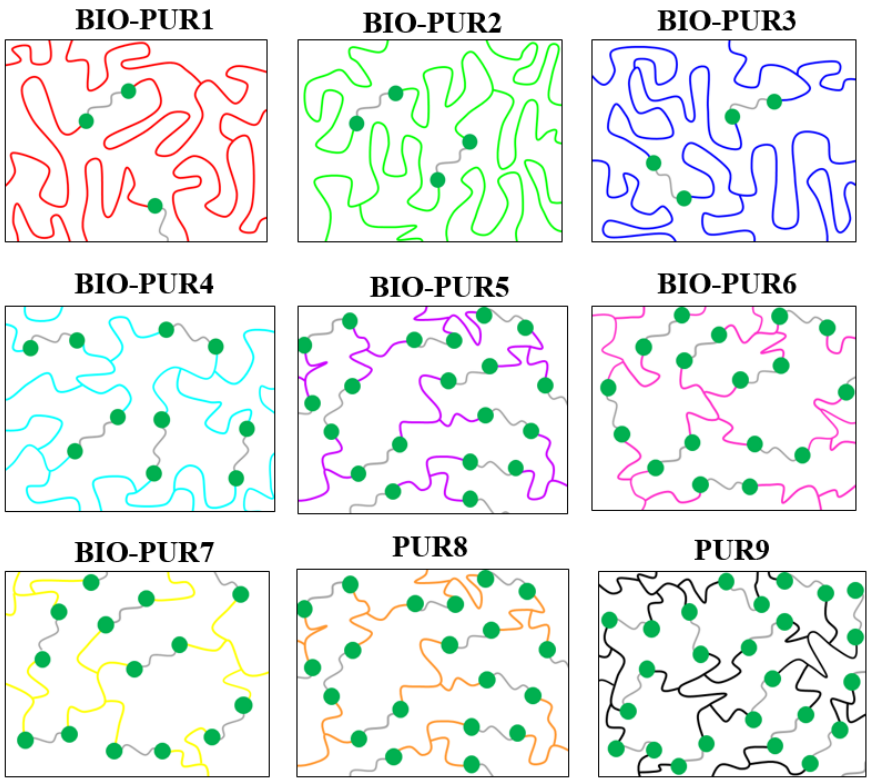

Figure 4.6. Scheme of the different three-dimensional networks of the BIO-PUR/PUR systems.

According to these results, the following systems were selected to compare the final properties of the cured resins. One flexible system (BIO-PUR1), two BIO-PUR rigid systems with different crosslink density (BIO-PUR4 and BIO-PUR5), and the petrochemical origin reference system with the highest properties (PUR9).

4.6.4.Thermal stability (TGA)

Figure 4.7 shows the results of the thermogravimetric curves for the selected BIO-PUR and PUR systems.

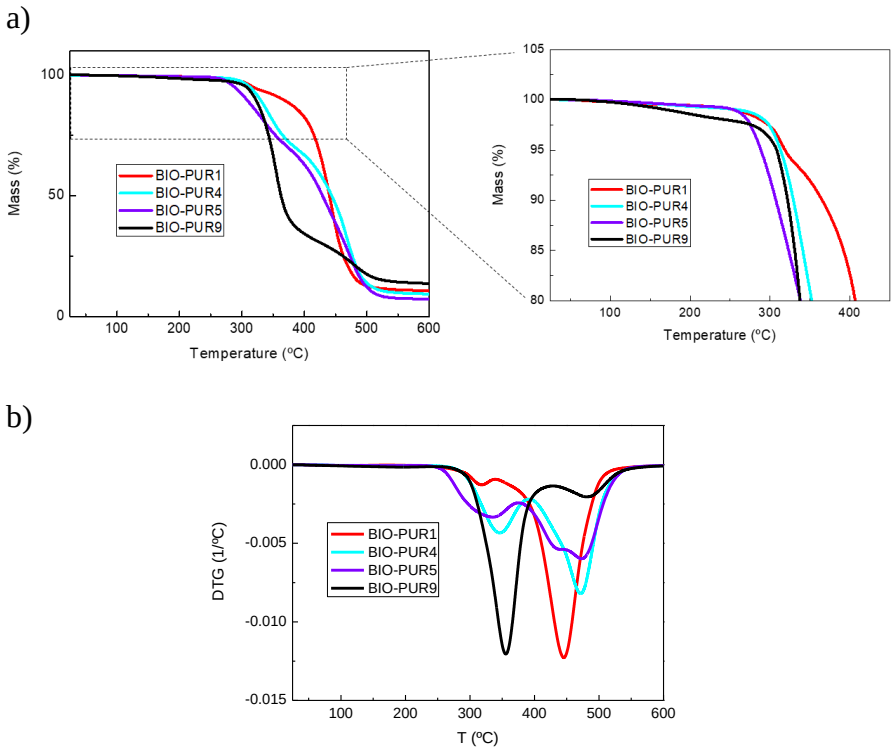

Figure 4.7. a) TG curves b) DTG curves for the BIO-PUR and PUR systems

The thermal stability of PURs was related with the structural differences in the reactants. Two regions were clearly appreciated in the decomposition of all analysed systems. The first one corresponds to the dissociation of urethane bonds (200-350 ºC) and the second region (370–500 ºC) to the polyol degradation and the residues formed during the previous degradation steps that further degrade to form char residue [31].

As shown in *Figure 4.7* in all studied formulations the weight loss started at temperatures higher than 200 ºC so it can be concluded that all BIO-PUR/PURs systems had a suitable thermal stability. The onset of weight loss was similar for all studied systems except for BIO-PUR5 and PUR9 where degradation started at a slightly lower temperature. It is reported that the degradation onset temperature of PURs depends both on urethane groups density and structural differences [32,33]. The degradation onset temperature sifts to lower temperatures as polyol I_{OH} and functionality increases. Javni et al. analysed the thermal stability of different polyurethanes synthesized from polyols derived from different vegetable oils and observed that those synthesized with polyols containing double bonds in their structure presented lower thermal stability and more complex degradation mechanism [32,34,35]. Therefore, the lower thermal stability observed for BIO-PUR5 could be attributed to its high urethane density (*Figure* 4.6 *and Table 4.4)* and to its unsaturated chain as shown in the 3600-2575 cm^{-1} interval of the FTIR spectra of the selected polyurethanes polyol (*Figure 4.8*).

Moreover, several differences between the different systems in terms of percentage of weight loss of each region could be appreciated. *Figure 4.7* shows that in the urethane cleavage temperature region the PUR9 presented the largest mass loss (around 62%). This system was

based on the polyol with the highest OH index and as previous results demonstrated the higher crosslinking density (*Figure* 4.6). The BIO-PUR4 and BIO-PUR5 also presented large mass loss in the urethane cleavage region (27% and 31%). Conversely, when the crosslink density is significantly lower, the mass loss is not large (6%) as for BIO-PUR1 with I_{OH} < 100 mg KOH g^{-1}.

In the second temperature region, the opposite effect could be appreciated. The mass loss in that region decreased with the crosslinking density. In this step polyol degradation occurred and also the oxidation of the char residue. Therefore, system based on low OH index polyols (BIO-PUR1), showed a significative mass loss. Moreover, PUR9 presented the higher residue due to the higher content of aromatic isocyanate used in its synthesis.

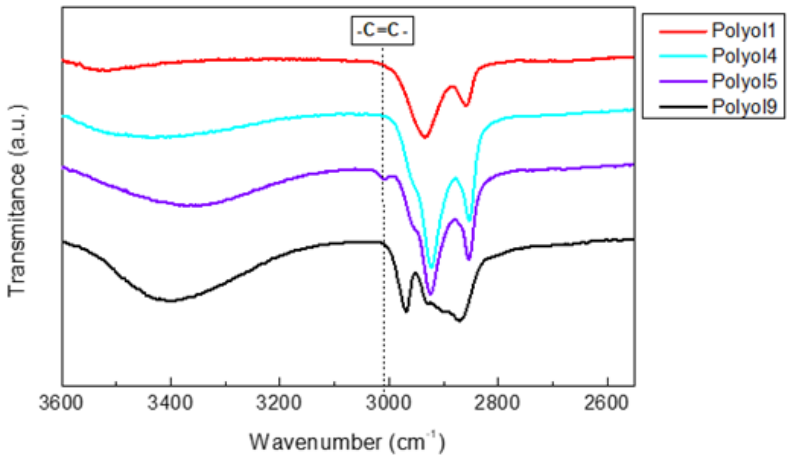

Figure 4.8. FTIR spectra of selected polyurethane polyols in the 3600-2575 cm^{-1} interval.

4.6.5.Mechanical properties

Table 4.5 summarizes the results of flexural tests for the BIO-PUR/PUR systems.

Table 4.5. Flexural properties of PUR/BIO-PUR systems.

Systems	Flexural strength	Flexural modulus	Flexural strain to failure
	MPa	*GPa*	*%*
BIO-PUR1	10.8 ± 1.6	0.01 ± 0.00	No break
BIO-PUR4	73.7 ± 2.0	1.85 ± 0.01	6.4 ± 0.3
BIO-PUR5	92.8 ± 4.3	2.17 ± 0.07	6.6 ± 0.7
PUR9	115.0 ± 1.3	3.13 ± 0.02	6.0 ± 0.0

Flexural modulus values are in accordance with the DMA tests results. BIO-PUR1 system presented low flexural strength and modulus and a high elastic deformation. Samples did not break during the test and they recovered the initial deformation. (Figure 4.9).

Figure 4.9. Flexural test for BIO-PUR1.

In general, the properties for the rest of the BIO-PURs were satisfactory. BIO-PUR5 presents very promising results. However, the modulus was still lower than the reference petrochemical origin. Nevertheless, these properties could be further enhanced by the addition of other components on the formulation such cross-linking agents to increase the network rigidity [24,36].

4.7. CONCLUSIONS

In this chapter different BIO-PUR/PUR systems based on different biobased polyols and petrochemical based polyols were investigated in order to understand the effect of biobased polyols characteristics on the resin viscosity, reactivity and final properties.

Rheology, DSC, DMA, TGA and flexural test results show that BIO-PUR/PURs behaviour are closely related to the polyol's hydroxyl index value, functionality and hydroxy group type as well. The initial viscosity of the resin depends on polyols initial viscosity, which is associated to their chemical structure. The BIO-PURs showed wide variety of reactivities, including fast curing if the functionalities and hydroxy index values were high. In the same way, high functionality and high hydroxy index polyols led to high crosslinking density BIO-PURs with high modulus and high T_g values.

Formulations based on polyols with low functionalities ($f < 3$) and low hydroxyl index value (IOH < 200 mg KOH g^{-1}) like BIO-PUR1-3, presented high initial viscosity, low reactivity and they were very flexible materials. These types of biobased polyols are not suitable for structural applications.

On the other hand, due to the good balance of biobased polyols functionality ($f \geq 3$) and hydroxyl index value ($I_{OH} > 200$ mg KOH g^{-1}) BIO-PUR4-7 showed high reactivities. Moreover, all these systems showed T_g value higher than 90 ºC. Among all BIO-PURs, BIO-PUR5 presented a promising combination of low viscosity before curing, high reactivity, high T_g and good mechanical properties for the target application. The flexural modulus seemed to be the only factor to be improved in order to get properties equivalent to the petrochemical origin structural PUR system (PUR9). However, this property could be further enhanced by the addition of other components on the formulation.

4.8. REFERENCES

[1] Bobade, S. K.; Paluvai, N. R.; Mohanty, S.; Nayak, S. K.: Bio-Based Thermosetting Resins for Future Generation: A Review. *Polym. - Plast. Technol. Eng.* (2016), *55*.

[2] Calvo-Correas, T.; Martin, M. D.; Retegi, A.; Gabilondo, N.; Corcuera, M. A.; Eceiza, A.: Synthesis and Characterization of Polyurethanes with High Renewable Carbon Content and Tailored Properties. ACS Sustainable Chemistry and Engineering, **4** (2016). http://doi:10.1021/acssuschemeng.6b01578.

[3] Biermann, U.; Friedt, W.; Lang, S.; Lühs, W.; Machmüller, G.; Metzger, J. O.; Rüsch gen. Klaas, M.; Schäfer, H. J.; Schneider, M. P.: New Syntheses with Oils and Fats as Renewable Raw Materials for the Chemical Industry. Angewandte Chemie International Edition, **39** (2000). http://doi:10.1002/1521-3773(20000703)39:13<2206::aid-anie2206>3.0.co;2-p.

[4] Gandini, A.: Polymers from renewable resources: A challenge for the future of macromolecular materials. Macromolecules, **41** (2008). http://doi:10.1021/ma801735u.

[5] Lligadas, G.; Ronda, J. C.; Galiá, M.; Cádiz, V.: Plant oils as platform chemicals for polyurethane synthesis: Current state-of-the-art. *Biomacromolecules* (2010), *11*.

[6] Sardon, H.; Mecerreyes, D.; Basterretxea, A.; Avérous, L.; Jehanno, C.: From Lab to Market: Current Strategies for the Production of Biobased Polyols. *ACS Sustain. Chem. Eng.* (2021), *9*.

[7] Kyriacos, D.: *Biobased polyols for industrial polymers*;

[8] Calvo-Correas, T.; Gabilondo, N.; Alonso-Varona, A.; Palomares, T.; Corcuera, M. A.; Eceiza, A.: Shape-memory properties of crosslinked biobased polyurethanes. European Polymer Journal, **78** (2016). http://doi:10.1016/j.eurpolymj.2016.03.030.

[9] Zhang, L.; Huang, M.; Yu, R.; Huang, J.; Dong, X.; Zhang, R.; Zhu, J.: Bio-based shape memory polyurethanes (Bio-SMPUs) with short side chains in the soft segment. Journal of Materials Chemistry A, **2** (2014). http://doi:10.1039/c4ta01640h.

[10] Zhao, X.; Dong, R.; Guo, B.; Ma, P. X.: Dopamine-Incorporated Dual Bioactive Electroactive Shape Memory Polyurethane Elastomers with Physiological Shape Recovery Temperature, High Stretchability, and Enhanced C2C12 Myogenic Differentiation. ACS Applied Materials and Interfaces, **9** (2017). http://doi:10.1021/acsami.7b10583.

[11] Cui, B.; Wu, Q. Y.; Gu, L.; Shen, L.; Yu, H. bin: High performance bio-based polyurethane elastomers: Effect of different soft and hard segments. Chinese Journal of Polymer Science (English Edition), **34** (2016). http://doi:10.1007/s10118-016-1811-7.

[12] Wendels, S.; Avérous, L.: Biobased polyurethanes for biomedical applications. *Bioact. Mater.* (2021), *6*.

[13] Pan, X.; Webster, D. C.: New biobased high functionality polyols and their use in polyurethane coatings. ChemSusChem, **5** (2012). http://doi:10.1002/cssc.201100415.

[14] Patil, C. K.; Rajput, S. D.; Marathe, R. J.; Kulkarni, R. D.; Phadnis, H.; Sohn, D.; Mahulikar, P. P.; Gite, V. V.: Synthesis of bio-based polyurethane coatings from vegetable oil and dicarboxylic acids. Progress in Organic Coatings, **106** (2017). http://doi:10.1016/j.porgcoat.2016.11.024.

[15] Noreen, A.; Zia, K. M.; Zuber, M.; Tabasum, S.; Zahoor, A. F.: Bio-based polyurethane: An efficient and environment friendly coating systems: A review. *Prog. Org. Coatings* (2016), *91*.

[16] Sahoo, S.; Mohanty, S.; Nayak, S. K.: Biobased polyurethane adhesive over petroleum based adhesive: Use of renewable resource. *J. Macromol. Sci. Part A Pure Appl. Chem.* (2018), *55*.

[17] Tenorio-Alfonso, A.; Sánchez, M. C.; Franco, J. M.: A Review of the Sustainable Approaches in the Production of Bio-based

Polyurethanes and Their Applications in the Adhesive Field. *J. Polym. Environ.* (2020), *28*.

[18] Gadhave, R. V.; Mahanwar, P. A.; Gadekar, P. T.: Bio-Renewable Sources for Synthesis of Eco-Friendly Polyurethane Adhesives—Review. Open Journal of Polymer Chemistry, **07** (2017). http://doi:10.4236/ojpchem.2017.74005.

[19] Gama, N. V.; Soares, B.; Freire, C. S. R.; Silva, R.; Neto, C. P.; Barros-Timmons, A.; Ferreira, A.: Bio-based polyurethane foams toward applications beyond thermal insulation. Materials and Design, **76** (2015). http://doi:10.1016/j.matdes.2015.03.032.

[20] Kurańska, M.; Cabulis, U.; Auguścik, M.; Prociak, A.; Ryszkowska, J.; Kirpluks, M.: Bio-based polyurethane-polyisocyanurate composites with an intumescent flame retardant. Polymer Degradation and Stability, **127** (2016). http://doi:10.1016/j.polymdegradstab.2016.02.005.

[21] Peyrton, J.; Avérous, L.: Structure-properties relationships of cellular materials from biobased polyurethane foams. *Mater. Sci. Eng. R Reports* (2021), *145*.

[22] Echeverria-Altuna, O.; Ollo, O.; Calvo-Correas, T.; Harismendy, I.; Eceiza, A.: Effect of the catalyst system on the reactivity of a polyurethane resin system for RTM manufacturing of structural composites. Express Polymer Letters, **16**, 234–247 (2022). http://doi:10.3144/expresspolymlett.2022.19.

[23] Kim, T. H.; Kim, M.; Lee, W.; Kim, H.-G.; Lim, C.-S.; Seo, B.: Synthesis and Characterization of a Polyurethane Phase Separated to Nano Size in an Epoxy Polymer. Coatings, **9**, 319 (2019). http://doi:10.3390/coatings9050319.

[24] Morales-Cerrada, R.; Tavernier, R.; Caillol, S.: Fully Bio-Based Thermosetting Polyurethanes from Bio-Based Polyols and Isocyanates. Polymers, **13**, 1255 (2021). http://doi:10.3390/polym13081255.

[25] Petrović, Z. S.; Guo, A.; Javni, I.; Cvetković, I.; Hong, D. P.: Polyurethane networks from polyols obtained by

hydroformylation of soybean oil. Polymer International, **57**, 275–281 (2008). http://doi:10.1002/pi.2340.

[26] Zhang, C.; Madbouly, S. A.; Kessler, M. R.: Biobased Polyurethanes Prepared from Different Vegetable Oils. ACS Applied Materials & Interfaces, **7**, 1226–1233 (2015). http://doi:10.1021/am5071333.

[27] Colby, R. H.; Fetters, L. J.; Graessley, W. W.: The melt viscosity-molecular weight relationship for linear polymers. Macromolecules, **20**, 2226–2237 (1987). http://doi:10.1021/ma00175a030.

[28] Ionescu, M.; Petrović, Z. S.; Wan, X.: Primary hydroxyl content of soybean polyols. JAOCS, Journal of the American Oil Chemists' Society, **85** (2008). http://doi:10.1007/s11746-008-1210-5.

[29] Kurańska, M.; Prociak, A.: The influence of rapeseed oil-based polyols on the foaming process of rigid polyurethane foams. Industrial Crops and Products, **89**, 182–187 (2016). http://doi:10.1016/j.indcrop.2016.05.016.

[30] Dutta, A. S.: Polyurethane Foam Chemistry. In *Recycling of Polyurethane Foams*; Elsevier, (2018); pp. 17–27.

[31] Latere Dwan'isa, J. P.; Mohanty, A. K.; Misra, M.; Drzal, L. T.; Kazemizadeh, M.: Biobased polyurethane and its composite with glass fiber. Journal of Materials Science, **39** (2004). http://doi:10.1023/B:JMSC.0000017770.55430.fb.

[32] Javni, I.; Petrović, Z. S.; Guo, A.; Fuller, R.: Thermal stability of polyurethanes based on vegetable oils. Journal of Applied Polymer Science, **77** (2000). http://doi:10.1002/1097-4628(20000822)77:8<1723::AID-APP9>3.0.CO;2-K.

[33] Monteavaro, L. L.; Riegel, I. C.; Petzhold, C. L.; Samios, D.: Thermal stability of soy-based polyurethanes. Polímeros, **15** (2005). http://doi:10.1590/s0104-14282005000200018.

[34] Kaikade, D. S.; Sabnis, A. S.: Polyurethane foams from vegetable

oil-based polyols: a review. *Polym. Bull.* (2022).

[35] Ristić, I. S.; Bjelović, Z. D.; Holló, B.; Mészáros Szécsényi, K.; Budinski-Simendić, J.; Lazić, N.; Kićanović, M.: Thermal stability of polyurethane materials based on castor oil as polyol component. Journal of Thermal Analysis and Calorimetry, **111**, 1083–1091 (2013). http://doi:10.1007/s10973-012-2497-x.

[36] Tan, A. C. W.; Polo-Cambronell, B. J.; Provaggi, E.; Ardila-Suárez, C.; Ramirez-Caballero, G. E.; Baldovino-Medrano, V. G.; Kalaskar, D. M.: Design and development of low cost polyurethane biopolymer based on castor oil and glycerol for biomedical applications. Biopolymers, **109** (2018). http://doi:10.1002/bip.23078.

5

BIO-PUR SYSTEM OPTIMIZATION

5. BIO-PUR SYSTEM OPTIMIZATION

5.1. GRAPHICAL ABSTRACT 126
5.2. ABSTRACT 127
5.3. INTRODUCTION 128
5.4. EXPERIMENTAL 129
5.4.1. Materials 129
5.4.2. Samples preparation 132
5.5. CHARACTERIZATION 132
5.5.1. Rheological characterization 132
5.5.2. Differential scanning calorimetry (DSC) 133
5.5.3. Dynamic mechanical analysis (DMA) 134
5.5.4. Mechanical properties 134
5.6. RESULTS AND DISCUSSION 134
5.6.1. Rheological characterization 134
5.6.2. Differential scanning calorimetry (DSC) 136
5.6.3. Dynamical mechanical analysis (DMA) 138
5.6.4. Mechanical properties 140
5.6.5. Modelling and process simulation 141
5.7. CONCLUSIONS 148
5.8. REFERENCES 149

5.1. GRAPHICAL ABSTRACT

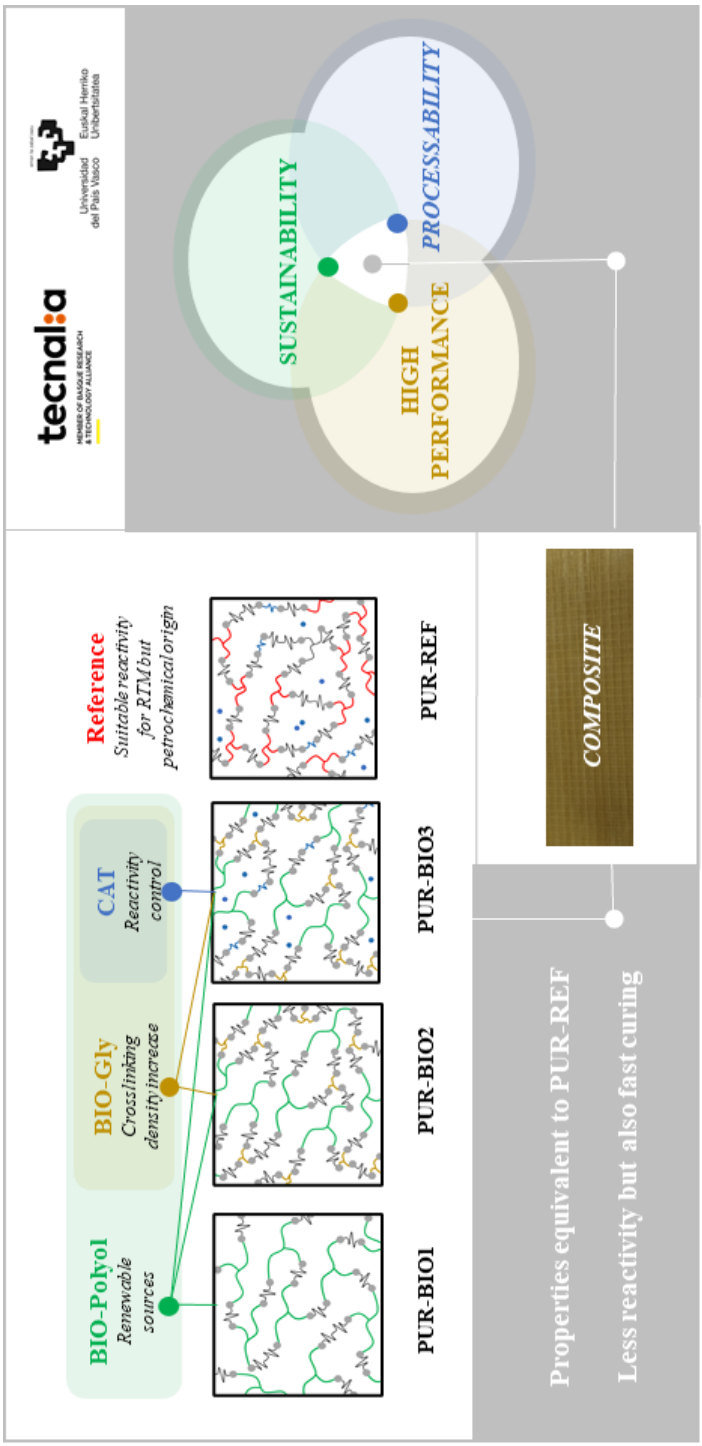

5.2. ABSTRACT

In the previous chapter we observed that using a high functionality and high hydroxyl index biobased polyol, it was possible to synthesize high-performance BIO-PUR with a promising combination of low viscosity, high reactivity, high T_g and good mechanical properties for structural composites. However, the flexural modulus should be improved to achieve properties equivalent to the petrochemical origin structural PUR.

In order to optimize the BIO-PUR formulation the high functionality (f=3) and hidroxyl value (I_{OH} = 400 mg KOH g-1) castor oil-based polyol was used combined with a biobased glycerol (BIO-Gly) to increase the crosslinking density and improve final properties

The viscosity and reactivity of the different resins were studied by means of rheology and Differential scanning calorimetry (DSC). Thermal and mechanical properties were studied by Dynamic mechanical analysis (DMA) and flexural tests. Furthermore, the RTM process of a representative composite part was simulated

The properties of the BIO-PUR resin systems were strongly influenced by the addition of biobased glycerol and its effect in the crosslink density giving a high-performance BIO-PUR with the required final properties for composite structural applications.

5.3. INTRODUCTION

As previously mentioned, the intensive investigation on BIO-PURs, there is not a high-performance formulation suitable for structural applications such as automotive parts[1–3].

The BIO-PUR characteristics are directly correlated to polyols nature, so a good selection of the biobased polyol is critical. In the previous chapter it was observed that using a high functionality and high hydroxyl index castor oil-based polyol, it was possible to synthesize BIO-PURs that could be suitable for structural applications. However, some of the properties such the elastic modulus was still lower than the reference petrochemical origin PUR. Nevertheless, these properties could be further enhanced by the addition of other components on the formulation such cross-linking agents to increase the network rigidity [4,5].

In order to achieve the desired rigidity, besides castor oil-based polyol, a biobased glycerol, BIO-Gly, was used in the synthesis of BIO-PUR. Glycerol was proven to be efficient for increasing the crosslinking density, Tg and toughness in non-structural BIO-PURs due to its low molecular weight [6–8]. Moreover, glycerol can be produced from renewable resources as byproduct in transesterification reaction in biodiesel plants or also in saponification and hydrolysis reactions in oleochemical plants [9].

Another aspect that has to be considered is the BIO-PUR reactivity. A biobased alternative suitable for structural composites

should have low initial viscosity, latency and fast cure to allow fast and low-cost manufacturing processes such RTM [10]. For this purpose, a delayed action catalyst based on epoxide and LiCl was added to the BIO-PUR formulation

The viscosity and reactivity of the different BIO-PUR resin systems were studied by means of rheology and Differential scanning calorimetry (DSC).

Furthermore, to evaluate the effect of BIO-Gly on the final properties, dynamic mechanical analysis (DMA) and flexural tests were performed. PUR-BIO systems characteristics were compared with one non-biobased PUR system suitable for RTM, which was used like a reference resin.

In order to evaluate the different alternatives and find the best process parameters of the RTM manufacturing a representative automotive composite part was simulated with ESI's PAM-RTM software.

Results showed the suitability of developed BIO-PUR formulation for structural automotive applications.

5.4. EXPERIMENTAL

5.4.1.Materials

In this work an MDI based commercial isocyanate (Voraforce TR 1500-Isocyanate, NCO equivalent weight = 136 g eq^{-1} and viscosity =

130 mPa s) supplied by Dow Chemical was employed. NCO content was determined according to the ASTM D2572-97.

In the case of polyols, two different components were used. The first polyol, used as a reference, was a petrochemical origin polyether-polyol, supplied by Dow Chemical (Voraforce TR 1551-Polyol, I_{OH} = 527 mg KOH g^{-1} and viscosity = 750 mPa s). The second polyol derived from castor oil was supplied by Vertellus (Polycin T-400, I_{OH} = 400 mg KOH g^{-1} and viscosity = 1500 mPa s). Hydroxyl number of Voraforce 1551 and Polycin T-400 were determined according to ASTM D 4274-88.

A biobased glycerol, BIO-Gly, supplied by Sigma Aldrich, was used as low-molecular-weight-crosslinking modulator.

The catalyst employed was a two-component system formed by an epoxide (1,4-butanediol diglycidyl ether, BDDE) and a halide salt (LiCl) dissolved in a low molecular mass biobased cycloaliphatic diol (1,4:3,6-dianhydro-D-glucitol or D-isosorbide, DAS). All the catalysts components were supplied by Sigma Aldrich.

Four PUR systems were synthesised, three biobased and one petroleum based as reference. The isocyanate index was maintained constant (equal to 1.2) for all the PUR systems studied. Designation and composition of the PUR systems are summarized in *Table 5.1*. All formulations are based on 100 parts by weight of polyol (pbw).

Table 5.1. Summary of synthesized polyurethanes

System	Component' s ratio (pbw)						Renewable content (%)
	Part A			Part B			
	Polyol	*Glycerol*	*BDDE*	*Isocyanat*	*LiCl*	*DAS*	
PUR-REF	100	-	7	181	3	12	4
BIO-PUR1	100	-	-	117	-	-	37
BIO-PUR2	100	22	-	233	-		29
BIO-PUR3	100	22	7	267	2	9	27

In the case of the glycerol containing mixtures (BIO-PUR2 and BIO-PUR3) the BIO-Gly was previously mixed with the biobased polyol. The reaction components were prepared as shown in *Figure 5.1*.

The addition of the catalysts (PUR-REF and BIO-PUR3) was performed following the same protocol as in Chapter 3.

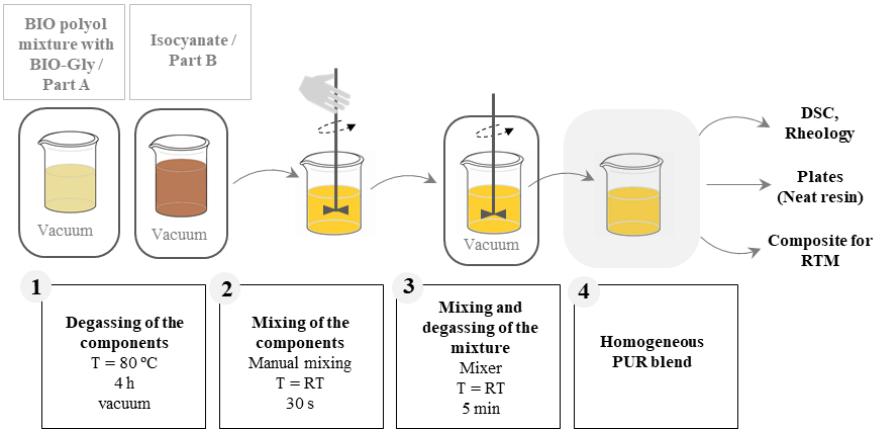

Figure 5.1. Polyurethane resin system preparation.

5.4.2.Samples preparation

The neat plates were manufactured by casting the resin into mould and curing in an oven at 120 ºC during 1 hour.

5.5. CHARACTERIZATION

5.5.1. Rheological characterization

Rheological tests were carried out on a HAAKE RheoStress 6000 Rheometer (Thermo Fisher Scientific, Massachusetts, USA), running in an oscillating stress mode at a frequency of 1 Hz. Amplitude was held constant in the Linear Viscoelastic Range (LVR) throughout the test. A

gap separation of 1 mm and disposable parallel plates of 60 mm diameter were used. Experiments were performed at dynamic or temperature sweep test conditions. Temperature sweep tests were performed from 25 to 200 ºC at a constant heating rate of 5 ºC min^{-1}. Storage and loss moduli, G' and G'' respectively, and complex viscosity, η*, were measured over temperature.

5.5.2. Differential scanning calorimetry (DSC)

Differential scanning calorimetry (DSC) tests were carried out on a TA Instruments DSC Q100 (TA Instruments, New Castle, USA) calorimeter in both dynamic and isothermal conditions. The dynamic experiments were performed from 20 to 200 ºC at three heating rates 5, 10 and 20 ºC min^{-1}. Isothermal experiments were performed at temperatures ranging from 50 to 120 ºC. All samples were subjected to a subsequent dynamic scan from 20 to 200 ºC at 10 ºC min^{-1} to determine the residual heat of reaction and the glass transition temperature, T_g, of the cured material. The T_g was taken as the midpoint of the heat capacity change and the total heat of reaction (H_T) was calculated from the integration of the area of the exothermic peaks.

The curing rates ($d\alpha/dt$) from the heat flow curves obtained in the dynamic and isothermal DSC tests equation (5.1) were integrated to calculate the degree of cure (α) profiles equation (5.2).

$$H = \frac{dH}{dt} = \frac{d\alpha}{dt} H_T \qquad (5.1)$$

$$\alpha = \int_0^t \frac{d\alpha}{dt} dt \qquad (5.2)$$

where *H* is the instantaneous heat evolved during the polymerisation reaction of the resin, and H_T is the total heat of the curing process.

5.5.3.Dynamic mechanical analysis (DMA)

Dynamic mechanical analysis (DMA) tests were carried out using the Gabo Eplexor100N (Netzch, Selb, Germany) dynamic mechanical analyser. Temperature scans were performed from -40 to 200 ºC at 2 ºC min^{-1} heating rate and at a frequency of 1 Hz. The sample dimensions were 2.2 x 5 x 50 mm^3. The T_g of the PUR resin systems was taken at the temperature value of the maximum of tan δ [5,11].

5.5.4.Mechanical properties

The flexural tests were carried out at RT using a Instron 5967 (Instron, Norwood, USA) equipment, with a 3-point bending device, according to ISO 178 standard

5.6. RESULTS AND DISCUSSION

5.6.1.Rheological characterization

Viscosity results from oscillatory temperature sweep test of from formulated systems are shown in *Figure 5.2.*

Temperature sweep rheology tests show the high reactivity of BIO PUR1. The viscosity decreased with temperature until the curing started accompanied by an abrupt increase of viscosity at 70ºC, which means that this system will start to react in a few seconds at the target process temperatures and will not have the necessary latency.

In the case of BIO-PUR2 and BIO-PUR3 the results showed the improvement on two ways, the reactivity control and the decrease of initial viscosity. BIO-PUR2 reactivity and viscosity evolution were comparable with the PUR-REF, petrochemical origin catalysed system. These two effects are attributed to the glycerol incorporation on the formulation. This cross-linking agent presents very low viscosity at RT, which has caused the BIO-PUR2 and BIO-PUR3 initial viscosity decrease. On the other hand, the secondary and lower reactivity hydroxy groups of the glycerol have delayed the BIO-PURs cure reaction. The addition of the catalyst to the BIO-PUR, decreased further the reactivity as in can be seen in the BIO-PUR3 viscosity evolution curve. In this case, the viscosity increase starts at 85 ºC, making the system suitable for a broader range of RTM process temperatures.

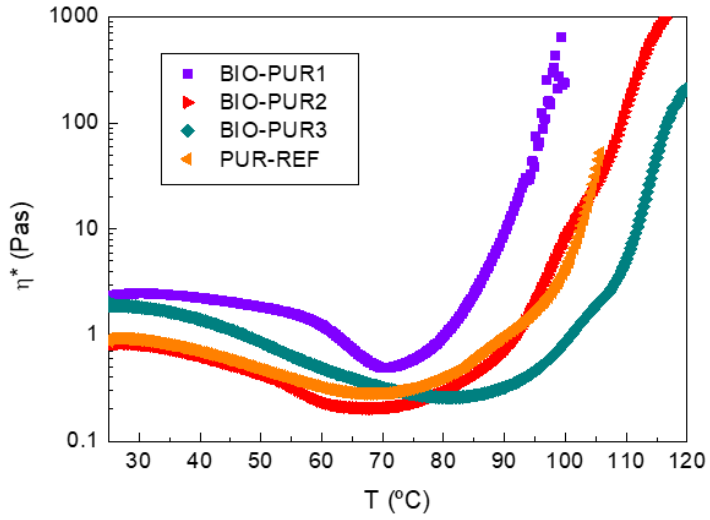

Figure 5.2. Complex viscosity evolution with temperature for different PUR systems.

5.6.2.Differential scanning calorimetry (DSC)

The curing reaction of BIO-PUR1, BIO-PUR2, BIO-PUR3 and PUR-REF was also characterized by both dynamical and isothermal DSC tests *Figure 5.3.*

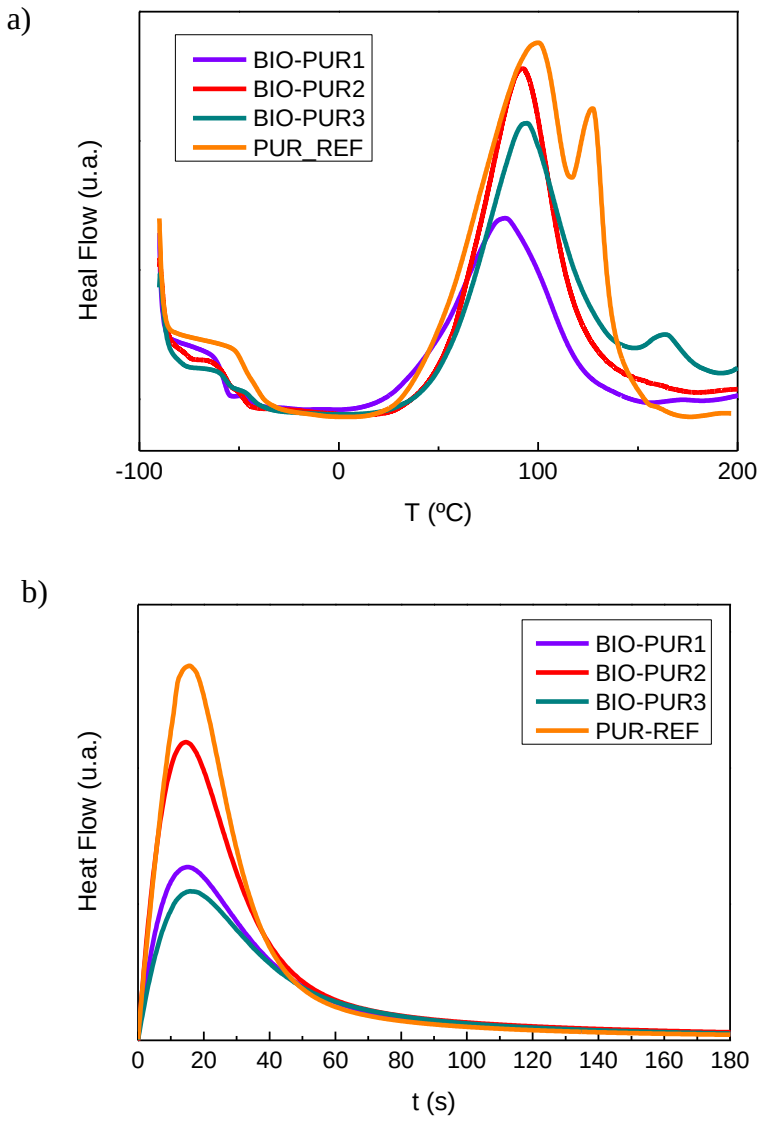

Figure 5.3 a) Dynamic DSC thermograms and b) isothermal DSC thermograms for the different PUR systems.

Figure 5.3a shows the thermograms obtained in dynamic conditions for the different systems at 10 ºC min^{-1}. As can be seen in the *Figure 5.3a*, the reaction is delayed for the BIO-PUR2 and BIO-PUR3 systems, suporting the retuls obatined on rheology tests. The BIO-PUR1 system peak has a maximum at 83 ºC, whereas it appears at 91 and 94 ºC for BIO-PUR2 and BIO-PUR3, respectively. Moreover, in the case of BIO-PUR3 and the reference system, the shape of the heat flow curve changes and a second peak can be appreciated at higher temperatures. This is attributed to the two-step catalytic mechanism as observed previuosly in Chapter 3.

Another critical issue for ultra-fast cure resins is the heat released during curing. Due to the fast heat production speed the resins can have temperature instabilities, especially in the case of thick laminates such as in the target application, hindering their processability. The total heat of reaction, taken as the value obtained at 10 ºC min^{-1} was 301 J g-1 for the PUR-REF system whereas for the biobased systems BIO-PUR1, BIO-PUR2 and BIO-PUR3 the heats were 121, 205 and 175 J g^{-1}respectively.

The total heat of reaction increased with the increase of I_{OH}, which is mainly related with the total hydroxyl or isocyanate groups content. This is the reason why the PUR-REF and BIO-PUR2 presented higher total heat of reaction. Moreover, other factors should be also considered like the functionality and polyols chemical structure. This is the reason why BIO-PUR1 presented lower heat of reaction than BIO-PUR2, BIO-PUR3 and PUR-REF.

BIO-PUR3 presented lower heat of reaction than the uncatalyzed system BIO-PUR2. As observed in Chapter 3, this is related to the catalyst components preparation. The components were mixed with the

isocyanate to form urethane prepolymer during the components preliminary preparation. In this step, some isocyanate groups react with hydroxyl groups in order to produce urethane groups and the heat released in this step was not measured in the later DSC cure.

Figure 5.3b shows the results obtained in the isothermal tests at 120 ºC (target process temperature). In the case of BIO-PUR1 maximum degrees of cure at 120 ºC 0.99-1 (full cure) are obtained whereas for PUR-BIO2 and PUR-BIO3 the maximum at 120 ºC are 0.97 and 0.96 respectively. The reference petrochemical origin system, PUR-REF, has a maximum degree of cure of 0.94. In all the cases, the maximum degree of cure atained is considered good enough to avoid postcuring.

5.6.3.Dynamical mechanical analysis (DMA)

Figure 5.4 shows the dynamic mechanical curves (storage modulus and tan δ) as a function of temperture for the PUR systems. The obtained values are summarized in *Table 5.2*.. The T_g of each material is taken the temperature value of the maximum of tan δ. The T_g of BIO-PUR1 gives value of 119 ºC, which is insufficient for automotive composite parts where a minimun of 120ºC is targeted as for PUR-REF, with a T_g of 124 ºC. On the other hand, for the BIO-PUR2 and BIO-PUR3 the values are higher, 167 ºC and 161 ºC respectively.

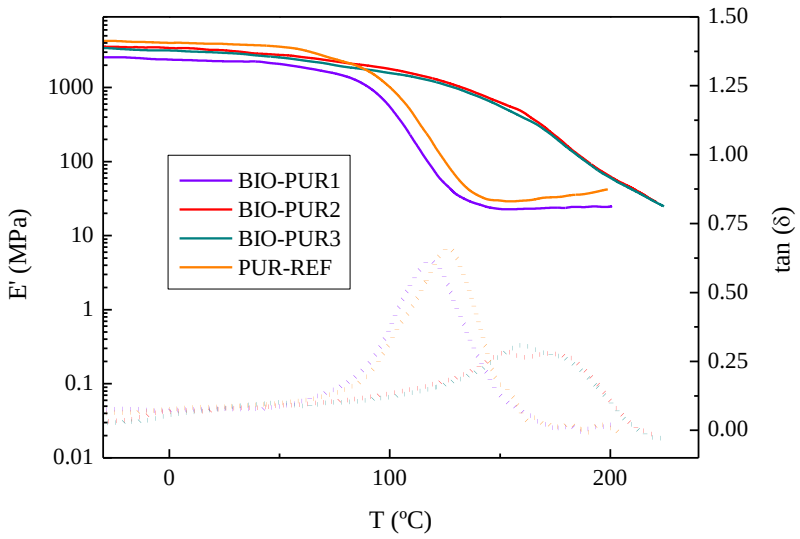

Figure 5.4. Curves of loss factor (tan δ, dashed line) and storage modulus (E', continuous line) vs temperature of different PUR systems.

Table 5.2. RT Storage modulus and T_g values for the different BIO-PUR/PUR systems.

System	T_g	E' (25 ºC)
	ºC	GPa
PUR-REF	124	3.4
BIO-PUR1	119	2.3
BIO-PUR2	167	3.2
BIO-PUR3	161	3.0

The changes in T_g are attributed to the low moculear weitght and high functionality of the BIO-Gly that produces an increase of the crosslinking density of the PURs. Moreover, the storage modulus is also affected by the decrease on the network mobility, ivcreasing significantly in the BIO-PUR2 and BIO-PUR3 systems compared with BIO-PUR1.

Figure 5.5 shows a schematic representation of the three-dimensional network of the PUR systems BIO-PUR1, BIO-PUR2, BIO-PUR3 and PUR-REF based on these results.

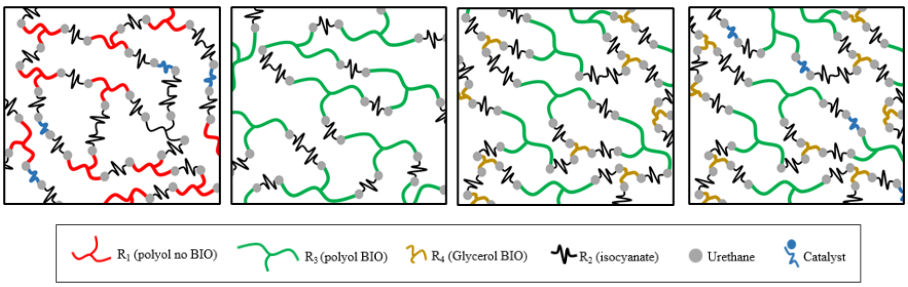

Figure 5.5. Scheme of the three-dimensional network of the different PUR systems.

5.6.4.Mechanical properties

Table 5.3 summarizes the mechanical properties of the PUR systems. It could be observed that with the addition of BIO-Gly as cross-linking agent, the flexural modulus and strength increases. Moreover, the BIO-PUR2 and BIO-PUR3 maintain the flexural strain, compared to BIO-PUR1. The results obtained in the flexural tests modulus are in accordance with those of the the DMA tests. BIO-PUR1 presents very promising results but the modulus was still lower than the reference petrochemical origin. However, when the glycerol was incorporated such in the BIO-PUR2 and BIO-PUR3 the mechanical properties were comparable with the petrochemical origin reference system properties showing their suitability for structural applications. It was also observed that the addition of the catalyst didn’t produce any significant difference on the mechanical properties.

Table 5.3. Flexural properties of the PUR systems.

Systems	Flexural strength	Flexural modulus	Flexural strain
	MPa	*GPa*	*%*
PUR-REF	139.0 ± 1.6	3.3 ± 0.1	6.6 ± 0.2
BIO-PUR1	92.8 ± 4.3	2.2 ± 0.1	6.6 ± 0.7
BIO-PUR2	124.2 ± 2.3	2.9 ± 0.1	6.9 ± 0.3
BIO-PUR3	127.6 ± 0.9	3.0 ± 0.1	6.5 ± 0.1

5.6.5.Modelling and process simulation

Next step was to evaluate the suitability of the developed systems (BIO-PUR2 and BIO-PUR3) for the target application. For this purpose, the RTM process was simulated. The composite part simulated was a leaf spring reinforced with 47% fibre volume content of high fatigue resistance (ultra-fatigue) unidirectional glass fibre. These parts are normally produced with a linear, lateral injection strategy with the resin inlet at the middle point of the part and the outlets at the ends (*Figure 5.6a*) so for the evaluations, only half length of the real part was considered.

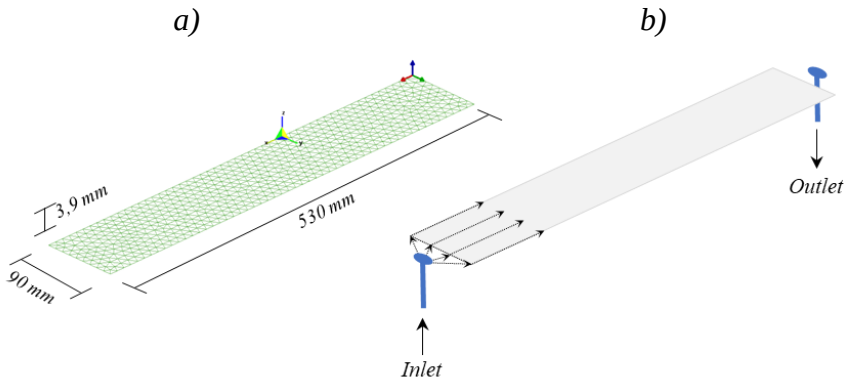

Figure 5.6. a) Mesh and b) injection strategy used in the simulation.

The flow of the polyurethane resin through the glass fibre fabric can be described by Darcy's law *(3.8)*.

$$Q = -\frac{S\,K}{\phi\eta^*}\nabla P \tag{5.3}$$

where Q denotes the resin flow rate, K is the preform permeability, S the cross-sectional area, ϕ the porosity, η* the resin viscosity and P represents the pressure. For the preform, a nominal permeability of 1.35e $^{-10}$ m^2 was considered for this fibre volume content [12].

On the other hand, as mentioned previously, resin viscosity depends on resin temperature and time. So, the curing reaction and viscosity evolution were modelled to obtain the rheo-kinetic equations.

For the cure kinetic modelling, the degree of cure curves obtained from the dynamic and isothermal DSC tests were fitted to the Kamal-Sourour equation *(3.3)* [13]. In order to consider the diffusion effect and have a good fitting in all the degree of cure ranges, we completed with a diffusion factor F(α) *(3.3)* [14].

$$\frac{d\alpha}{dt} = \left(k_1 e^{-\frac{E1}{T}} + k_2 e^{-\frac{E2}{T}}\alpha^m\right)(1-\alpha)^n F(\alpha) \tag{5.4}$$

$$F(\alpha) = \frac{1}{1 + e^{(Ed(\alpha-\alpha_c))}} \tag{5.5}$$

where

$$E_d = E_{d1} + E_{d2}\,T \tag{5.6}$$

and

$$\alpha_c = \alpha_{c1} + \alpha_{c2}\,T \tag{5.7}$$

are temperature dependent adjustable parameters.

In this equation α is the degree of cure, dα/dt is the reaction rate, n and m the reaction orders and T the temperature. The variables k_1, E_1

and k_2, E_2 are the preexponential factors and activation energies of the n^{th} and m^{th} order reactions, respectively and $F(\alpha)$ corresponds to the diffusion factor. The kinetic model parameters for each of the BIO-PUR2 and BIO-PUR3 are summarised in *Table 5.4.*

Table 5.4. Kinetic model parameters for the different BIO-PUR3.

		BIO-PUR2	**BIO-PUR3**
K_1	s^{-1}	2.59E+09	2.04E+09
E_1	ºK	5.76E+04	1.01E+04
K_2	s^{-1}	7.32E+05	7.57E+04
E_2	ºK	6.55E+03	5.56E+03
m		2.42E-01	4.96E-01
n		2.02E+00	2.39E+00
α_{c1}		-3.08E-01	-9.71E-01
α_{c2}		3.41E-03	5.00E-03
E_{d1}		-1.71E+02	7.28E+02
E_{d2}		8.10E-01	2.77E+01

As it can be seen in *Figure 5.7* there is a good correlation between the experimental results and the proposed models.

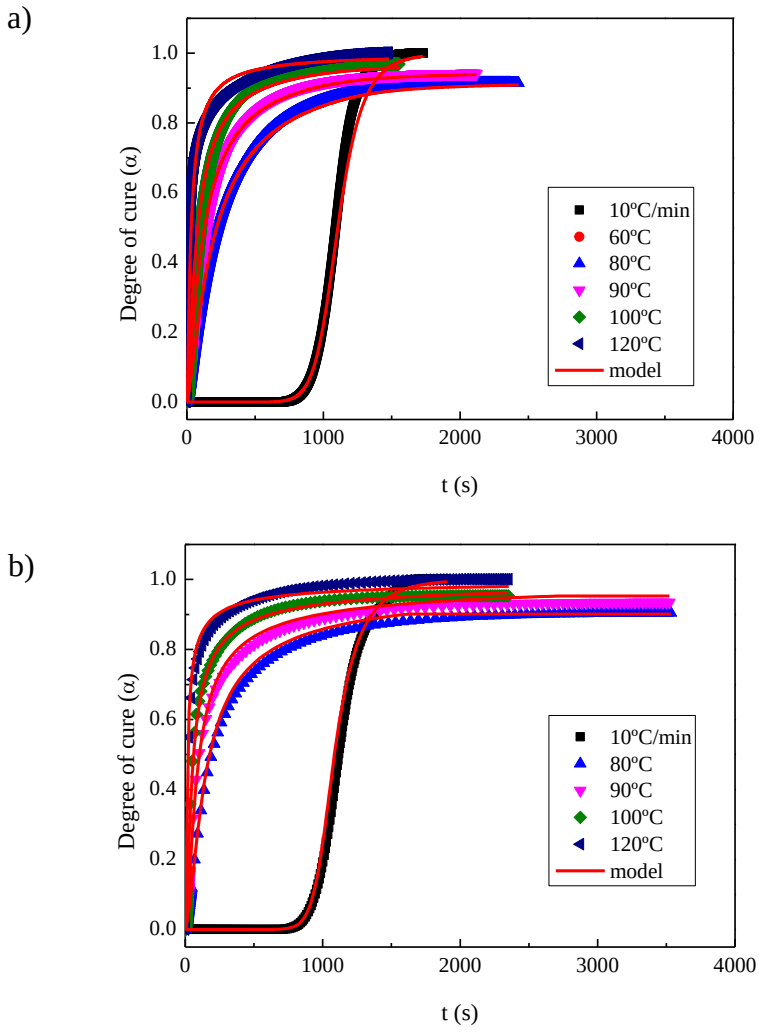

Figure 5.7. Degree of cure curves from DSC isothermal and dynamic tests(symbols) and models fitting (red lines) for a) BIO-PUR2 and b) BIO-PUR3.

For the viscosity modelling, the results from the time and temperature sweeps tests for BIO-PUR2 and BIO-PUR3 were fitted to the following equation based on Castro-Macosko model *(3.7)*[15]:

$$\eta^* = \eta_0 e^{\frac{E}{T}} \frac{1}{(1-\alpha)}^{p1+p2\alpha} \qquad (5.8)$$

where η* is the resin viscosity at a given degree of cure (α), temperature (T) and activation energy (E), and η_0, p1 and p2 are adjustable parameters. The viscosity model parameters for each of the BIO-PUR2 and BIO-PUR3 are summarised in *Table 5.5.*

As it can be seen in the figure bellow, there was a good agreement between the experimental results and model for both systems.

Table 5.5 Viscosity model parameters.

		BIO-PUR2	**BIO-PUR3**
η_0	Pa s	1.73E-07	2.93E-06
E	ºK	7011	6300.2
p1		-2.2	-4.4
p2		10.8	10.0

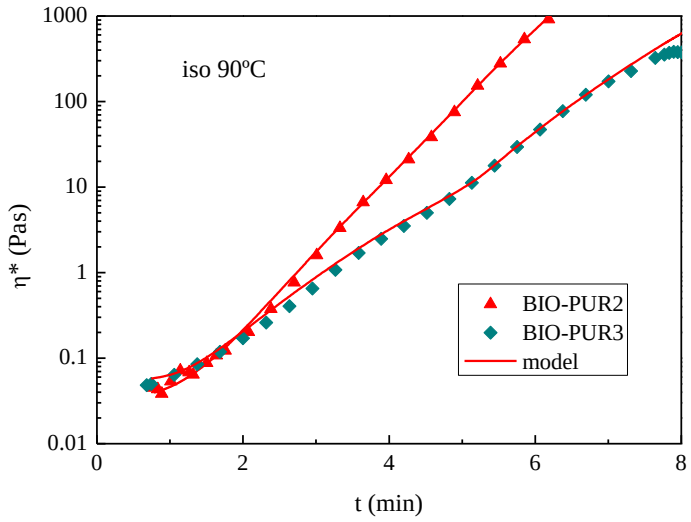

Figure 5.8. Viscosity evolution with time at 90 ºC for BIO-PUR2 and BIO-PUR3. Experimental results (symbols) and model (red lines).

The temperature used for the simulations was 120 ºC, which is a standard temperature to produce composite automotive parts. Also, two different injection strategies were considered, at constant pressure and a constant flow.

In the case of constant pressure injections, the simulations have been carried out at 70 bar. BIO-PUR2 system simulation results are satisfactory (*Figure 5.9*). Simulations show the processability of BIO-PUR2 at moderate pressures. At pressures higher than 70 bar this system can fill the mould in a few seconds. After the mould filling the curing was completed in eight minutes without the needed post-curing process. The BIO-PUR2 provided the good combination of enough latency and fast cure to be suitable for RTM. BIO-PUR3 system had a longer filling time due to its higher initial viscosity but showed a latent behaviour, achieving a curing degree and viscosity of 0.34 and 612 mPas respectively after the filling. Also, it required 3 additional minutes to reach the full curing compared to BIO-PUR 2.

The simulations at constant flow rate of 1 Kg min^{-1} and 100 bar maximum pressure strengthen the previous results. The results show that it is possible to fill the mould with both systems with similar filling times. However, for the BIO-PUR3 system the maximum pressure is reached.

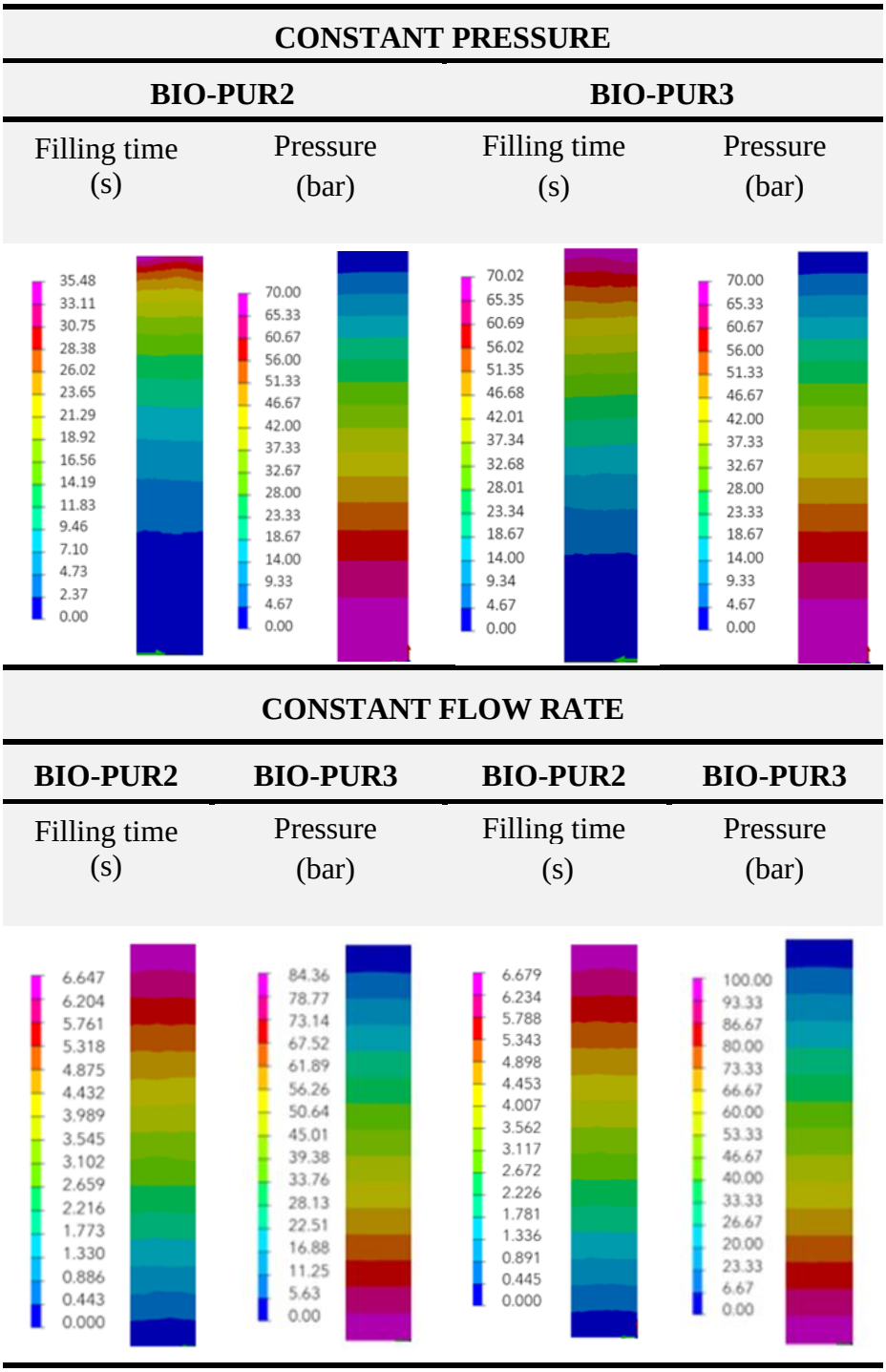

Figure 5.9. Leaf spring RTM process simulation.

5.7. CONCLUSIONS

The addition of a biobased glycerol, BIO-Gly to a high functionality and high hydroxyl value castor oil-based polyol was proven to be efficient for increasing the crosslinking density, T_g and mechanical properties of a structural BIO-PUR.

Moreover, the system showed a viscosity profile similar to the reference petrochemical origin structural PUR system with the required latency and reactivity. The addition of a delayed action catalyst allowed to further delay the curing if necessary.

The process simulation of the target composite part (leaf spring) at industrial conditions (120ºC and high-medium pressures) showed both catalyzed and uncatalyzed systems suitability. However, for the catalyzed systems both process times and maximum pressures were higher.

5.8. . REFERENCES

[1] Zhang, J.; Yao, M.; Chen, J.; Jiang, Z.; Ma, Y.: Synthesis and properties of polyurethane elastomers based on renewable castor oil polyols. Journal of Applied Polymer Science, 136 (2019). http://doi:10.1002/app.47309.

[2] Zhang, L.; Zhang, M.; Hu, L.; Zhou, Y.: Synthesis of rigid polyurethane foams with castor oil-based flame retardant polyols. Industrial Crops and Products, 52 (2014). http://doi:10.1016/j.indcrop.2013.10.043.

[3] Ionescu, M.; Radojčić, D.; Wan, X.; Shrestha, M. L.; Petrović, Z. S.; Upshaw, T. A.: Highly functional polyols from castor oil for rigid polyurethanes. European Polymer Journal, 84 (2016). http://doi:10.1016/j.eurpolymj.2016.06.006.

[4] Tan, A. C. W.; Polo-Cambronell, B. J.; Provaggi, E.; Ardila-Suárez, C.; Ramirez-Caballero, G. E.; Baldovino-Medrano, V. G.; Kalaskar, D. M.: Design and development of low cost polyurethane biopolymer based on castor oil and glycerol for biomedical applications. Biopolymers, 109 (2018). http://doi:10.1002/bip.23078.

[5] Morales-Cerrada, R.; Tavernier, R.; Caillol, S.: Fully Bio-Based Thermosetting Polyurethanes from Bio-Based Polyols and Isocyanates. Polymers, 13, 1255 (2021). http://doi:10.3390/polym13081255.

[6] Meiorin, C.; Calvo-Correas, T.; Mosiewicki, M. A.; Aranguren, M. I.; Corcuera, M. A.; Eceiza, A.: Comparative effects of two different crosslinkers on the properties of vegetable oil-based polyurethanes. Journal of Applied Polymer Science, 137 (2020). http://doi:10.1002/app.48741.

[7] Hejna, A.; Kirpluks, M.; Kosmela, P.; Cabulis, U.; Haponiuk, J.; Piszczyk, Ł.: The influence of crude glycerol and castor oil-based

polyol on the structure and performance of rigid polyurethane-polyisocyanurate foams. Industrial Crops and Products, 95 (2017). http://doi:10.1016/j.indcrop.2016.10.023.

[8] Calvo-Correas, T.; Mosiewicki, M. A.; Corcuera, M. A.; Eceiza, A.; Aranguren, M. I.: Linseed oil-based polyurethane rigid foams: Synthesis and characterization. In Journal of Renewable Materials; (2015); Vol. 3.

[9] Tan, H. W.; Abdul Aziz, A. R.; Aroua, M. K.: Glycerol production and its applications as a raw material: A review. Renew. Sustain. Energy Rev. (2013), 27.

[10] Echeverria-Altuna, O.; Ollo, O.; Calvo-Correas, T.; Harismendy, I.; Eceiza, A.: Effect of the catalyst system on the reactivity of a polyurethane resin system for RTM manufacturing of structural composites. Express Polymer Letters, 16, 234–247 (2022). http://doi:10.3144/expresspolymlett.2022.19.

[11] Kim, T. H.; Kim, M.; Lee, W.; Kim, H.-G.; Lim, C.-S.; Seo, B.: Synthesis and Characterization of a Polyurethane Phase Separated to Nano Size in an Epoxy Polymer. Coatings, 9, 319 (2019). http://doi:10.3390/coatings9050319.

[12] Gorka Garate; · Isabel Harismendy·; Oihane Echeverria-Altuna ·; Julian Estevez: A dynamic data driven application system for real-time simulation of resin transfer moulding processes. International Journal of Material Forming, 15, 1–11 (2022).

[13] Kamal, M. R.; Sourour, S.: Kinetics and thermal characterization of thermoset cure. Polymer engineering and science, 13, 59–64 (1973). http://doi:10.1002/pen.760130110.

[14] Chern, C. S.; Poehlein, G. W.: A kinetic model for curing reactions of epoxides with amines. Polymer engineering and science, 27, 788–795 (1987). http://doi:10.1002/pen.760271104.

[15] Castro, J. M.; Macosko, C. W.; Perry, S. J.: Viscosity changes during urethane polymerization with phase separation. Polymer communications, 25, 82–87 (1984).

6

BIO-PUR SYSTEM OPTIMIZATION

6. BIO-PUR SYSTEM OPTIMIZATION

6.1. GRAPHICAL ABSTRACT 152
6.2. ABSTRACT 153
6.3. INTRODUCTION 154
6.4. EXPERIMENTAL 160
6.4.1. Materials 160
6.5. CHARACTERIZATION 161
6.5.1. Permeability test 161
6.5.2. Void content 163
6.5.3. Dynamic mechanical analysis (DMA) 163
6.5.4. Mechanical properties 163
6.5.5. Density 164
6.5.6. Fibre and void Volume Fraction 164
6.6. RESULTS AND DISCUSSION 164
6.6.1. Permeability 164
6.6.2. Void content 167
6.6.3. Composite manufacturing and testing 173
6.6.4. Devopment of the DDDAS process control system 177
6.7. CONCLUSIONS 192
6.8. REFERENCES 194

6.1. GRAPHICAL ABSTRACT

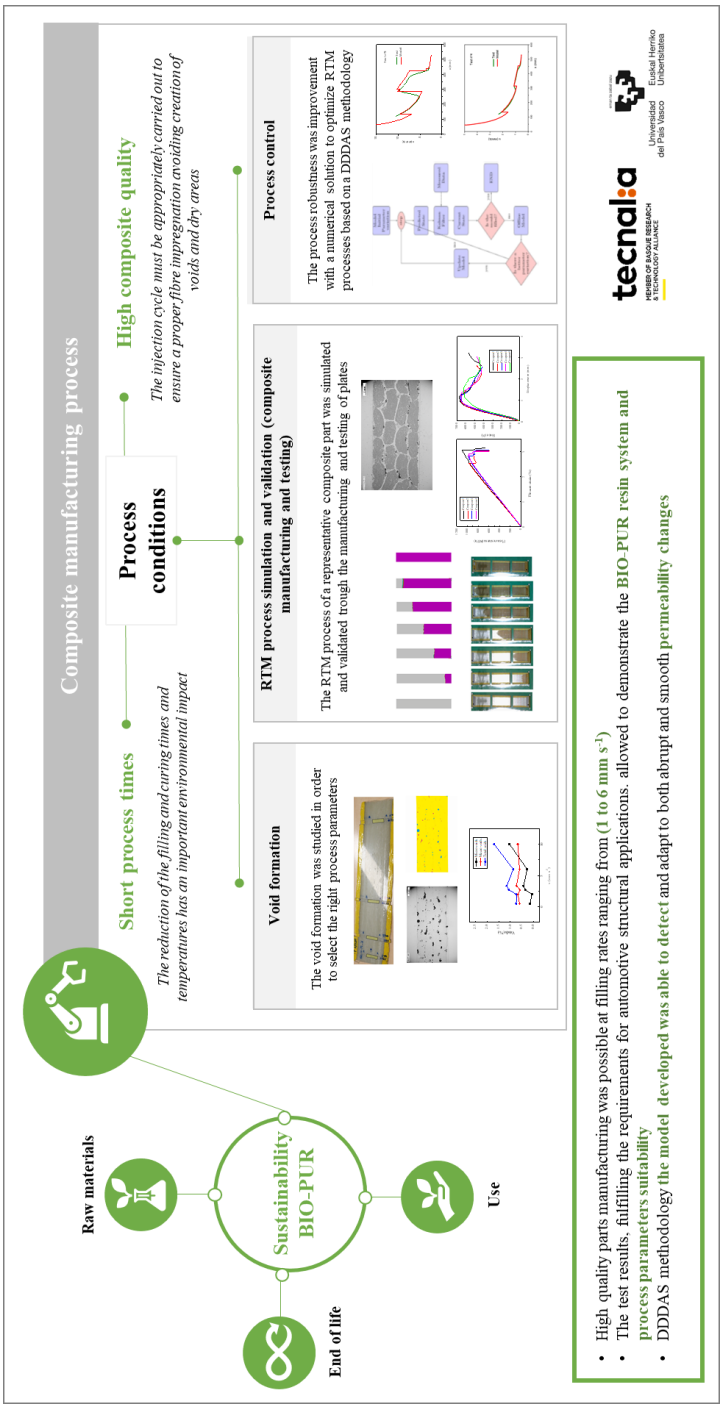

6.2. ABSTRACT

As mentioned before, sustainability should be considered in all the aspects, including the composite manufacturing process. In the RTM process the filling of the mould remains the limiting step of the whole process, and the reduction of the filling and curing times and temperatures has an important environmental impact.

On the other hand, the injection cycle must be appropriately carried out to ensure a proper fibre impregnation avoiding creation of voids and dry areas that lead to defective and scrap parts. In addition, the final part quality is very sensitive to unavoidable variations in the raw material parameters, in particular the permeability fabric stacks, resulting in unexpected resin flow patterns. These, in turn, may cause unacceptable content of dry spots and voids.

In this chapter, the influence of the filling rate on the void formation was studied in order to select the right process parameters and optimize the manufacturing process.

Once the parameters selected, the RTM process of a representative composite part was simulated and validated trough the manufacturing and testing of plates. The quality obtained was good, fulfilling the requirements for automotive structural applications.

Finally, to improve the process robustness a numerical solution to optimize RTM processes based on a DDDAS methodology, taking permeability as stochastic was studied. The suitability of the proposed

model was tested and validated under different process parameters variations like pressure and preform permeability.

6.3. INTRODUCTION

Resin transfer moulding (RTM) has become one of the most widely used processes to manufacture medium size reinforced composite parts. To further enhance the sustainability of composites based on BIO-PUR it is necessary to improve the process efficiency ensuring the best possible quality of the produced parts.

The quality of composite components fabricated by RTM depends not only on materials, resin and fibre, but also on the filling process itself.

In the case of Newtonian fluids, the motion of fluids through porous fibre structure is governed by this well-known Darcy's law.

$$Q = -\frac{S\,K}{\phi\,\eta^*}\nabla P \qquad (6.1)$$

where Q denotes the resin flow rate, K is the preform permeability, S is the cross-sectional area, ϕ is the porosity, η* is the resin viscosity, and P represents the pressure.

The main factors that influence the resin motion are the pressure gradient, the resin viscosity, which depends on time and temperature, and fibre permeability [1].

The filling of the mould remains the limiting step of the whole process, and the reduction of the filling time has an important impact on the overall cost reduction. However, the injection cycle has to be appropriately carried out to ensure a proper fibre impregnation. Indeed, a partial fibre impregnation leads to the creation of voids.

Composite parts porosity is a critical factor due to its considerable influence on physical and thermomechanical properties [2,3].

Moreover, in components subjected to cyclical loads is a major issue because they can radically influence the resistance to fatigue [4,5]. D. Huelsbusch et al. observed the void formation in their polyurethane systems and the influence in the fatigue resistance. They explained that matrix cracks can grow immediately due to pores under cyclic loading. This results in higher energy loss and heating that leads to an acceleration of damage development with the number of cycles to failure ten times smaller [6].

Investigation of voids in composites started around half a century ago and is still an active research field in composites community. The voids can be classified based on their location (*Figure 6.1*), micro-voids are defined as the interstitial spaces between the filaments in the fibre tows and the macro-voids are the gaps between the tows[7].

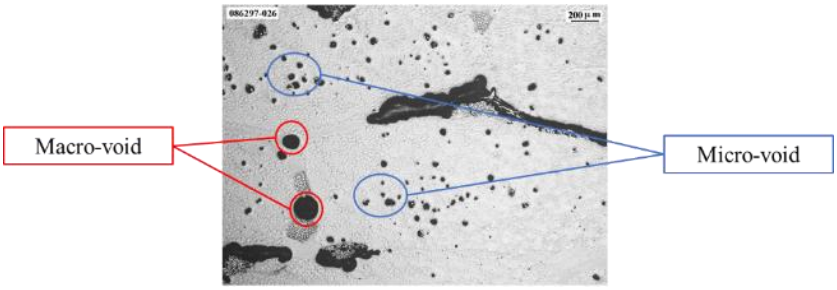

Figure 6.1. Example of micro-void and macro-void in RTM manufactured composite.

The voids are generated by different mechanisms: mechanical air entrapment during resin flow, gas created due to chemical reactions during cure, nucleation, leakage, cavitation or uneven resin curing [2,8-10]. Nevertheless, the most common void formation in the RTM is due to air entrapment [11-13].

The void formation is directly associated with the velocity of the impregnation. The amount and type of voids directly depend on this parameter [14-17]. The creation of micro and macro pores is due to the double scale flow of the resin during the RTM process. Because of the fibre structure, the resin can easily flow in open channels between the tows with less viscous resistance than in the inter-tows due to the balance between the two types of forces involved, the viscous forces and capillarity (*Figure 6.2*).

As *Figure 6.3* shows, when the impregnation velocity is low, the dominant force is the capillarity. The resin advance causes the generation of macro-voids between tows gaps. Conversely, when the velocity of the flow front is very high, viscous forces are dominant: The resin flows

preferably between the gaps in the tows and micropores into tows are generated.

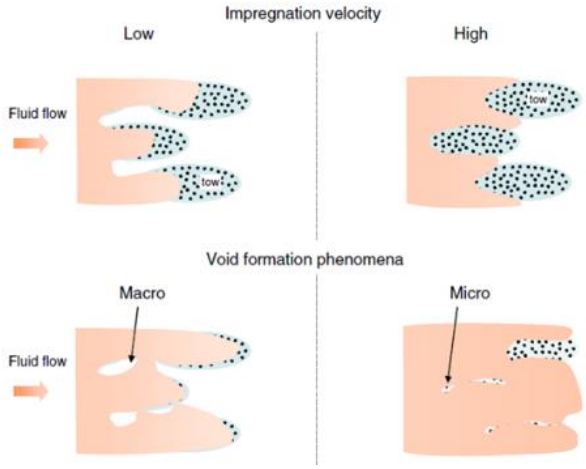

Figure 6.2. Schematic relationship between voids formation and the impregnation velocity [18].

Researchers have demonstrated that the percentage of macro/micro-voids is nearly a logarithmic function of the fluid flow velocity[18-21]. So, to select the optimal process parameters, the influence of the filling rate on the void formation should be considered.

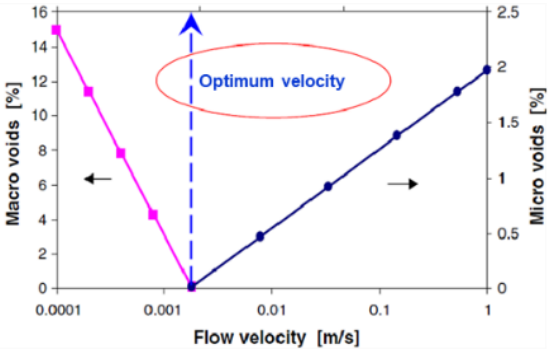

Figure 6.3. Relationship between macro and micro voids and the mould filling velocity[18].

In addition, the final part quality is very sensitive to unavoidable variations in the raw material parameters, in particular the permeability fabric stacks, resulting in unexpected resin flow patterns. These, in turn, may cause unacceptable content of dry spots and voids. So, improve process robustness it would be necessary to develop process control systems able to predict and correct the outcomes of these deviations.

Usually models to simulate the manufacturing processes use a static combination of parameters that represents the behaviour of the real system. The disadvantage lies at the variability of the parameters of the design phase in the real-time process. As the values of those parameters are not static but stochastic, the outputs of these simulated models often present significant deviations from those of the corresponding real processes [22,23].

Parameters such as permeability and porosity cannot be estimated accurately beforehand as a consequence of preform architecture variability due to different handling and storage conditions or shear deformations during the forming/draping stage, nesting effects during lay-up, low resistance channels along the preform, as well as accidental misplacement of the preform in the mould [24]. Several experimental and simulation studies have outlined the stochastic nature of permeability. Standard deviations up to 20% were observed during permeability measurements[25-29], while according to other results permeability standard deviation can reach values up to 30% [30].

To circumvent this stochastic nature of permeability DDDAS (Dynamic Data Driven Application Systems) methods can be applied [31]. With the DDDAS the simulation can process online field data from

measures and adapt to those measurements. DDDAS systems have been mostly applied in Computational Science and Engineering and Mathematics, and also been some research in the field of Environmental Science [32] or Materials Science [33]. However, only a few examples can be found for composite materials [34,35]. These examples address only mechanical properties and not manufacturing processes, excepting the work of Chinesta et al [36], where Hybrid Twins Features of which DDDAS systems are a constitutive part were illustrated for RTM.

In this chapter the influence of the filling rate on the void formation was studied to select the right process parameters and optimize the manufacturing process of a reinforced composite part. For this purpose, plates were manufactured at different pressures and test coupons were extracted at different filling rates and studied by optical microscopy.

Once the parameters selected, a representative composite part was simulated with ESI's PAM-RTM software and validated trough the manufacturing and testing of its physical (density, void content), thermal (DMA) and mechanical (ILSS, Flexural) properties.

Finally, in order to improve the process robustness a numerical solution to optimize RTM processes based on a DDDAS, taking permeability as stochastic was studied. The proposed model was tested and validated under different process parameters variations like pressure and preform permeability.

6.4. EXPERIMENTAL

6.4.1.Materials

Reinforcements

A unidirectional glass fibre specifically developed for components subjected to cyclic loadings (Ultra Fatigue UD) supplied by Saertex, was selected as reinforcement. Fibre properties are summarized in Table 1.

Table 6.1. Fibre properties.

Weaving pattern	E-glass unidirectional non-crimp fabric (NCF)
Areal weight	1176 ± 64 g/m2
Powder	Huntsman XB 6078 10 ± 2 g/m2
Sewing thread	Polyester 76 dtex 12 ± 3 g/m2

Preforming was carried out under in a vacuum table at 150ºC for 90 seconds.

Resins

The composition of the PUR resin used for this study is shown in the *Table 6.2*.

Table 6.2. Summary of synthesized polyurethanes.

System	Component's ratio (pbw)					
	Part A			***Part B***		
	Polyol	*Glycerol*	*BDDE*	*Isocyanate*	*LiCl*	*DAS*
BIO-PUR3	100	22	7	267	2	9
	Renewable content (%)					
	27					

In the permeability and DDDAS part to take into account the possible interaction of the resins and the binder a commercial low viscosity epoxy supplied by Resoltech (1800/1805) was used as the infiltration fluid. This resin has a constant viscosity of 25 cps at the experiment's temperature/times.

6.5. CHARACTERIZATION

6.5.1.Permeability test

Permeability tests were carried out on a sensorized self-heated steel mould with a glass window frame in the upper side to see the flow front progression (*Figure 6.4*). The mould is equipped with a camera in order to see and record all the phenomena involved in the process. An *in situ* developed software automatically calculates the resin filing rate and permeability.

Permeability tests were performed at 60 ºC and constant pressures ranging from 0.75 to 2 bars.

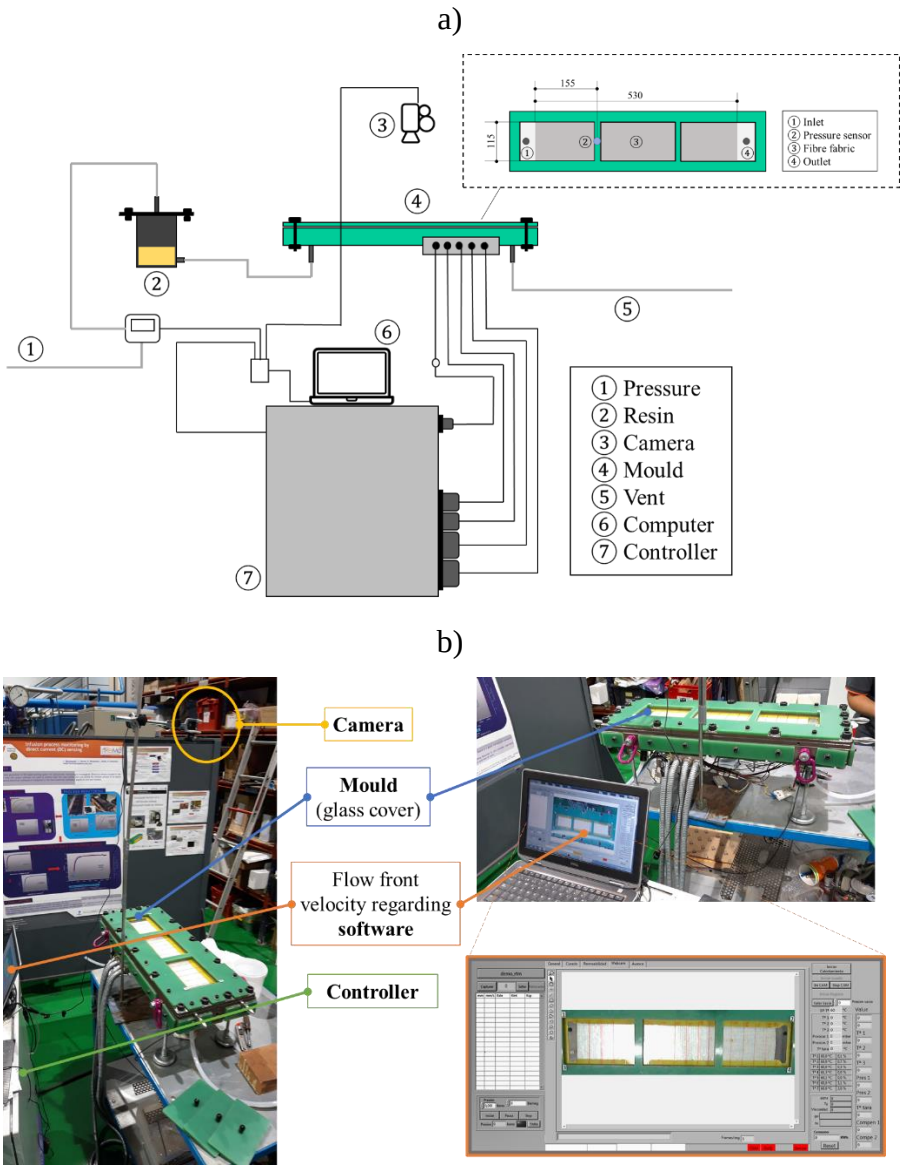

Figure 6.4. a) Schematic diagram of the test equipment and RTM mould. b)RTM test equipment and software picture.

Permeability is calculated from the flow velocity with the LSF method (least square fit) in order to obtain accurate values.

6.5.2.Void content

The voids of fabricated composites were studied by optical microscopy (Eclipse MA200, Nikon). Sample images were obtained at RT. The sample were embedded in epoxy resin (EpoFix resin / Epofix Hardener, STRUERS).

The image analysis software Olympus Stream 2.3.3., was used to determine the percentage of voids.

6.5.3.Dynamic mechanical analysis (DMA)

Dynamic mechanical analysis (DMA) tests were carried out using the Gabo Eplexor100N (Netzch, Selb, Germany) dynamic mechanical analyser. Temperature scans were performed from -40 to 200 ºC at 2 ºC min^{-1} heating rate and at a frequency of 1 Hz. The sample dimensions were 2.2 x 5 x 50 mm^3. The T_g of the PUR resin systems was taken at the temperature value of the maximum of tan δ [37,38].

6.5.4.Mechanical properties

The flexural tests were carried out at RT using an Instron 5500R6025 (Instron, Norwood, USA) equipment, with a 3-point bending device, according to ISO 14125. Moreover, ASTM D2344 tests were carried according to ASTM 2-344.

6.5.5.Density

The density of the developed resin and the composite plate was determined in accordance with the liquid displacement method (ASTM D792-20).

6.5.6.Fibre and void Volume Fraction

The burn-off method described in ASTM D3171-22 was used to determine the fibre volume fraction, Vf, and the void volume fraction, Vv, of the composite samples.

6.6. RESULTS AND DISCUSSION

6.6.1.Permeability

For the permeability calculation by the average method, Darcy's equation was rearranged to;

$$x^2 = \frac{2K_{av}\Delta Pt}{\phi\mu} \tag{6.2}$$

were ΔP denotes the pressure gradient, K_{av} the permeability determined by average method, ϕ the composite porosity and μ the resin viscosity.

Permeability value was obtained directly using the straight-line slope.

Elementary method

This method uses the average values of the flow front velocity to obtain the macroscopic value of the permeability. The impregnation velocity, for specific time (v_t), was calculated using the sample pairs (x_i, t_i) that describe the flow front position evolution with time i (6.3).

$$v_t = \frac{1}{2}\left(\frac{x_{t+1} - x_t}{t_{t+1} - t_t} + \frac{x_t - x_{t-1}}{t_t - t_{t-1}}\right) \quad (6.3)$$

Permeability values were calculated with equation (6.4) for each time step and then averaged.

$$K_{ele} = \frac{1}{\mu}\frac{dP/dx}{v_t \Phi} \quad (6.4)$$

where the pressure gradient is evaluated by equation *(6.5)* and K_{ele} is the permeability determined by elementary method.

$$dP/dx = \frac{P_0(t)}{x_f(t)} \quad (6.5)$$

where the P_0 denotes the pressure at x_0 point (preform initial point) and x_f is the flow front position.

Interpolation method

The permeability determined by this method represent the best global fit from experimental data.

$$K_{int} = \frac{a^2 \mu}{2\Phi} \quad (6.6)$$

where a parameter is calculated by equation *(6.7)*(6.5) and K_{int} is the permeability determined by interpolation method.

$$a = \frac{\sum x_f \sqrt{I_t}}{\sum I_t} \tag{6.7}$$

and I parameter for specific time is determined by equation *(6.8)*.

$$I_t = I_{t-1} + (\frac{P_{0_{t-1}} + P_{0_t}}{2})(t_t - t_{t-1}) \tag{6.8}$$

Single-point method

The single point method uses a single pair of (x_i, I_i) to a rapid approximation of permeability (K_{sp}).

$$K_{sp} = \frac{x^2 \mu}{2 I_t \phi} \tag{6.9}$$

This method is based on the determination of the permeability value at a specific moment in a specific position. As it is a permeability value in one position, this value will give large errors in other positions. In this case, an average of the most representative positions was used for the calculations.

The results achieved for the glass fibre used in this work are shown in *Table 6.3* for a 47,5% Vf. The permeability values obtained with different calculation methods were similar. However, the value of the interpolation method was used, as it is considered the most reliable. Therefore, the permeability value considered in this work is 1.35E-10 m^2.

Table 6.3 Permeability value calculated with different method.

$K_{av}(m^2)$	K_{ele} (m^2)	$K_{int}(m^2)$	$K_{sp}(m^2)$
1,35E-10	1,38E-10	1,35E-10	1,30E-10

6.6.2.Void content

In order to study the effect of filling rate on void formation, plates were manufactured at constant pressures and test coupons were extracted at different filling rates ranging from 0.5 to 10mm s^{-1} and studied by optical microscopy. *Figure 6.5* shows the samples extraction areas.

Previous to the composite micro – macro void study, the morphology of the dry the fibre with the binder has been analysed in order to avoid interpretation errors. *Figure 6.6* shows the micrographs of fibreglass fabric. The binder after the preforming process presents an amorphous geometry similar to macro voids.

Figure 6.7 shows the micrographs and the image analysis of the composite samples. The different samples present micro and macro pores. In some cases, it was not easy to differentiate between the binder and the macro voids.

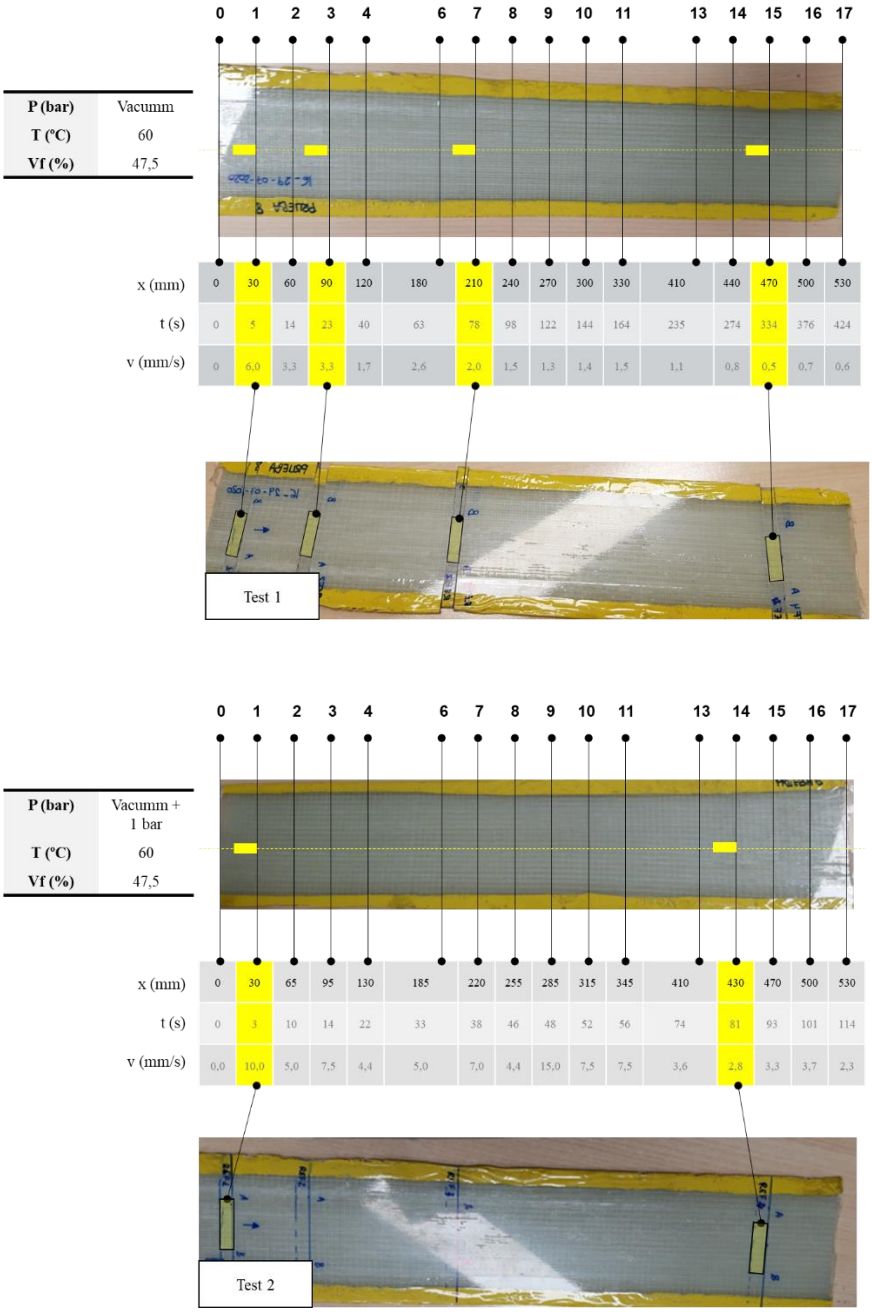

Figure 6.5. Samples extraction areas.

a) Before preforming

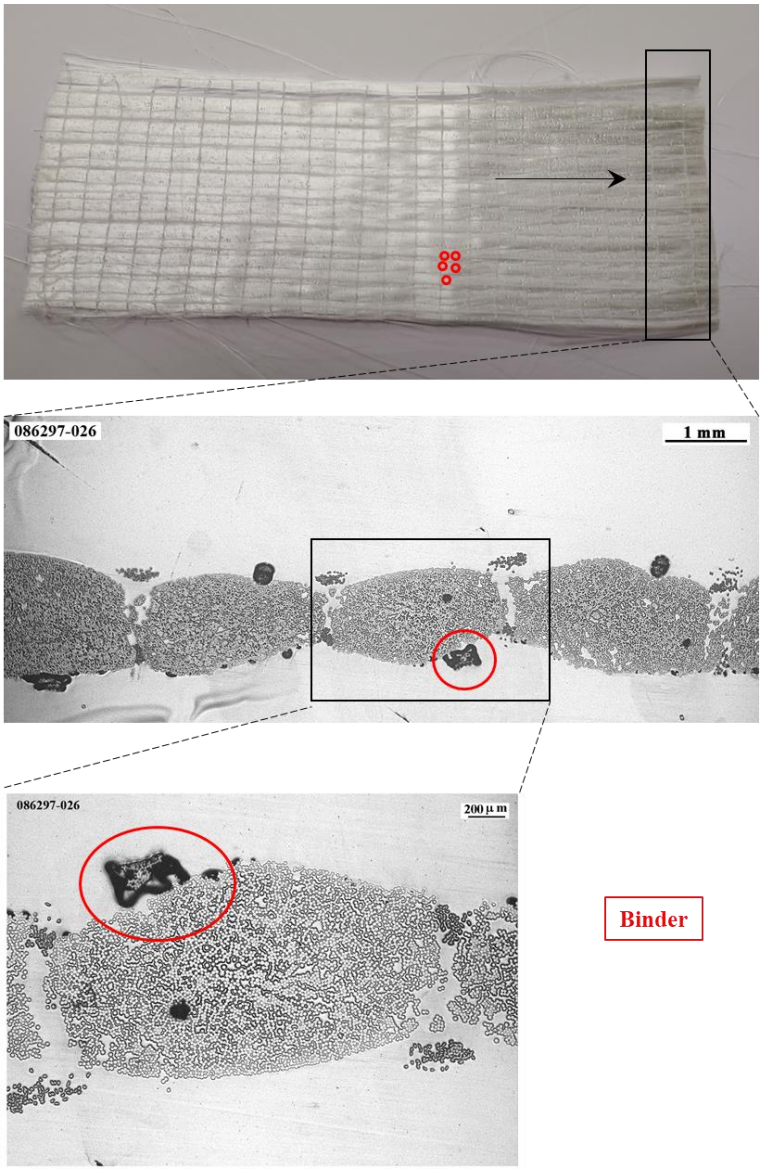

Figure 6.6. a) Glass fabric morphology before preforming.

b) After preforming

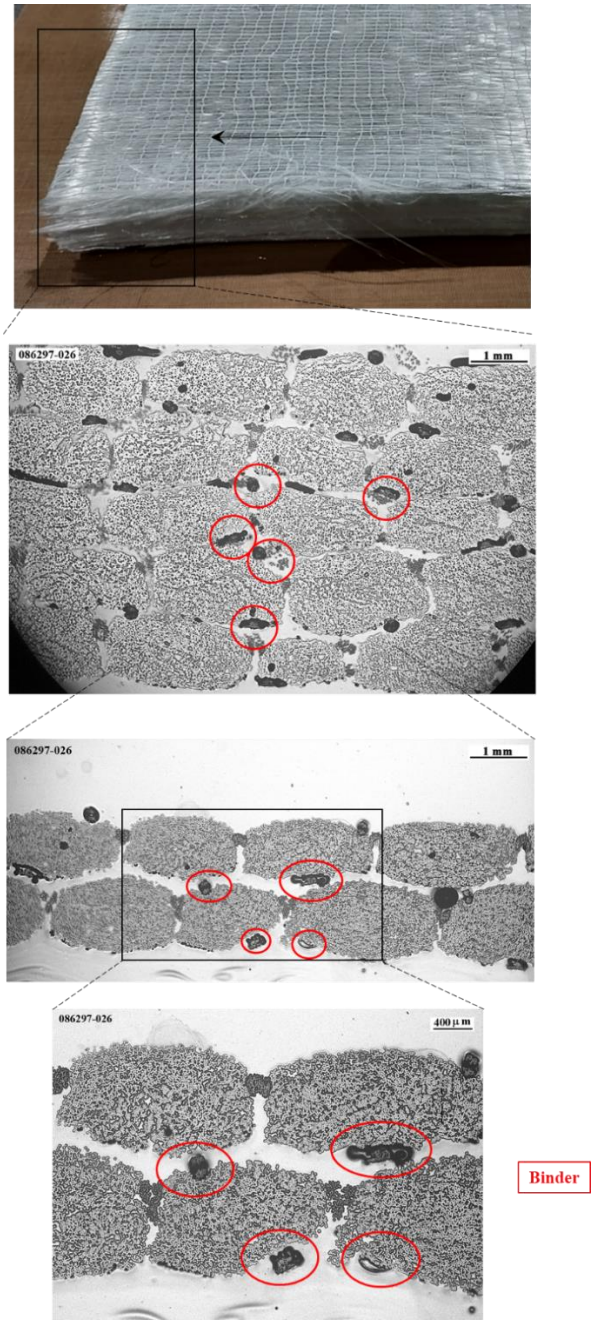

Figure 6.6. b) Glass fabric morphology after performing.

Velocity ($mm\ s^{-1}$)	Micrography	Void analysis
10.0	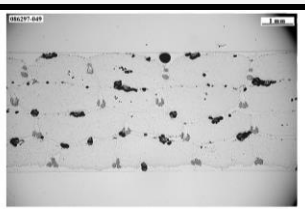	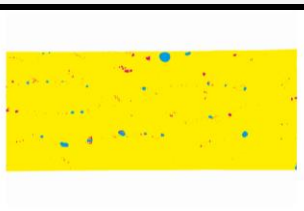
6.0	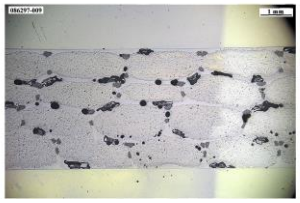	
3.3	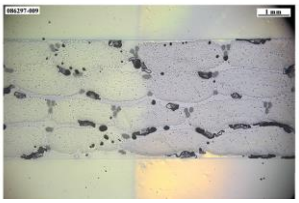	
2.7	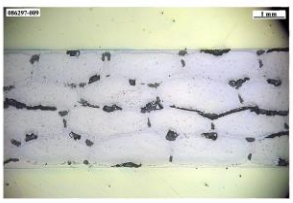	
2.0	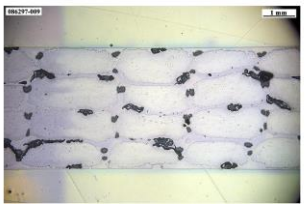	
0.5	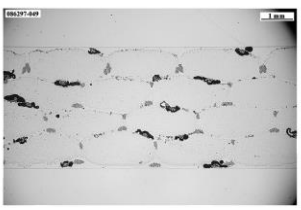	

Figure 6.7. Micrographs and processed images for the different composite samples (blue areas: macrovoids; red areas: microvoids).

Results show that with the selected process parameters, it was only possible to quantify the void content and impregnation velocity in a very narrow window (*Figure 6.8*). Void content of the composites was less than 2% in all the cases.

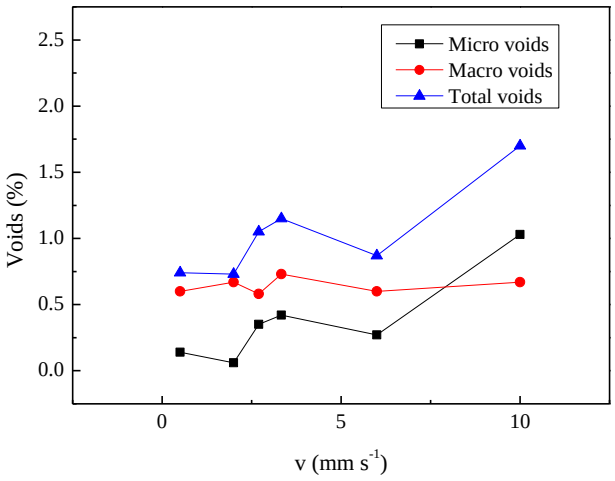

Figure 6.8. Void content for different impregnation velocity.

E. Ruiz et al. employed velocities ranging from 0.0001 to 1m s^{-1} were used to get the macro and micro void velocity relationship [18]. In this case, the equipment used, with a glass cover did not allow high flow front velocity, due to the pressure limit. As expected, the number of micro voids decreased at low velocities. However, in the case of macro voids the amount remained stable.

Based on these results, an impregnation velocity between 1 - 6 mm s^{-1} was considered optimal to manufacture structural composites with this reinforcement at a 47.5% fibre volume content.

6.6.3.Composite manufacturing and testing

Once the impregnation velocity range was selected, composite plates were manufactured and tested in order to further validate the BIO-PUR developed formulation suitability for structural composites.

The reinforcement and fibre content used was the same as in the target application process simulations (47,5% fibre volume content of high fatigue resistance (ultra-fatigue) unidirectional glass fibre) but, the process conditions had to be changed due to a 3 bar maximum injection pressure of the glass cover mould used. Also, in this case, the less reactive BIO-PUR3 system was selected. Moreover, the selected process temperature was also lower than the target 120 ºC. In this case, the filling was performed at 60 ºC and pressures ranging from 0.5 to of 3 bar and then postcured for 1 h at 120 ºC.

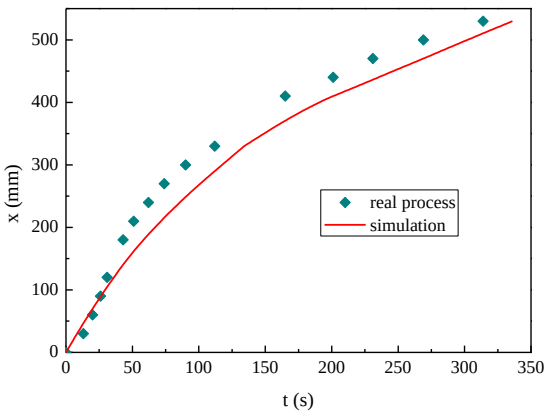

Figure 6.9. The flow front evolution for BIO-PUR3. Experimental (symbols) and simulation (red line) results.

Figure 6.9 shows the comparison between the experimental and simulation results. As can be seen although there is a good agreement and the models fitting could be considered good enough, the real process

has slightly quicker than the theoretical one. This is probably due to the presence of higher permeability zones that modified the flow pattern as can be seen in *Figure 6.10*.

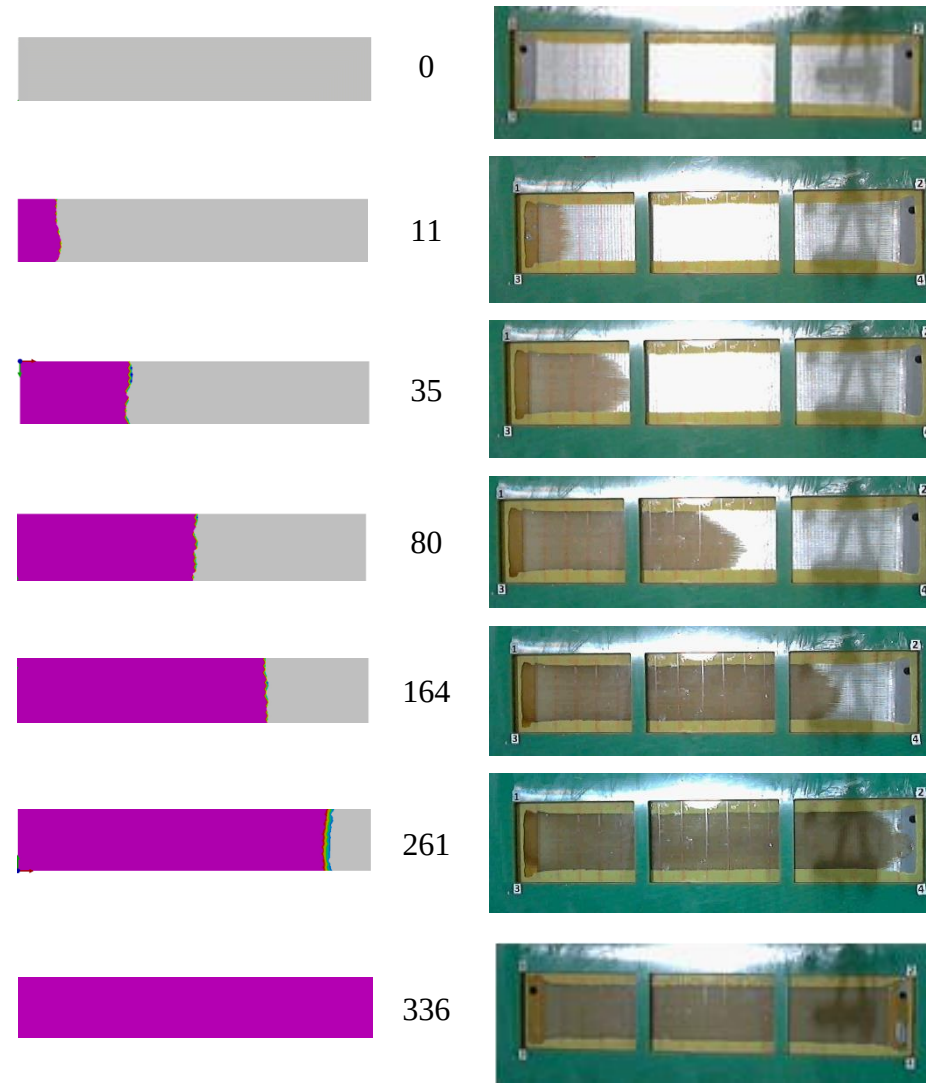

Figure 6.10. Comparison between the simulation and real RTM process with the BIO-PUR3 formulation.

Once manufactured, characterization tests were carried out to test the composite plate quality. *Figure 6.11* and *Figure 6.12* show the curves obtained in Flexural tests.

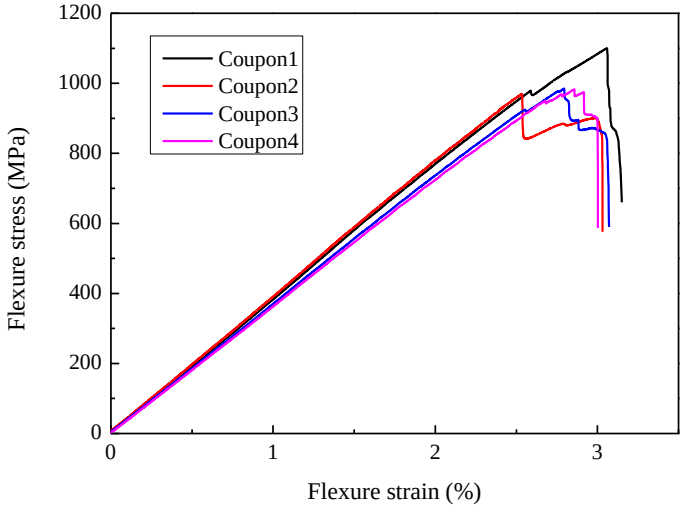

Figure 6.11. Flexural strength testing results for BIO-PUR composite plate.

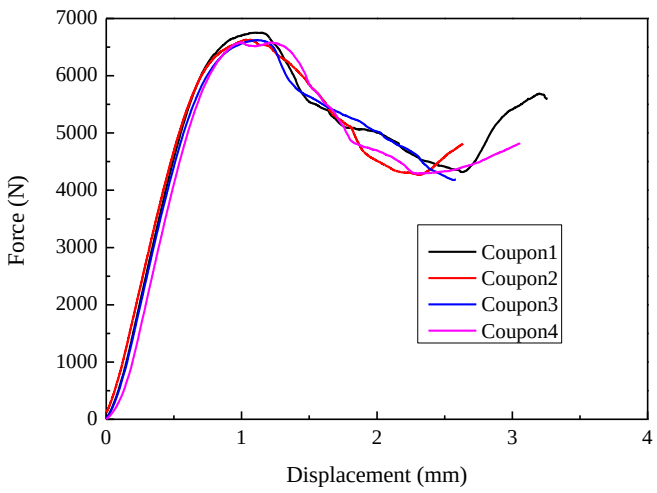

Figure 6.12. Interlaminar shear strength results for BIO-PUR composite plate.

The results are shown in *Table 6.4. T*he BIIO-PUR composite exhibit excellent mechanical properties with modulus and flexural strength of 35 GPa and1000 MPa respectively (*Figure 6.11*). ILSS value of the coupons, extracted at different plate lengths showed a very small deviation showing that a constant quality was attained (*Figure 6.12*). Void content of the coupons was less than 1.25% in all the cases. The fibre volume content was also constant and in accordance with the theorical one (47,5%).

Samples were also examined with optical microscopy. As can be seen in the *Figure 6.1*, a good and homogenous quality is obtained (Dark areas correspond to binder).

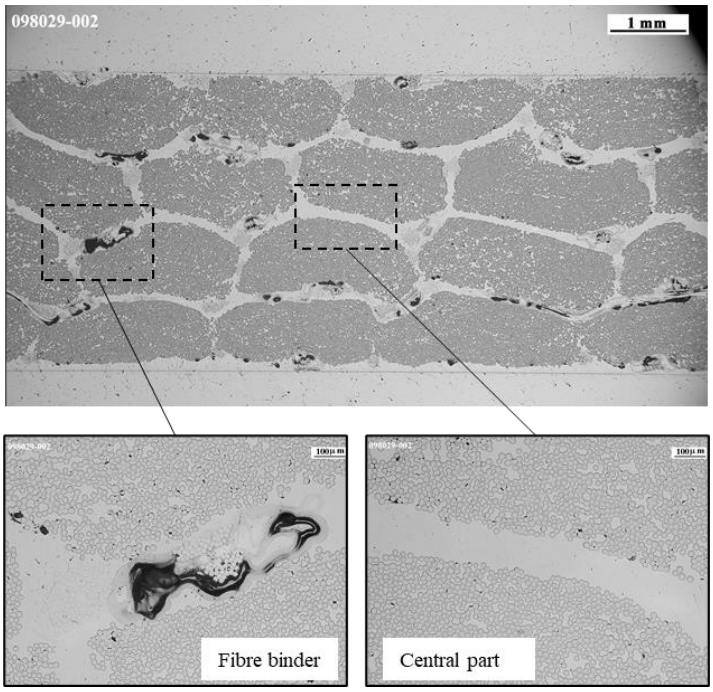

Figure 6.13. Composite plate micrographs.

Moreover, the T_g value is also higher than 120ºC, fulfilling the automotive structural parts requirements.

Table 6.4. Final properties of BIO-PUR based composite

BIO-PUR3		
Method	**Properties**	**Value**
Mechanical properties	**Flexural strength (**MPa)	1009 ± 61
	Flexural modulus (GPa)	36.8 ± 1.0
	Flexural strain (%)	2.8 ± 0.2
	ILLS (MPa)	65 ± 2
DMA	**T_g** (ºC)	138
Liquid displacement method	**Matrix density at 25 ◦C (ρ_m)** ($g\ cm^{-3}$)	1.21
Burn-off method	**Void content (Vv)** (%)	-0.28 ± 0.96
	Fibre volumen content (Vf) (%)	48.2 ± 0.9

6.6.4.Devopment of the DDDAS process control system

As shown in the previous section, even if the optimal filling rates are selected, there are still some deviations between the simulations and reality due to the presence of high permeability areas. So, in order to

improve the process robustness a numerical solution to optimize RTM processes based on a DDDAS is proposed in this section. The modelling activities were performed by the Department of Applied Mathematics of the Faculty of Engineering of Gipuzkoa in University of the Basque Country.

Proposed virtual offline model

The method of simulation consists in solving by finite differences the following 2D Initial Value Problem (IVP):

$$\begin{cases} v\,(x,t) = \dfrac{dx}{dt} = \dfrac{k\,(x)}{\mu}\nabla p\,(x,t) \\ x(0) = g \end{cases} \tag{6.10}$$

This IVP consists of Darcy's law for the filtration velocity of the flow in the i direction, plus a condition for the initial position of the front of the flow. Where v is the filling rate, k is the permeability tensor of order 2, μ is the viscosity (scalar), p is the pressure, x is the vector pointing to the front of the flow and g is the initial gap between the edge of the preform and the contour line. The IVP is defined in domain Ω. The boundary of the domain consists of the pressure contour, the impermeable boundary and the goal line.

Approximating the differentials by finite increments and assuming through each step a constant pressure gradient and a constant permeability tensor, we can iterate on the position of the front of the flow and generate simulations of the RTM processes for different variations

of the parameters. The pseudo-code of the generation of the theoretical simulations is presented here as Algorithm 1.

Algorithm 1 Generation of the RTM simulations.

Initialization : $n = 0$; $\boldsymbol{x}^0 = \boldsymbol{g}$; $t^0 = 0$;
while *all points at the goal line have not been reached* **do**
  Time step: $t^{n+1} = t^n + \Delta t$;
  for *every point at the front of the flow* **do**
    Calculate the pressure gradient ∇p^n at the point of the front of the flow;
    Approximate the filling rate at step n using Eq. 1;

$$\boldsymbol{v} = \frac{d\boldsymbol{x}}{dt} = -\frac{\boldsymbol{k}}{\mu}\nabla p^n \tag{2}$$

    Approximate the advance in position of the front at point $\boldsymbol{x}^n$ at step n;

$$\boldsymbol{a}^n = \Delta t \cdot v_i^n \tag{3}$$

    if *the advance* $\boldsymbol{a}^n$ *has crossed the impermeable boundary* **then**
      Apply a non-penetration condition

$$\boldsymbol{a}^n = \boldsymbol{a}_{in}^n + \left(\boldsymbol{a}_{out}^n - \left(\boldsymbol{a}_{out}^n \cdot \boldsymbol{n}\right)\boldsymbol{n}\right), \tag{4}$$

      where $\boldsymbol{n}$ stands for the normal vector at the impermeable vector (see Fig. 2);
    end
    if *the goal line has been crossed* **then**
      Apply a no-penetration condition using Eq. 4;
    end
    Approximate the position of the front at point $\boldsymbol{x}^{n+1}$ at step $n + 1$;

$$x_i^{n+1} = x_i^n + \boldsymbol{a}^n \tag{5}$$

  end
  if *all points on the goal line have been reached* **then**
    break;
  end
end

Proposed model for the DDDAS RTM simulation

The simulation proceeds using Algorithm 1, assigning at each of the points in the actual front (at each iteration step) a stochastic value of the permeability obtained from anormal Gaussian distribution that uses as mean the nominal value of the actual permeability of the simulation and a fixed standard deviation of 2.5% of the nominal permeability.

Figure 6.14 describes the way the DDDAS works. The model starts with an initial state of the RTM process. An initial discrete front of one hundred points located along the width of the mould at an initial separation from the injection line ($x = x_0$ mm). Another two hundred points are fixed at the impermeable boundary (in the case of our mould, $y = 0$ mm and $y = 125$ mm) and one hundred more are fixed at the goal line ($x = 530$ mm). The nominal value of permeability is set to an initial value.

The model uses both the estimate and the measured value to apply a Kalman filter that gives a new filtered current filling rate estimate. If the mould is not filled, the model checks whether there is a precalculated variation (permeability value) for the actual front position that gives a filling rate that is closer to the estimate than that of the actual variation. If there is one, the model updates the permeability value taking the corresponding value of the offline model that performs best.

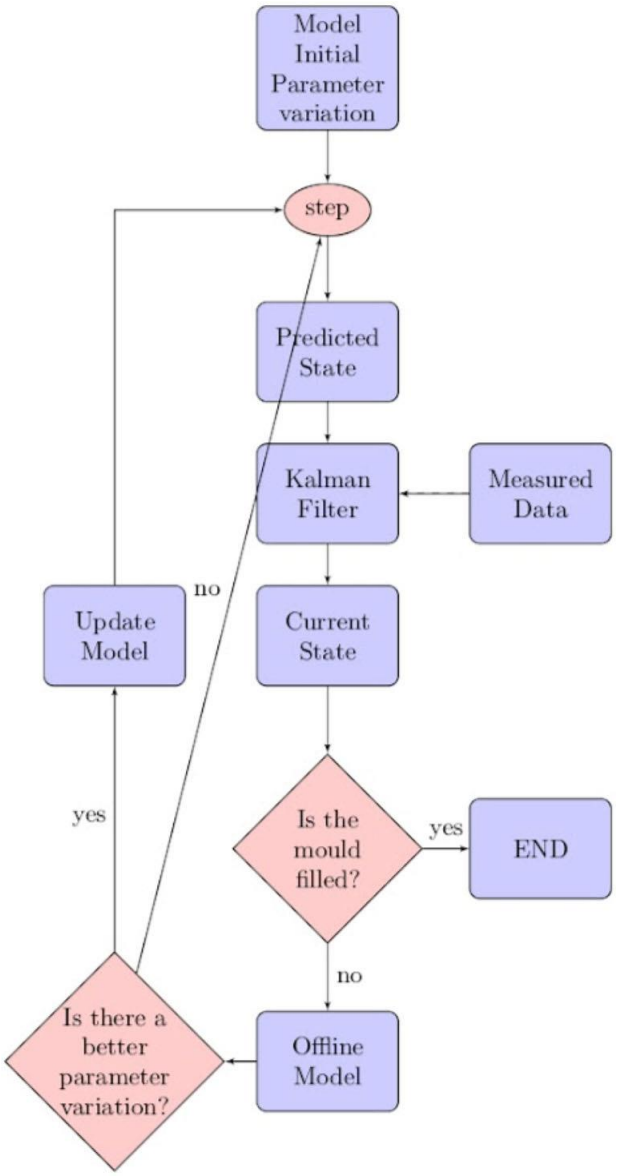

Figure 6.14. DDDAS flow chart.

The process goes on taking new steps using the new parameter until it finds new data (in that case the Filter + Current State + Update is repeated) or the mould has been filled (the points in the front have reached the goal line). The pseudo-code is detailed in Algorithm 2.

Algorithm 2 Generation of the DDDAS RTM simulation.

Initialization : $n = 0$; pick up values $\boldsymbol{x}^0$ and parameter $\boldsymbol{k}^0$ from a previously simulated variation; $t^0 = 0$;
while *all points at the goal line have not been reached*
do
  Time step: $t^{n+1} = t^n + \Delta t$;
  Take a single step to time t^{n+1} using Algorithm 1;
  if *there is collected data recorded for the current front position* t^{n+1} **then**
    Step 1 of the Kalman filter: Measure;
    Step 2 of the Kalman filter: Update;
    Step 3 of the Kalman filter: Estimate:
    - Look among the recorded simulations the variation that best approximates the estimated filling rate for the given front position;
    - Update parameter $\boldsymbol{k}$ to the new simulation;
  end
  if *all points on the goal line have been reached* **then**
    break;
  end
end

Model testing and validation

In order to check the suitability of the proposed model for detection and correction of permeability variation, different kind of preforms were prepared with the following configurations:

-Configuration 1: preforms constant permeability (4 layers of glass fabric)

-Configuration 2: preforms with different permeability zones.

For this purpose, the number of plies was reduced from 4 to 3 and 0 in a specific area of the preform as shown in the *Figure 6.15*.

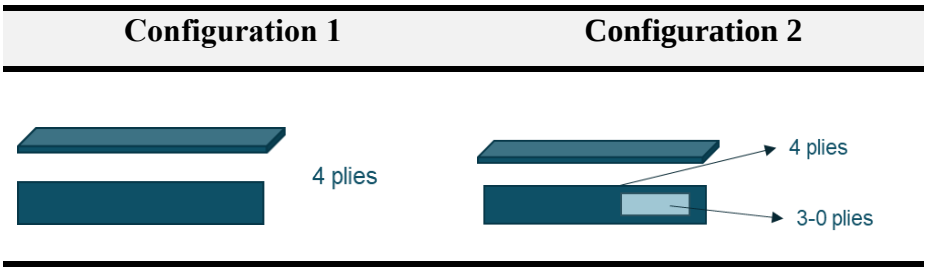

Figure 6.15. Preforms configuration.

Unidirectional laminar flow RTM tests were carried out at a constant pressure with the same equipment and materials as in the permeability tests.

The RTM injection test were performed at 60 ºC and pressure gradients ranging from 0.5 bar to 2.3 bars. Both visual and a pressure sensor form Kistler (Type 4001A, with temperature compensation) were used for the flow front position determination.

The model was tested under different preforms configurations and process conditions:

Test 1

The *Figure 6.16* show Test 1. configuration. It was performed with a constant permeability preform consisting of 4 plies of glass fabric, with a resultant fibre volume content Vf, of 47.5% and a nominal permeability of 1.35E-10 m^2. The test was carried out under controlled vacuum, at -0.73 bar.

As can be seen in *Figure 6.17*, the flow front was stable, with no race tracking and little difference between the saturated (full preform impregnated, dark grey) and unsaturated (preform partially impregnated,

lighter grey) areas. The sawtooth aspect of the flow front is due to the presence of high permeability channels between fibre tows.

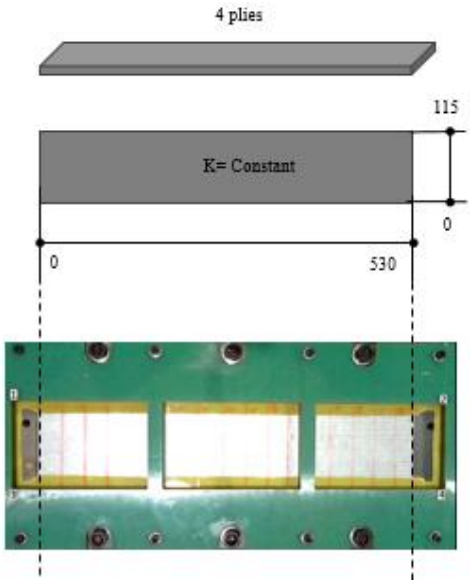

Figure 6.16. Test 1 configuration.

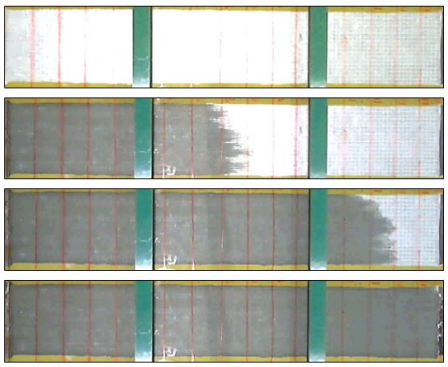

Figure 6.17 Flow front progression during Test1.

Figure 6.18 shows the results of the on-line model calculations for Test nº1. An onset permeability of 1.0E-10 m^2 was used in order to check the on-line adaptation ability of the model. As in can be seen in the figure, permeability value was quickly recalculated as soon as the

model received the real data from the experiment showing a good fitting between calculated and real filling rate values.

Permeability

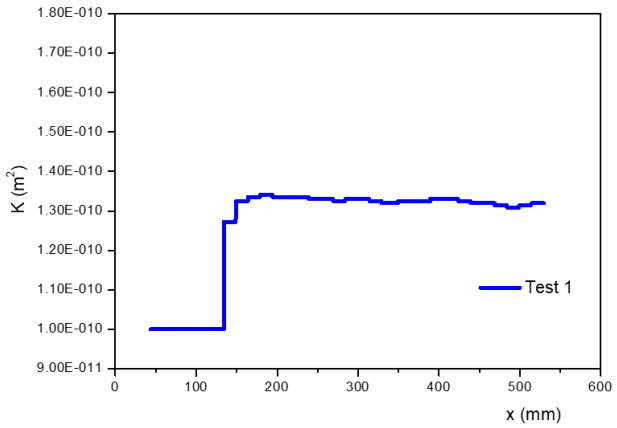

Filling rate

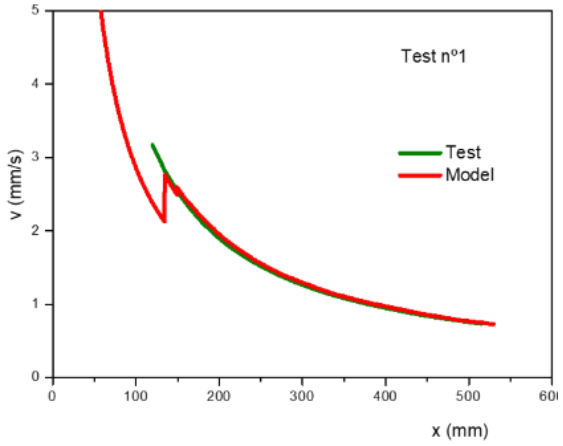

Figure 6.18 Model results for Test 1.

Test 2

Test 2 was performed with the same preform configuration as Test 1: a constant permeability preform, with a nominal permeability value of 1.35E-10m^2 (*Figure 6.16*Figure 6.19). The difference between

both tests was the pressure gradient applied. In this case the test was performed under vacuum (-0.98. bar) and a constant injection pressure of 1.04 bar, resulting in a pressure gradient of 2.02 bar.

The increase of the filling rate intensifies the effect of the high permeability channels and significantly increases the difference between the saturated and the unsaturated flow (*Figure 6.19*).

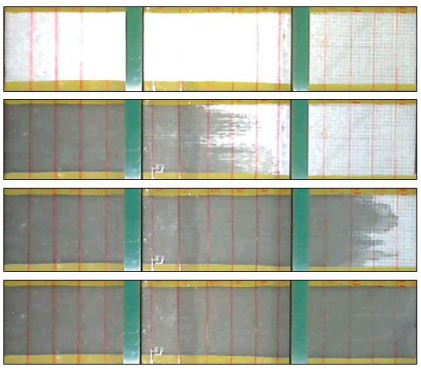

Figure 6.19 Flow front progression during Test 2.

Figure 6.20 shows the results of the on-line model calculations for Test nº2. Again, an onset permeability of 1.0 E-10 m^2 was used. As in can be seen in the figure, permeability value was quickly adapted to real data even at high filling rates.

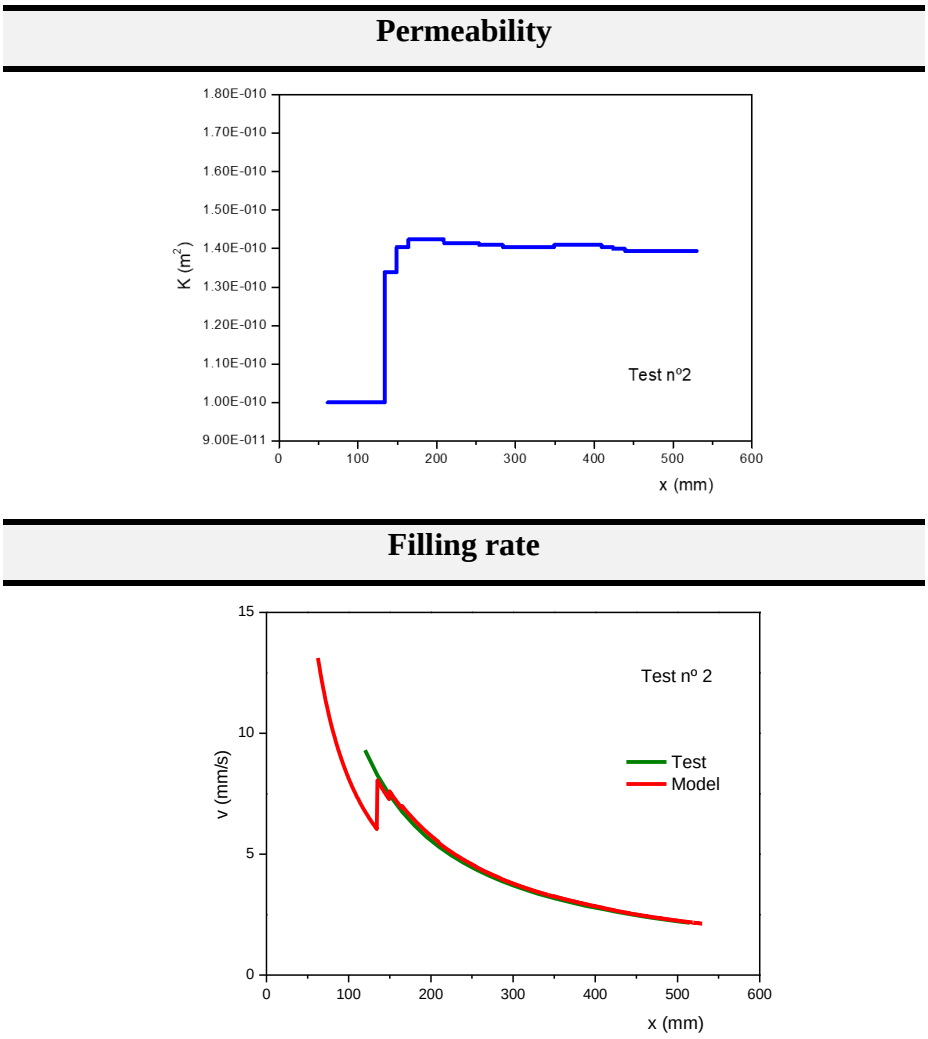

Figure 6.20 Model results for Test 2.

Test 3

Test 3 was performed with a variable permeability preform. For this purpose, the number of plies was reduced from 4 to 0 in a specific area of the preform (*Figure 6.21*). The test was carried out under vacuum (-0.98 bar) and at a constant injection pressure of 1.32 bar **(**pressure gradient of 2.30 bars).

As for Test 2, there was a significative difference between the saturated and the unsaturated flow rates. The filling rate dramatically increased in the high permeability window producing a turbulent flow with bubbles (*Figure 6.22*).

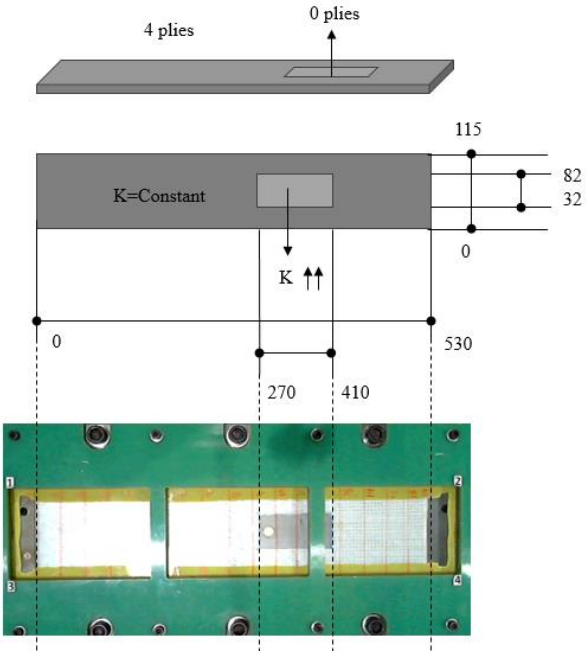

Figure 6.21. Test 3 configuration.

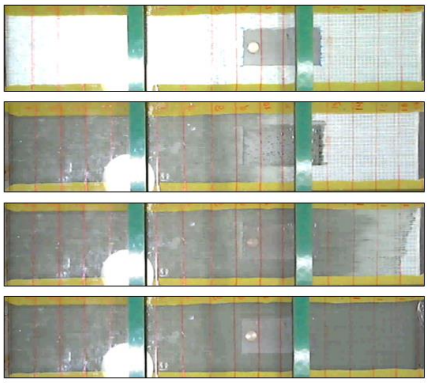

Figure 6.22 Flow front progression during Test nº3.

As shown in the *Figure 6.23* the model was able to detect an adapt to abrupt permeability changes giving a good prediction of filling rate.

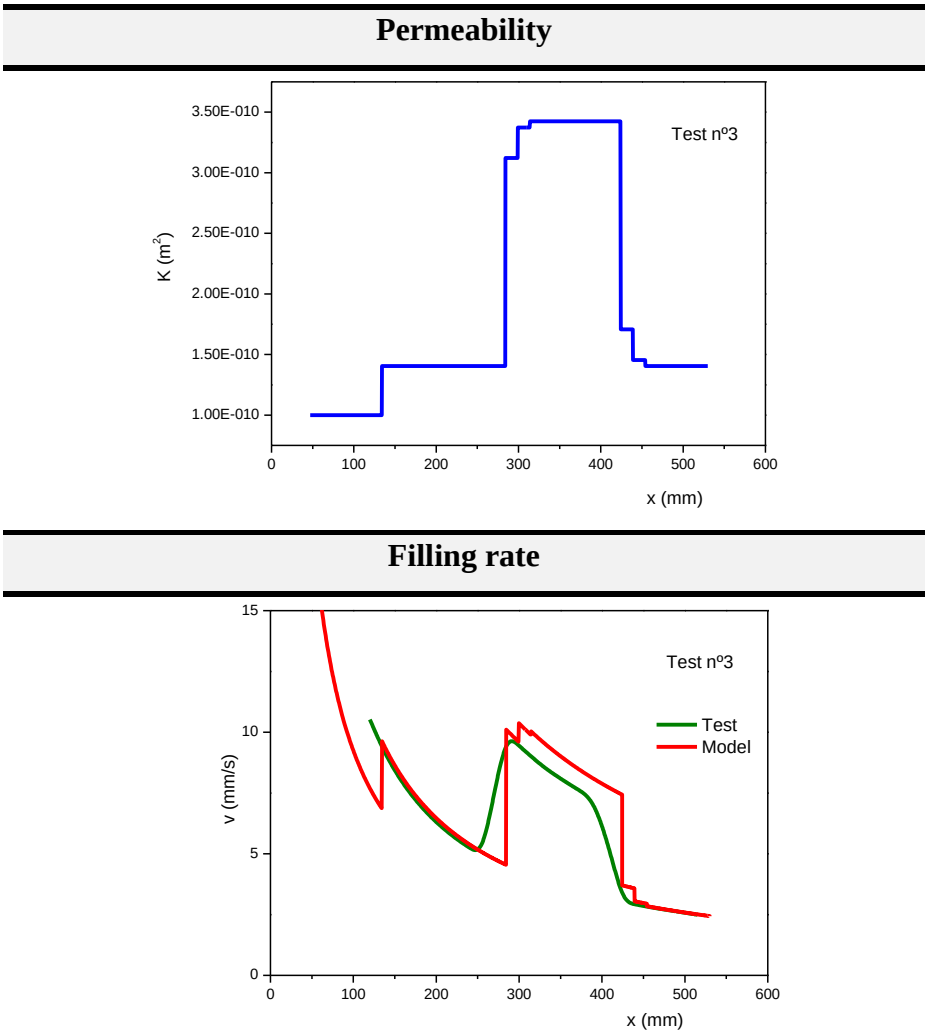

Figure 6.23 Model results for Test 3.

Test 4

The *Figure 6.24* shows Test 4. configuration. As Test 3, it was performed with a variable permeability preform. In this case, the number

of plies was reduced from 4 to 3 in a specific area of the preform, in a fibre volume variation from 47.5 to 35.6% in order to test the model at less extreme conditions. In addition, the test was carried out at lower filling rate, under a constant vacuum of 0.53 bar and no injection pressure applied.

In this case, as expected the change of the filling rate was significatively less pronounced. (*Figure 6.26*). However, as seen in the figure bellow (*Figure 6.25*), it could be clearly appreciated visually by a more unsaturated flow condition (light grey).

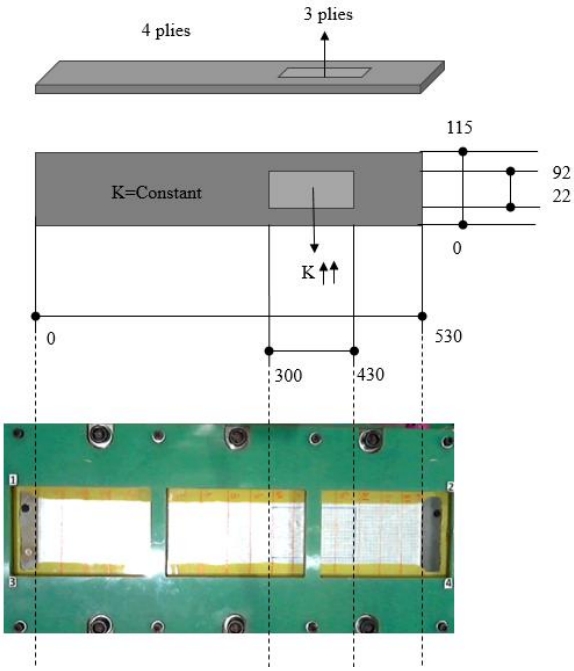

Figure 6.24. Test 4 configuration.

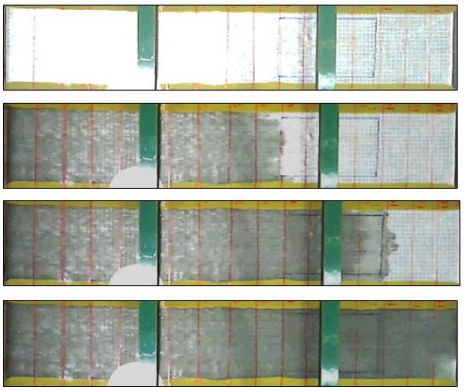

Figure 6.25 Flow front progression during Test nº4.

Figure 6.26 shows the model results for Test 4. Again, the model was able to detect and recalculate permeability changes. Even if the differences were less pronounced, the model was giving an accurate prediction of filling rate.

Permeability

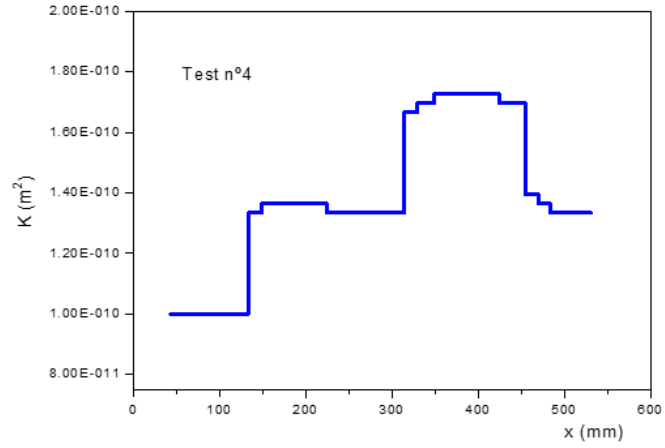

Filling rate

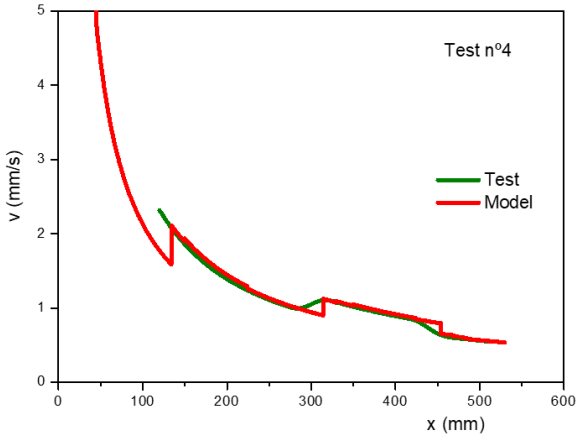

Figure 6.26 Model results for Test nº4.

6.7. CONCLUSIONS

In this chapter, the influence of the filling rate on the void formation was studied in order to select the right process parameters and optimize the manufacturing process. Although it was not feasible to perform the study in a broader range, results showed that it was possible

to manufacture high quality parts at filling rates ranging from (1 to 6 mm s^{-1})

Once the filling rates selected, manufacturing of a high fibre volume unidirectional glass fibre composite plate allowed to demonstrate the BIO-PUR resin system and process parameters suitability. The quality was good, with less than 2% of voids, and a T_g value higher than 120 ºC. Regarding the mechanical properties, a flexural modulus higher than 35 GPa and strength higher than 1000 MPa were obtained, fulfilling the requirements for automotive structural applications.

Finally, in order to improve the process robustness a numerical solution to optimize RTM processes based on a DDDAS methodology was developed. The model was able to detect and adapt to both abrupt and smooth permeability changes in the experiments, giving accurate predictions. The developed solution allows the online estimation of the evolution of the filling process and its uncertainty. This estimation can be utilized to carry out control and corrective actions during manufacturing, potentially increasing process efficiency, improving part quality and reducing process failures and defects.

6.8. REFERENCES

[1] Pierre Ferland; Dominique Guittard; Francois Trochu: concurrent methods for permeability measurement in Resin Transfer Molding. Polymer Composites, 17, 149–158 (1996).

[2] Mehdikhani, M.; Gorbatikh, L.; Verpoest, I.; Lomov, S. V.: Voids in fiber-reinforced polymer composites: A review on their formation, characteristics, and effects on mechanical performance. J. Compos. Mater. (2019), 53.

[3] Mendikute, J.; Baskaran, M.; Aretxabaleta, L.; Aurrekoetxea, J.: Effect of voids on the impact properties of Non-Crimp fabric carbon/epoxy laminates manufactured by liquid composite Moulding. Composite Structures, 297, 115922 (2022). http://doi:10.1016/j.compstruct.2022.115922.

[4] Huelsbusch, D.; Jamrozy, M.; Frieling, G.; Mueller, Y.; Barandun, G. A.; Niedermeier, M.; Walther, F.: Comparative characterization of quasi-static and cyclic deformation behavior of glass fiber-reinforced polyurethane (GFR-PU) and epoxy (GFR-EP). Materials Testing, 59, 109–117 (2017). http://doi:10.3139/120.110972.

[5] Daniel Huelsbusch; Yves Mueller; Gion A. Barandun; Michael Niedermeier; Frank Walther: Mechanical properties of GFR-polyurethane and-epoxy for impact-resistant applications under service-relevant temperatures. In Gion A. Barandun2, Michael Niedermeier3 and Frank Walther1; Proceedings of the ECCM17—17th European Conference on Composite Materials, (2016).

[6] Huelsbusch, D.; Jamrozy, M.; Mrzljak, S.; Walther, F.: Mechanism-Oriented Characterization of the Fatigue Behavior of Glass Fiber-Reinforced Polyurethane Based on Hysteresis and Temperature Measurements. Key Engineering Materials, 742,

629–635 (2017). http://doi:10.4028/www.scientific.net/KEM.742.629.

[7] Xu, Z.; Zhao, Y.; Wang, X.; Lin, T.: A thermally healable polyhedral oligomeric silsesquioxane (POSS) nanocomposite based on Diels–Alder chemistry. Chemical Communications, 49, 6755–6757 (2013). http://doi:10.1039/c3cc43432j.

[8] Afendi, M.; Banks, W. M.; Kirkwood, D.: Bubble free resin for infusion process. Composites Part A: Applied Science and Manufacturing, 36 (2005). http://doi:10.1016/j.compositesa.2004.10.030.

[9] Lundström, T. S.; Gebart, B. R.: Influence from process parameters on void formation in resin transfer molding. Polymer Composites, 15 (1994). http://doi:10.1002/pc.750150105.

[10] Lundström, T. S.; Gebart, B. R.; Lundemo, C. Y.: Void Formation in RTM. Journal of Reinforced Plastics and Composites, 12 (1993). http://doi:10.1177/073168449301201207.

[11] Park, C. H.; Lee, W.: Modeling void formation and unsaturated flow in liquid composite molding processes: A survey and review. J. Reinf. Plast. Compos. (2011), 30.

[12] Matsuzaki, R.; Seto, D.; Todoroki, A.; Mizutani, Y.: Void formation in geometry-anisotropic woven fabrics in resin transfer molding. Advanced Composite Materials, 23 (2014). http://doi:10.1080/09243046.2013.832829.

[13] Leclerc, J. S.; Ruiz, E.: Porosity reduction using optimized flow velocity in Resin Transfer Molding. Composites Part A: Applied Science and Manufacturing, 39 (2008). http://doi:10.1016/j.compositesa.2008.09.008.

[14] Patel, N.; Lee, L. J.: Modeling of void formation and removal in liquid composite molding. Part II: Model development and implementation. Polymer Composites, 17 (1996). http://doi:10.1002/pc.10595.

[15] Patel, N.; Lee, L. J.: Modeling of void formation and removal in liquid composite molding. Part I: Wettability analysis. Polymer Composites, 17 (1996). http://doi:10.1002/pc.10594.

[16] Labat, L.; Bréard, J.; Pillut-Lesavre, S.; Bouquet, G.: Void fraction prevision in LCM parts. EPJ Applied Physics, 16 (2001). http://doi:10.1051/epjap:2001104.

[17] Bréard, J.; Henzel, Y.; Trochu, F.; Gauvin, R.: Analysis of dynamic flows through porous media. Part I: Comparison between saturated and unsaturated flows in fibrous reinforcements. Polymer Composites, 24 (2003). http://doi:10.1002/pc.10038.

[18] Ruiz, E.; Achim, V.; Soukane, S.; Trochu, F.; Bréard, J.: Optimization of injection flow rate to minimize micro/macro-voids formation in resin transfer molded composites. Composites Science and Technology, 66 (2006). http://doi:10.1016/j.compscitech.2005.06.013.

[19] Spaid, M. A. A.; Phelan, F. R.: Modeling void formation dynamics in fibrous porous media with the lattice Boltzmann method. Composites Part A: Applied Science and Manufacturing, 29 (1998). http://doi:10.1016/S1359-835X(98)00031-1.

[20] Mahale, A. D.; Prud'homme, R. K.; Rebenfeld, L.: Characterization of voids formed during liquid impregnation of non-woven multifilament glass networks as related to composite processing. Composites Manufacturing, 4 (1993). http://doi:10.1016/0956-7143(93)90005-S.

[21] Lee, G. W.; Lee, K. J.: Mechanism of Void Formation in Composite Processing with Woven Fabrics. Polymers and Polymer Composites, 11 (2003). http://doi:10.1177/096739110301100706.

[22] Zhang, F.; Cosson, B.; Comas-Cardona, S.; Binetruy, C.: Efficient stochastic simulation approach for RTM process with random fibrous permeability. Composites Science and

Technology, 71, 1478–1485 (2011). http://doi:10.1016/j.compscitech.2011.06.006.

[23] Kostas Tifkitsis; Alex Skordos: Integration of stochastic process simulation and real time process monitoring of lcm sampe. In SAMPE Europe Conference 2018; Southampton, UK, (2018).

[24] Mesogitis, T. S.; Skordos, A. A.; Long, A. C.: Uncertainty in the manufacturing of fibrous thermosetting composites: A review. Composites Part A: Applied Science and Manufacturing, 57, 67–75 (2014). http://doi:10.1016/j.compositesa.2013.11.004.

[25] Potter, K.; Khan, B.; Wisnom, M.; Bell, T.; Stevens, J.: Variability, fibre waviness and misalignment in the determination of the properties of composite materials and structures. Composites Part A: Applied Science and Manufacturing, 39 (2008). http://doi:10.1016/j.compositesa.2008.04.016.

[26] Verleye, B.; Lomov, S. V.; Long, A.; Verpoest, I.; Roose, D.: Permeability prediction for the meso-macro coupling in the simulation of the impregnation stage of Resin Transfer Moulding. Composites Part A: Applied Science and Manufacturing, 41 (2010). http://doi:10.1016/j.compositesa.2009.06.011.

[27] Luthy, T.; Hintermann, M.; Mosler, H.; Ziegmann, G.; Ermanni, P.: Dependence of the 1-D permeability of fibrous media on the fibre volume content: Comparison between measurement and simulation. In Proceedings of the International Conference on Computer Methods in Composite Materials, CADCOMP; (1998).

[28] Hoes, K.; Dinescu, D.; Sol, H.; Parnas, R. S.; Lomov, S.: Study of nesting induced scatter of permeability values in layered reinforcement fabrics. Composites Part A: Applied Science and Manufacturing, 35 (2004). http://doi:10.1016/j.compositesa.2004.05.004.

[29] Desplentere, F.; Lomov, S. V.; Woerdeman, D. L.; Verpoest, I.; Wevers, M.; Bogdanovich, A.: Micro-CT characterization of variability in 3D textile architecture. Composites Science and Technology, 65 (2005). http://doi:10.1016/j.compscitech.2005.04.008.

[30] ENDRUWEIT, A.; MCGREGOR, P.; LONG, A.; JOHNSON, M.: Influence of the fabric architecture on the variations in experimentally determined in-plane permeability values. Composites Science and Technology, 66, 1778–1792 (2006). http://doi:10.1016/j.compscitech.2005.10.031.

[31] Darema, F.: Dynamic data driven applications systems: A new paradigm for application simulations and measurements. Lecture Notes in Computer Science (including subseries Lecture Notes in Artificial Intelligence and Lecture Notes in Bioinformatics), 3038 (2004). http://doi:10.1007/978-3-540-24688-6_86.

[32] Ouyang, Y.; Zhang, J. E.; Luo, S. M.: Dynamic data driven application system: Recent development and future perspective. Ecological Modelling, 204, 1–8 (2007). http://doi:10.1016/j.ecolmodel.2006.12.010.

[33] Ghnatios, C.; Masson, F.; Huerta, A.; Leygue, A.; Cueto, E.; Chinesta, F.: Proper Generalized Decomposition based dynamic data-driven control of thermal processes. Computer Methods in Applied Mechanics and Engineering, 213–216, 29–41 (2012). http://doi:10.1016/j.cma.2011.11.018.

[34] Patón Pozo, P. J.: Dynamic data driven applications systems (dddas) for multidisciplinary optimisation (mdo).

[35] Prudencio, E. E.; Bauman, P. T.; Williams, S. V.; Faghihi, D.; Ravi-Chandar, K.; Oden, J. T.: A Dynamic Data Driven Application System for Real-time Monitoring of Stochastic Damage. Procedia Computer Science, 18, 2056–2065 (2013). http://doi:10.1016/j.procs.2013.05.375.

[36] Chinesta, F.; Cueto, E.; Abisset-Chavanne, E.; Duval, J. L.; Khaldi, F. El: Virtual, Digital and Hybrid Twins: A New

Paradigm in Data-Based Engineering and Engineered Data. Archives of Computational Methods in Engineering, 27, 105–134 (2020). http://doi:10.1007/s11831-018-9301-4.

[37] Kim, T. H.; Kim, M.; Lee, W.; Kim, H.-G.; Lim, C.-S.; Seo, B.: Synthesis and Characterization of a Polyurethane Phase Separated to Nano Size in an Epoxy Polymer. Coatings, 9, 319 (2019). http://doi:10.3390/coatings9050319.

[38] Morales-Cerrada, R.; Tavernier, R.; Caillol, S.: Fully Bio-Based Thermosetting Polyurethanes from Bio-Based Polyols and Isocyanates. Polymers, 13, 1255 (2021). http://doi:10.3390/polym13081255.

7

OTHER APPLICATIONS: WIND ENERGY

7. OTHER APPLICATIONS: WIND ENERGY

7.1. GRAPHICAL ABSTRACT 202

7.2. ABSTRACT 203

7.3. INTRODUCTION 203

7.4. EXPERIMENTAL 205

7.4.1. Materials 205

7.5. CHARACTERIZATION 206

7.5.1. Mechanical properties 206

7.5.2. Density 207

7.5.3. Fibre and void volume fraction 207

7.6. RESULTS 207

7.6.1. Infusion process development 207

7.6.3. Composite manufacturing and testing 219

7.7. CONCLUSIONS 220

7.8. REFERENCES 222

7.1. GRAPHICAL ABSTRACT

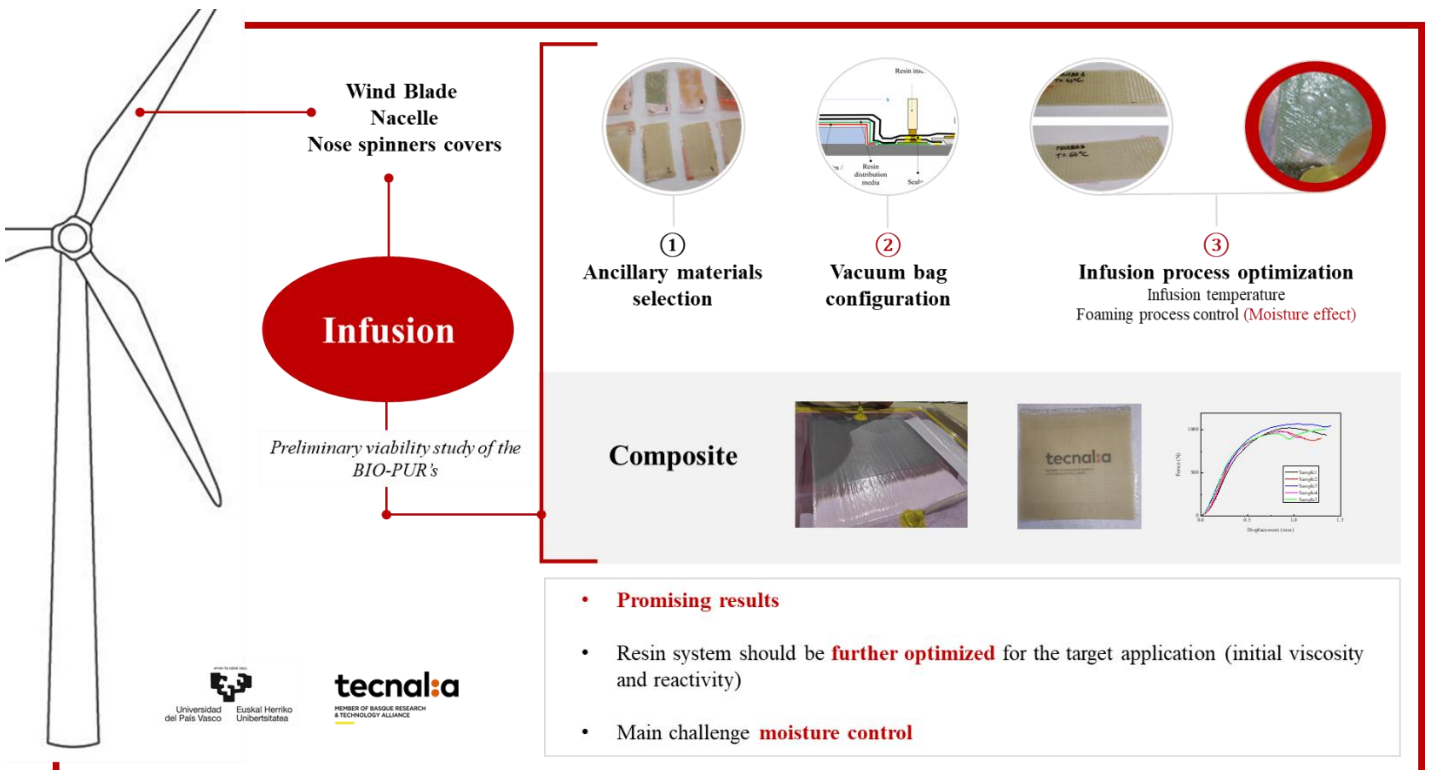

7.2. ABSTRACT

The development of wind energy is an important element of the strategy to limit global warming. As a green energy, it should be sustainable in all the aspects, that is why the sector is constantly seeking to design and manufacture their products with more sustainable materials . In this context, the BIO-PUR's resins systems developed in this PhD could be especially attractive for this application, mainly in the case of wind turbine blades but also for other components such nacelles or nose spinner covers. This is the reason why in this chapter we performed a preliminary viability study of the BIO-PUR's for the application. In this case, the manufacturing process studied was vacuum infusion. For this purpose, the infusion process had to be optimized in terms of ancillary materials and process parameters. Then, composite plates were manufactured and tested showing very promising properties.

7.3. INTRODUCTION

Climate change, economic growth, higher electricity prices and security of energy supply underscore the global need for locally produced renewable energy. In Europe alone, the ocean energy industry plans to deploy 100 GW of production capacity by 2050, meeting 10% of electricity demand, the equivalent of 76 million households.

Wind energy, and specifically offshore wind energy, is one of the most sustainable alternatives [1,2] due to its great efficiency. Therefore,

this technology arouses great interest [3,4]. However, despite being one of the most sustainable alternatives in terms of energy production, there are several aspects that should be improved, such as the sustainability of the materials and processes used in wind turbines.

Currently, between 85 and 90% of the total mass of wind turbines can be recycled [5,6] but the difficulty lies in the blades and other elements of the wind turbine such as the nacelle covers which are made of thermosetting matrix composites. Although there are different technologies for recycling blades and a growing number of companies offer recycling services, these solutions are not yet fully available or economically competitive [7].

On the other hand, the materials currently used are of petrochemical origin, that is, they are produced by refining fossil fuels, a process that generates significant amounts of CO_2.

The matrices for wind turbines blades manufacturing are typically polyester, vinyl ester or epoxy resins although for large blades such as in offshore wind turbines, where great mechanical and fatigue properties are required, epoxy resins are generally used [8,9].

Nowadays, work is being done on the development of biobased epoxy resins, recyclable acrylic resins and hardeners for epoxy resins with dynamic bonds [10-13]. A very interesting example is the development of Siemens Gamesa with a blade 81 meters long made of recyclable epoxy. The chemical structure of this new resin type makes possible to separate the resin from the other components at end of the blade's working life by dissolution of the matrix in acetic acid [14,15].

Another interesting development is the polyurethane resin developed by Covestro. Covestro partnered with the Chinese wind turbine giant Goldwind to develop the world's very first 64.2 m wind turbine blade entirely made of polyurethane resin – demonstrating the material's suitability as a cost-effective solution for wind turbines[16-18].

Although this PU resin technology has a petrochemical origin, it is claimed to improve rotor blade performance due to the resin enhanced mechanical properties, enabling reducing overall weight and material consumption. Also, it contributes to the blades manufacturing process sustainability, allowing a faster curing than when using epoxy resins.

In this chapter we performed a preliminary viability study of the developed BIOPUR's for the application. For this purpose, the infusion was optimized in terms of ancillary materials and process parameters. Then, composite plates were manufactured, and their quality was tested through micrographic and ILSS tests showing very promising results.

7.4. EXPERIMENTAL

7.4.1.Materials

Resin

The composition of the BIO-PUR3 resin used for this study is shown in the *Table 6.2*. As previously mentioned in the chapter 5, the

BIO-PUR3 system present the broader process time window, being the most suitable formulation for infusion.

Table 6.2.BIO-PUR3 resin formulation.

System	Components ratio (pbw)					
	Part A			***Part B***		
	Polyol	*Glycerol*	*BDDE*	*Isocyanate*	*LiCl*	*DAS*
BIO-PUR3	100	22	7	267	2	9
	Renewable content (%)					
	27					

Reinforcement

An unidirectional axial glass fibre used in wind blades, supplied by Axson technologies (Cergy-Pontoise, France) was selected as reinforcement. Fibre properties are summarized in Table 1.

Table 7.1. Fibre properties.

Weaving pattern	E-glass unidirectional axial non-crimp fabric (NCF)
Areal weight	962 ± 29 g m^{-2}
Sewing thread	Polyester 11 ± 0.3 g m^{-2}

7.5. CHARACTERIZATION

7.5.1.Mechanical properties

ILSS tests were carried out at RT according to ASTM 2344 using an Instron 5500R6025 (Instron, Norwood, USA) equipment.

7.5.2.Density

The density of the developed resin and the composite plate was determined in accordance with the liquid displacement method (ASTM D792-20).

7.5.3.Fibre and void volume fraction

The burn-off method described in ASTM D3171-22 was used to determine the fibre volume fraction, Vf, and the void volume fraction, Vv, of the composite samples.

7.6. RESULTS

7.6.1.Infusion process development

Ancillary materials selection

In order to validate the compatibility of BIO-PUR3 system with the usual infusion materials, different combinations of resin distribution media and Peel ply were studied. The materials used are summarized in the *Table 7.2*. The materials used in the different combination studied are summarised in *Table 7.3.*

The infusions made with different resin distribution media showed that the turbulent flow produced with the LowMesh3P95 during the process, favoured the creation of bubbles. Therefore, for the following infusions, *Greenflow75* was selected.

On the other hand, the *Econostitch G* Peel Ply was bonded to the sample and couldn’t be removed. Although both the *Release Ply C* and

60BR showed a good behaviour, the *Release Ply C* was selected due to its lower price. *60BR* peel ply is specific for high temperatures and it was not necessary in this case.

Table 7.2. Commercial infusion materials.

Resin distribution media	
Greenflow75	*LowMesh3P95*
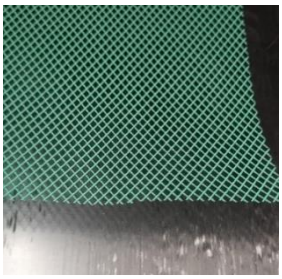	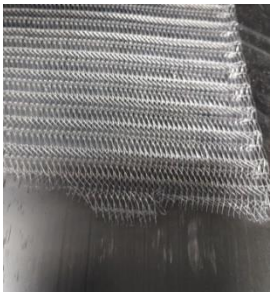
Release film / Peel Ply	
Econostitch G	*Release Ply C*
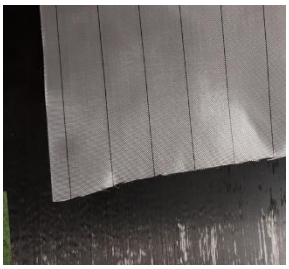	

60BR

Table 7.3. Ancillary materials combinations studied.

System	Distribution media	Pell ply
INFU-1	*LowMesh3P95*	*Econostitch G*
INFU-2	*Greenflow75*	*Release Ply C*
INFU-3	*LowMesh3P95*	*Release Ply C*
INFU-4	*Greenflow75*	*60BR*

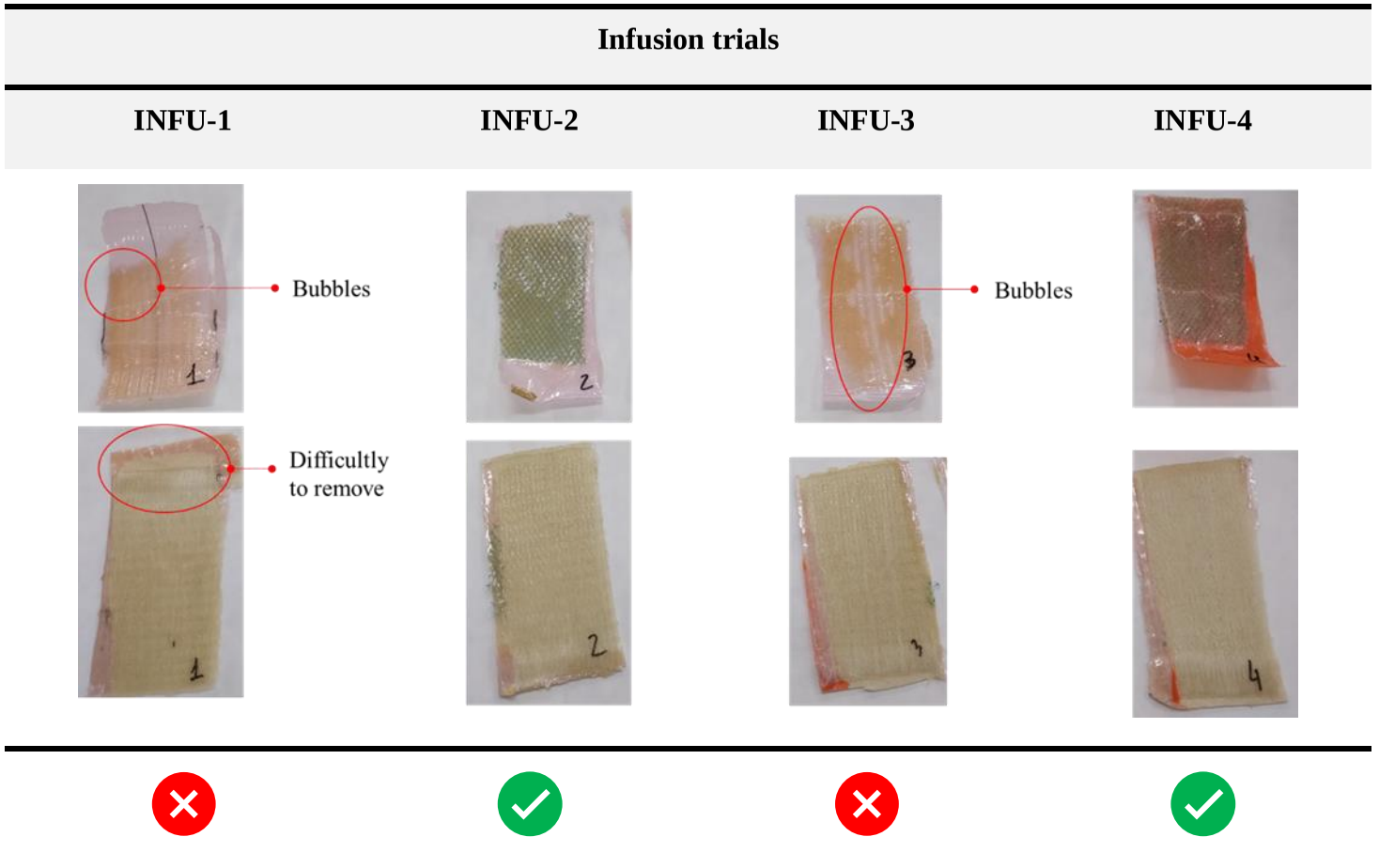

Figure 7.1. Results of BIO-PUR3 infusion trials with the different ancillary materials combinations.

Vacuum bag configuration

The double infusion bag (*Figure 7.2*) was selected in this work. This method is commonly used in industrial process to tight process control enabling repeatable fibre volumes percent and improving consistency of infused laminates [19].

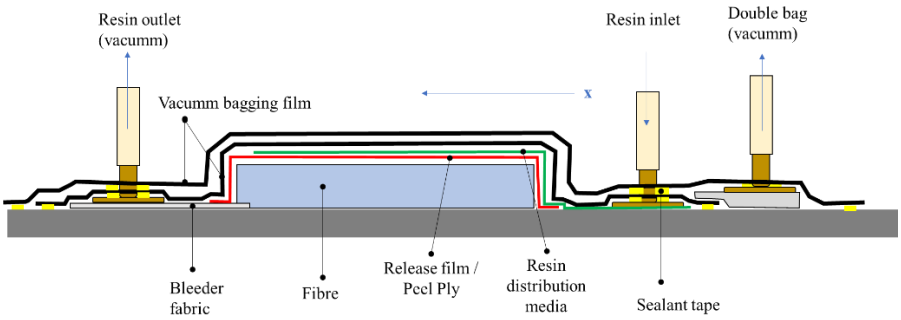

Figure 7.2. Double infusion bag configuration.

Infusion process optimization

In order to select the suitable infusion parameters, the infusion temperature, and moisture effect was analysed.

Infusion temperature

As seen in the previous chapter BIO-PUR3 used in this study was developed to enable a quick RTM process at 120 ºC. This is the reason why it is not optimal for RT manufacturing.

Currently, the wind blade infusion process is performed at low temperatures, usually RT. Nevertheless, the BIO-PUR3 presents a viscosity value higher than 200 mPa at RT which is the maximum optimal value for infusion resins. This case, infusions were performed at

different temperatures: RT, 40 and 60 ºC to compare and select the best combination viscosity/resin reactivity.

The pictures presented in *Figure 7.3* show that the filling at RT was very slow and, in the inlet, a high amount of BIO-PUR3 has accumulated. However, the fibre impregnation was fast enough to avoid the resin accumulation at 40 ºC and 60 ºC.

After these preliminary infusions with the BIO-PUR3 resin at different temperatures, it was noticed that the polyurethanes tend to foam in the curing stage and the appearance of bubbles was observed (*Figure 7.3*). This phenomenon also happens in the case of petrochemical origin PUR for infusion [16-18].

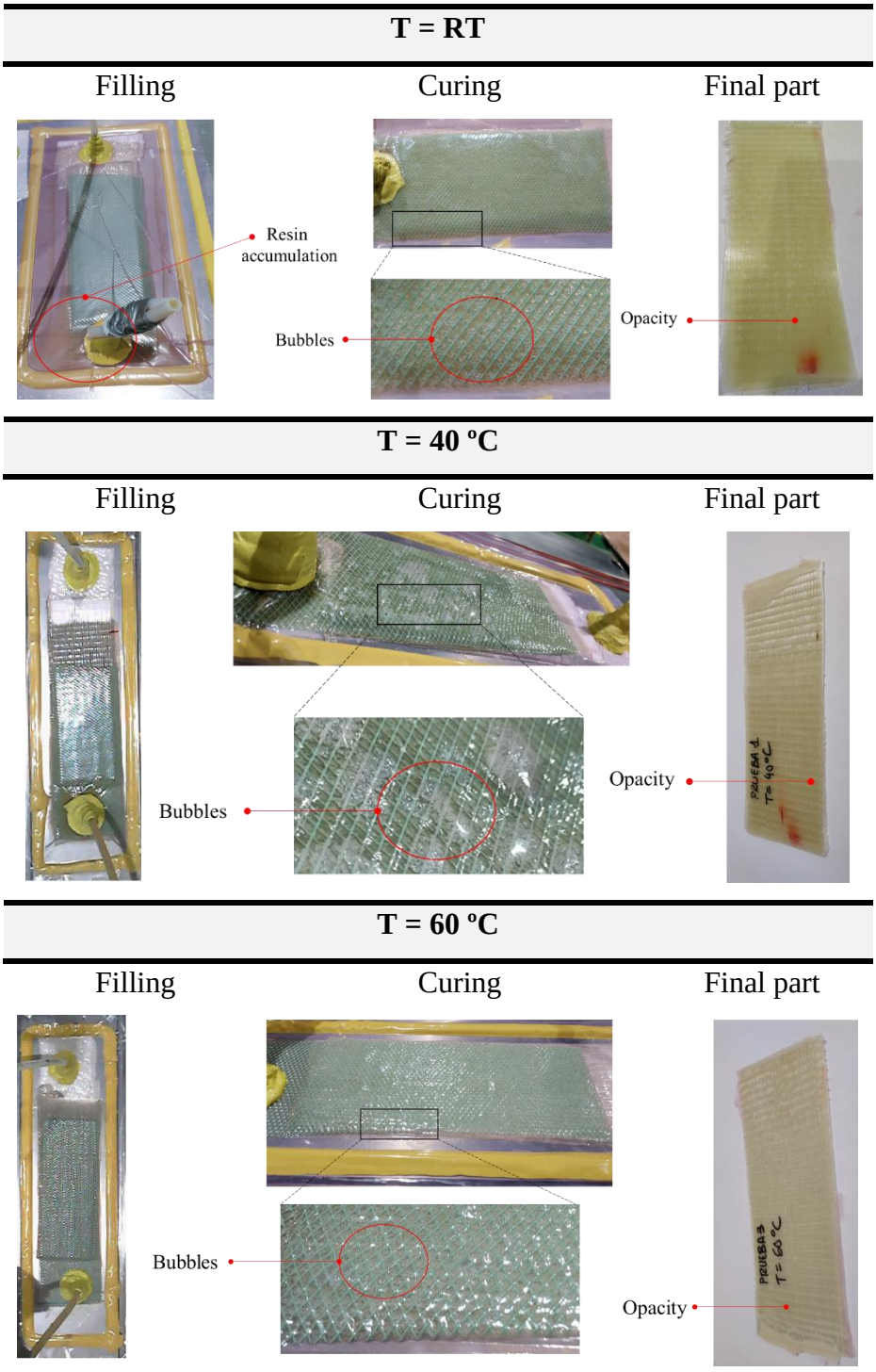

Figure 7.3. BIO-PUR3 infusion at different temperatures.

Foaming process control

PURs foaming was studied in detail. One of the main reasons of this phenomenon is the capability of isocyanate to react with water to form urea and CO_2 groups. Because of that, the control of this reaction is a critical factor in the case of PURs.

Composites for wind turbine blades are reinforced with high-performance glass fabrics and these fibres are hygroscopic and tend to absorb moisture. The *Figure 7.4* shows that the fibre moisture content of the fibre stored in the warehouse is enough to react with isocyanate and cause the resin foaming.

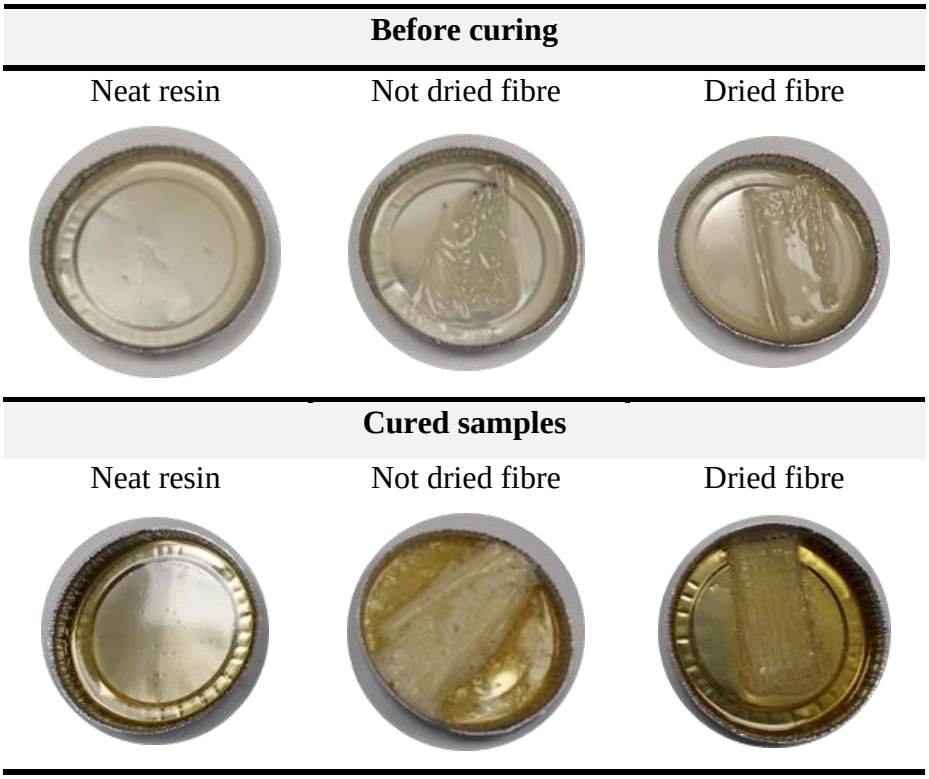

Figure 7.4. Fibre moisture effect.

Avoiding foaming of BIO-PUR3 is one of the major challenges for the validation of this resin for the infusion process. For this reason, different strategies were studied to control the moisture effect in the infusion process.

1. Incorporation in the formulation of moisture scavengers

One of the most used strategy to control the moisture effect in PURs is the moisture scavenger integration in the PUR formulation [20,21]. There is a wide variety of moisture scavengers based on different technologies in the market. One of the most attractive alternatives is the system based on mono-oxazolidines [22-23]. The oxazolidine reacts with the water and prevents the generation of CO_2 leading to defect free PURs [24]. Zeolites are natural aluminium-silicate and one of the most common moisture scavengers [20,25,26]. They show an extremely high porosity and cationic exchange capacity. This is the reason why zeolites are used as smell binder, molecular sieve or filter media. In order to avoid the foaming of BIO-PUR3, these components were incorporated in the formulation. Two commercial mono-oxazolidines, Incozol 2 provided by Incorez Limited (Preston, United Kingdom) and LithoFill provided by Lithos Natural GmbH (Ennsdorf, Austria), were employed as moisture scavengers. However, the results were not satisfactory employing 3% of moisture scavenger. The BIO-PUR3 presented bubbles in both cases (Figure *7.5*).

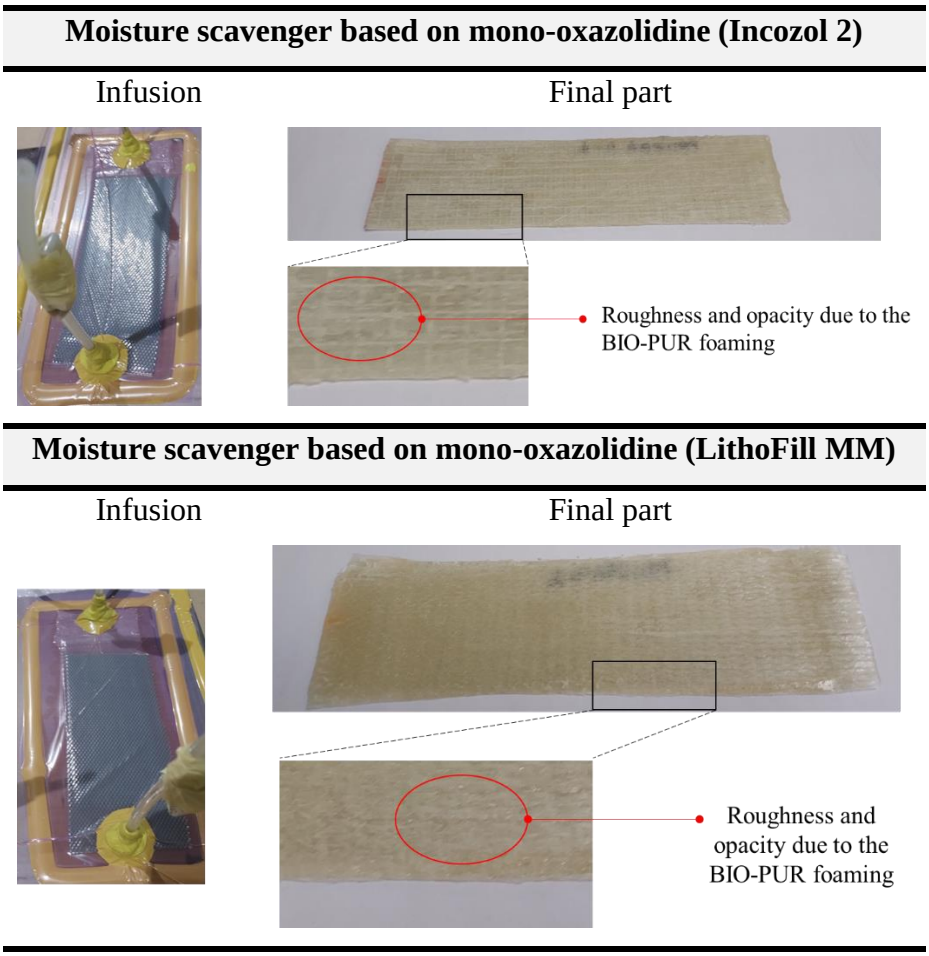

Figure 7.5. BIO-PUR3 infusion trial with moisture scavengers.

2. Vacuum Assisted Process (VAP®)

The incorporation of a specific membrane in the infusion assembly was studied. Vacuum Assisted Process (VAP®) uses the properties of modern, semi-permeable membrane systems to remove trapped air and gas during resin infusion.

Nevertheless, the composite fabricated foamed, showing that this VAP system is not the final solution for this type of issues (*Figure 7.6*).

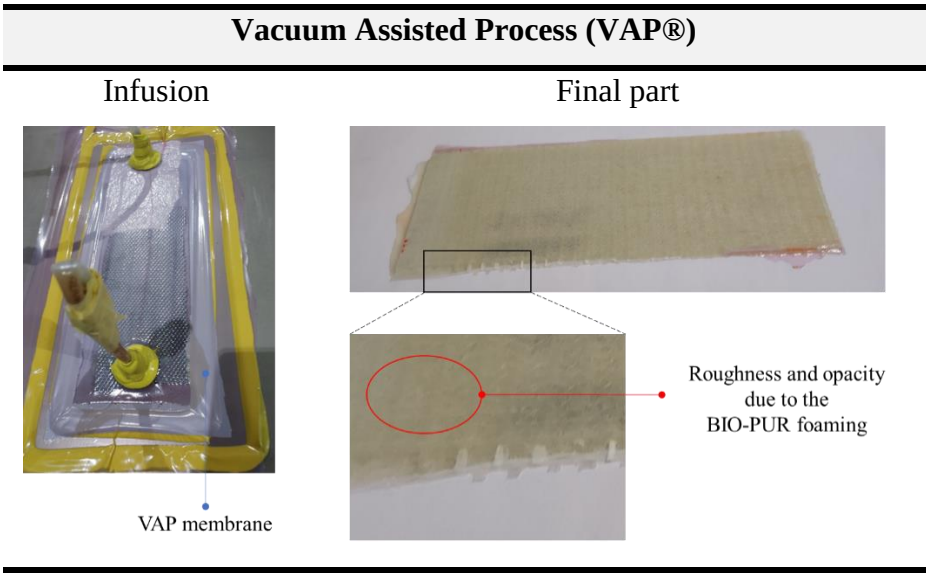

Figure 7.6. Infusion trial with Vacuum Assisted Process.

3. *Fibre drying*

In order to prevent the BIO-PUR3 foaming, the final strategy studied was to eliminate the moisture drying the fibres (120 ºC for 1 hour) before the infusion process. This strategy presents the disadvantage of adding a previous process step of drying the infusion materials, increasing the process time and the amount of energy consumption. The results shown in *Figure 7.7* demonstrate the suitability of this strategy. The composite plate manufactured presented only some slight foaming evidence in the dry areas but not in the fully saturated and the general aspect better.

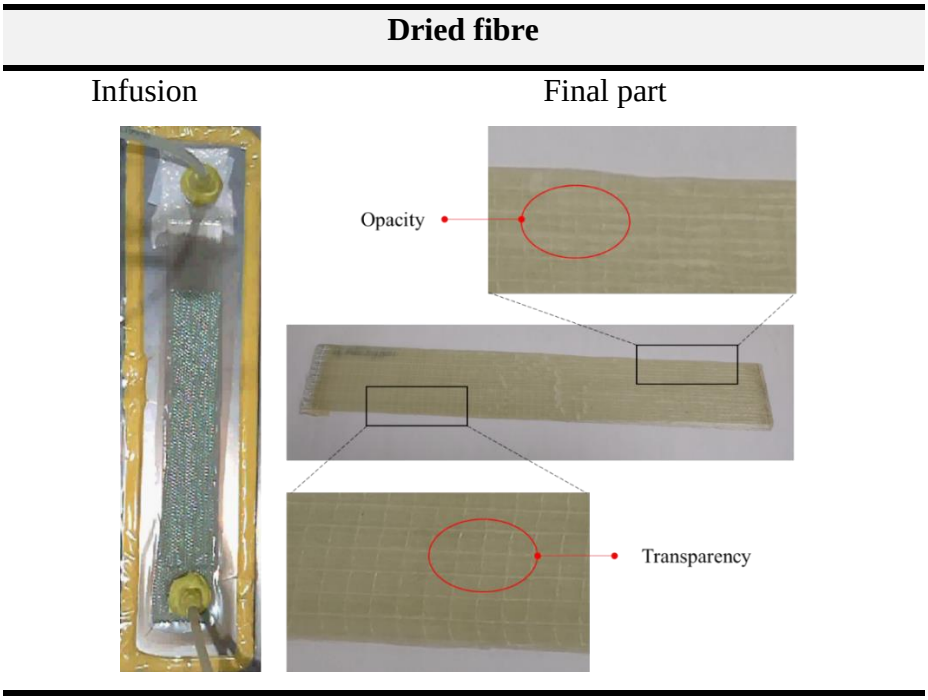

Figure 7.7. BIO-PUR3 infusion with previously dried glass fabric.

7.6.2.Composite sample fabrication

Based on the previous results, the following infusion process parameters were selected (*Figure 7.8*).

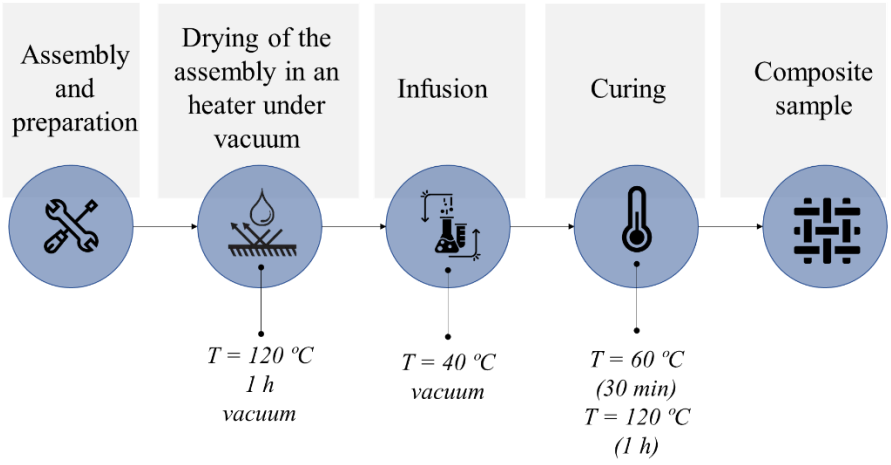

Figure 7.8. BIO-PUR3 infusion process parameters.

Three composite plates of different sizes were manufactured with the established work method and the selected infusion parameters. The three parts presented a good appearance as shown in *Figure 7.9.*

Infusion with optimum parameters	
Small plate (200 x 90 mm)	
Infusion	Final part
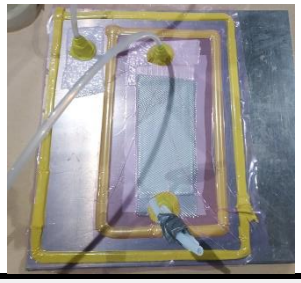	
Medium plate (300 x 300 mm)	
Infusion	Final part
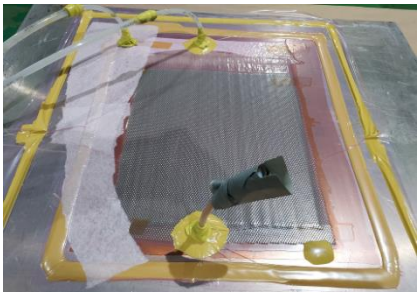	
Big plate (350 x 450 mm)	
Infusion	Final part
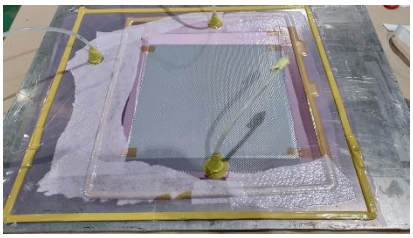	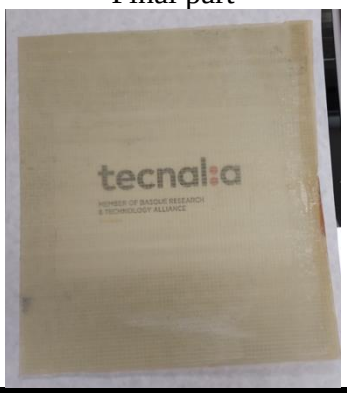

Figure 7.9. Infusion manufactured BIO-PUR3 composite plates.

Although the reinforcement was fully impregnated, the filling stopped before reaching the outlet because of the resin reaction and consequent increase of viscosity. The resin viscosity increases caused a filling showdown at 23 minutes.

7.6.3.Composite manufacturing and testing

In order to validate the BIO-PUR3 formulation suitability for the infusion process the composite big plate was tested mechanically and the void content was determined to analyse the composite quality. *Figure 7.10* shows the force-displacement curves obtained in the ILSS tests of the different coupons.

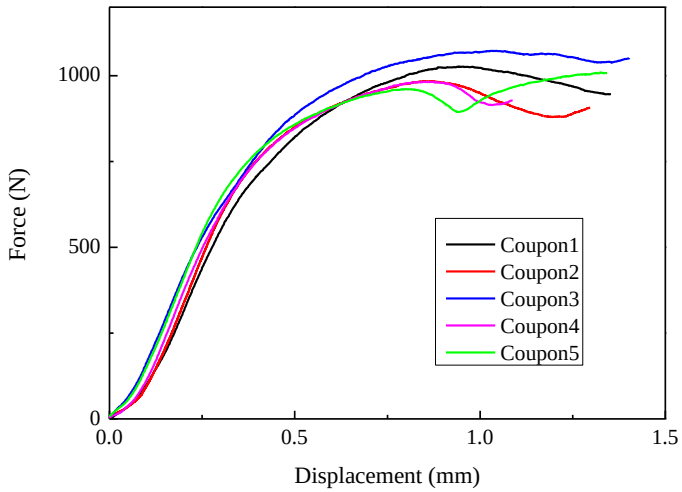

Figure 7.10. Interlaminar shear strength results for infused BIO-PUR3 composite plate.

The tests results are shown in *Table 7.4*. The BIO-PUR3 composite exhibit good final properties. ILSS value of the coupons, extracted at different plate lengths showed a very small deviation showing that a constant quality was attained. Void content of the samples

was less than 0,72% in all the cases. The fibre volume content was also constant and in accordance with the theoretical one (57,1%).

Table 7.4. Final properties of BIO-PUR3 based composite

BIO-PUR3 composite (infusion)		
Method	**Properties**	**Value**
Mechanical properties	**ILLS** (MPa)	45 ± 1
Burn-off method	**Void content (Vv)** (%)	0.46 ±0.23
	Fibre volumen content (Vf) (%)	57.56± 0.21

7.7. CONCLUSIONS

In this chapter the suitability of the developed BIO-PUR resin system for infusion was studied.

The resin viscosity made necessary to increase the process temperature from RT to 40 ºC, even for small composite plates manufacturing and process time window was narrow. The resin tested, BIO-PUR3, was designed for short cycle times RTM manufacturing at 120 ºC. Although the resin system should be further optimized for the target application, the results are considered promising.

The main challenge of BIO-PUR3 was the moisture control. Due to the isocyanate capability to react with water and form CO_2, the resin tends to foam. However, with the adequate selection of process

parameters high quality composites based on BIO-PUR could be manufactured. The composite samples presented good quality (only 0.5% of voids) and high mechanical properties (ILLS 45 MPa).

7.8. REFERENCES

[1] BOEM: Renewable Energy on the Outer Continental Shelf.

[2] IRENA: Wind Energy Available online: https://www.irena.org/wind (accessed on Jul 20, 2022).

[3] Cavazzi, S.; Dutton, A. G.: An Offshore Wind Energy Geographic Information System (OWE-GIS) for assessment of the UK's offshore wind energy potential. Renewable Energy, 87 (2016). http://doi:10.1016/j.renene.2015.09.021.

[4] Manson H.: The markets: Renewable energy .

[5] Sánchez, R. G.; Pehlken, A.; Lewandowski, M.: On the Sustainability of Wind Energy Regarding Material Usage. Acta Technica Corviniensis - Bulletin of Engineering, 7 (2014).

[6] WindEurope: Accelerating Wind Turbine Blade Circularity. Thematic reports, (2020).

[7] Tarigan, P. B.: A new Circular Economy Action Plan For a cleaner and more competitive Europe. Journal of Chemical Information and Modeling, 53 (2013). http://doi:10.1017/CBO9781107415324.004.

[8] Broøndsted, P.; Nijssen, R. P. L.: Advances in wind turbine blade design and materials;

[9] Mishnaevsky, L.; Branner, K.; Petersen, H. N.; Beauson, J.; McGugan, M.; Sørensen, B. F.: Materials for wind turbine blades: An overview. Materials (Basel). (2017), 10.

[10] Guelcher, S. A.; Gallagher, K. M.; Didier, J. E.; Klinedinst, D. B.; Doctor, J. S.; Goldstein, A. S.; Wilkes, G. L.; Beckman, E. J.; Hollinger, J. O.: Synthesis of biocompatible segmented polyurethanes from aliphatic diisocyanates and diurea diol chain extenders. Acta Biomaterialia, 1 (2005). http://doi:10.1016/j.actbio.2005.02.007.

[11] Konieczny, J.; Loos, K.: Green polyurethanes from renewable isocyanates and biobased white dextrins. Polymers, 11 (2019). http://doi:10.3390/polym11020256.

[12] Wang, B.; Ma, S.; Xu, X.; Li, Q.; Yu, T.; Wang, S.; Yan, S.; Liu, Y.; Zhu, J.: High-Performance, Biobased, Degradable Polyurethane Thermoset and Its Application in Readily Recyclable Carbon Fiber Composites. ACS Sustainable Chemistry and Engineering, 8 (2020). http://doi:10.1021/acssuschemeng.0c02330.

[13] Madbouly, S. A.; Zhang, C.; Kessler, M. R.: Bio-based Plant Oil Polymers and Composites;

[14] Ferrari, F.; Esposito Corcione, C.; Striani, R.; Saitta, L.; Cicala, G.; Greco, A.: Fully Recyclable Bio-Based Epoxy Formulations Using Epoxidized Precursors from Waste Flour: Thermal and Mechanical Characterization. Polymers, 13, 2768 (2021). http://doi:10.3390/polym13162768.

[15] Siemens Gamesa: Siemens Gamesa pioneers wind circularity: launch of world's first recyclable wind turbine blade for commercial use offshore Available online: https://www.siemensgamesa.com/newsroom/2021/09/launch-world-first-recyclable-wind-turbine-blade (accessed on Aug 22, 2022).

[16] Manson H.: Covestro delivers first order of polyurethane resin for wind blades.

[17] Covestro: Covestro polyurethane resin composites: an easy choice for wind turbine blades Available online: https://solutions.covestro.com/en/highlights/articles/stories/2020/covestro-polyurethane-solutions-easy-choice-wind-turbine-rotor-blades (accessed on Aug 15, 2022).

[18] Covestro: Covestro, Goldwind and LZ Blades develop world's first 64.2-meter polyurethane wind turbine blade Available online: https://www.covestro.com/press/covestro-goldwind-and-

lz-blades-develop-worlds-first-642-meter-polyurethane-wind-turbine-blade/ (accessed on Aug 22, 2022).

[19] Gardiner, G.: Double-bag infusion: 70% Fiber volume? Composites Technology, 16 (2010).

[20] Chattopadhyay, D. K.; Raju, K. V. S. N.: Structural engineering of polyurethane coatings for high performance applications. Prog. Polym. Sci. (2007), 32.

[21] Sharmin, E.; Zafar, F.: Polyurethane: An Introduction. In Polyurethane; (2012).

[22] Robinson, G. N.; Alderman, J. F.; Johnson, T. L.: New oxazolidine-based moisture scavenger for polyurethane coating systems. Journal of Coatings Technology, 65 (1993).

[23] Ming, S.; Hong, C.; Jun, G.; Jingxin, L.: Synthesis of polyoxazolidines and their application in moisture-curable polyurethane. Journal of Adhesion Science and Technology, 30 (2016). http://doi:10.1080/01694243.2016.1145785.

[24] Thomas, A.: Improving polyurethane surface coatings Part 2: Use of oxazolidines and aldimines. Surface Coating International, 98, 223–230 (2015).

[25] Pfenninger, A.: Manufacture and Use of Zeolites for Adsorption Processes. In; (1999).

[26] Somdee, P.; Lassú-Kuknyó, T.; Kónya, C.; Szabó, T.; Marossy, K.: Thermal analysis of polyurethane elastomers matrix with different chain extender contents for thermal conductive application. Journal of Thermal Analysis and Calorimetry, 138 (2019). http://doi:10.1007/s10973-019-08183-y.

8

END OF LIFE / RECYCLABILITY

8. END OF LIFE / RECYCLABILITY

8.1. GRAPHICAL ABSTRACT 226

8.2. ABSTRACT 227

8.3. INTRODUCTION 227

8.4. EXPERIMENTAL 234

8.4.1. Materials 234

8.4.2. Synthesis 235

8.5. CHARACTERIZATION 237

8.5.1. Characterization of Triol-DA and BHET 237

8.5.2. Characterization of BIO-PUR-DA and BIO-PUR-R systems 238

8.6. RESULTS 240

8.6.1. Synthesis of BIO-PUR containing dynamic covalent bonds (BIO-PUR-DA) 240

8.6.2. Synthesis of BIO-PUR with recycled components 252

8.7. CONCLUSIONS 260

8.8. REFERENCES 262

8.1. GRAPHICAL ABSTRACT

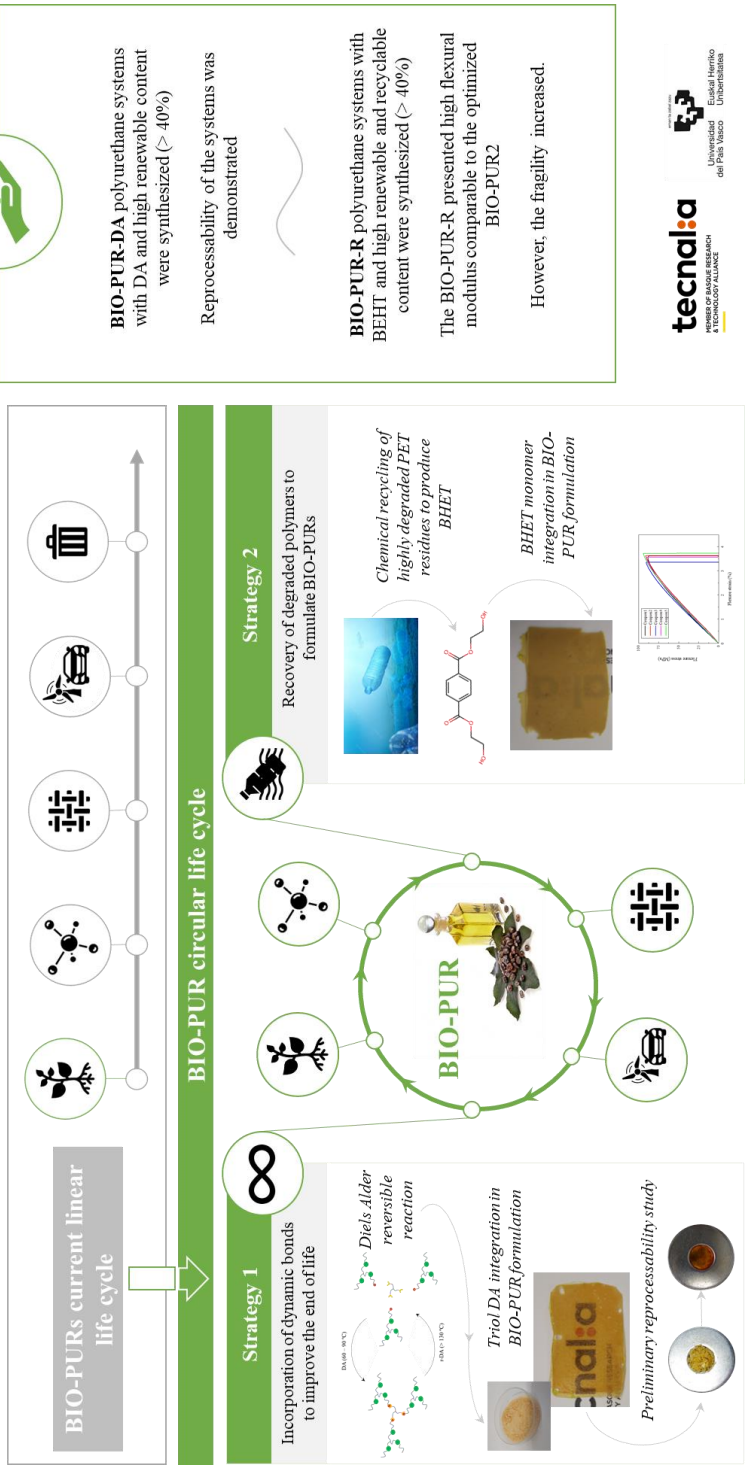

8.2. ABSTRACT

In this chapter a valid end of life option for the newly developed sustainable BIO-PUR formulation was explored with the incorporation of reversible/dynamic covalent bonds to increase recyclability. The technology is based on the development of specifically engineered polyols with reversible Diels Alder (DA) cleavage points. The DA/r-DA reaction thermo-reversibility was analysed by DSC and FTIR. The curing of the BIO-PUR system with Diels Alder cleavage points (BIO-PUR-DA) was analysed by means of DSC and resin plates were manufactured to carry out preliminary studies of the novel formulation reprocessability.

Moreover, the incorporation of recycled monomers in the BIO-PUR was also investigated adding bis(2-hydroxyethyl) terephthalate (BHET), a monomer obtained after the glycolysis of highly degraded marine PET to the BIO-PUR formulation (BIO-PUR-R). The effect of integrating BHET in the BIO-PUR formulation instead of glycerol on the reactivity was studied by DSC and rheological tests. In addition, coupons were manufactured and tested by DMA and flexural tests.

8.3. INTRODUCTION

PUR resin systems used for high-performance composite structures react to crosslink and cure into rigid three-dimensional infusible networks that cannot be depolymerized, reformed, reused or recycled. This is one of the main disadvantages of BIO-PUR with regard

of environmental impact. Covalent adaptable networks (CAN) with dissociative or associative dynamic or reversible bonds could be very promising approach to achieve thermally reprocessable or recyclable PURs [1-5] (*Figure 8.1*) to improve the PUR circularity.

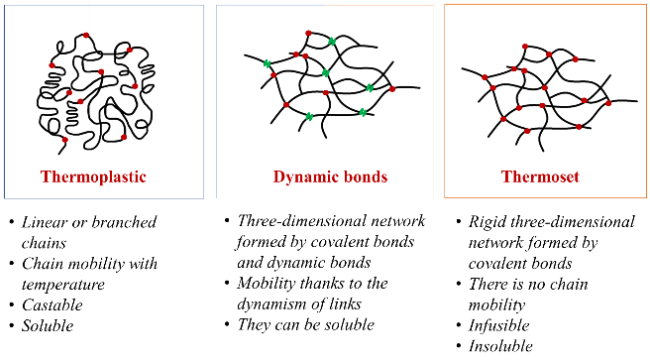

Figure 8.1.CAN advantages compared to thermoplastic and thermoset common polymers.

Reversible covalent bonds can be divided into two groups, depending on their exchange mechanism (*Figure 8.2*): (a) dissociative CANs, where an existing bond is broken before a new bond is formed, and (b) associative CANs, where the cleavage of the exiting bond and the formation of a new one is concerted [2].

A typical example for a dissociative CAN reaction is given by Diels-Alder based polymers. Diels-Alder (DA) reaction is highly efficient, simple and can be repeatedly healed through only the application of heat for the occurrence of the retro Diels-Alder (r-DA) reaction (*Figure 8.3*) [2,6-11].

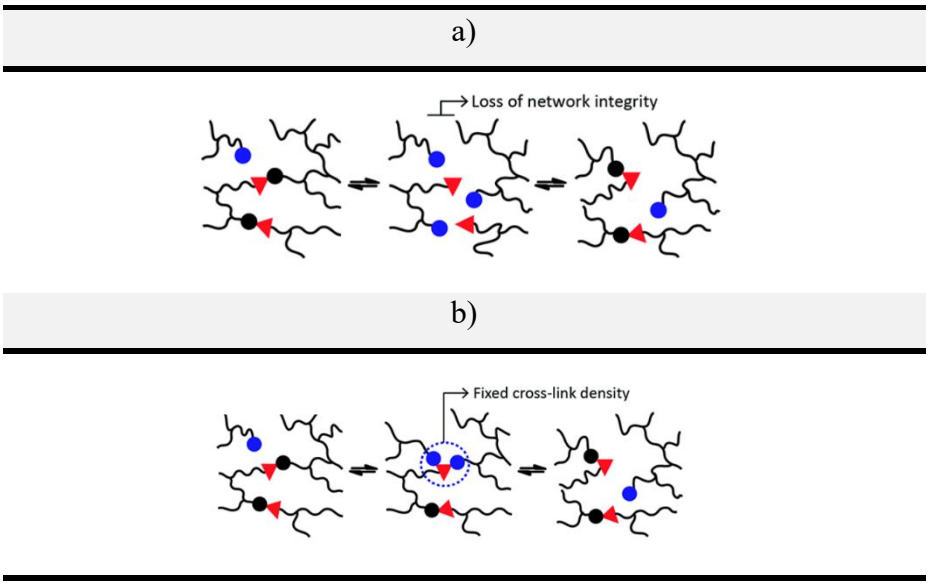

Figure 8.2. a) Dissociative and b) associative CANs reversible reaction mechanism [12]..

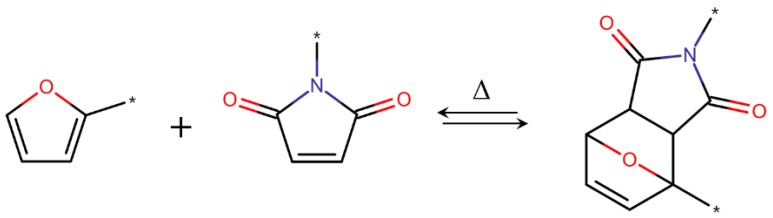

Figure 8.3.Diels Alder reaction.

The proposal of introducing cleavable bonds into thermosetting resin provides a new strategy for the gentle recovery of fibres from the composite. The temperature range at which the process takes place depends on several factors, such as the polymer backbone, crosslinking density, crosslinking moieties, and macromolecular architecture. These factors also influence the general properties of the materials, making them highly tuneable regarding their processing temperatures and mechanical performance.

In addition to dynamic bonds, recent publications focus on the subproducts obtained from the depolymerization/repolymerization of fossil based products like poly(ethylene terephthalate) (PET), in order to reduce the environmental impact [13]. As it is well known, PET represents a high percentage of the plastic waste, both from urban and marine origin. The main process for the valorisation of PET residues is the mechanical recycling, however it is not suitable for highly degraded PET.

In a recent publication, it is in fact demonstrated that chemical recycling of highly degraded PET marine litter produces a subproduct that can be successfully used to this scope [119,120]. Bis(2-hydroxyethyl) terephthalate (BHET) (*Figure 8.4*) is the monomer obtained after the glycolysis of marine and urban PET, and as it is reported, is a suitable hydroxylated component for the synthesis of polyurethanes providing stiffness to the obtained polyurethane [16,17].

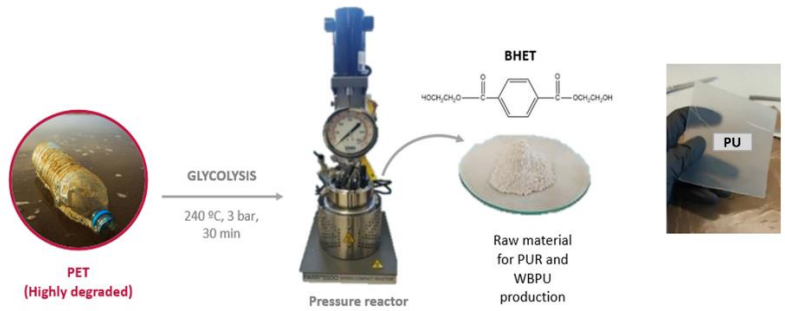

Figure 8.4. BHET monomer obtained after the PET glycolysis and a polyurethane synthesised from it [18].

BIO-PUR resins developed in this work are derived from renewable sources (vegetable oil), but they still present some environmentally drawbacks like their linear life cycle *(Figure 8.5)*.

Two research lines have been identified to further improve the BIO-PUR sustainability; the incorporation of dynamic bonds to improve the end of life of the composites manufactured with the BIO-PUR and the recovery of degraded polymers to obtain monomers and their integration into the BIO-PUR formulation (*Figure 8.6*). This work was performed with the collaboration of the 'Materials + Technologies' research group of the University of the Basque Country (EHU/UPV) which are focussing their research work on the incorporation of dynamic bonds in thermosets and on the chemical recycling of PET.

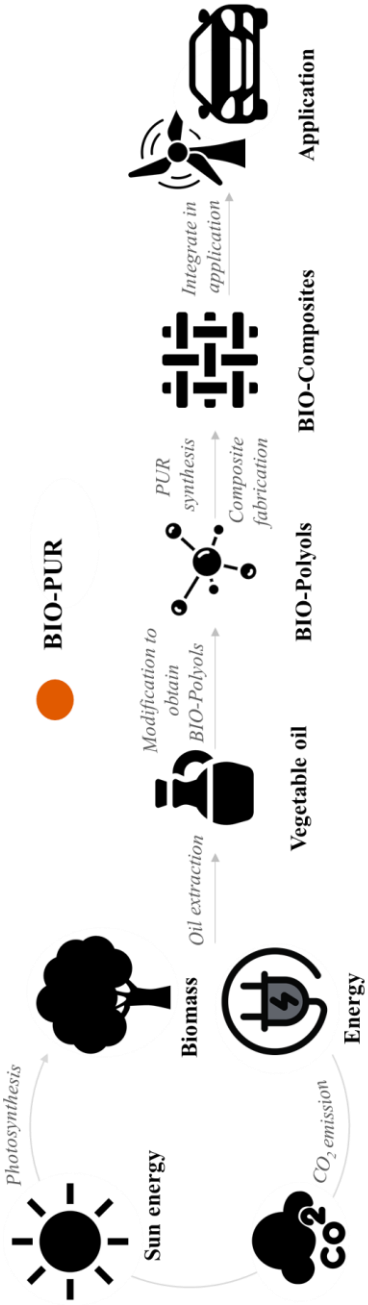

Figure 8.5.BIO-PURs linear life cycle.

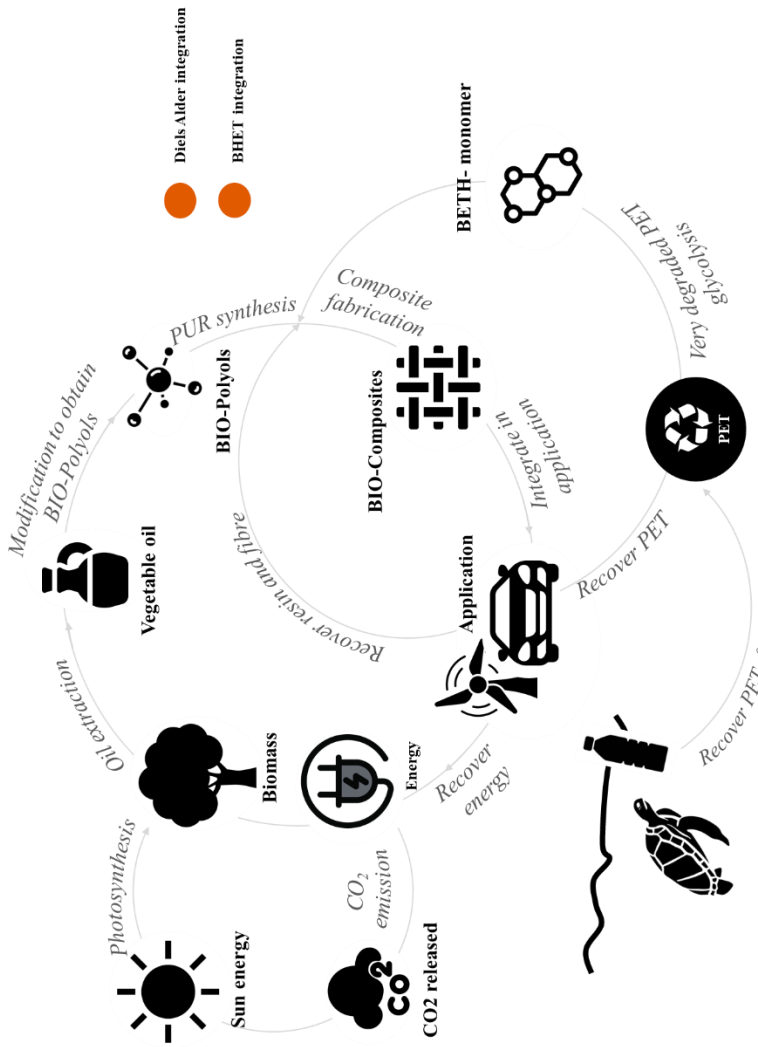

Figure 8.6.BIO-PUR circular materials.

Dynamics bonds were incorporated in the BIO-PUR adding a novel triol with DA (Triol-DA) into the formulation (BIO-PUR-DA). The effect of the triol in the curing has been analysed by DSC tests. Moreover, DSC and FTIR evaluated the DA/r-DA reaction thermo-reversibility, and some preliminary tests have been carried out to study the new formulation reprocessability. Moreover, the novel BIO-PUR-DA systems has been compared with the BIO-PUR2 optimized system.

In the other hand, the BHET obtained in the glycolysis of PET has been incorporated in the BIO-PUR (BIO-PUR-R). DSC and rheology analysis were performed in order to study the formulation reactivity. Moreover, the viability of the developed systems was evaluated by DMA and flexural tests. In order to validate the BIO-PUR-R systems, it has been compared with the BIO-PUR2 formulation.

To clearly differentiate the two strategies, the results of this chapter are divided into two large sections: the synthesis of BIO-PUR containing dynamic covalent bonds (BIO-PUR-DA) and the synthesis of BIO-PUR with recycled components (BIO-PUR-R).

8.4. EXPERIMENTAL

8.4.1.Materials

GMT-EHU/UPV group kindly provided the Triol-DA and BHET employed in the synthesis of BIO-PUR-DA and BIO-PUR-R polyurethanes, respectively. The polyol and isocyanate are those selected in previous chapters for the development of BIO-PUR for structural

applications, Polycin T-400 (Vertellus) and Voraforce TR 1500-Isocyanate (Dow Chemical), respectively. For the preparation of the BIO-PUR-DA systems, the solid Triol-DA was diluted in a reactive biobased glycol such as 1,3-propanediol (PD, Quimidroga, S.A.). Materials used in the BIO-PUR-DA and BIO-PUR-R are summarized in the *Table 8.1*.

Table 8.1. Components used in the BIO-PUR-DA and BIO-PUR-R formulation.

	Polyol	Triol-DA	PD	BHET	Isocyanate
I_{NCO} (%)	---	---	---	---	30.79
I_{OH} (mg KOH g^{-1})	400	247.26	201.0	441.7	---
f	3	3	2	2	---
Equivalent weight (g eq^{-1})	140.3	226.7	279.1	127.0	136.4
Recycled content (%)	---	---	---	100	---
Renewable content (%)	80	43	100	---	---

8.4.2.Synthesis

Two BIO-PUR-DA and one BIO-PUR-R polyurethane systems were synthesised mixing at RT the Part A, constituted by hydroxylated components, and Part B, isocyanate component.

The isocyanate index was maintained constant (equal to 1.2) for all the systems studied. Subsequently, the mixture was heated at 105 ºC for 3 h in the case of BIO-PUR-DA and at 120 ºC for 1 h in the case of BIO-PUR-R in order to obtain the cured polyurethane. The designation, composition, renewable content, DA adduct content and recycled

material content of all the systems are summarized in Table 8.2. All formulations are based on 100 parts by weight of polyol (pbw).

Table 8.2. Summary of synthesized BIO-PUR-DA and BIO-PUR-R systems.

BIO-PUR-DA1				
	Polyol	PD	Triol-DA	Isocyanate
Equivalent (mol)	1.5	0,75	0,75	3,6
Equivalent weight (g eq^{-1})	140.3	279,1	226,7	136,4
Weight (g)	100	99,5	80,8	233,0
Triol-DA content (%)			15.7	
Renewable content (%)			41.7	
BIO-PUR-DA2				
	Polyol	PD	Triol-DA	Isocyanate
Equivalent (mol)	1	1	1	3,6
Equivalent weight (g eq^{-1})	140.2	279,1	226,7	136,4
Weight (g)	100.0	199,0	161,6	350,1
Triol-DA content (%)			19.9	
Renewable content (%)			43.0	
BIO-PUR-R				
	Polyol		BHET	Isocyanate
Equivalent (mol)	0.6		0,4	1,2
Equivalent weight (g eq^{-1})	140.3		127,0	136,4
Weight (g)	100.0		60,4	194,5
Recycled material content (%)			17.0	
Renewable content (%)			22.5	

8.5. CHARACTERIZATION

8.5.1.Characterization of Triol-DA and BHET

The chemical structure of the synthesized raw materials was analysed by Fourier transform infrared spectroscopy (FTIR) or proton nuclear magnetic resonance (^{1}H NMR). FTIR was carried out on a Nicolet Nexus FTIR spectrometer equipment with an ATR Golden Gate (Specac) accessory. The spectra were performed averaging 32 scans in the range from 4000 to 650 cm^{-1} with a resolution of 2 cm^{-1}. Liquid–state ^{1}H NMR measurements were conducted with an Avance Bruker 500 spectrometer equipped with a BBO probe with gradient in Z axis, at a frequency of 500 MHz, number of scans 64, spectral window of 5000 Hz and recovery delay of 1s.

Molecular weight distribution was determined by gel permeation chromatography (GPC). Weight average molecular weight (Mw) and number average molecular weight (Mn) values have been determined by GPC, using a Thermo Fisher Scientific chromatograph (Waltham, Massachusetts, USA), equipped with an isocratic Dionex UltiMate 3000 pump and a RefractoMax 521 refractive index detector. The separation has been carried out at 30 °C within four Phenogel GPC columns from Phenomenex with 5 µm particle size and porosities of 10^5, 10^3, 100, and 50 Å, located in an UltiMate 3000 thermostated column compartment. THF was used as mobile phase at a flow rate of 1 mL min^{-1}. Samples have been prepared by solving in THF at 1 wt% and filtering using nylon

filters with a pore size of 2 µm. Mw and Mn have been reported as weight average based on monodisperse polystyrene standards.

Thermal properties were determined by differential scanning calorimetry (DSC) and thermogravimetric analysis (TGA). DSC analysis has been carried out from 25 °C up to 300 °C with a heating rate of 10 °C min^{-1} under nitrogen atmosphere in a Mettler Toledo DSC3+ equipment (Columbus, Ohio, USA) provided with a robotic arm and an electric intracooler as refrigerator unit. Between 5 and 10 mg of sample have been encapsulated in aluminium pans. TGA were performed in a TGA/SDTA851 Mettler Toledo (Columbus, Ohio, USA) equipment. Samples were heated from RT to 800 ºC at a heating rate of 10 ºC min^{-1} under nitrogen atmosphere.

8.5.2. Characterization of BIO-PUR-DA and BIO-PUR-R systems

The viscosity evolution during resin curing was evaluated by rheological analysis. Rheological tests were carried out on a HAAKE RheoStress 6000 Rheometer (Thermo Fisher Scientific, Massachusetts, USA), running in an oscillating stress mode at a frequency of 1 Hz. Amplitude was held constant in the Linear Viscoelastic Range (LVR) throughout the test. A gap separation of 1 mm and disposable parallel plates of 60 mm diameter were used. Experiments were performed at dynamic or temperature sweep test conditions. Temperature sweep tests were performed from 25 to 200 ºC at a constant heating rate of 5 ºC min^{-1}. Storage and loss moduli, G' and G'' respectively, and complex viscosity, η*, were measured over temperature.

The resin curing and Diels-Alder reaction thermo-reversibility were evaluated by differential scanning calorimetry (DSC) tests on a TA Instruments DSC Q100 (TA Instruments, New Castle, USA) calorimeter. The curing was analysed by dynamic experiments, which were performed from -90 to 225 ºC at 20 ºC min^{-1} heating rate. Diels Alder reaction thermo-reversibility were evaluated, for that the triol was subjected to various heating and cooling scans, which are summarized in *Figure 8.9.*

The evolution of the functional groups involved in the DA/r-DA themo-reversible reaction was monitored by Fourier transform infrared spectroscopy (FTIR) in a Nicolet Nexus FTIR spectrometer equipment with an ATR Golden Gate (Specac) accessory. The thermomechanical stability of the synthesised polyurethanes was analysed by dynamic mechanical analysis (DMA). DMA tests were carried out using the Gabo Eplexor100N (Netzch, Selb, Germany) dynamic mechanical analyser. Temperature scans were performed from -40 to 200 ºC at 2 ºC min^{-1} heating rate and at a frequency of 1 Hz. The sample dimensions were 2.2 x 5 x 50 mm^3. The Tg of the PUR resin systems was taken at the temperature value of the maximum of tan δ, Tα [19,20].

Mechanical behaviour of the synthesised polyurethanes has been analysed by flexural tests. The analysis was carried out at RT using a Instron 5967 (Instron, Norwood, USA) equipment, with a 3-point bending device, according to ISO 178 standard.

8.6. RESULTS

8.6.1. Synthesis of BIO-PUR containing dynamic covalent bonds (BIO-PUR-DA)

A DA adduct containing triol synthesized from a trismaleimide and furfuryl alcohol (*Figure 8.7*), kindly provided by the GMT-EHU/UPV group (Triol-DA), has been employed to incorporate covalent bonds in the BIO-PUR formulations.

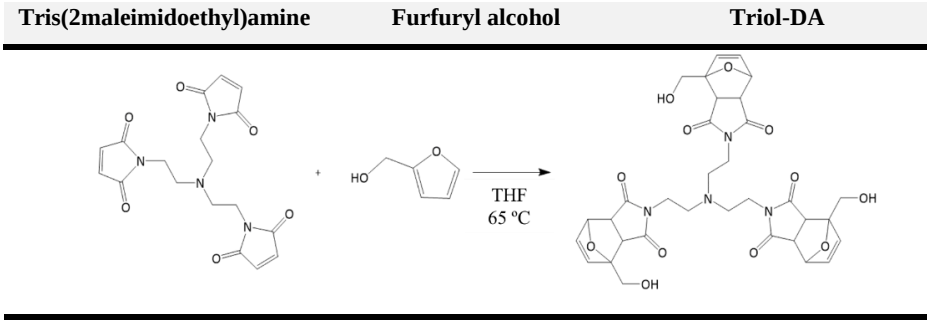

Figure 8.7. Scheme of the synthesis of the DA adduct containing triol.

The tris(2-maleimidoethyl) amine and furfuryl alcohol were mixed at 65 ºC at a stoichiometric ratio under constant mixing for 16 hours. After the reaction time, the triol was dried on a vacuum oven, and characterized by FTIR. This triol is a partially biobased component since the furfuryl alcohol is obtained from polysaccharides or sugars from vegetable renewable sources. A renewable content of 43% was calculated from the weight percentage of the renewable components.

Figure 8.8 shows the FTIR spectrum of the synthesized triol. The characteristic broad band between 3200 and 3600 cm^{-1}attributed to the stretching vibration of hydroxyl groups and the band around 1000 cm^{-o1}, related to the C-O stretching, confirmed the presence of the primary alcohol. The bands at 3078 and 2951 cm^{-1} are attributed to stretching vibration of =CH and –CH groups, respectively. The band at 1768 cm^{-1}, characteristic of the stretching vibration of DA adduct carbonyl group, the signal at 1152 cm^{-1} related to asymmetric stretching vibration of C-O-C bond and the band at 733 cm^{-1} due to the deformation out of the plane of the =C-H confirmed the presence of the DA adduct [21,22].

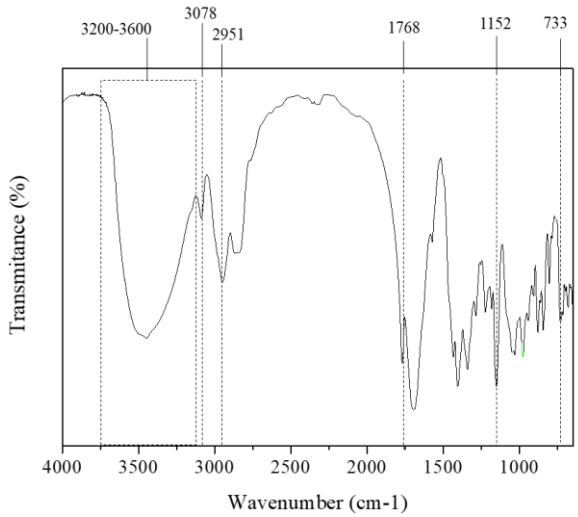

Figure 8.8. FTIR of the synthesized triol.

Before the synthesis of DA containing polyurethanes, the thermo-reversibility of the DA adduct was evaluated. The synthesized triol was characterized by DSC. The triol was subjected to various heating and cooling scans, which are summarized in *Figure 8.9*.

Figure 8.9a shows the results of cycle 1 constituted by five consecutive steps. In this cycle, a first dynamic heating sweep (10 ºC

min^{-1}) was carried out up to 200 ºC followed by a controlled cooling and an isothermal annealing of 3 h at 65 ºC and finishing with a second dynamic scan (10 ºC min^{-1}) up to 200 ºC. The thermogram of the first scan shows three stages: triol fusion, DA opening reaction and maleimide homopolymerization [23]. DA formation at 65 ºC was not possible due to the maleimide homopolymerization in the first scan, consequently the second scan did not present the r-DA. Therefore, the first step of cycle 2 and 3 was modified as shown in *Figure 8.9*b and *Figure 8.9*c.

Figure 8.9b-c present results of cycle 2 and cycle 3, in both cycles first dynamic sweeps (10 ºC min^{-1}) were carried out up to 160 ºC and 140 ºC respectively, continued by a controlled drop including an isothermal step at 65 ºC for 3 h and followed by a second heating (10 ºC min^{-1}) up to 200 ºC. In the case of cycle 3, there was an isothermal step of 1 hour once the target heating temperature (140 ºC) was reached.

In both cases, the maleimide groups formed during the r-DA were available for the subsequent DA formation during the isothermal step for 3 h at 65 ºC. The reversible DA reaction occurred. In addition, in the thermograms of the second scans of the two cycles, the retro reaction of the DA could be observed indicating that the DA had been re-formed during isothermal step. In the case of cycle 3, which had more time for the reversible reaction and the same time for the formation of the DAs again, the second scan showed a slight difference with the others.

Therefore, not only the temperature at which r-DA is brought can affect reprocessability and recyclability, but time also plays an important

role in the degree or magnitude of that reprocessability and recyclability takes place.

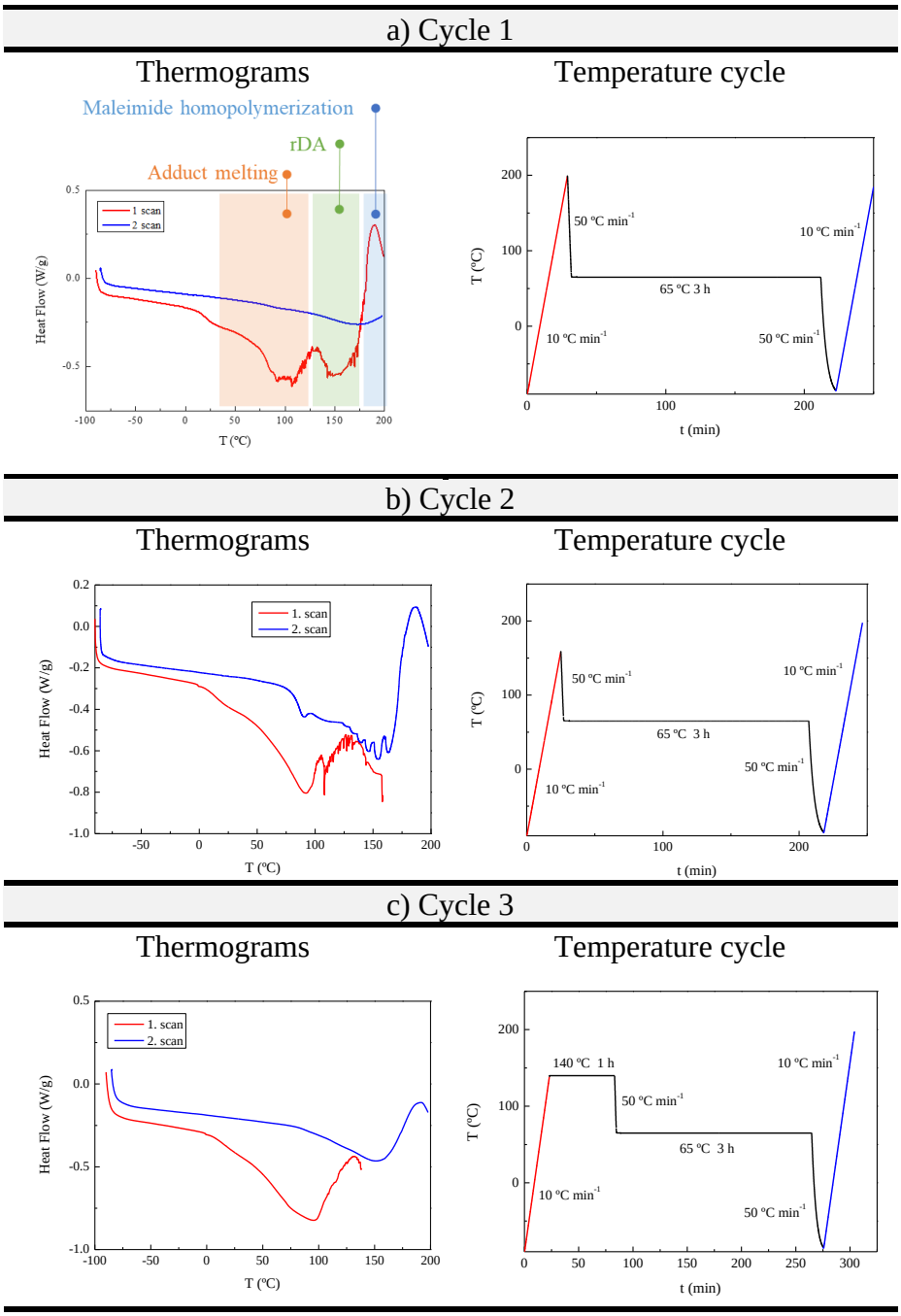

Figure 8.9.Triol-DA thermograms for the different heating and cooling cycles.

Once the thermo-reversibility of the triol with the DA adduct corroborated, a BIO-PUR with including this component (BIO-PUR-DA) was synthesized. The scheme of the synthesis and thermo-reversibility is shown in *Figure 8.10*.

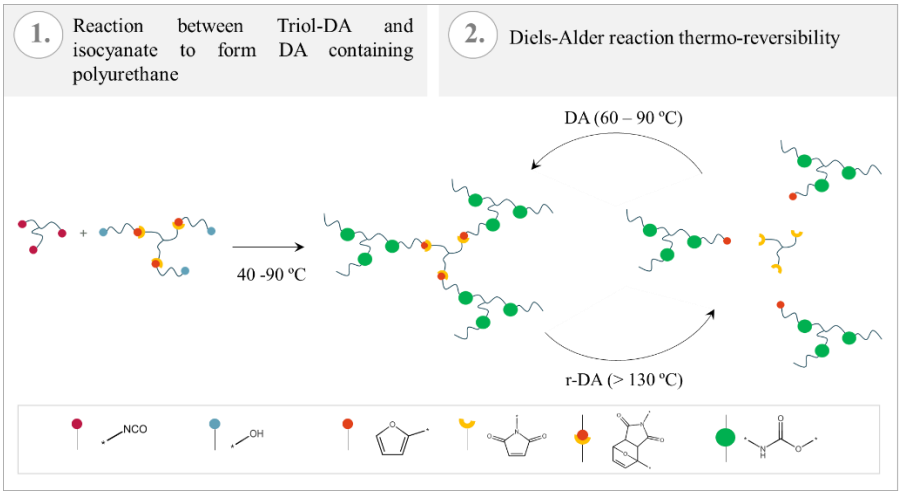

Figure 8.10.Schema of the strategy to integrate the DA adduct in the BIO-PUR formulation.

The DA adduct was solid at RT, which is the temperature used for the preparation of polyurethane resin mixture, and therefore a reactive solvent of Triol-DA was employed. 1,3-Propanediol was selected in order to maintain as high as possible the Triol-DA content in the formulation and also according to previous miscibility tests. As shown in *Figure 8.11*, Triol-DA and PD presented good miscibility among them and with pMDI, obtaining a homogeneous dispersion of BIO-PUR-DA before curing.

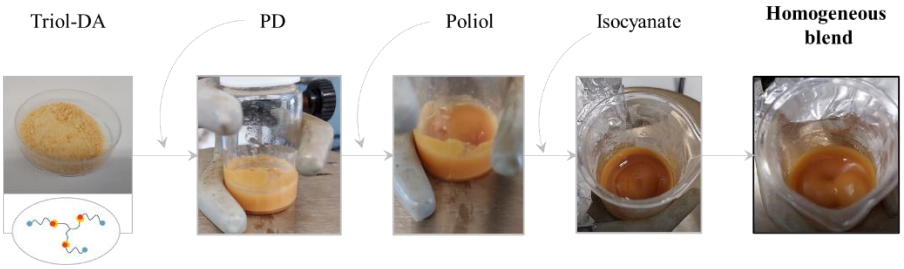

Figure 8.11. Triol- DA appearance at RT and miscibility of the components.

The curing reaction of BIO-PUR-DAs was characterised by dynamic DSC tests at 10 ºC min^{-1} (*Figure 8.12*). In both systems the first peak is attributed to the curing reaction which can be overlapped with DA adduct fusion and r-DA reaction and followed by maleimide homopolymerization. In the BIO-PUR-DA2 system, the maleimide homopolymerization reaction was more intense, due to the higher adduct content.

As can be observed, the BIO-PUR-DA1 and BIO-PUR-DA2 systems showed curing peak maximums at 95 and 90 ºC, quite similar to BIO-PUR2 (92 ºC). Therefore, and in order to avoid the r-DA reaction during the resin curing, a temperature between the curing peak maximum and the starting of the r-DA reaction was selected (105 ºC).

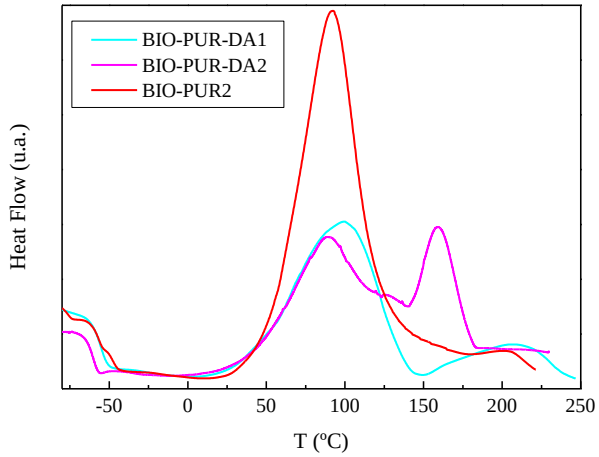

Figure 8.12. DSC thermograms of BIO-PUR-DA systems and BIO-PUR2.

BIO-PUR-DAs plates were prepared by casting and curing at 105 ºC for 1 h (*Figure 8.13*).

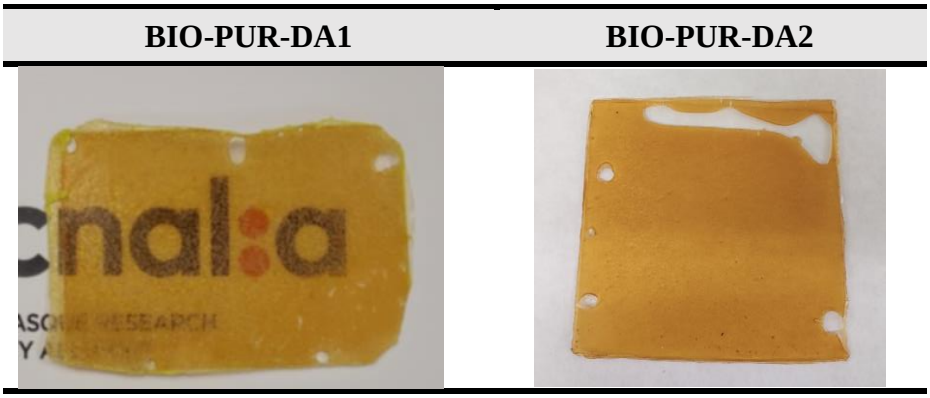

Figure 8.13.BIO-PUR-DA plates

As expected according to components functionality and content, BIO-PUR-DA2 presented higher flexibility due to the higher content of PD component, both difunctional and aliphatic, which contributes more to chain extension than to crosslinking providing chain mobility (*Figure*

8.13). The BIO-PUR-DA1 showed higher rigidity and could be more suitable for structural application, and this is the reason why it was selected for the subsequent study.

A preliminary thermo-reversibility study was preformed, where the BIO-PUR-DA1 was subjected to various heating and cooling cycles (*Figure 8.14*) and analysed by FTIR (*Figure 8.15*). The evolution of the bands characteristic of furfuryl group at 1017, 914 and 724 cm^{-1} [21,22,24], maleimide group at 813 and 696 cm^{-1} [22,24,25] and DA adduct at 765 cm^{-1} [22,25] were analysed.

After the first heating at 120 ºC for 1 h and subsequent fast cooling out of the oven, the characteristic band of isocyanate group at 2270 cm^{-1} disappeared, suggesting that polymerization was not completed at 105 ºC. Moreover, new bands related with furfuryl group at 914 and 724 cm^{-1} and with maleimide group at 696 cm^{-1} could be seen, suggesting the occurrence of r-DA reaction.

The ability of DA adduct re-formation was also analysed. Once the sample is heated at 120 ºC for 1 h, it was cooled down up to 80 ºC and annealed at this temperature for 5 h in an oven, leaving it inside to reach RT. No significant variations were observed in the characteristic bands of furan and maleimide, suggesting that the maleimide and furan groups generated by the r-DA reaction were not recombined by the DA reaction during the annealing at 80 °C. This could indicate that 5 h and 80 ºC are not enough to coupling DA adduct in the polyurethane plate. Yasuda el al. Reported 60 ºC for 48 h for the coupling of DA adduct in healing tests [25].

The effect of the temperature on the extension of r-DA reaction was also analysed. The BIO-PUR-DA1 plate was subjected to 160 ºC for 1 h in an oven and cooled down fast out of the oven. As can be seen, the intensity of the characteristic bands of the maleimide group at 813 and 696 cm^{-1} increased. Moreover, the band attributed to DA adduct at 765 cm^{-1} slightly decreased. This suggests that the extension of r-DA reaction is favoured at the higher temperature studied, as also reported by other authors. Yasuda et al. reported onset temperatures in the range of 140-150 ºC for the r-DA reaction of cured products[25]. Moreover, the additional cooling up to 80 ºC, annealing the sample at this temperature for 5 h in an oven and leading to cool down to RT in the oven, results in a decrease of the maleimide band intensity at 696 cm^{-1}respect to the band of DA adduct at 765 cm^{-1}, suggesting that the maleimide and furan groups generated by the r-DA reaction at 160 ºC were partially recombined by the DA reaction during the annealing at 80 °C. The obtained preliminary results, in agreement with previous DSC results, confirmed that the synthesised BIO-PUR-DA1 experienced successfully the thermo-reversible r-DA/DA reactions.

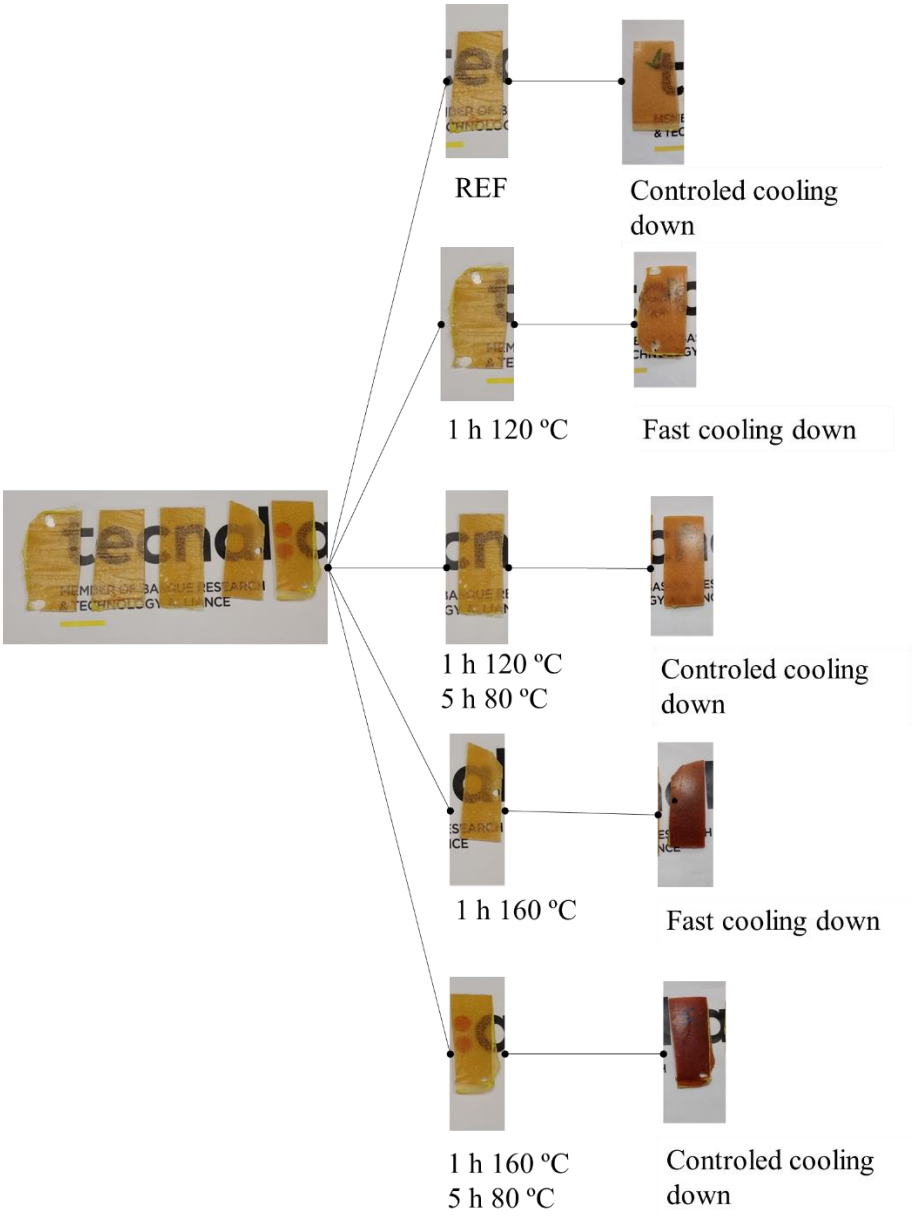

Figure 8.14.BIO-PUR-DA1temperature cycles.

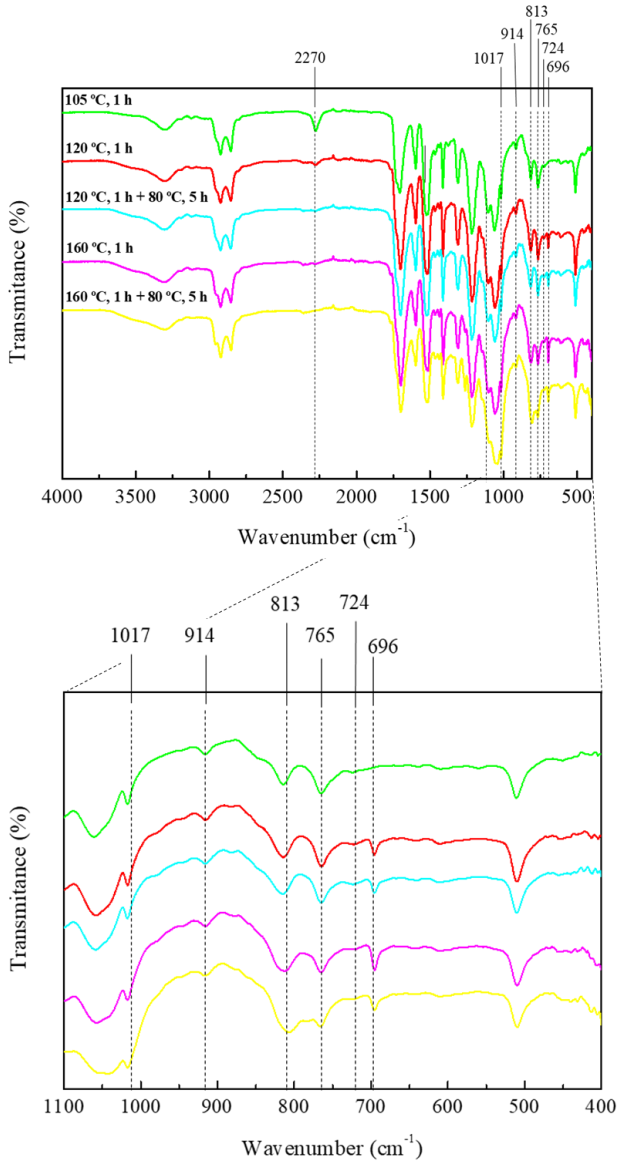

Figure 8.15. FTIR of BIO-PUR-DA1after temperature cycles.

Based on the previous results, to study the reprocessability of the BIO-PUR-DA1, a grinded plate was heated in the press under 15 bar for 1h at 160 ºC to enable r-DA reaction and then a controlled cooling was carried out holding at 80 ºC 5 h to allow the DA reaction (*Figure 8.16).*

The process was repeated to verify that the reprocessing capacity was not lost after the first test. The results were promising (*Figure 8.16*) showing the capability of forming a new plate.

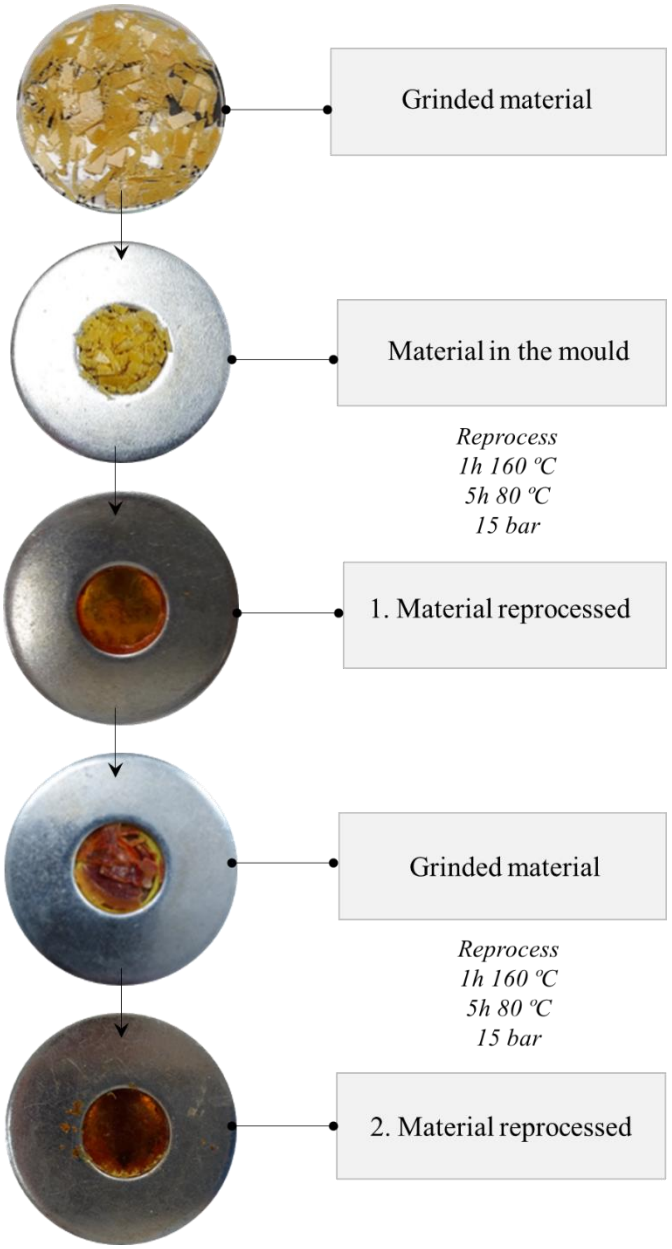

Figure 8.16. Preliminary tests of BIO-PUR-DA1 reprocessability.

8.6.2. Synthesis of BIO-PUR with recycled components

The second strategy was the synthesis of PUR using recycled monomers. For that purpose, bis(2-hydroxyethyl) terephthalate, BHET, kindly provided by the GMT-EHU/UPV group was used. The BHET was obtained by glycolysis of PET bottles collected in the sea according to a previously optimized protocol [14]. Briefly, glycolysis was performed in a closed reactor using ethylene glycol (EG) with a ratio of PET:EG of 1:3, under a pressure of 3 bar, at 220 ºC and during 30 min. The obtained mixture was filtered with excess of water, and the fraction rich in BHET recovered and dried at 60 °C under vacuum. The BHET was characterized by FTIR, ^{1}H NMR, GPC, DSC and TGA before its use in the synthesis of PUR.

The chemical structure of BHET was analysed by FTIR and ^{1}H NMR (*Figure 8.17)*. FTIR spectrum (*Figure 8.17a)* shows the characteristic stretching vibration of hydroxyl group at 3442 cm^{-1}, the double band attributed to stretching vibration of ester carboxyl group at 1712 cm^{-1} and 1690 cm^{-1} and the absorption band of aromatic group at 1508 cm^{-1} [26]. ^{1}H NMR spectrum (*Figure 8.17b)* shows a peak at 8.1 ppm assigned to protons of the aromatic ring, a, b, c and d, a signal attributed to hydroxyl groups at 4.95 ppm, the peak assigned to methylene groups (-CH_2-) adjacent to the -OH groups at 3.73 ppm and the signal of methylene groups (-CH_2-) adjacent to the -COO groups at 4.33 ppm. The peak around 2.5 ppm belongs to DMSO-d6 used as solvent and the peak at 3.3 can be attributed to residual H_2O [26].

a)

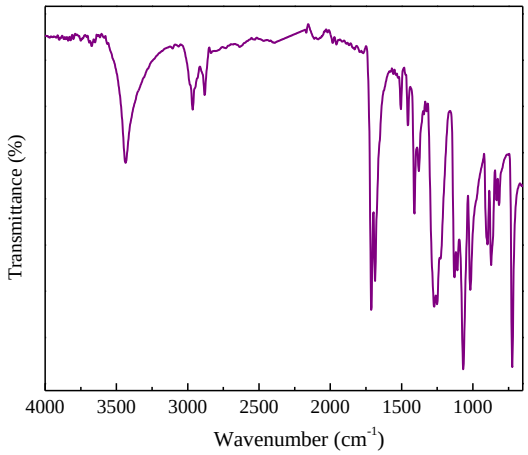

b)

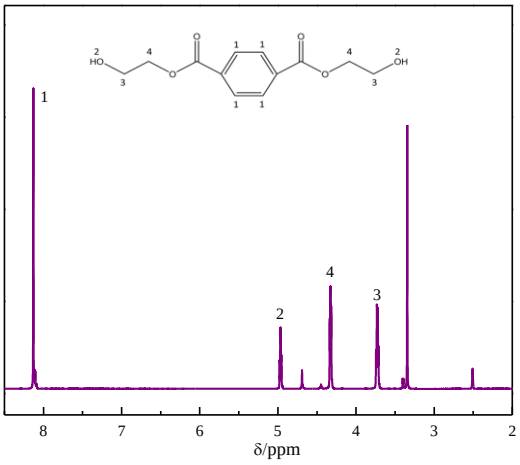

Figure 8.17. a) *FTIR and b) ^{1}H NMR spectra of the BHET obtained from PET glycolysis.*

The obtained BHET was also analyzed by GPC (*Figure 8.18*). As can be observed, BHET shows two peaks centred at 36 and 41 min retention times, ascribed to BHET dimer (Mn = 380-393 g mol^{-1} and Mw = 384-396 g mol^{-1} according to polystyrene standard) that represents a 3%, and to the BHET monomer (Mn = 168-176 g mol^{-1} and Mw = 172-

180 g mol^{-1}), respectively. The obtained results confirmed that the obtained fraction is mainly constituted by the BHET monomer.

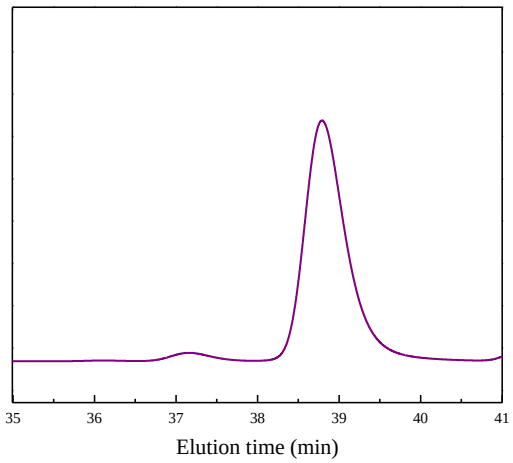

Figure 8.18. GPC chromatogram of the BHET obtained from PET glycolysis.

BHET was also thermally characterized. DSC thermogram (*Figure 8.19a*) shows a prominent melting peak around 113 °C attributed to BHET monomer and a small melting enthalpy centred at 213 °C attributed to the crystalline structures formed by the BHET dimers. Regarding thermal stability, the first weight loss observed by TGA is related to the degradation of BHET monomer, whereas the second one centred at 433 °C to the degradation of PET formed during the thermogravimetric analysis (*Figure 8.174b)* [27].

a)

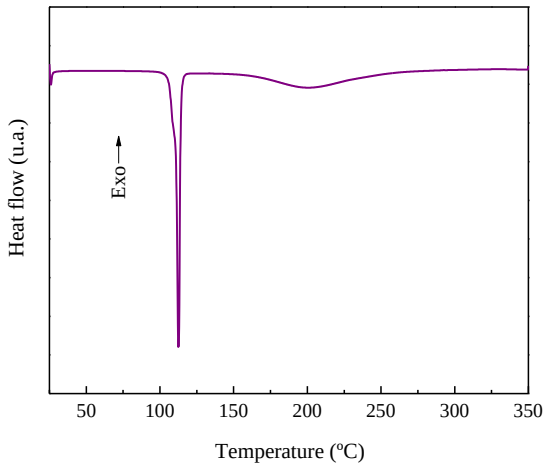

b)

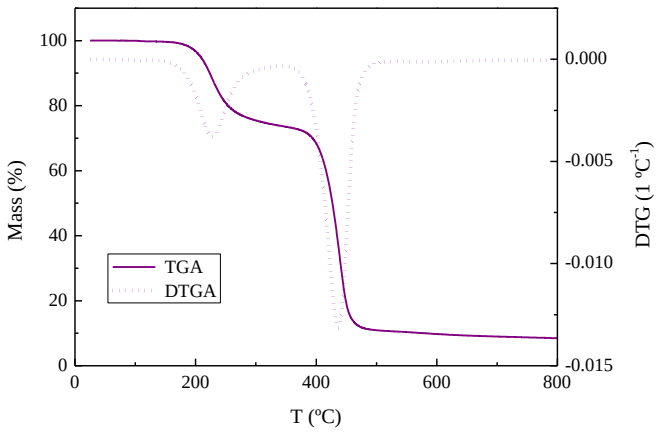

Figure 8.19. *a) DSC and b) mass loss (lines) and derivative (dot line) of the BHET obtained from PET glycolysis.*

The structural and thermal analysis results confirmed that the glycolyzed product recovered from the glycolysis of highly degraded marine PET consist on BHET with high purity, which will be investigated in the synthesis of PUR.

The BHET is solid at RT but the monomer presented good miscibility with the polyol under stirring. After 20 min under 1000 rad min^{-1} a homogeneous dispersion was obtained (Part A), which can be

mixed and react with the isocyanate (Part B). BIO-PUR-R plate was prepared by casting and curing 1 h at 120 ºC (*Figure 8.20*).

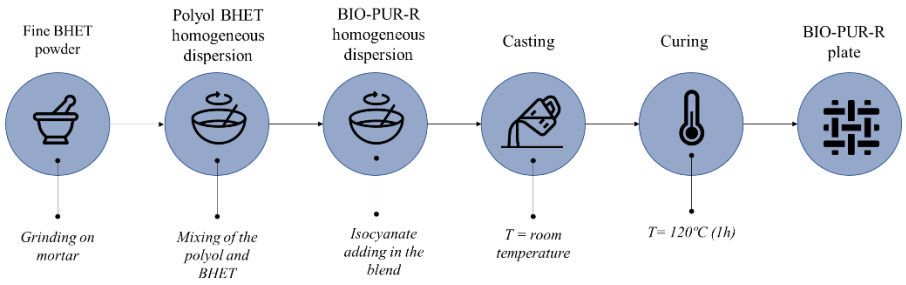

Figure 8.20. BIO-PUR-R plate preparation.

Viscosity evolution results from oscillatory temperature sweeps of BIO-PUR-R system are shown in *Figure 8.21*. The new formulation was compared with the BIO-PUR2 system optimized for leaf spring RTM manufacturing process.

Temperature sweep rheology tests show that BIO PUR-R reactivity is similar to the BIO-PUR2 reactivity (*Figure 8.21*). However, the initial viscosity increased. This effect is attributed to the BHET incorporation in the formulation. This monomer is solid at RT and presents a high melting point (113 ºC) making BIO-PUR-R viscosity higher than BIO-PUR2.

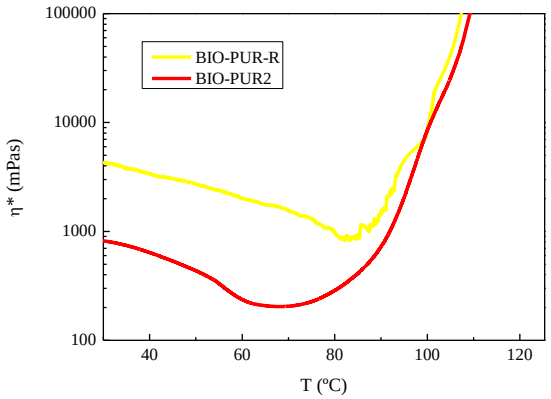

Figure 8.21.Viscosity evolution with temperature for BIO-PUR-R and BIO-PUR2 systems.

The curing reaction of BIO-PUR-R was also characterized by dynamical DSC tests and compared with the BIO-PUR2 optimized formulation. *Figure 8.22* shows the thermograms obtained at 10 ºC min^{-1}.

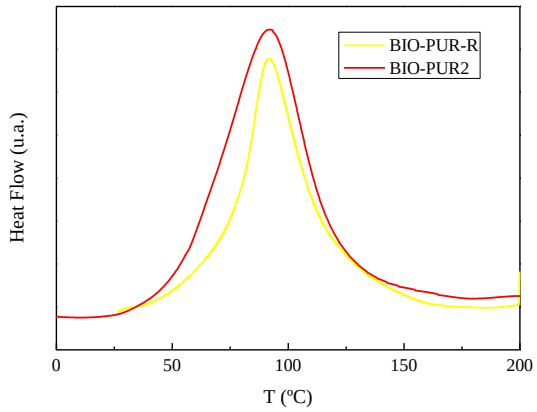

Figure 8.22. Dynamic DSC thermograms.

As can be seen in the *Figure 8.22*, the reaction is similar for the BIO-PUR2 and BIO-PUR-R systems at termperatures higher than 80 ºC, suporting the results obatined on the rheology tests. The BIO-PUR

system peak has a maximum at 92 ºC, whereas it appears at 91 ºC for BIO-PUR2. However, BIO-PUR-R was less reactive at temperatures lower than 80 ºC, problably due to it's higher viscosity.

Another critical factor for ultra-fast cure resins is the heat released during curing. As mentioned before, the fast heat production speed the resins curing producing temperature instabilities. The total heat of reaction, taken as the value obtained at 10 ºC min^{-1} was 205 J g^{-1} for the BIO-PUR2 system whereas for the BIO-PUR-R the heat was 130 J g^{-1}, which is a satisfactory result. As previously discussed, the lower total heat of reaction could be related with the lower total hydroxyl or isocyanate groups content of BIO-PUR-R.

Once the suitability of the system evaluated, plates were prepared by casting and curing at 120 ºC for 1 h (*Figure* 8.23) and tested to determine the final properties.

Figure 8.23. BIO-PUR-R plate.

Figure 8.24 shows the tan δ results of BIO-PUR-R and BIO-PUR2 polyurethanes. The Tg of each material is taken as the temperature value of the maximum of tan δ. As can be seen in the *Figure 8.24* the BIO-PUR2 T_g value (167 ºC) is higher than BIO-PUR-R T_g (138 ºC). This is attributed to the higher cross-linking density of BIO-PUR2

system. Even so, the BIO-PUR-R fulfilled the automotive structural parts requirements (T_g > 120 ºC).

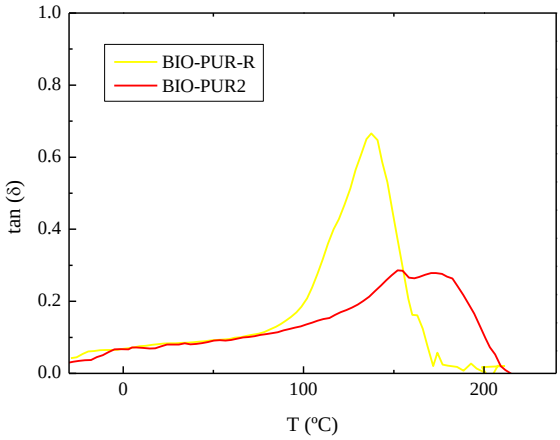

Figure 8.24. BIO-PUR-R and BIO-PUR2 curves of tan δ vs temperature.

BIO-PUR-R sample was also mechanically characterized (*Figure 8.25*) and compared to BIO-PUR2. *Table 5.3* summarizes the flexural mechanical properties of the BIO-PUR-R and BIO-PUR2 systems. It could be observed that with the addition of BHET the flexural modulus value was comparable to the optimized BIO-PUR2 system. Nevertheless, due to the BHET incorporation the BIO-PUR-R fragility increased and the flexural strength and flexural strain values were lower than the BIO-PUR2. The results of the DMA test demonstrated the lower crosslinking density of the BIO-PUR2 than BIO-PUR-R, being this the reason to higher flexural strength and flexural strain. The maintenance of the modulus was associated to the BHET aromatic rings.

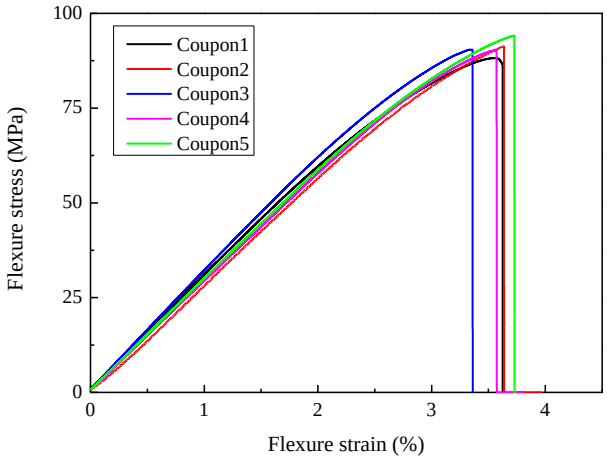

Figure 8.25. Flexural strength testing results for BIO-PUR composite plate.

Table 8.3. Flexural properties of the BIO-PUR2 and BIO-PUR-R systems.

Systems	Flexural strength	Flexural modulus	Flexural strain
	MPa	*GPa*	*%*
BIO-PUR2	124,2 ± 2,3	2,9 ± 0,1	6,9 ± 0,3
BIO-PUR-R	90,9 ± 2,2	3,0 ± 0,1	3,6 ± 0,15

8.7. CONCLUSIONS

In this chapter a valid end of life option for the newly developed sustainable BIO-PUR formulation was explored with the incorporation of dynamics bonds adding a novel triol with DA (Triol-DA) into the

formulation (BIO-PUR-DA). BIO-PUR-DA polyurethane systems with high renewable content, up to 40%, were synthesised.

The reprocessability of the systems was demonstrated with the production of two successful consecutive reprocess cycles.

Results show that temperature is not the only factor affecting r-DA/DA reprocessability and recyclability, time also plays an important role in the degree or magnitude of that reprocessability and recyclability takes place.

Regarding the incorporation of recycled monomers in the BIO-PUR adding BHET, rheology and DSC tests show that the reactivity of the system is similar to the reference BIO-PUR2 formulation at temperatures higher than 80 ºC, whereas viscosity is higher. The reaction was also less exothermic than the reference system.

The BIO-PUR-R presented high T_g value, 138 ºC, higher than 120 ºC, fulfilling the automotive structural parts requirements. However, the BIO-PUR2 presented a higher T_g, 167 ºC, due to higher cross-linking density.

The BIO-PUR-R presented a high flexural modulus, comparable to the optimized BIO-PUR2. However, the crosslinking density decrease resulted in a higher fragility, and the flexural strength and flexural strain values were lower than the BIO-PUR2.

8.8. REFERENCES

[1] Jin, Y.; Lei, Z.; Taynton, P.; Huang, S.; Zhang, W.: Malleable and Recyclable Thermosets: The Next Generation of Plastics. Matter, 1, 1456–1493 (2019). http://doi:10.1016/j.matt.2019.09.004.

[2] Yang, Y.; Xu, Y.; Ji, Y.; Wei, Y.: Functional epoxy vitrimers and composites. Prog. Mater. Sci. (2021), 120.

[3] Cárdenas, C. B.; Gayraud, V.; Rodriguez, M. E.; Costa, J.; Salaberria, A. M.; de Luzuriaga, A. R.; Markaide, N.; Keeryadath, P. D.; Zapatería, D. C.: Study into the Mechanical Properties of a New Aeronautic-Grade Epoxy-Based Carbon-Fiber-Reinforced Vitrimer. Polymers, 14 (2022). http://doi:10.3390/polym14061223.

[4] Ruiz de Luzuriaga, A.; Markaide, N.; Salaberria, A. M.; Azcune, I.; Rekondo, A.; Grande, H. J.: Aero Grade Epoxy Vitrimer towards Commercialization. Polymers, 14, 3180 (2022). http://doi:10.3390/polym14153180.

[5] Ruiz De Luzuriaga, A.; Martin, R.; Markaide, N.; Rekondo, A.; Cabañero, G.; Rodríguez, J.; Odriozola, I.: Epoxy resin with exchangeable disulfide crosslinks to obtain reprocessable, repairable and recyclable fiber-reinforced thermoset composites. Materials Horizons, 3 (2016). http://doi:10.1039/c6mh00029k.

[6] Orozco, F.; Li, J.; Ezekiel, U.; Niyazov, Z.; Floyd, L.; Lima, G. M. R.; Winkelman, J. G. M.; Moreno-Villoslada, I.; Picchioni, F.; Bose, R. K.: Diels-Alder-based thermo-reversibly crosslinked polymers: Interplay of crosslinking density, network mobility, kinetics and stereoisomerism. European Polymer Journal, 135, 109882 (2020). http://doi:10.1016/j.eurpolymj.2020.109882.

[7] Du, P.; Liu, X.; Zheng, Z.; Wang, X.; Joncheray, T.; Zhang, Y.: Synthesis and characterization of linear self-healing

polyurethane based on thermally reversible Diels-Alder reaction. RSC Advances, 3 (2013). http://doi:10.1039/c3ra42278j.

[8] Liu, Y. L.; Chuo, T. W.: Self-healing polymers based on thermally reversible Diels-Alder chemistry. Polym. Chem. (2013), 4.

[9] Tian, Q.; Yuan, Y. C.; Rong, M. Z.; Zhang, M. Q.: A thermally remendable epoxy resin. Journal of Materials Chemistry, 19 (2009). http://doi:10.1039/b811938d.

[10] Bai, N.; Saito, K.; Simon, G. P.: Synthesis of a diamine cross-linker containing Diels-Alder adducts to produce self-healing thermosetting epoxy polymer from a widely used epoxy monomer. Polymer Chemistry, 4 (2013). http://doi:10.1039/c2py20611k.

[11] Turkenburg, D. H.; Fischer, H. R.: Diels-Alder based, thermo-reversible cross-linked epoxies for use in self-healing composites. Polymer, 79 (2015). http://doi:10.1016/j.polymer.2015.10.031.

[12] Denissen, W.; Winne, J. M.; Du Prez, F. E.: Vitrimers: Permanent organic networks with glass-like fluidity. Chem. Sci. (2016), 7.

[13] Law, K. L.; Narayan, R.: Reducing environmental plastic pollution by designing polymer materials for managed end-of-life. Nat. Rev. Mater. (2022), 7.

[14] Mendiburu-Valor, E.; Mondragon, G.; González, N.; Kortaberria, G.; Eceiza, A.; Peña-Rodriguez, C.: Improving the Efficiency for the Production of Bis-(2-Hydroxyethyl) Terephtalate (BHET) from the Glycolysis Reaction of Poly(Ethylene Terephtalate) (PET) in a Pressure Reactor. Polymers, 13, 1461 (2021). http://doi:10.3390/polym13091461.

[15] Mendiburu-Valor, E.; Mondragon, G.; González, N.; Kortaberria, G.; Martin, L.; Eceiza, A.; Peña-Rodriguez, C.: Valorization of urban and marine PET waste by optimized chemical recycling. Resources, Conservation and Recycling,

184, 106413 (2022). http://doi:10.1016/j.resconrec.2022.106413.

[16] Jamdar, V.; Kathalewar, M.; Dubey, K. A.; Sabnis, A.: Recycling of PET wastes using Electron beam radiations and preparation of polyurethane coatings using recycled material. Progress in Organic Coatings, 107, 54–63 (2017). http://doi:10.1016/j.porgcoat.2017.02.007.

[17] Cevher, D.; Sürdem, S.: Polyurethane adhesive based on polyol monomers BHET and BHETA depolymerised from PET waste. International Journal of Adhesion and Adhesives, 105, 102799 (2021). http://doi:10.1016/j.ijadhadh.2020.102799.

[18] Eider Mendiburu-Valor; Tamara Calvo-Correas; Loli Martin; Isabel Harismendy; Cristina Peña-Rodriguez; Arantxa Eceiza: Synthesis and characterization of sustainable polyurethanes from renewable and recycled feedstocks. . Journal of Cleaner Production 2022 (under review),.

[19] Kim, T. H.; Kim, M.; Lee, W.; Kim, H.-G.; Lim, C.-S.; Seo, B.: Synthesis and Characterization of a Polyurethane Phase Separated to Nano Size in an Epoxy Polymer. Coatings, 9, 319 (2019). http://doi:10.3390/coatings9050319.

[20] Morales-Cerrada, R.; Tavernier, R.; Caillol, S.: Fully Bio-Based Thermosetting Polyurethanes from Bio-Based Polyols and Isocyanates. Polymers, 13, 1255 (2021). http://doi:10.3390/polym13081255.

[21] Turkenburg, D. H.; Durant, Y.; Fischer, H. R.: Bio-based self-healing coatings based on thermo-reversible Diels-Alder reaction. Progress in Organic Coatings, 111 (2017). http://doi:10.1016/j.porgcoat.2017.05.006.

[22] Sugane, K.; Takagi, R.; Shibata, M.: Thermally healable/heat-resistant properties of thermosets bearing dynamic and thermally stable bonds formed by the Diels-Alder and thiol-maleimide “click” reactions. Reactive and Functional Polymers, 131 (2018). http://doi:10.1016/j.reactfunctpolym.2018.08.001.

[23] Dolci, E.; Michaud, G.; Simon, F.; Boutevin, B.; Fouquay, S.; Caillol, S.: Remendable thermosetting polymers for isocyanate-free adhesives: a preliminary study. Polymer Chemistry, 6, 7851–7861 (2015). http://doi:10.1039/C5PY01213A.

[24] Zhong, Y.; Wang, X.; Zheng, Z.; Du, P.: Polyether-maleimide-based crosslinked self-healing polyurethane with Diels-Alder bonds. Journal of Applied Polymer Science, 132 (2015). http://doi:10.1002/app.41944.

[25] Yasuda, K.; Sugane, K.; Shibata, M.: Self-healing high-performance thermosets utilizing the furan/maleimide Diels-Alder and amine/maleimide Michael reactions. Journal of Polymer Research, 27 (2020). http://doi:10.1007/s10965-019-1986-z.

[26] Imran, M.; Kim, B. K.; Han, M.; Cho, B. G.; Kim, D. H.: Sub- and supercritical glycolysis of polyethylene terephthalate (PET) into the monomer bis(2-hydroxyethyl) terephthalate (BHET). Polymer Degradation and Stability, 95 (2010). http://doi:10.1016/j.polymdegradstab.2010.05.026.

[27] Chen, C. H.: Study of glycolysis of poly(ethylene terephthalate) recycled from postconsumer soft-drink bottles. III. Further investigation. Journal of Applied Polymer Science, 87 (2003). http://doi:10.1002/app.11694.

9

CONCLUSIONES FINALES Y SUGERENCIAS PARA FUTUROS TRABAJOS

9. CONCLUSIONES FINALES Y SUGERENCIAS PARA FUTUROS TRABAJOS

9.1. CONCLUSIONES GENERALES 268

9.2. TRABAJOS FUTUROS 272

9.3. PUBLICACIONES Y CONTRIBUCIONES A CONGRESOS ...281

9.4. REFERENCIAS 285

9.1. CONCLUSIONES GENERALES

En este trabajo se han desarrollado formulaciones de base poliuretano más sostenibles específicas para aplicaciones estructurales y viables para el proceso de RTM.

Para ello se ha trabajado en aportar soluciones en cuanto al control de la reactividad, origen de las materias primas, eficiencia del proceso y fin de vida.

Control de la reactividad:

Se han estudiado diferentes sistemas catalíticos basados en un epóxido combinado con LiCl para aportar latencia PUR's. Se ha visto que la adición del LiCl provoca que la sal y el epóxido formen un alcóxido que acelera la reacción y empeora su latencia. La adición de un diol o monol en la formulación hace que el LiCl quede encapsulado por la formación de puentes de hidrógeno entre los grupos uretano generados proporcionando la latencia necesaria en la primera parte del proceso.

Cuando la reacción progresa el calor generado rompe estos puentes de hidrógeno y permite que se forme el alcóxido acelerando la última parte del curado. La incorporación del diol (DAS) resulta ser más efectiva que el monol, obteniéndose el perfil de reactividad deseado y una Tg final de 133 ºC, evitando el postcurado.

La simulación del proceso de RTM de una ballesta de suspensión demuestra la viabilidad del sistema a las temperaturas y presiones utilizadas habitualmente en la industria (120 ºC, 70-100 bar).

Incorporación de componentes de origen vegetal en la formulación

Se han sintetizado BIO-PURs a partir de polioles derivados de aceites vegetales de diferentes índices de hidroxilo y funcionalidades y se ha estudiado el efecto de dichas características en sus propiedades.

Los polioles biobasados con alta funcionalidad ($f \geq 3$) e índices de hidroxilo (I_{OH} > 200 mg KOH g^{-1}) resultan ser más viables para la aplicación debido a que presentan altas reactividades y T_g's, siendo el más prometedor el Polycin 400, derivado del aceite de ricino. El sistema con este poliol presenta una muy buena combinación de baja viscosidad, alta reactividad, alta T_g y las propiedades mecánicas necesarias para la aplicación objetivo.

El único factor a mejorar es el módulo elástico, que resulta inferior al de la resina de referencia de origen petroquímico. Sin embargo, se ha visto que las propiedades finales (térmicas y mecánicas) se pueden mejorar con la adición de un agente de entrecruzamiento basado biobasado como el glicerol. Con el glicerol se obtiene un valor del módulo equivalente y una T_g superior a la resina de referencia.

Además, se ha visto que el poliol seleccionado (Polycin 400) aporta latencia al sistema, presentando un perfil de viscosidad sin catalizar similar al del sistema de referencia con un catalizador de acción retardada. La adición del sistema catalítico permite retrasar todavía más la reacción en caso de ser necesario (RTM a baja presión).

De nuevo, la simulación del proceso de RTM ha permitido demostrar la viabilidad del sistema (tanto sin catalizar como catalizado) para la aplicación objetivo.

Mejora de la eficiencia del proceso

Para la mejora de la calidad del proceso de fabricación, se ha estudiado la influencia de la velocidad de llenado en la porosidad fabricando y ensayando probetas extraídas a diferentes velocidades. Aunque no ha sido posible el estudio en el rango deseado, se ha visto que es posible fabricar componentes de buena calidad a velocidades entre 1 y 6 mm s^{-1}.

Una vez seleccionado el rango de velocidades de llenado óptimo, se han fabricado y ensayado placas de composite de BIO-PUR reforzado con fibra de vidrio obteniéndose una buena calidad, con menos de un 2% de poros y una Tg mayor de 120 ºC. Con respecto a las propiedades mecánicas, se alcanza un módulo superior a 35 GPa y resistencia mayor que 1000 MPa, cumpliéndose con creces los requisitos para piezas de automoción estructurales.

Por otra parte, se ha desarrollado un modelo basado en la metodología DDAS de cara a mejorar la robustez del proceso. Este modelo es capaz de detectar y predecir los cambios en la velocidad de llenado debidos a variaciones en la permeabilidad y permitiría la implementación de sistemas de control capaces de corregir en tiempo real estas desviaciones.

Otras aplicaciones

Además, y dada la creciente demanda de resinas más sostenibles en diferentes sectores se ha estudiado la viabilidad del sistema desarrollado para otras aplicaciones como la eólica, utilizándose en este caso para la fabricación el proceso de infusión.

En este caso, la viscosidad del sistema resulta demasiado alta a temperatura ambiente por lo que ha sido necesario aumentar la temperatura de proceso a 40 ºC. La resina está optimizada para ciclos cortos de RTM a temperaturas de 120 ºC por lo que sería necesario reformularla para la aplicación. Sin embargo, los resultados obtenidos son prometedores.

Se ha visto que el principal reto es el control de la humedad, ya que la resina tiende a absorber agua y formar CO_2, con la consiguiente formación de burbujas.

No obstante, se ha demostrado con una selección adecuada de los parámetros del proceso es posible fabricar piezas de composite de alta calidad (con sólo un 0.5% de porosidad)

Fin de vida y circularidad

Por último, para la mejora del fin de vida del BIO-PUR desarrollado se ha explorado la opción de integrar enlaces dinámicos. Para ello, se ha desarrollado un triol con enlaces dinámicos de tipo Diels-Alder (Triol-DA) que se ha agregado a la formulación (BIO-PUR-DA).

Se han sintetizado sistemas BIO-PUR-DA con alto contenido renovable de hasta un 40%, demostrándose mediante ensayos

consecutivos de reprocesamiento la reprocesabilidad de los sistemas desarrollados.

Por otra parte, los resultados han mostrado que la temperatura no es el único factor que afecta la capacidad de reprocesamiento y reciclabilidad de r-DA/DA, el tiempo también juega un papel importante en el grado o magnitud de la capacidad de reprocesamiento y reciclabilidad.

La T_g y las propiedades mecánicas del BIO-PUR-R obtenidas en los ensayos de DMA y de flexión muestran que la T_g es más baja y el sistema es más frágil que el BIO-PUR2. Sin embargo, la T_g obtenida cumple con los requisitos de la aplicación (T_g > 120 ºC) y el módulo de flexión es equivalente al del sistema optimizado. La menor densidad de reticulación del sistema con BHET hace que la T_g, resistencia y deformación a flexión se vean reducidos.

El contenido renovable y reciclado del poliuretano BIO-PUR-R desarrollado fue de hasta un 40%.

9.2. TRABAJOS FUTUROS

Basándose en los resultados obtenidos, se han identificado las siguientes líneas en las que sería interesante continuar investigando

Validación de las formulaciones a fatiga

En este trabajo se ha demostrado que el sistema BIO-PUR desarrollado permite fabricar piezas de composite de alta calidad y

propiedades mecánicas equivalentes a las resinas de origen petroquímico.

Sin embargo, el estudio se ha realizado mediante ensayos estáticos. Una de las propiedades más interesantes para la aplicación objetivo y donde los PU's podrían aportar mayores ventajas es la resistencia a la fatiga. Esta propiedad es muy dependiente de la configuración de la pieza y, en el caso de las ballestas de suspensión, los fabricantes comunicaron que son muy sensibles a las tensiones residuales provocadas por diferencias en el grado de curado debido a su gran espesor [1-4].

Por ello, se considera necesario ensayar probetas con una relación de aspecto muy cercano al real. Actualmente se está trabajando en esta línea, en la que se han podido llevar a cabo algunos avances en la fabricación de un demostrador (530 mm x 85 mm x 25 mm) que posteriormente se ensayará a fatiga (*Figura 9.1*).

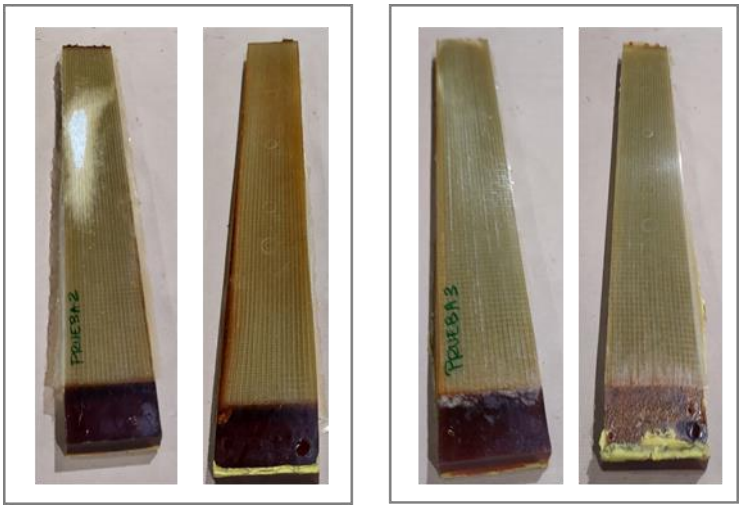

Figura 9.1. Fotos de las pruebas de la fabricación del demostrador de ballesta.

Aumento del contenido de componente biobasado en las formulaciones

A pesar de que las formulaciones de resinas desarrolladas entran dentro de la categoría de bio-basadas por tener un porcentaje BIO mayor del 20% (29%) sería interesante trabajar en aumentar este porcentaje, por ejemplo, con la utilización de polioles con un mayor porcentaje de carbono renovable, a pesar de que probablemente no existan alternativas comerciales. En este trabajo los polioles utilizados presentaban un contenido carbono renovable máximo del 80%.

Por otra parte, también sería interesante aumentar el porcentaje de componente bio y/o sostenible en el composite con la incorporación de fibras naturales como cáñamo, yute o fibras recicladas y estudiar su viabilidad para piezas estructurales de automoción u otras aplicaciones [5-9].

Mejora de la eficiencia del proceso

Se ha visto que el modelo basado en DDDAS es capaz de detectar y predecir los cambios en la velocidad de llenado debidos a variaciones en la permeabilidad. El siguiente paso sería la implementación en un molde sensorizado y validación de un sistema de control con este modelo, verificando su capacidad de corregir on-line los parámetros de proceso (presión o velocidad de alimentación) para que el proceso se realice a una velocidad óptima en la que no se produzcan porosidades o áreas secas.

Otras aplicaciones

En este trabajo, se ha realizado un estudio preliminar, demostrándose la viabilidad del sistema desarrollado para otras aplicaciones como la eólica y el proceso de infusión. Sin embargo, se ha visto que sería necesario mejorar algunos aspectos de cara a su implementación como la viscosidad y reactividad del sistema. En ese sentido se prevé colaborar con Covestro que ha desarrollado un sistema de PU's de muy baja viscosidad optimizado para la infusión de palas. Actualmente se está en proceso de firma de un NDA.

Por otra parte, se considera que estas resinas podrían ser de interés para el campo de la energía offshore, tanto para eólica como para otros sectores, por lo que se está estudiando el comportamiento de estos materiales en ambiente marino en el laboratorio flotante HarshLab de Tecnalia [10].

Para ello, se han fabricado probetas por infusión y se han colocado en la zona atmosférica y en la zona de inmersión, con el fin de estudiar su viabilidad en aplicaciones como las palas de los aerogeneradores o estructuras de plataformas flotantes. Para llevar a cabo el estudio es necesario mantener las probetas durante 3 y 6 meses por lo que se espera tener estos resultados en breve.

La *Figura 9.2c* muestra el aspecto de las probetas después de 1 mes de inmersión.

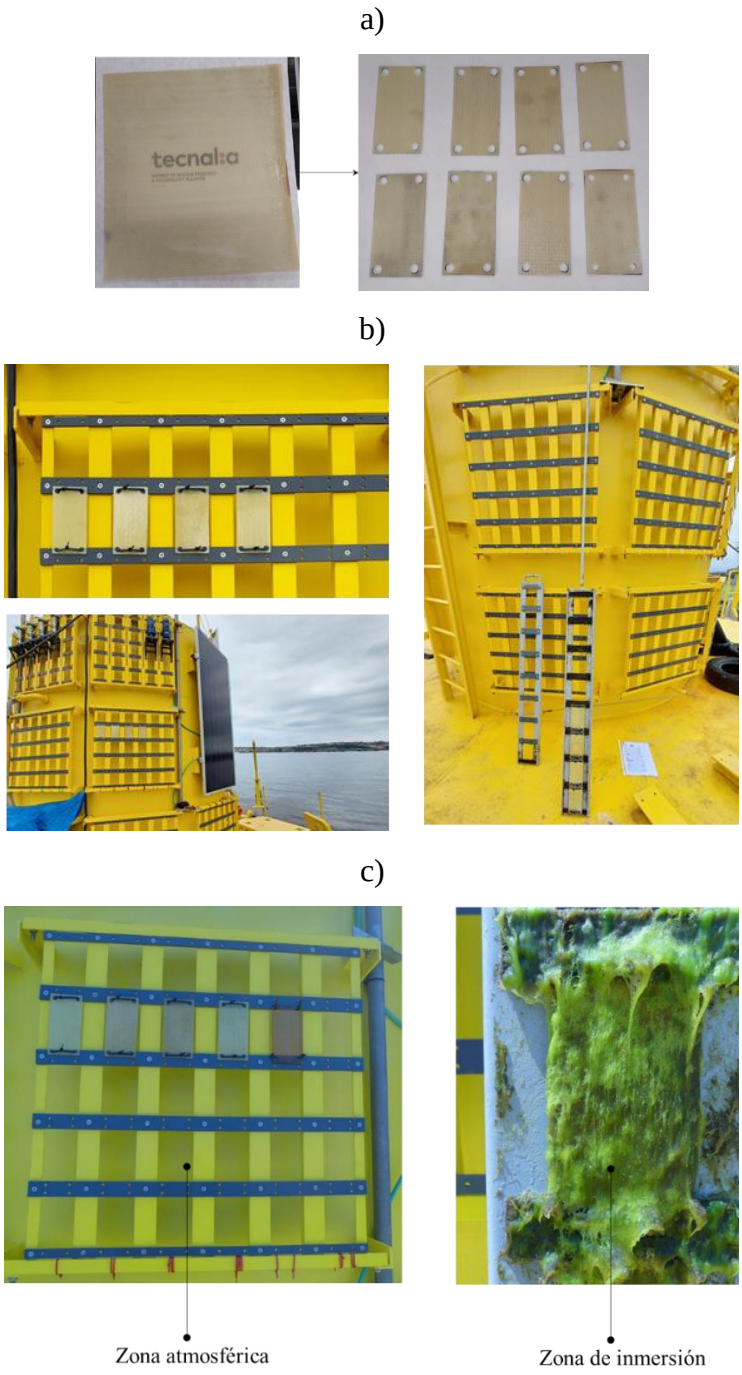

Figura 9.2. a) Probetas para el ensayo en el HarshLab, b) Las probetas colocadas en el HarshLab y c) el aspecto de las probetas tras 1 mes.

Resinas para paneles fotovoltaicos

Otra de las energías renovables en el que los composites y en concreto las resinas sostenibles presentan un gran interés es la energía solar fotovoltaica.

Los módulos fotovoltaicos Solarface desarrollados por Tecnalia (WO2016038000) consisten en un composite transparente en el que se embeben las células fotovoltaicas permitiendo la fabricación de módulos fotovoltaicos estructurales de gran ligereza. En este sentido los BIO-PUR podrían ser una alternativa más sostenible que las resinas epoxi de origen petroquímico utilizadas actualmente.

Sin embargo, las resinas para esta aplicación deben ser transparentes y el isocianato utilizado en la formulación presenta un color amarillento debido a su naturaleza del isocianato (pMDI). Se ha realizado un ensayo preliminar en la EQE (External Quantum Efficiency) a muestras de resina sin reforzar tanto del BIO-PUR desarrollado en este trabajo (BIO-PUR3) como a un BIO-PUR sintetizado a partir de un isocianato transparente de base MDI. La muestra con MDI presenta valores que se podrían acercar más a los mínimos necesarios (muestras de composite) por lo que se seguirá trabajando en esta línea.

a)

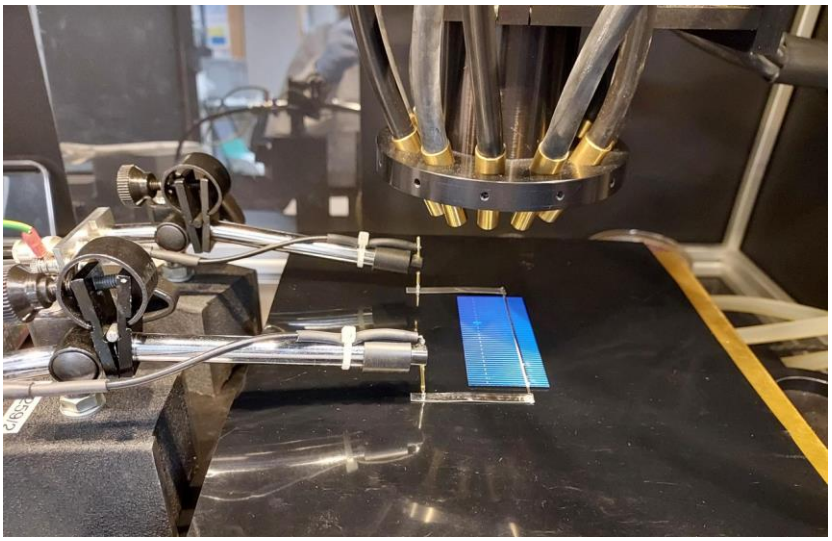

b)

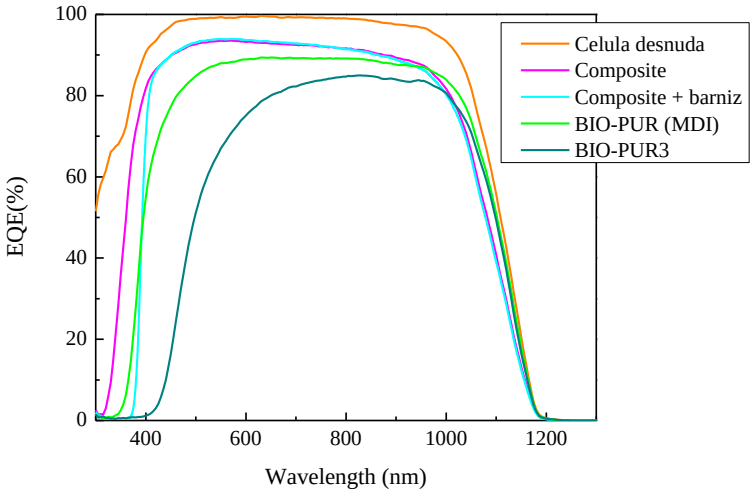

Figura 9.3. a) Ensayo preliminar en la EQE (External Quantum Efficiency) y b) Resultados en los que se presentan eficiencia cuántica frente a longitud de ondapara los diferentes sistemas.

Fin de vida y circularidad

A lo largo de estos años se ha comprobado que a pesar de que el aumento de la circularidad de los materiales composites es un tema que se considera crítico en diferentes sectores (automoción, eólica, fotovoltaica...) queda aún mucho camino por recorrer. En este trabajo se han explorado nuevas líneas de investigación para la mejora de fin de vida y circularidad de los BIO-PUR desarrollados. Se han obtenido resultados muy prometedores tanto con la incorporación de enlaces de dinámicos de tipo Diels-Alder para mejorar su reciclabilidad como con la utilización de BHET proveniente de PET reciclado. Por lo tanto, se va a continuar trabajando y colaborando en estas dos líneas considerada como estratégicas tanto para Tecnalia como para el grupo de la GMT-EHU/UPV.

Incorporar elementos reciclados

En este trabajo se ha visto viable incorporar elementos componentes derivados de plásticos reciclados como el BHET. Se han podido fabricar BIO-PUR-R con un 40% de contenido reciclable y biobasado. Sin embargo, la incorporación del BHET a pesar de que se obtengan un módulo equivalente al sistema de BIO-PUR optimizado, aumenta la fragilidad del material. El siguiente paso sería modificar la formulación para aumentar la tenacidad del material. Esto se podría hacer por varias vías. En este trabajo se ha substituido totalmente el glicerol por el BHET por lo que se podrían evaluar diferentes grados de sustitución de glicerol utilizando diferentes relaciones de glicerol:BHET.

También se podrían utilizar otros polioles biobasados con mayor peso equivalente para lograr una mayor flexibilidad, pero con mayor funcionalidad para mantener el grado de reticulación al máximo posible.

Por otra parte, habría que optimizar los parámetros de proceso y fabricar placas de composite con esta formulación y caracterizar las propiedades finales (T_g y propiedades mecánicas)

Fin de vida

En este trabajo se ha visto que es posible incorporar enlaces dinámicos en los BIO-PUR para obtener nuevas formulaciones, BIO-PUR-DA1 reprocesables por lo que se considera interesante seguir investigando en esta línea. El siguiente paso sería realizar el estudio reológico del BIO-PUR-DA1 para analizar los tiempos de relajación de la resina a diferentes temperaturas, con el objeto de caracterizar y optimizar su termo-reversibilidad. Por otra parte, también sería necesario optimizar los parámetros de proceso y fabricar placas de composite con esta formulación y caracterizar las propiedades finales (T_g y propiedades mecánicas) y también desarrollar el proceso de reciclado.

9.3. PUBLICACIONES Y CONTRIBUCIONES A CONGRESOS

En el marco de este trabajo se han realizado las siguientes contribuciones científicas.

Artículos indexados

Autores:	Oihane Echeverria-Altuna, Olatz Ollo, Tamara Calvo-Correas, Isabel Harismendy, Arantxa Eceiza
Titulo:	Effect of the catalyst system on the reactivity of a polyurethane resin system for RTM manufacturing of structural composites
Revista:	eXPRESS Polymer Letters
Año:	2022
Factor de impacto:	3.952 (JCR 2021)
Ranking:	POLYMER SCIENCE 27/90 (JCR 2021)

Autores:	Gorka Garate, Isabel Harismendy, Oihane Echeverria-Altuna, Julián Estévez
Titulo:	A dynamic data driven application system for real-time simulation of resin transfer moulding processes
Revista:	International Journal of Material Forming
Año:	2022
Factor de impacto:	2.378 (JCR 2021)
Ranking:	ENGINEERING, MANUFACTURING 35/51 (JCR 2021) MATERIALS SCIENCE, MULTIDISCIPLINARY 244/345 (JCR 2021) METALLURGY & METALLURGICAL ENGINEERING 28/79 (JCR 2021)

Autores:	Oihane Echeverria-Altuna, Olatz Ollo, Isabel Harismendy, Arantxa Eceiza
Titulo:	Desarrollo de formulaciones de PUR más sostenibles para aplicaciones estructurales
Revista:	Revista de Materiales Compuestos
Año:	2022
Factor de impacto:	N/A-JCR
Ranking:	N/A-JCR

Autores:	Oihane Echeverria-Altuna, Olatz Ollo, Izaskun Larraza, Isabel Harismendy, Arantxa Eceiza
Titulo:	Effect of the biobased polyol's chemical structure in high performance thermoset polyurethane properties
Revista:	Polymer
Año:	2022 enviado y en revisión
Factor de impacto:	4.432 (JCR 2021)
Ranking:	POLYMER SCIENCE 22/90 (JCR 2021)

Autores:	Oihane Echeverria-Altuna, Olatz Ollo, Izaskun Larraza, Isabel Harismendy, Arantxa Eceiza
Titulo:	Development of a novel biobased polyurethane resin system for structural composites
Revista:	Polymer
Año:	2022 enviado
Factor de impacto:	4.432 (JCR 2021)
Ranking:	POLYMER SCIENCE 22/90 (JCR 2021)

Autores:	Oihane Echeverria-Altuna, Olatz Ollo, Eider Mendiburu, Isabel Harismendy, Arantxa Eceiza
Titulo:	Development of a biobased polyurethane resin with recycled BHET for structural composites
Año:	En preparación

Contribuciones a congresos

Autores:	Oihane Echeverria-Altuna, Olatz Ollo, Tamara Calvo-Correas, Olatz Ollo, Isabel Harismendy, Arantxa Eceiza
Titulo:	Desarrollo de nuevas formulaciones de resinas PUR de altas prestaciones para procesos de alta cadencia de producción de componentes estructurales
Conferencia:	XIII Congreso Nacional de Materiales Compuestos (MATCOMP 2019)
Contribución:	Poster
Año:	2019
Lugar:	Vigo (España)

Autores:	Oihane Echeverria-Altuna, Olatz Ollo, Tamara Calvo-Correas, Olatz Ollo, Isabel Harismendy, Arantxa Eceiza
Titulo:	RTM prozesurako ezaugarriak eta prestazio altuak dituzten Bio-Poliuretano formulazio berrien garapena
Conferencia:	Materialen Zientzia eta Teknologia V. Kongresua
Contribución:	Presentación oral
Año:	2021
Lugar:	Bilbo (España)

Autores:	Oihane Echeverria-Altuna, Olatz Ollo, Tamara Calvo-Correas, Olatz Ollo, Isabel Harismendy, Arantxa Eceiza
Titulo:	Thermoset polyurethanes based on biobased polyols for LCM processes
Conferencia:	GEPSLAP2022
Contribución:	Presentación flash y poster
Año:	2022
Lugar:	Donostia (España)

Autores:	Oihane Echeverria-Altuna, Olatz Ollo, Isabel Harismendy, Arantxa Eceiza
Titulo:	Desarrollo de formulaciones de PUR más sostenibles para aplicaciones estructurales
Conferencia:	XIV Congreso Nacional de Materiales Compuestos
Contribución:	Presentación oral
Año:	2022
Lugar:	Sevilla (España)

Otras contribuciones

Webminar

Autores:	Oihane Echeverria-Altuna, Isabel Harismendy, Arantxa Eceiza
Titulo:	Nuevos poliuretanos más sostenibles y de altas prestaciones
Webminar:	Webminar AEMAC
Contribución:	Presentación oral

Artículo (Blog Tecnalia)

Autores:	Oihane Echeverria-Altuna, Isabel Harismendy.
Titulo:	Materiales y procesos más sostenibles para el sector de la automoción
Lugar:	Blog de Tecnalia
Contribución:	Artículo
Año:	2021

9.4. REFERENCIAS

[1] Michaud, D. J.; Beris, A. N.; Dhurjati, P. S.: Curing behavior of thick-sectioned RTM composites. Journal of Composite Materials, 32 (1998). http://doi:10.1177/002199839803201402.

[2] Huntsman: What are the specific advantages when it comes to manufacturing leaf springs? Available online: https://www.huntsman-transportation.com/EN/applications/applications-for-composites/leaf-spring.html (accessed on Aug 26, 2022).

[3] Stewart, R.: Wind turbine blade production – new products keep pace as scale increases. Reinforced Plastics, 56, 18–25 (2012). http://doi:10.1016/S0034-3617(12)70033-4.

[4] Maguire, J. M.; Nayak, K.; Ó Brádaigh, C. M.: Novel epoxy powder for manufacturing thick-section composite parts under vacuum-bag-only conditions. Part II: Experimental validation and process investigations. Composites Part A: Applied Science and Manufacturing, 136, 105970 (2020). http://doi:10.1016/j.compositesa.2020.105970.

[5] Gilmar Lima; Giuseppe Santachè: PUGgreen:a new bio-resin concept for composite processing. Jec Composites Magazine, 146, 46–49 (2022).

[6] Terry, J. S.; Taylor, A. C.: The properties and suitability of commercial bio-based epoxies for use in fiber-reinforced composites. Journal of Applied Polymer Science, 138 (2021). http://doi:10.1002/app.50417.

[7] Pil, L.; Bensadoun, F.; Pariset, J.; Verpoest, I.: Why are designers fascinated by flax and hemp fibre composites? Composites Part A: Applied Science and Manufacturing, 83 (2016). http://doi:10.1016/j.compositesa.2015.11.004.

[8] Dixit, S.; Goel, R.; Dubey, A.; Shivhare, P. R.; Bhalavi, T.: Natural fibre reinforced polymer composite materials - A review. Polym. from Renew. Resour. (2017), 8.

[9] Peças, P.; Carvalho, H.; Salman, H.; Leite, M.: Natural fibre composites and their applications: A review. Journal of Composites Science, 2 (2018). http://doi:10.3390/jcs2040066.

[10] Tecnalia: Floating laboratory in a real offshore environment (HarshLab) Available online: https://www.tecnalia.com/en/infrastructure/floating-laboratory-in-a-real-offshore-environment-harshlab (accessed on Aug 22, 2022).

ANEXO I

Figuras y tablas

Figuras

Capítulo 2

Figura 2.1. Composite para soluciones estructurales ligeras en automoción. *12*
Figura 2.2.Piezas estructurales en composite *13*
Figura 2.3. Etapas principales del proceso RTM. *18*
Figura 2.4. Formación del grupo uretano. *20*
Figura 2.5.. El grupo isocianato y sus estructuras de resonancia. *20*
Figura 2.6. Estructura de los poliuretanos termoplásticos. *26*
Figura 2.7. Estructura de los poliuretanos termoestables (red tridimensional). *28*
Figura 2.8.Propiedades de los PUR. *29*
Figura 2.9. Retos que presentan los poliuretanos. *32*
Figura 2.10. Ciclo de vida de materiales. *33*

Capítulo 3

Figure 3.1. b) Part A preparation of the catalysed systems and c) Part B preparation of the catalysed systems. *64*
Figure 3.2. a) Ideal viscosity evolution for the PUR RTM resin systems and b) complex viscosity evolution with temperature for the different PUR. *68*
Figure 3.3. Complex viscosity evolution with time at different temperatures, a) PUR-REF, b) PUR-CAT1, c) PUR-CAT2 and d) PUR-CAT3. ..... *69*
Figure 3.4. Gel time vs temperature for the studied PUR systems. *70*

Figure 3.5. Scheme of the salt encapsulation. a) Salt dissociation in DAS and BDG and b) urethane formation with DAS or BDG and salt encapsulation. *72*

Figure 3.6. Dynamic DSC thermograms for the different PUR systems at a) 5 ºC min^{-1}*, b) 10 ºC* min^{-1} *and c) 20 ºC* min^{-1}*, and d) isothermal DSC thermograms for the different PUR systems at 120 ºC.* *74*

Figure 3.7. a) Scheme of the catalyst mechanism, catalyst production in situ and polyurethane curing. *76*

Figure 3.8. Polyurethane three-dimensional network for PUR-REF, PUR-CAT2 and PUR-CAT3 systems. *77*

Figure 3.9. Degree of cure curves from DSC isothermal and dynamic tests (symbols) and models fitting (lines), a) PUR-REF, b) PUR-CAT2 and c) PUR-CAT3, and d) maximum degree of cure at different temperatures. *81*

Figure 3.10. Viscosity evolution with time at 80 and 90 ºC for PUR-REF and PUR-CAT2 systems. Experimental results (symbols) and the rheological model (red lines). *83*

Figure 3.11. a) Injection strategy and b) mesh used in the simulation of a reinforced leaf spring. *84*

Figure 3.12. Leaf spring simulation at 120ºC with constant pressure for PUR-REF. *86*

Figure 3.13. Leaf spring simulation at 120ºC with constant pressure for PUR-CAT2. ..... *87*

Figure 3.14. Leaf spring simulation at 120ºC with constant flow rate for PUR-REF and PUR-CAT2. ..... *88*

Capítulo 4

Figure 4.1. a) BIO-PUR/ PUR sample preparation and b) resin plates casting process. 102
Figure 4.2. Complex viscosity evolution with temperature of the different BIO-PUR and PUR. 107
Figure 4.3. Dynamic DSC thermograms. 108
Figure 4.4. BIO-PURs and PURs plates. 109
Figure 4.5. Curves of loss factor (tan δ, dashed line) and storage modulus (E', continuous line) vs temperature. a) Flexible BIO-PUR systems flexural geometry and b) Rigid BIO-PUR and PUR systems. 110
Figure 4.6. Scheme of the different three-dimensional networks of the BIO-PUR/PUR systems. 112
Figure 4.7. a) TG curves b) DTG curves for the BIO-PUR and PUR systems 113
Figure 4.8. FTIR spectra of selected polyurethane polyols in the 3600-2575 cm^{-1} interval. 115
Figure 4.9. Flexural test for BIO-PUR1 116

Capítulo 5

Figure 5.1. Polyurethane resin system preparation. 132
Figure 5.2. Complex viscosity evolution with temperature for different PUR systems. 135
Figure 5.3 a) Dynamic DSC thermograms and b) isothermal DSC thermograms for the different PUR systems. 136
Figure 5.4. Curves of loss factor (tan δ, dashed line) and storage modulus (E', continuous line) vs temperature of different PUR systems. 139

Figure 5.5. Scheme of the three-dimensional network of the different PUR systems. 140
Figure 5.6. a) Mesh and b) injection strategy used in the simulation. 141
Figure 5.7. Degree of cure curves from DSC isothermal and dynamic tests(symbols) and models fitting (red lines) for a) BIO-PUR2 and b) BIO-PUR3. 144
Figure 5.8. Viscosity evolution with time at 90 ºC for BIO-PUR2 and BIO-PUR3. Experimental results (symbols) and model (red lines). .. 145
Figure 5.9. Leaf spring RTM process simulation. 147

Capítulo 6

Figure 6.1. Example of micro-void and macro-void in RTM manufactured composite. 156
Figure 6.2. Schematic relationship between voids formation and the impregnation velocity [18]. 157
Figure 6.3. Relationship between macro and micro voids and the mould filling velocity[18]. 157
Figure 6.4. a) Schematic diagram of the test equipment and RTM mould. b)RTM test equipment and software picture. 162
Figure 6.5. Samples extraction areas. 168
Figure 6.6. Glass fabric morphology b) after performing. 170
Figure 6.7. Micrographs and processed images for the different composite samples (blue areas: macrovoids; red areas: microvoids). 171
Figure 6.8. Void content for different impregnation velocity. 172
Figure 6.9. The flow front evolution for BIO-PUR3. 173

Figure 6.10. Comparison between the simulation and real RTM process with the BIO-PUR3 formulation. *174*
Figure 6.11. Flexural strength testing results for BIO-PUR composite plate. *175*
Figure 6.12. Interlaminar shear strength results for BIO-PUR composite plate. *175*
Figure 6.13. Composite plate micrographs. *176*
Figure 6.14. DDDAS flow chart. *181*
Figure 6.15. Preforms configuration. *183*
Figure 6.16. Test 1 configuration. *184*
Figure 6.17 Flow front progression during Test1. ..... *184*
Figure 6.18 Model results for Test 1. ..... *185*
Figure 6.19 Flow front progression during Test 2. ..... *186*
Figure 6.20 Model results for Test 2. ..... *187*
Figure 6.21. Test 3 configuration. *188*
Figure 6.22 Flow front progression during Test nº3. ..... *188*
Figure 6.23 Model results for Test 3. ..... *189*
Figure 6.24. Test 4 configuration. *190*
Figure 6.25 Flow front progression during Test nº4. ..... *191*
Figure 6.26 Model results for Test nº4. ..... *192*

Capítulo 7

Figure 7.1. Results of BIO-PUR3 infusion trials with the different ancillary materials combinations. *209*
Figure 7.2. Double infusion bag configuration. *210*
Figure 7.3. BIO-PUR3 infusion at different temperatures. *212*
Figure 7.4. Fibre moisture effect. *213*
Figure 7.5. BIO-PUR3 infusion trial with moisture scavengers. *215*

Figure 7.6. Infusion trial with Vacuum Assisted Process. 216
Figure 7.7. BIO-PUR3 infusion with previously dried glass fabric... 217
Figure 7.8. BIO-PUR3 infusion process parameters. 217
Figure 7.9. Infusion manufactured BIO-PUR3 composite plates. 218
Figure 7.10. Interlaminar shear strength results for infused BIO-PUR3 composite plate. 219

Capítulo 8

Figure 8.1.CAN advantages compared to thermoplastic and thermoset common polymers. 228
Figure 8.2. a) Dissociative and b) associative CANs reversible reaction mechanism [12].. 229
Figure 8.3.Diels Alder reaction. 229
Figure 8.4. BHET monomer obtained after the PET glycolysis and a polyurethane synthesised from it [18]. 230
Figure 8.5.BIO-PURs linear life cycle. 232
Figure 8.6.BIO-PUR circular materials. 233
Figure 8.7. Scheme of the synthesis of the DA adduct containing triol. 240
Figure 8.8. FTIR of the synthesized triol. 241
Figure 8.9.Triol-DA thermograms for the different heating and cooling cycles. 243
Figure 8.10.Schema of the strategy to integrate the DA adduct in the BIO-PUR formulation. 244
Figure 8.11. Triol- DA appearance at RT and miscibility of the components. 245
Figure 8.12. DSC thermograms of BIO-PUR-DA systems and BIO-PUR2. 246

Figure 8.13.BIO-PUR-DA plates *246*
Figure 8.14.BIO-PUR-DA1temperature cycles..... *249*
Figure 8.15. FTIR of BIO-PUR-DA1after temperature cycles. *250*
Figure 8.16. Preliminary tests of BIO-PUR-DA1 reprocessability.... *251*
Figure 8.17. a) FTIR and b) ^{1}*H NMR spectra of the BHET obtained from PET glycolysis.* *253*
Figure 8.18. GPC chromatogram of the BHET obtained from PET glycolysis. *254*
Figure 8.19. a) DSC and b) mass loss (lines) and derivative (dot line) of the BHET obtained from PET glycolysis...... *255*
Figure 8.20. BIO-PUR-R plate preparation..... *256*
Figure 8.21.Viscosity evolution with temperature for BIO-PUR-R and BIO-PUR2 systems. *257*
Figure 8.22. Dynamic DSC thermograms...... *257*
Figure 8.23. BIO-PUR-R plate...... *258*
Figure 8.24. BIO-PUR-R and BIO-PUR2 curves of tan δ vs temperature. *259*
Figure 8.25. Flexural strength testing results for BIO-PUR composite plate. *260*

Capítulo 9

Figura 9.1. Fotos de las pruebas de la fabricación del demostrador de ballesta. *273*
Figura 9.2. a) Probetas para el ensayo en el HarshLab, b) Las probetas colocadas en el HarshLab y c) el aspecto de las probetas tras 1 mes. *276*

Figura 9.3. a) Ensayo preliminar en la EQE (External Quantum Efficiency) y b) Resultados en los que se presentan eficiencia cuántica frente a longitud de ondapara los diferentes sistemas. 278

ANEXO III

Figura A.1. Espectro infrarrojo de los polioles Voraforce TR 1551-Polyol, Lupranol 3300 y Lupranol 3422. 306
Figura A.2. Espectro infrarrojo de los polioles Emerox 14060 y Emerox 14090. 308
Figura A.3. Espectro infrarrojo de los polioles Priplast 3186 y Priplast 4F. 309
Figura A.4. Espectro infrarrojo de los polioles Polycin T-400, Polycin T-12 y Polycin M-280. 310
Figura A.5. Espectro infrarrojo del diisocianato pMDI. 312

Tablas

Capítulo 2

Tabla 2.1.Fabricantes de ballestas de composite.....15
Tabla 2.2. Tecnologías y materiales empleados en la fabricación de ballestas de composite.....16
Tabla 2.3. Isocianatos más utilizados en la síntesis de los poliuretanos. 22
Tabla 2.4. Isocianatos biobasados comerciales.....23
Tabla 2.5. Resinas poliuretano termoestables comerciales. 30

Capítulo 3

Table 3.1. Designation and composition of synthesised thermoset polyurethanes. 62
Table 3.2. Kinetic model parameters for the different PUR resin systems. 79
Table 3.3. Viscosity model parameters.....82

Capítulo 4

Table 4.1. Propesties of polyols. 100
Table 4.2. Summary of synthesized BIO-PUR/PUR systems.....101
Table 4.3. Total heat of cure reaction of different BIO-PUR/PUR's systems.....109
Table 4.4. Crosslinking density and T_g values of different BIO-PUR/PUR systems.....111
Table 4.5. Flexural properties of PUR/BIO-PUR systems.....116

Capítulo 5

Table 5.1. Summary of synthesized polyurethanes 131
Table 5.2. RT Storage modulus and T_g values for the different BIO-PUR/PUR systems. 139
Table 5.3. Flexural properties of the PUR systems. 141
Table 5.4. Kinetic model parameters for the different BIO-PUR3..... 143
Table 5.5 Viscosity model parameters. 145

Capítulo 6

Table 6.1. Fibre properties. 160
Table 6.2. Summary of synthesized polyurethanes. 161
Table 6.3 Permeability value calculated with different method. 167
Table 6.4. Final properties of BIO-PUR based composite 177

Capítulo 7

Table 7.1. Fibre properties. 206
Table 7.2. Commercial infusion materials. 208
Table 7.3. Ancillary materials combinations studied. 208
Table 7.4. Final properties of BIO-PUR3 based composite 220

Capítulo 8

Table 8.1. Components used in the BIO-PUR-DA and BIO-PUR-R formulation. 235
Table 8.2. Summary of synthesized BIO-PUR-DA and BIO-PUR-R systems. 236
Table 8.3. Flexural properties of the BIO-PUR2 and BIO-PUR-R systems. 260

ANEXO III

Tabla A.1 Principales propiedades de los polioles empleados en la síntesis de poliuretanos. 305
Tabla A.2. Asignación de los picos significativos del espectro FTIR de los polioles Voraforce TR 1551-Polyol, Lupranol 3300 y Lupranol 3422. 307
Tabla A.3. Asignación de los picos significativos del espectro FTIR de los polioles Emerox 14060 y Emerox 14090. 308
Tabla A.4. Asignación de los picos significativos del espectro FTIR de los polioles Priplast 3186 y Priplast 4F. 309
Tabla A.5. Asignación de los picos significativos observados en el espectro FTIR de los polioles Polycin T-400, Polycin T-12 y Polycin M-280. 311
Tabla A.6. Propiedades de la fibra Ultra Fatigue UD utilizado en el proceso RTM. 313
Tabla A.7. Propiedades de la fibra utilizado en el proceso de infusión. 313

ANEXO II

Abreviaturas y símbolos

α	Grado de curado
ΔP	Gradiente de presión
^{1}H NMR	Resonancia magnética nuclear de protones
BDDE	1,4-butanodiol diglicidil éter
BDG	Dietilenglicol dibutil éter
BDMAEE	2-[2-(dimetilamino)etoxi]-N,N-dimetiletanamina
BHET	Bis(2-Hidroxyethil) tereftalato
BIO-Gly	Glicerol biobasado
BIO-PUR	Poliuretanos termoestables de origen vegetal
CAN	Redes adaptables covalentes
C-RTM	Moldeo por transferencia de resina de alta presión por compresión
dα/dt	Velocidad de curado
DA	Diels Alder
DA	Diels Alder
DABCO	1,4-diazabiciclo[2.2.2]octano
DAS	1,4:3,6-dianhidro-D-glucitol o D-isosorbide
DDDAS	Sistemas de aplicación basados en datos dinámicos
DDI	diisocianato de dimerilo
DMA	Análisis mecánico diferencial
DSC	Calorimetría diferencial de barrido
E, E_1, E_2	Energía de activación
$E'_{T\alpha+50}$	Módulo de almacenamiento en la región elastica
f	Funcionalidad de los polioles
F(α)	Factor de difusión
FTIR	Espectrofotómetro de transformada de Fourier
G'	Módulo de almacenamiento
G''	Módulo de perdida
GPC	Cromatografía de permeación por gel

H	Calor instantáneo desarrollado durante la reacción de polimerización de la resina
H_{12}MDI	Diciclohexilmetano-4,4'-diisocianato metileno-bis-(4-isocianatociclohexano)
HDI	1,6- Hexametilen diisocianato
HP-RTM	Moldeo por transferencia de resina de alta presión
H_T	Calor total de la reacción
ILSS	Resistencia al cizallamiento interlaminar
I_{OH}	Índice de hidroxilo
IPDI	Isoforone diisocianato
IVP	Problema de valor inicial
K	Permeabilidad de la preforma
k_1, k_2	Factor preexponencial (ecuación Kamal-Sourour)
K_{av}, K_{ele}, K_{int}, K_{sp}	Valores de permeabilidad determinadas por diferentes métodos de cálculo (basado en el promedio, el método elemental, basado en la interpolación y el basado en el punto único)
LCM	Proceso de moldeo por vía líquida de composites
L-LDI	Diisocianato de etil ester L-lisina
LLTI	Triisocianato de etil ester L-lisina
LSF	Ajuste por mínimos cuadrados
LVR	Rango Viscoelástico Lineal
MDI	4,4’-Difenil metano diisocianato
Mn	Peso Molecular Promedio en Número
Mw	Peso molecualar
n^{th}, m^{th}	Orden de reacción
P	Presión
ϕ	Porosidad
PET	Politereftalato de etileno
pMDI	4,4’-Difenil metano diisocianato polimérico

PUR	Poliuretanos termoestables
Q	Flujo de la resina
R	Constante universal de los gases ideales (8.314 J mol^{-1} K^{-1})
rDA	Reacción de Retro-Diels-Alder
R-RIM	Inyección de resina reforzada
RT	Temperatura ambiente
RTM	Moldeo por transferencia de resina
S	Área transversal
S-RIM	Inyección de resina estructural
T	Temperatura
TDI	2,4- o 2,6-Tolueno diisocianato
T_g,	Transición vítrea
TGA	Análisis termogravimétrico
THF	Tetrahidrofurano
T_m	Temperatura de fusión
TPU	Poliuretanos termoplásticos
UD	Unidireccional
v	Velocidad de impregnación de la resina
VAP	Proceso asistido por vacío
Vf	Volumen de fibra de composite
VOC	Compuestos orgánicos volátiles
Vv	Volumen de poros
x	Posición del frente de flujo
η^*	Viscosidad de la resina
η_0, p_1, p_2	Parámetros ajustables (ecuación Castro-Macosko)

ANEXO III

Materiales

En este trabajo se han utilizado polioles comerciales tanto de origen petroquímico como de origen renovable.

Entre los de origen petroquímico, se han utilizado tres polioles de tipo polieter, Voraforce TR 1551-Polyol [1], amablemente suministrado por Dow Chemical (Milano, Italia), y los Lupranol 3300 y Lupranol 3422, derivados de glicerol y sorbitol respectivamente [2], amablemente suministrados por Basf Española (Barcelona, España).

Entre los de origen renovable, se han utilizado siete polioles comerciales derivados de diferentes aceites vegetales, como los Emerox 14060 y Emerox 14090 derivados de aceite de palma [3], amablemente suministrado por Emery (Cincinnati, USA), los Priplast 3186 y Priplast 4F derivados de varios tipos de aceites [4,5] , amablemente suministrado por Croda Ibérica (Barcelona, España), y los Polycin T-400, Polycin T-12 y Polycin M-280 derivados de aceite de aceite de ricino [6], amablemente suministrados por Bercen de Vertellus (Denham Springs, USA).

En la Tabla A.1 se resumen las principales propiedades de los polioles utilizados en este trabajo, proporcionadas por el proveedor o determinadas en su defecto, como el índice de hidroxilo (I_{OH}), la funcionalidad (f), la viscosidad a 25 ºC, el peso equivalente y el contenido de carbono renovable en el caso de los biobasados. El índice de hidroxilo se ha determinado mediante valoración según la norma ASTM D 4274-05 [7].

Tabla A.1 Principales propiedades de los polioles empleados en la síntesis de poliuretanos.

	I_{OH}	**f**	**Viscosity at 25 ºC**	**Renewable content**	**Equivalent weight**
	mg KOH g^{-}		*mPas*	*%*	*g OH eq^{-1}*
Polyol-1	60	3.1	24600	73	935
Polyol-2	86	2.5	5000	80	652
Polyol-3	71	>2	11000	56	790
Polyol-4	203	4	27050	60	276
Polyol-5	400	3	1500	80	141
Polyol-6*	330	4	3000	80	170
Polyol-7	280	4	1385	80	200
Polyol-8**	400	3	373	0	140
Polyol-9**	490	5	22750	0	114

* 25% of secondary OH groups according to data sheet
** 100% of secondary OH groups according to data sheet

Los polioles utilizados en este trabajo también han sido caracterizados espectroscópicamente mediante FTIR con la finalidad de determinar los principales grupos funcionales y el tipo de poliol. Los resultados relativos a esta caracterización se muestran en la *Figura A.1, Figura A.2, Figura A.3 y Figura A.4.*

La *Figura A.1* muestra los espectros FTIR de los polioles de origen petroquímico.

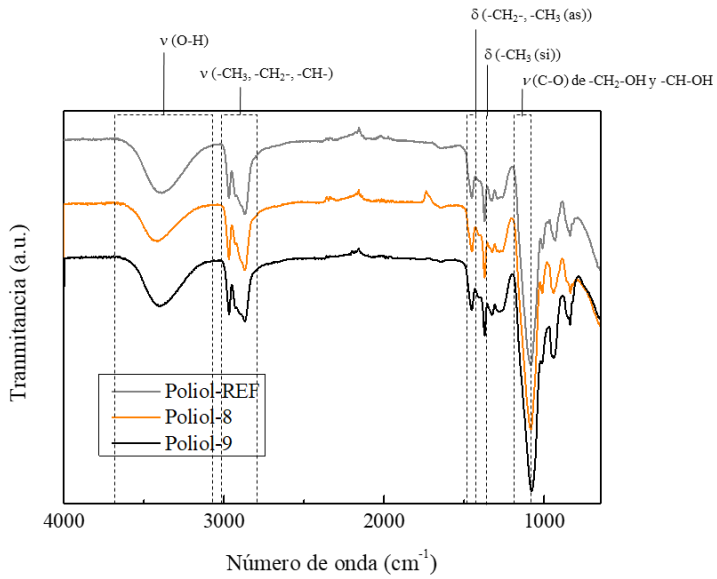

Figura A.1. Espectro infrarrojo de los polioles Voraforce TR 1551-Polyol, Lupranol 3300 y Lupranol 3422.

Como se observa en la *Figura A.*1, los tres polioles presentan espectros muy similares. No se observan diferencias apreciables ni en las posiciones de las bandas, ni en las intensidades. En la *Tabla A.*2 se detallan las principales bandas del espectro infrarrojo, así como la asignación de las bandas significativas observadas en los espectros FTIR.

Tabla A.2. Asignación de los picos significativos del espectro FTIR de los polioles Voraforce TR 1551-Polyol, Lupranol 3300 y Lupranol 3422.

Número de onda	Asignación
3650-3050	ν (O-H)
2970, 2915, 2865	ν (-CH_3, -CH_2, -CH)
1476-1450	δ (-CH_2, CH_3 (as))
1379	δ (- CH_3 (si))
1196-1015	ν (C-O) de -CH_2-OH y -CH-OH

Del análisis FTIR de los polioles Voraforce TR 1551-Polyol, Lupranol 3300 y Lupranol 3422 se confirma que son polioles de tipo poliéter con alto contenido de grupos hidroxilo.

En lo que respecta a los polioles biobasados, la *Figura A.2*, *Figura A.3* y *Figura A.4* muestran los espectros FTIR de los polioles suministrados por Emery, Croda y Vertellus, respectivamente. En la *Tabla A.3, Tabla A.4 y Tabla A.5* se detallan las principales bandas del espectro FTIR y la asignación de las bandas.

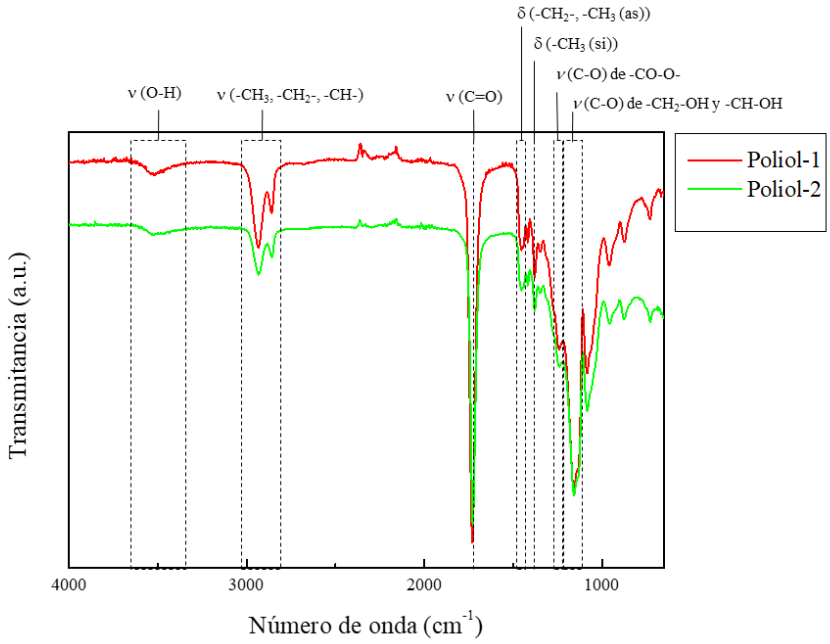

Figura A.2. Espectro infrarrojo de los polioles Emerox 14060 y Emerox 14090.

Tabla A.3. Asignación de los picos significativos del espectro FTIR de los polioles Emerox 14060 y Emerox 14090.

Número de onda (cm^{-1})	Asignación
3660-3290	ν (O-H)
-, 2931, 2857	ν (-CH_3, -CH_2-, -CH-)
1726	ν (C=O)
1488-1426	δ (-CH_2-, -CH_3 (as))
1370	δ (-CH_3 (si))
1264-1221	*ν* (C-O) de -CO-O-
1202-1091	*ν* (C-O) de -CH_2-OH y -CH-OH

La principal diferencia reside en la intensidad de la banda correspondiente a la vibración de tensión del grupo hidroxilo, menor en el caso de los polioles suministrados por Emery de acuerdo al menor I_{OH} de estos polioles, así como en la presencia de la banda correspondiente a

la vibración de tensión del grupo carbonilo. Estos resultados confirman que los polioles Emerox 14060 y Emerox 14090 son polioles de tipo poliéster con bajo contenido de grupos hidroxilo.

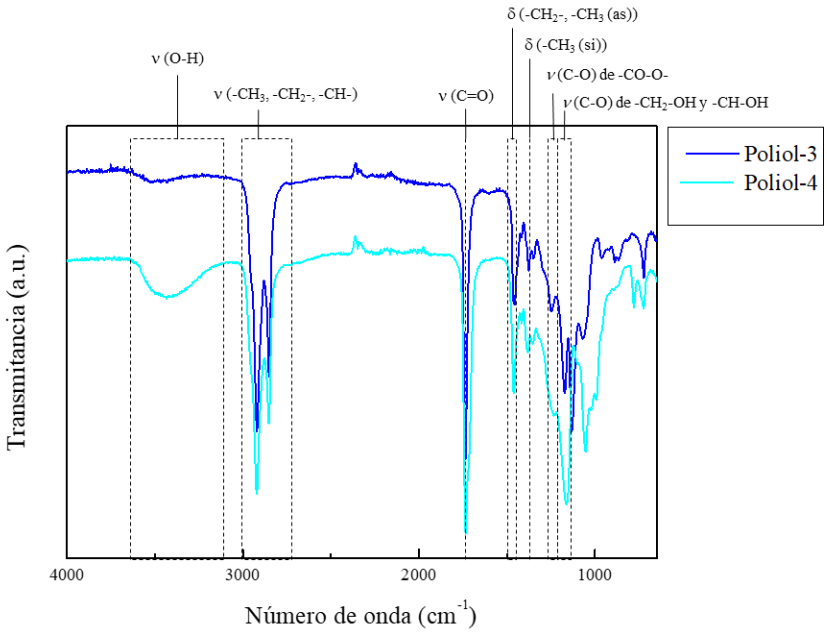

Figura A.3. Espectro infrarrojo de los polioles Priplast 3186 y Priplast 4F.

Tabla A.4. Asignación de los picos significativos del espectro FTIR de los polioles Priplast 3186 y Priplast 4F.

Número de onda (cm^{-1})	**Asignación**
3640-3125	ν (O-H)
2954, 2920, 2853	ν (-CH_3, -CH_2-, -CH-)
1741	ν (C=O)
1477-1445	δ (-CH_2-, -CH_3 (as))
1355	δ (-CH_3 (si))
1270-1219	*ν* (C-O) de -CO-O-
1219-1127	*ν* (C-O) de -CH_2-OH y -CH-OH

En este caso se observan ligeras diferencias entre los espectros de los polioles suministrados por Croda, sobre todo en lo que respecta a las intensidades de las bandas. El espectro del poliol Priplast 3186 es similar al de los polioles Emerox 14060 y Emerox 14090, de acuerdo a que presentan I_{OH} similares. En el caso del poliol Priplast 4F, se observa un aumento de la intensidad de las bandas 3640-3125 y 1219-1127 cm^{-1}, asociadas con la vibración de tensión del enlace O-H y C-OH de los compuestos hidroxilados, debido al mayor I_{OH} de este poliol. Ambos polioles presentan la banda característica de la vibración de tensión del grupo carbonilo, así como del enlace C-O del grupo éster, por lo que se trata de polioles de tipo poliéster.

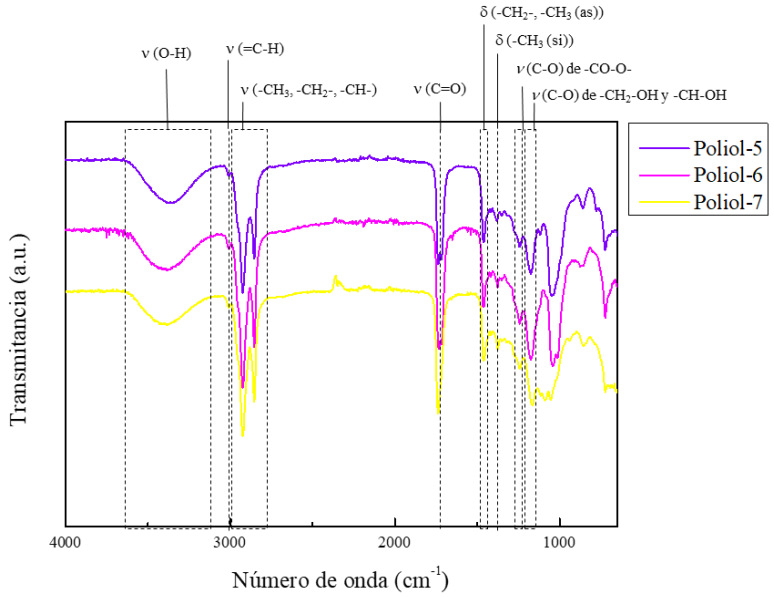

Figura A.4. Espectro infrarrojo de los polioles Polycin T-400, Polycin T-12 y Polycin M-280.

Tabla A.5. Asignación de los picos significativos observados en el espectro FTIR de los polioles Polycin T-400, Polycin T-12 y Polycin M-280.

Número de onda (cm^{-1})	Asignación
3645-3100	ν (O-H)
3008	ν (=C-H)
2957, 2923, 2853	ν (-CH_3, -CH_2-, -CH-)
1737	ν (C=O)
1490-1444	δ (-CH_2-, -CH_3 (as))
1360	δ (-CH_3 (si))
1264-1220	ν (C-O) de -CO-O-
1220-1136	ν (C-O) de -CH_2-OH y -CH-OH

La principal diferencia con respecto al resto de los polioles biobasados reside en la banda a 3008 cm^{-1} del enlace =C-H de carbonos insaturados., lo cual indica que estos dobles enlaces no se han utilizado para incorporar los grupos hidroxilo en poliol. El aceite de ricino es uno de los pocos aceites vegetales que naturalmente contienen grupos hidroxilo. En particular, contiene el triglicérido de ácido ricinoleico (87-90 %), que posee grupos hidroxilo reactivos en el ácido graso, con un valor medio de 2,7 por unidad [8]. En lo que respecta a las bandas relacionadas con el grupo hidroxilo, a 3645-3100 y 1220-1136, las intensidades son ligeramente superiores a las observadas en el poliol Priplast 4F, ya que presentan mayores valores de I_{OH}, entre 280-400 mg KOH g^{-1}. Entre los diferentes Polycin, el Polycin 400 presenta intensidades mayores, de acuerdo con su mayor I_{OH}. Las bandas relacionadas con el grupo carbonilo confirman que se trata de polioles de tipo poliéster.

En lo que respecta al isocianato empleado en la síntesis de los poliuretanos, se ha utilizado un isocianato polimérico aromático basado

en diisocianato de 4,4'-difenilmetano (pMDI), Voraforce TR 1500-Isocyanate [1], amablemente suministrado por Dow Chemical (Milano, Italia), con una viscosidad de 130 mPa s y un equivalente NCO de 136 g eq^{-1}. El equivalente isocianato se ha determinado según la norma ASTM D2572-97 [9]. En la *Figura A.5* se muestra el espectro FTIR del isocianato empleado, así como la fórmula química.

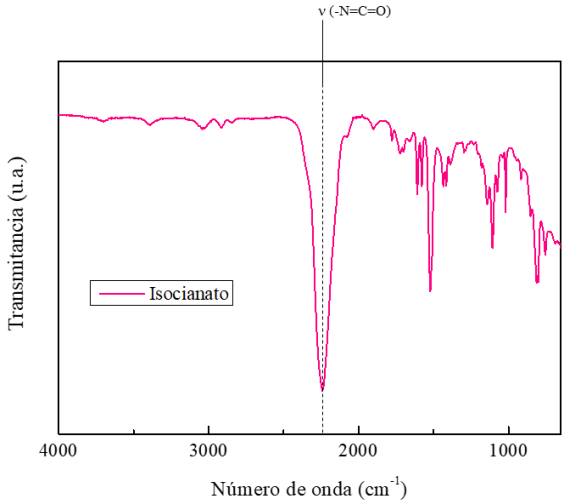

Figura A.5. Espectro infrarrojo del diisocianato pMDI.

Como se puede ver en el espectro FTIR, la banda más característica de este compuesto es la que aparece centrada a 2265 cm^{-1} y corresponde a la vibración de tensión del grupo –N=C=O. Esta banda disminuye, o desaparece completamente, con el avance de la reacción.

En lo que respecta a los compuestos hidroxilados de baja masa molecular se han utilizado etilenglicol y glicerol suministrados por Sigma Aldrich - Merk, (Darmstadt, Alemania). Aprovechando sus diferentes funcionalidades, y en función del contenido, se han sintetizado poliuretanos con diferentes densidades de entrecruzamiento.

En el desarrollo de los catalizadores se han empleado un epóxido (diglicidil éter de 1,4-butanodiol, BDDE) y cloruro de litio (LiCl) como constituyentes base. Como componentes de encapsulación de los catalizadores se han empleado un diol cíclico de base biológica de bajo peso molecular (1,4:3,6-dianhidro-D-glucitol o D-isosorbida, DAS) o un monool alifático de bajo peso molecular (dietilenglicol butil éter, BDG). Todos los componentes de los catalizadores fueron suministrados por Sigma Aldrich - Merk, (Darmstadt, Alemania).

En lo que respecta a los refuerzos utilizados en los composites, se han seleccionado dos tejidos de vidrio. Uno de ellos, el tejido unidireccinal de vidrio específico para piezas sujetas a cargas cíclicas (Ultra Fatigue UD) suministrado por Saertex (Saerbeck, Alemania) se ha utilizado para la fabricación por RTM. Las propiedades de la fibra seleccionada para RTM se presentan en la Tabla A.6.

Tabla A.6. Propiedades de la fibra Ultra Fatigue UD utilizado en el proceso RTM.

Tipo de tejido	Tejido de vidrio unidireccional
Gramaje	1176 ± 64 g m^{-2}
Aglomerante	Huntsman XB 6078 10 ± 2 g m^{-2}
Hilo de costura	Poliester 76 dtex 12 ± 3 g m^{-2}

En el caso de los composites fabricados por infusión se ha seleccionado un tejido unidireccional utilizado en las palas eólicas, suministrado por Axon technologies (Cergy-Pontoise, Francia). Las propiedades de la fibra se exponent en la *Tabla A.7.*

Tabla A.7. Propiedades de la fibra utilizado en el proceso de infusión.

Tipo de tejido	Tejido de vidrio unidireccional
Gramaje	962 ± 29 g m^{-2}
Hilo de costura	Poliester 11 ± 0.3 g m^{-2}

REFERENCIAS

[1] Dow: Dow Available online: https://www.dow.com/en-us/pdp.voraforce-systems.188527z.html#overview (accessed on Aug 26, 2022).

[2] Basf: Basf España Available online: https://chemicals.basf.com/global/en/Monomers/isocyanates-and-polyols/polyols.html (accessed on Aug 26, 2022).

[3] Emery: Emery Available online: https://www.emeryoleo.com/ (accessed on Aug 26, 2022).

[4] Croda: Croda.

[5] Sardon, H.; Mecerreyes, D.; Basterretxea, A.; Avérous, L.; Jehanno, C.: From Lab to Market: Current Strategies for the Production of Biobased Polyols. ACS Sustain. Chem. Eng. (2021), 9.

[6] Vertellus: Vertellus Available online: https://vertellus.com/products/ polycin-gr-polyol-series/ (accessed on Aug 26, 2022).

[7] ASTM: Standard Test Method for Testing Polyurethane Raw Materials: Determination of Hydroxyl Numbers of Polyols (D4274). ASTM Standard, (2005).

[8] Morales-Cerrada, R.; Tavernier, R.; Caillol, S.: Fully Bio-Based Thermosetting Polyurethanes from Bio-Based Polyols and Isocyanates. Polymers, 13, 1255 (2021). http://doi:10.3390/polym13081255.

[9] Society, A. C.: Standard Test Method for Isocyanate Groups in Urethane Materials or Prepolymers 1. Current, 06 (1998).